Development of small molecule modifiers of microRNA functions and targeted activation of caged morpholino oligomers

by

Rohan Surendra Kumbhare

B.S. Chemistry, IISER Pune, India 2013

M.S. Chemistry, IISER Pune, India 2013

Submitted to the Graduate Faculty of the

Dietrich School of Arts and Sciences in partial fulfillment

of the requirements for the degree of

Doctor of Philosophy

University of Pittsburgh

2020

UNIVERSITY OF PITTSBURGH

DIETRICH SCHOOL OF ARTS AND SCIENCES

This dissertation was presented

by

Rohan Surendra Kumbhare

It was defended on

June 18, 2020

and approved by

Paul Floreancig, Professor, Department of Chemistry

Seth Horne, Associate Professor, Department of Chemistry

Subha Das, Assistant Professor, Department of Chemistry, Carnegie Mellon University

Dissertation Director: Alexander Deiters, Professor, Department of Chemistry

Development of small molecule modifiers of microRNA functions and targeted activation of caged morpholino oligomers

Rohan Surendra Kumbhare, PhD

University of Pittsburgh, 2020

MicroRNAs (miRNAs) are small non-coding RNA molecules (~22-nucleotides long) and constitute up to 60% of human genes. miRNAs are primarily involved in gene silencing by binding to the 3'-untranslated region (3'-UTR) of messenger RNAs (mRNAs), leading to translational inhibition or mRNA cleavage. The liver-specific miR-122 plays a critical role in the replication of Hepatitis C virus (HCV) while the progression of many cancer types is affected by the downregulation of miR-21. The first part of the thesis focuses on the design, synthesis, and identification of small molecule inhibitors of miR-122 and miR-21. Upon identification of the hit molecules identified by high throughput screening of small molecule libraries by, previously developed, miR-122 and miR-21 reporter assays, structure-activity relationship (SAR) studies were undertaken and lead molecules exhibiting improved activity were selected. The lead molecules were further explored for their mode of action in the modulation of miR-122 and miR-21.

In the second part of the thesis, strategies for selective activation of gene regulation by morpholino oligomers (MOs) were explored. Topologically constrained or caged MOs exhibit poor to none target sequence binding by Watson-Crick base-pair complementarity. Caging of MOs can be achieved by construction of bi-functional linkers for joining both the ends of linear MOs. Gene silencing with spatiotemporal resolution can be achieved by targeted activation and

linearization of these caged MOs. In this study, a number of projects with small molecule-mediated and selective enzyme (β-lactamase)-mediated activation strategies were undertaken.

In the final part of the thesis, other methodologies utilizing light activation to mediate gene regulation were explored. The maturation process of nascent mRNAs proceeds by attaching the mRNA 5'-end with a modified guanosine triphosphate cap and polyadenylation on the 3'-end. The mRNA translation can be modulated by modifications to the 5'-cap as the cap interactions with initiation factors like eIF4E are crucial for the assembly of translational machinery. A closer look at eIF4E and 5'-cap interactions revealed multiple positions of caging with a photocleavable group for light-mediated activation of mRNA translation. Strategies involving the incorporation of two caged cap analogs and caged guanosine triphosphate were pursued.

Table of contents

List of tables

List of figures

List of abbreviations

2’-fluoro-RNA	2’-fluoro-modified RNA
2’-*O*-alkyl-RNA	2’-*O*-alkyl-RNA
2DCS	two-dimensional combinatorial screening
3’-UTR	3’-untranslated region
5’-UTR	5’-untranslated region
AdoMet	*S*-adenosylmethionine
AGO2 (Ago2)	Argonaute2
AMOs	anti-miRNA oligonucleotides
AP-1	Activator Protein 1
ARCA	anti-reverse cap analog
AREs	AU-rich elements
ASOs	antisense oligonucleotides
ATP	adenosine monophosphate
Bcl2	B-cell lymphoma 2
B-CLL	B-cell chronic lymphocytic leukemia
C. elegans	*Caenorhabditis elegans*
CAL B	*Candida Antarctica* Lipase B
CAT-1	cationic amino acid transporter 1
cat-ELCCA	catalytic enzyme-linked click chemistry assay
CDI	1,1'-carbonyldiimidazole
CDKN1A	cyclin-dependent kinase inhibitor 1A
cMO	caged morpholino oligomer
c-MYC	cellular myelocytomatosis
COSY	^{1}H-^{1}H Correlation Spectroscopy
CuAAC	Copper(I)-catalysed Azide-Alkyne Cycloaddition
DBU	1,8-Diazabicyclo[5.4. 0]undec-7-ene
DCC	*N*,*N'*-Dicyclohexylcarbodiimide
DCM	dichloromethane
DCP2	decapping protein 2
DEACM	7-(diethylamino)coumarin caging group
DEACM-MN	diethylaminocoumarylidenemalononitrilemethyl caging group
DEAE	diethylaminoethanol
DGCR8	DiGeorge syndrome critical region

DIAD	diisopropyl azodicarboxylate
DIPEA	*N*,*N*-Diisopropylethylamine
DMAP	4-dimethylaminopyridine
DMEDA	*N*,*N*′-Dimethylethylenediamine
DMF	*N*,*N*-dimethylformamide
DMNB	4,5-dimethoxy-2-nitrobenzyl caging group
DMSO	dimethyl sulfoxide
DNA	deoxyribonucleic acid
DSC	*N*,*N*′-Disuccinimidyl carbonate
dsRNAs	double-stranded RNAs
EBV	Epstein-Barr virus
EDC	1-ethyl-3-(3-dimethylaminopropyl)carbodiimide
EDG	electon donating group
EGFP	enhanced green fluorescent protein
eIF4E	Eukaryotic Translation Initiation Factor 4E
EMSA	electrophoretic mobility shift assay
ESI	electrospray ionization
Et_3N	triethylamine
EWG	electron withdrawing group
FRET	fluorescence resonance energy transfer
FXR1	fragile-X-mental-retardation-related protein 1
GAPDH	glyceraldehyde 3-phosphate dehydrogenase
GDP	guanosine diphosphate
GMP	guanosine monophosphate
GTP	guanosine triphosphate
HATU	1-[Bis(dimethylamino)methylene]-1*H*-1,2,3-triazolo[4,5-b]pyridinium 3-oxide hexafluorophosphate
HCC	hepatocellular carcinoma
HCTU	*O*-(1*H*-6-Chlorobenzotriazole-1-yl)-1,1,3,3-tetramethyluronium hexafluorophosphate
HCV	hepatitis C virus
HIC1	hypermethylated in cancer 1
HMBC	^{1}H-^{13}C Heteronuclear Multiple Bond Correlation
HNFs	hepatocyte nuclear factors
HOBt	Hydroxybenzotriazole
HOMO	highest occupied molecular orbital
HPLC	high-performance liquid chromatography
HRMS	high resolution mass spectrometry

HRP	horseradish peroxide
HSQC	^{1}H-^{13}C Heteronuclear Single Quantum Correlation
HTS	high-throughput screen
iEDDA	inverse electron-demand Diels-Alder
IR	infrared
IRES	Internal Ribosomal Entry Site
IVT	*in vitro* transcription
JAK-STAT	Janus kinase-signal transducer and activator of transcription
LCMS	Liquid chromatography–mass spectrometry
LETFs	liver-enriched transcription factors
LiHMDS	lithium hexamethyldisilazide
LiOH	lithium hydroxide
LNA	locked nucleic acid
LUMO	lowest unoccupied molecular orbital
MALDI-TOF	Matrix-Assisted Laser Desorption/Ionization time-of-flight
MBL	metallo-β-lactamase
MeI	iodomethane
MeOH	methanol
microRNPs	miRNA-protein complexes
miRISC	miRNA-induced silencing complex
miRNA (miR)	microRNA
MNI	4-methoxy-7-nitroindoline
MO	morpholino oligomer
MRE	miRNA response element
mRNA	messenger RNA
MRSA	methicillin-resistant *Staphylococcus aureus*
MSN	mesoporous silica nanoparticles
NAG	*N*-acetylglucosamine
NAM	*N*-acetylmuramic acid
NASH	non-alcoholic steatohepatitis
NB	2-nitrobenzyl caging group
NHS	*N*-Hydroxysuccinimide
NMR	nuclear magnetic resonance
NPOM	6-nitropiperonyloxymethyl caging group
ntl (*ntla*)	no tail
PAIN	pan-assay interference
PBPs	penicillin-binding proteins

PD	pharmacodynamics
PDB	Protein Data Bank
PDCD4	programmed cell death protein 4
PEG	polyethylene glycol
PK	pharmacokinetics
Pol II	RNA polymerase II
ppm	parts per million
pre-miRNA	precursor miRNA
pri-miRNAs	primary microRNAs
PS-DNA	phosphorothioate-modified DNA
PTEN	phosphatase and tensin homolog
RECK	reversion-inducing cysteine-rich protein with Kazal motifs
RISC	RNA-induced silencing complex
Rluc	*Renilla* luciferase
RNA	ribonucleic acid
RNAi	RNA interference
ROESY	^{1}H-^{1}H Rotational Frame Nuclear Overhauser Effect Spectroscopy
RT-qPCR	Quantitative reverse transcription polymerase chain reaction
SAR	structure-activity relationship
shRNA	short hairpin RNA
siRNA	small interfering RNA
snRNAs	small nuclear RNAs
snRNPs	small nuclear ribonucleoproteins
SPAAC	Strain-Promoted Azide-Alkyne Cycloaddition
SPRY2	Sprouty2
StARTS	SAR studies through sequencing
TBAB	tetrabutylammonium bromide
TBAF	*tetra*-n-butylammonium fluoride
TBDMSCl	*tert*-butyldimethylsilyl chloride
TBDPSCl	*tert*-butyldiphenylsilyl chloride
TBHP	*tert*-butyl hydroperoxide
TBTA	Tris[(1-benzyl-1*H*-1,2,3-triazol-4-yl)methyl]amine
TCEP	*tris*(2-carboxyethyl)phosphine
TEAB	triethylammonium bicarbonate
TFA	trifluoroacetic acid
THF	tetrahydrofuran
TLC	thin layer chromatography

T_m	melting temperature
TNFα	cytokine tumor necrosis factor α
TOCSY	^{1}H-^{1}H Total Correlation Spectroscopy
TRBP	transactivation response element RNA-binding protein
TsOH	*p*-toluene sulfonic acid
TSTU	*N*,*N*,*N*′,*N*′-Tetramethyl-*O*-(*N*-succinimidyl)uronium tetrafluoroborate
VMP1	Vacuole Membrane Protein 1
XPO5	Exportin 5
XRN1	exoribonuclease 1
XTT	2,3-Bis-(2-methoxy-4-nitro-5-sulphenyl)-2*H*-tetrazolium-5-carboxanilide
γPNA	gamma-modified peptide nucleic acid

1.0 Introduction to microRNAs

MicroRNAs (miRNAs) are small non-coding single-stranded RNA molecules 20-25 nucleotides in length which are involved in posttranscriptional gene regulation.[1] With over 2,654 miRNAs reported in humans,[2] miRNAs control up to 21% of the protein-coding genes.[3] These act by binding to 3'-untranslated region (UTR) of mRNAs which results in repression of transcription and gene silencing.[4] In 1993, *lin-4* was the first miRNA to be discovered by Ambros and co-workers.[4] *Lin-4* was found to be regulated in the early development of *Caenorhabditis elegans (C. elegans)* larvae. The *lin-4* gene encoded 2 short oligonucleotide transcripts (22 and 61 nucleotides in length) which bind to the 3'-UTR of *lin-14* mRNA via an antisense RNA-RNA interaction. In 2000, the Ruvkun lab reported another *C. elegans* microRNA, *let-7*.[5] The Ruvkun lab determined that a 21-nucleotide RNA encoded by let-7 gene is complementary to elements in the 3'-UTR of the regulatory heterochronic genes *lin-14*, *lin-28*, *lin-41*, *lin-42* and *daf-12*, which specify the timing of *C. elegans* developmental events.[5] These miRNAs were subsequently found to be a subset of small non-coding RNAs in *C. elegans*, *Drosophila*, and humans.[6-8]

1.1 MicroRNA biogenesis

In the canonical pathway, miRNAs are usually transcribed by RNA polymerase II or III (Pol II or Pol III) from independent genomic transcription units or from introns of protein coding genes (**Figure 1-1**).[9] Pol II/III produces miRNAs (pri-miRNAs) which are 100- to 1,000-nucleotide long double-stranded RNAs (dsRNAs).[10] These long RNA molecules are recognized

by a 'Microprocessor' protein complex comprised of RNAse III endonuclease (Drosha) and dsRNA-binding protein (DiGeorge syndrome critical region, DGCR8) in the nucleus, which cleaves pri-miRNA to a ~70-100 nucleotide precursor miRNA (pre-miRNA) having a 3' overhang of 2 nucleotides with 5' and 3' termini with phosphate and hydroxyl groups, respectively (**Figure 1-1**).[11-12] DGCR8 recognizes N^6-methyladenylated GGAC and other motifs within the pri-miRNA.[13] Pre-miRNA is exported by Exportin 5 (XPO5) with the help of RanGTP.[14] The double-stranded pre-miRNA is protected by the XPO5:RanGTP complex during nuclear export and is cleaved by another RNAse III endonuclease, Dicer, in conjunction with transactivation response element RNA-binding protein (TRBP), resulting in removal of the terminal loop which liberates a ~22 nucleotide miRNA-miRNA* duplex in the cytoplasm.[15] This duplex is loaded into an Argonaute (AGO) protein complex in an ATP-dependent manner.[16] AGO protein in addition to Dicer:TRBP complex forms the RNA-induced silencing complex (RISC) containing the single-stranded mature miRNA (guide strand), while miRNA* (passenger strand) is expelled and degraded in the intermediate maturation steps.[17-18] The strand with lower 5'-stability or with 5'-uracil is preferentially loaded onto AGO2 as the guide strand, forming the miRNA-induced silencing complex (miRISC).[19] miRNAs direct the miRISC to the 3'-UTR of target mRNA containing the complementary sequence, called the miRNA response element (MRE).[20] MREs containing miRNAs with exact complementarity to 3'-UTR lead to mRNA degradation induced by AGO2 endonuclease activity.[21] More commonly, partial miRNA:MRE complementarity results in translational repression,[22] mRNA poly(A)-deadenylation (initiated by poly(A)-deadenylase PAN2/3 and completed by CCR4-NOT complexes),[22-23] and decapping (facilitated by decapping protein 2, DCP2,[24] and associated proteins, followed by 5′−3′ degradation by exoribonuclease 1, XRN1[25]) (**Figure 1-1**). In many cases, a functional miRNA:MRE duplex forms via the 5'seed

region (nucleotides 2-8),[26-27] and additional pairing at the 3' end improves the stability and specificity of the miRNA:MRE complex.[28] A single miRNA can bind to hundreds of mRNAs, giving each miRNA powerful control over gene regulation.[29]

Other modes of action include silencing effects of gene regulation by binding to 5'-UTR and coding regions,[30-31] while transcriptional activation via miRNAs bound to the promoter region have been reported.[32] Two miRNA-protein complexes (microRNPs), fragile-X-mental-retardation-related protein 1 (FXR1) and AGO2, are associated with the upregulation of translation in AU-rich elements (AREs) present in the 3'-UTR in serum-starved HEK293 cells.[33] Under cell cycle arrest induced by serum starvation, the cytokine tumor necrosis factor α (TNFα) AREs are upregulated by FXR1 and AGO2 with the help of several miRNAs including let-7; however, these microRNPs repress translation in proliferating cells.

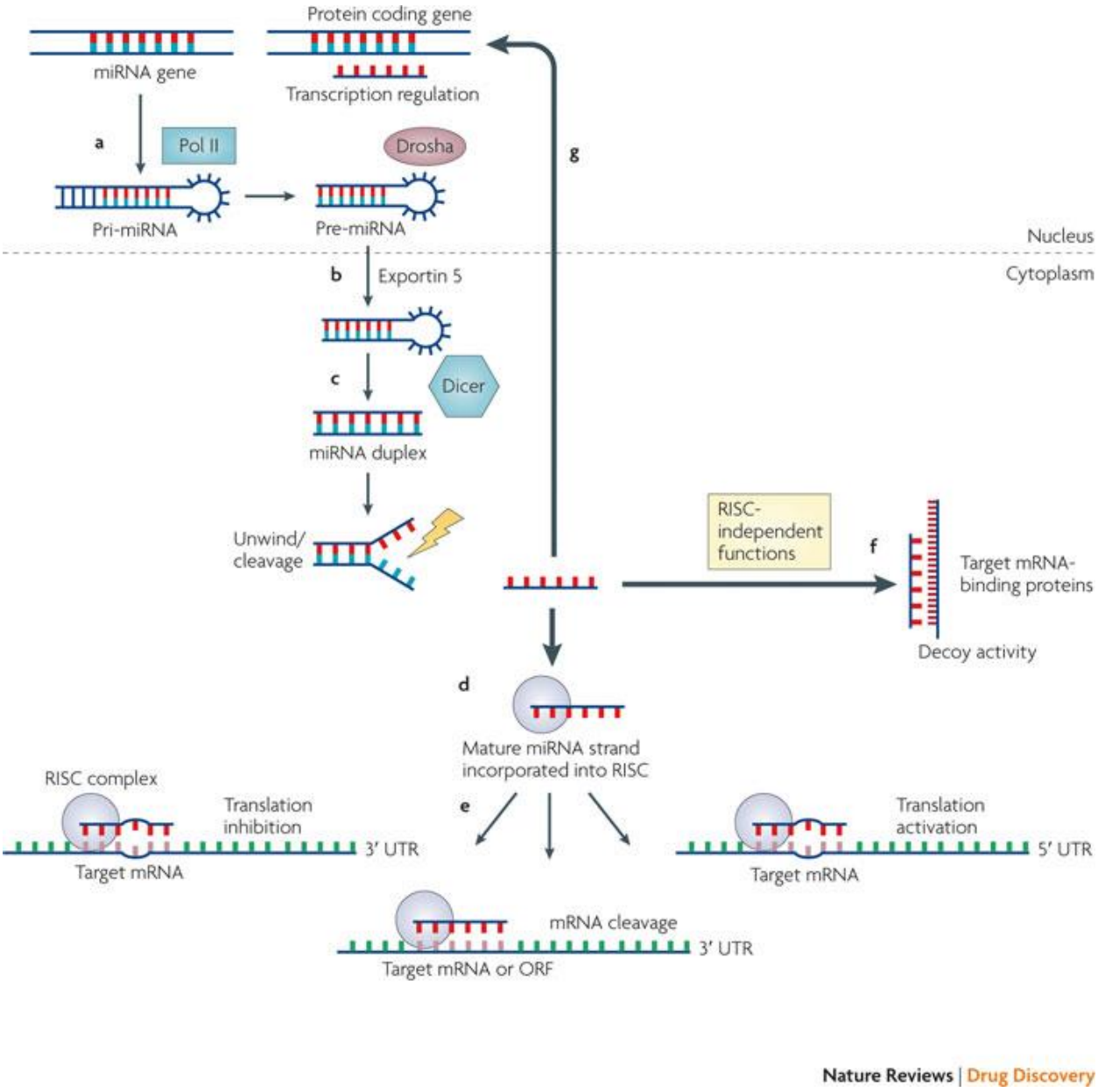

Figure 1-1 The canonical pathway of miRNA biogenesis.

The endogenous miRNA gene is transcribed and processed into mature miRNA, which is then loaded onto RISC complex. This mature RISC complex binds to the target mRNA and leads to translational repression or degradation of mRNA. Adapted from *Nat. Rev. Drug Discovery*, **2010**, 9 (10), 775.[34]

1.2 MicroRNAs as potential drug targets

miRNAs are dysregulated in hundreds of human diseases.[35-36] In particular, miRNAs play a variety of roles in cancer development and proliferation.[37] A study of solid tumor samples from 540 patients including lung, breast, stomach, prostate, colon and pancreatic cancers have shown abnormal miRNA expression profiles.[38] Furthermore, miRNA expression profiling studies show signature patterns associated with various tumor types, which helps identify common gene targets of deregulated miRNAs.[39] These signature patterns can classify human cancers by developmental lineage and differentiation state (**Figure 1-2**).[40]

Individual miRNAs have been found to promote or to suppress tumorigenesis. The involvement of miRNAs in human cancers was first found in the study to identify tumor suppressor genes in B-cell chronic lymphocytic leukemia (B-CLL) by the Croce group; miR-15 and miR-16 genes are located at frequently deleted region 13q14 in the majority of B-CLL cases.[41] Later it was found out that the miR15a-miR16-1 cluster represses B-cell lymphoma 2 (Bcl2) protein, in turn inducing apoptosis in B-CLL cells.[42] A study showed that knockdown of miR-15a resulted in tumorigenesis in the mouse prostate, while restoration in expression of miR-15a and miR-16-1 was marked by tumor growth arrest, apoptosis, and regression in mouse prostate tumor xenografts.[41] The miR-17-92 gene cluster is responsible for the upregulation of cellular myelocytomatosis (c-MYC) resulting in the activation of transcription factor E2F1, which promotes excessive cell proliferation.[43] Restoring the process of cell aging and apoptosis was achieved by inhibition of miR-17-92 activity. Additionally, hypermethylated in cancer 1 (HIC1) was observed to be downregulated by oncomiR miR-128, resulting in increased cell invasion, proliferation, and reduced apoptosis in breast cancer tissues.[44] These studies suggest that tumor

suppressor miRNAs downregulate tumor promoting genes or oncogenes, while oncomiRs inhibit translation of tumor suppressor genes.

Along with the role of miRNAs in cancer progression, several viral miRNAs have been identified. The first viral-encoded miRNAs were cloned from a Burkitt's lymphoma cell line infected by Epstein-Barr virus (EBV).[45] Several other viral miRNAs have also been discovered in adenovirus,[46] polyoma virus,[47] and several subtypes from the herpesvirus family.[45] Viruses are also capable of regulating miRNAs endogenous to the host cells for their own benefit. In the case of EBV infection, the cellular level of miR-155 is upregulated.[48] Higher expression of miR-155 may prevent cellular apoptosis.[49] Even if miRNAs are not directly regulated by viruses, cellular expression of miRNAs are important for maintaining viral replication. In resting $CD4^+$ T cells, miR-28, miR-125b, miR-150, miR-223, and miR-382 expression is maintained at high levels as compared to activated $CD4^+$ T cells, making activated cells more susceptible to HIV-1 infection.[50] Taken together, these results show that miRNAs play a crucial role in viral infection and replication.

Correlations between autoimmune, hepatic, and neurodegenerative diseases and cellular miRNAs have been studied. miRNA expression profiles of multiple sclerosis (MS) patients and healthy controls have revealed multiple miRNA signatures.[51] Specifically, miR-145 was found to be upregulated in controls, whereas increased expression of miR-34a, miR-155, and miR-326 was observed in MS patients. Abnormal levels of miR-29c, miR-34a, miR-155, and miR-200b were observed in a non-alcoholic steatohepatitis (NASH) mouse model of [52] along with 23 more miRNAs identified in tissue samples from NASH human patients.[53] miRNA's role in neurodegenerative diseases is poorly understood. miRNA expression profiling revealed abnormal levels of miR-30b, miR-30c, and miR-26a in patients of Parkinson's disease compared to healthy

individuals.[54] Similarly, in patients with Alzheimer's disease, the expression levels of miR-29a, miR-29b-1, and miR-9 were found to be significantly decreased, implying a functional relevance of miRNA-mediated regulation in disease pathogenesis.[55] From 2004 to 2009, a study indicated that among 192 dysregulated miRNAs in human cancers, almost 168 of them are overexpressed.[56]

In general, miRNAs serve as important factors in various regulatory pathways, and miRNA dysregulation has been implicated in several disease initiation and progression. Typically, as miRNAs do not require exact sequence complementarity for gene regulation, a single miRNA can regulate different gene networks resulting in tumorigenesis and metastasis.[57-58] For example, in case of hepatic cancer stem cells, a gene regulatory map shows that 7 upregulated miRNAs results in 274 downregulated genes, while 9 downregulated miRNAs results in 62 upregulated genes.[59] The control that these few miRNAs exert over many genes emphasizes the importance of targeting miRNAs as an appealing strategy for cancer therapies.[60]

MicroRNA	Genomic location	Expression in patients	Deregulation mechanism	Function	Targets	Experimental data	Therapeutic strategy
miR-15a–miR-16-1	13q31	Down in CLL[24], prostate cancer[44] and pituitary adenomas[45]	Genomic loss[24]; mutations[30]; positive regulation by p53 (REFS 58–59)	Tumour suppressor	*BCL-2* (REF. 61), *MCL1* (REF. 61)	*In vitro* overexpression induces apoptosis in CLL and prostate cancer cells[24,44]; *in vivo* silencing causes CLL in mice[62]	Mimics; vector-based (viral); drugs
Let-7a-2	11q24	Down in lung[46], colon[33] breast[31], ovarian[50] and stomach cancer[27]	Negative regulation by MYC[70]	Tumour suppressor	*KRAS*, *NRAS*[46], *CDK6*, *CDC25A*[124], *HMGA2* (REF. 124), *MYC*[64]	*In vitro* overexpression reduces cell growth in lung, breast and colon cancer cells[46,48–49]; *In vivo* overexpression reduces breast and lung tumour burden in mice[48,124]	Mimics; vector-based (viral); drugs
miR-29b-1–miR-29a miR-29b-2–miR-29c	7q32 1q30	Down in NPM1 wild-type AML[39], CLL[30], lung[28] and breast cancer[31], cholangiocarcinoma[41], lymphoma[43], hepatocarcinoma[42] and rhabdomyosarcoma[40]	Genomic loss[63]; negative regulation by MYC[60]; positive regulation by p53 (REF. 59)	Tumour suppressor	*MCL1*, *CDK6* (REFS 41,63) *TCL1*, *DNMT1* (REFS 118–125), *DNMT3α*, *DNMT3β*[110]	*In vitro* overexpression induces apoptosis, inhibits cell proliferation and induces DNA hypomethylation in several cancers[41,63,118,119]; *in vivo* overexpression inhibits tumorigenicity in AML, liver and lung cancer in mice[42,63,119]	Mimics; vector-based (viral); drugs
miR-34a miR-34b and miR-34c	1p36 11q23	Down in colon, lung, breast, kidney and bladder cancer, neuroblastoma[34] and melanoma cell lines[126]	Methylation regulation[65,126]; positive regulation by p53 (REFS 58–59); deletion	Tumour suppressor	*CDK4*, *CDK6*, (REFS 65,127) *CCNE2*, *CCND1* (REFS 127–128), *MET*, *MYC*[127,129], *CREB*, *E2F3* (REFS 130,131), *BCL-2* (REF. 131)	*In vitro* overexpression induces cell cycle arrest, apoptosis and inhibits cell proliferation[61–62]	Mimics; vector-based (viral); drugs
miR-26a	3p22	Down in liver cancer[93]	Negative regulation by MYC[60]	Tumour suppressor	*CCND2*, *CCNE2* (REF. 93)	Restoration of miR-26 inhibits MYC-induced liver cancer[93]	Vector-based (viral)
miR-155	21q21	Up in high risk CLL[30], AML[32,39], lung[28], colon[33], breast cancer[31] and in lymphomas[37–38]	Positive regulation by NF-κB[118]	Oncogene	*SHIP1*, *CEBPB*[71,73]	Overexpression in HSC-induced myeloid proliferation and blocks erythropoiesis in mice[72]; *in vivo* overexpression in lymphocytes induces pre-B lymphoma and leukaemia in mice[71]	Antisense oligonucleotides; miR-mask; miRNA sponges; drugs
miR-17-92	13q22	Up in lung[28], breast[31], colon[33] and stomach cancer[27], myeloma[36] and t(11q23) AML[132]	Amplification[23]; positive regulation by E2F and MYC[133]	Oncogene	*BIM*, *PTEN*[27,70], *CDKN1A*[27]	Cooperates with MYC to induce lymphoma[73]; *in vivo* overexpression in lymphocytes induces lymphoid proliferation and autoimmunity in mice[72]	Antisense oligonucleotides; miR-mask; miRNA sponges; drugs
miR-21	17q23	Up in pancreas[33], breast[31], lung[28], prostate and stomach cancer[23], CLL[30], AML[32], myeloma[39] and gliobastoma[34]	Positive regulation by IL-6 and GF1α[134–135]	Oncogene	*PDCD4*, *PTEN*[67–68], *TPM1* (REF. 136)	*In vitro* silencing enhances apoptosis in glioblastoma, lung, breast and hepatocarcinoma cell lines[66–70]	Antisense oligonucleotides; miR-mask; miRNA sponges; drugs
miR-372 miR-373	19q13	Up in testicular germ cell tumours and in breast cancer[31,130]	Unknown	Oncogene	*LATS2* (REF. 137)	Neutralizes the p53 pathway *in vitro*[137]; *in vivo* overexpression stimulated cancer cell invasion[130]	Antisense oligonucleotides; miR-mask; miRNA sponges; drugs

AML, acute myeloid leukaemia; BCL-2, B-cell lymphoma protein-2; CCN, cyclin; CDC, cell division cycle; CDKN1A, cyclin-dependent kinase inhibitor 1A; CEBPB, CCAAT/enhancer binding protein β; CLL, chronic lymphocytic leukaemia; CREB, cAMP response element-binding protein; DNMT, DNA methyltransferase; HMGA2, high mobility group AT-hook 2; HSC, haematopoietic stem cells; IL-6, interleukin-6; KRAS, v-Ki-ras2 Kirsten rat sarcoma viral oncogene homologue; LATS2, LATS, large tumour suppressor, homologue 2; MCL1, myeloid cell leukaemia sequence 1 (BCL-2-related); NF-κB, nuclear factor-κB; NPM1, nucleophosmin (nucleolar phosphoprotein B23, numatrin); NRAS, neuroblastoma RAS viral (v-ras) oncogene homologue; PDCD4, programmed cell death 4; PTEN, phosphatase and tensin homologue; SHIP1, Src homology 2 domain-containing inositol 5-phosphatase 1; TPM1, tropomyosin 1.

Figure 1-2 Involvement of miRNAs in cancer.

Adapted from *Nat. Rev. Drug Discovery*, **2010**, 9 (10), 775.[34]

1.3 Nucleic acid and small molecule modifiers of miRNA function

In light of the crucial role of miRNAs in cancer development and progression, directed efforts to target specific miRNAs have been evaluated as therapeutics. A large subset of miRNAs are overexpressed in cancer cells;[36] hence, strategies to downregulate these oncogenic miRNA are of considerable interest.[34, 61] A common approach is the use of antisense oligonucleotides. Antisense oligonucleotides (ASOs), specifically antagomirs or anti-miRNA oligonucleotides (AMOs) in this context, are synthetic oligonucleotides which have exact base-pair complementarity with the target miRNA. These oligonucleotides bind to the target mature miRNA, rendering the miRNA ineffective or inducing miRNA degradation.[62] As an example, this strategy was successfully shown to target miR-2 and miR-13 in *Drosophila* embryos.[63] To further increase stability, nuclease resistance, and binding specificity, 2'-*O*-methyl oligonucleotides,[64-65] 2'-*O*-methyl-modified cholesterol-conjugated single-stranded RNA analogs with phosphorothioate linkages,[66] and 2'-F modified oligonucleotides[67] have been employed (**Figure 1-3**). Exceptional hybridization affinity towards miRNAs is seen in Locked Nucleic Acids (LNA) constructs. LNA nucleosides have a "locked" ribose ring, freezing the sugar-phosphate backbone in a C3'-*endo*, RNA-like conformation. LNA constructs have been successfully used in mice as anti-miR-155[68] and anti-miR-122[69] agents. Santaris Pharma is pursuing LNA anti-miR-122 drug as a hepatitis C treatment, named Miravirsen (SPC3649); this has become the first microRNA-targeted drug to enter clinical trials (Phase 2).[70] Morpholinos are synthetic oligomer molecules containing DNA bases attached to a backbone of methylenemorpholine rings linked through phosphoramidate groups (**Figure 1-3**).

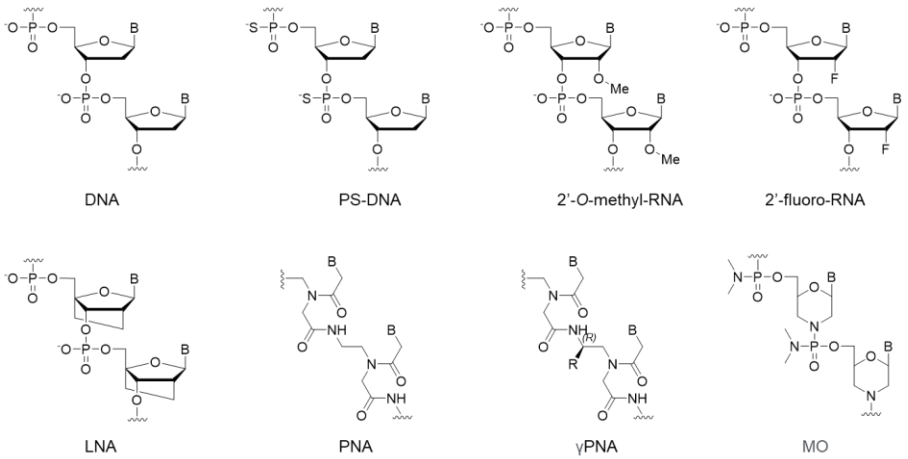

Figure 1-3 Structures of chemical modifications for AMOs.

DNA: non-modified deoxyribonucleic acid; PS-DNA: phosphorothioate-modified; 2'-*O*-alkyl-RNA: 2'-*O*-methyl-ribonucleic acid; 2'-fluoro-RNA: 2'-fluoro-modified ribonucleic acid; LNA: locked nucleic acid; PNA: peptide nucleic acid; γPNA: gamma-modified peptide nucleic acid with R = miniPEG; MO: morpholino oligomer

In another strategy for targeting oncogenic miRNAs, multiple binding sites for a target miRNA are transcribed in tandem in mammalian expression vectors, creating miRNA sponges or decoys. On injected into cells, these constructs compete with the target miRNA binding sites on mRNAs for binding to the endogenous miRNA. As these sponges have multiple binding sites for the target miRNA, they "soak up" the cognate miRNA, making it unavailable to hybridize with the 3'-UTR of mRNAs. A strategy developed by Choi and coworkers used antisense morpholinos complementary to miR-430 binding sites to target mRNA, acting as "miRNA-masks."[71] These morpholinos compete with miRNAs for binding to target mRNA, thus inhibiting miRNA's repression of mRNA expression.

In addition to these strategies for suppressing oncogenic miRNAs, several non-viral and viral strategies have been developed to deliver tumor-suppressing miRNAs in cells. The non-viral strategies include liposome-, nanoparticle-, antibody-, hydrogel-, and polymer-based miRNA

delivery.[72-73] Synthetic modification of the DNA backbone with phosphorothioate linkages is the most widely studied modification. miRNA mimics and small molecule activators are other non-viral strategies. Adenovirus-associated viral vectors coding for miRNAs have been used in viral-based strategies (**Figure 1-4**).[72-73]

Strategy	Limitations	Advantages	Experimental data	Solutions and future directions
2′-*O*-methyl phosphorothiolate oligonucleotides	Delivery; short serum half-life; poor cellular uptake; off-target effects; limited biological effects	Safe; improved stability; nuclease resistance; increased binding affinity	*In vitro* and *in vivo* data; animal models; Phase I, Phase II and Phase III clinical trials[39–41,61,63]	Improve delivery
2′-*O*-methyl phosphorothiolate oligonucleotides with cholesterol backbone	Toxicity; requires high doses	Good bioavailability	*In vitro* and *in vivo* (animals)[39]	Improve safety profile
Locked nucleic acid	Off-targets effects; potential dose toxicity effects	Safe; good biodistribution; effective	*In vitro* and *in vivo* (mice and chimpanzees); human trials ongoing[41,64,65,91–94]	Detailed pharmacokinetic, pharmacodynamic and toxicity studies in humans; develop tissue-specific delivery
Liposome–oligonucleotide complexes	Toxicity; hypersensitivity; potential dose toxicity effects	Improved stability and delivery	*In vitro* and *in vivo* (animals)[108,111–113]	Develop better formulations
Polymer–nanoparticle oligonucleotide complexes	Off-target effects; potential dose toxicity effects	Improved stability and delivery; minimal toxicity	*In vitro* and *in vivo* (animals)[101,112]	Develop tissue-specific delivery (antibody tagging)
miR-mask	Limited scope (one target); delivery	Effects are gene-specific; no off-target effects	*In vitro* studies[98]	Achieve delivery *in vivo*; assess activity *in vivo*
miRNA sponge	Delivery; off-targets effects	Able to silence a family of miRNAs	*In vitro* studies[95–97]	Achieve delivery *in vivo*; assess activity *in vivo*
Adenovirus-associated vectors coding for miRNAs	Potential dose toxicity effects; off-target effects	Safe, efficient transduction; long-term expression	*In vitro* and *in vivo* (animals); human trials for small interfering RNA; Phase I, Phase II and Phase III trials[101,102]	More extensive animal data is needed (in particular with other tumours)

Figure 1-4 Limitations and advantages of miRNA targeting technologies.

Strategies including phosphorothioate oligonucleotides to miRNA sponges inhibit oncogenic miRNAs while adenovirus-associated vectors are technologies implemented for upregulating tumor suppressor miRNAs. Adapted from *Nat. Rev. Drug Discovery*, **2010**, 9 (10), 775.[34]

Although ASOs have shown therapeutic potential, a number of challenges stem from their poor bioavailability, difficult delivery, limited cell penetration, and toxicity. Toxicity from ASOs mostly comes from the immunostimulatory off-target effects of oligonucleotide therapeutics.[74] A number of carriers have been developed including nanoparticles and liposomes, but these

technologies are far from perfect. For example, Gilleron and co-workers conducted an analytical imaging-based study using fluorescence and electron microscopy to track transport and release of siRNAs from lipid nanoparticles. They showed that only 1-2% of siRNA payload was released into cytosol.[75]

Conversely, small molecules are a unique strategy for targeting specific miRNAs. Small molecules, usually with molecular weight < 800 Da, can be tuned to have ideal drug properties, good solubility, high cellular uptake, good bioavailability, and an ideal pharmacokinetics/pharmacodynamics (PK/PD) profile.[56] miRNAs exist as a number of structures with grooves, pockets and hairpin loops on the surface, which can act as potential targets for small molecules. As explained in miRNA biogenesis, miRNAs are processed in a multi-step manner with a number of enzymes involved. Thus, small molecules can target miRNA processing at 3 levels: pre-transcriptional, transcriptional and posttranscriptional, unlike ASOs which only target mature miRNAs.

Over the years, RNA molecules were not considered an attractive target for small molecule therapeutics because of their structural flexibility, highly electronegative surfaces, and the lack of miRNA X-ray structural information. However, a number of approaches have been employed recently to discover new small molecules controlling miRNA function, broadly classified as biochemical assays, cell-based assays, or computational and rational design.[76] The small molecule modifiers target various key intermediates and processes in the miRNA biogenesis pathway, namely, inhibition of transcription; inhibition of pri-miRNA, and pre-miRNA processing in the nucleus; inhibition of Dicer processing; and inhibition of mature miRNA function in the cytoplasm.[76]

The development of *in vitro* biochemical assays to monitor miRNA maturation has helped enable discovery of small molecule inhibitors of miRNA activity. Prominent advantages of biochemical assays include high throughput and robust screening procedures with few components required for these assays, especially in comparison to cell-based screening assays. These assays detect direct small molecule binding to key RNA intermediates in the biogenesis pathway. Secondary assays have been constructed to monitor the enzymatic functions of the protein machinery involved in the biogenesis pathway. These efforts have led to the development of fluorescence-based assays, catalytic chemiluminescence-based assays, and microarray assays. Microarray technology is important in the high-throughput monitoring of small molecule-RNA interactions.[77] In this technology, a small molecule library is covalently immobilized onto a microarray plate and incubated with a fluorescently-labelled RNA molecule. Following washing steps, the fluorescence can be monitored to identify the bound RNA. This strategy has been utilized for screening peptide-[78] and peptoid-based miRNA inhibitors.[79] A recent approach developed by the Schneekloth lab involved screening a small molecule library against a Cy5-labelled pre-miR-21 hairpin immobilized onto a microarray plate.[80] Compounds **1** and **2** were identified to bind to pre-miR-21 by measuring the melting temperature (K_D = 2.3 μM and 700 nM, respectively) (**Figure 1-5**). The Disney lab designed and developed a unique platform for probing RNA-motifs and chemical interactions simultaneously, named the microarray-based two-dimensional combinatorial screening (2DCS) approach.[81-82] In the 2DCS approach, a collection of azide-modified small molecules were immobilized onto an agarose-containing microarray slide and incubated with a ^{32}P-labelled RNA library with modifications at specific locations on RNA. The bound RNAs were excised from the slide and then amplified and sequenced. Four aminoglycosides were identified to bind to specific RNA motifs: neomycin preferentially bound to GA pairs,

tobramycin preferred internal loops with GG pairs, kanamycin A preferred internal loops containing pyrimidine–pyridimine pairs, and neamine preferred various internal loops, especially GA pairs. Other studies utilizing microarray-based approaches helped identify compound **3** to be a potent topoisomerase inhibitor binding the Dicer cleavage site on pre-miR-21 (**Figure 1-5**).[83]

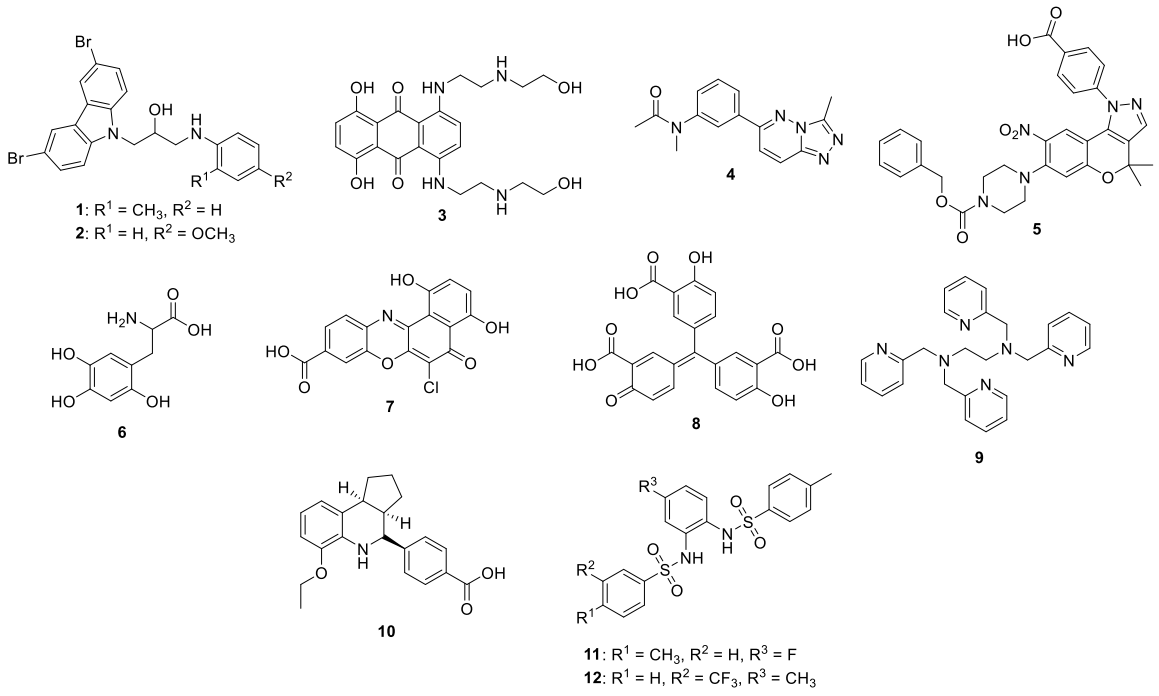

Figure 1-5 Structures of small molecule miRNA inhibitors identified by biochemical assays.

Adapted from *MicroRNAs in Diseases and Disorders*, **2019**, 323.[76]

Fluorescence resonance energy transfer (FRET) assays were also developed to identify small molecule inhibitors of miRNA maturation. The Arenz lab was the first to develop FRET assays using fluorophore-labeled precursor miRNAs, similar to molecular beacons.[84-85] Installation of a 5′ fluorophore and a 3′ fluorescence quencher at the termini of a pre-miRNA hairpin enabled efficient FRET monitoring of Dicer-mediated cleavage. This assay was employed to identify RNA-binding aminoglycosides.[86-89] Hall and co-workers developed tailored FRET

assays for targeting specific miRNA-protein interactions, which were utilized to identify compound **4** as an inhibitor of abnormal cell lineage protein 28 (LIN28)-pre-let-7 interaction (**Figure 1-5**).[90] Another FRET assay entailing site-specific incorporation of an unnatural amino acid for fluorescent labelling of the LIN28 protein and a FRET acceptor was developed by Park and co-workers.[91] Upon screening 4500 drug-like compounds in this assay, **5** (IC_{50} = 4 μM) was identified as an inhibitor of the LIN28-let-7 interaction (**Figure 1-5**). In alternate FRET-based approaches, compounds **6**, **7**,[92] **9**, and **10**[93] were also identified as small molecule inhibitors of the LIN28-let-7 interaction, while **8** was identified as an inhibitor of miRNA-RISC loading (**Figure 1-5**).[94]

The Garner lab designed and developed the unique approach of the catalytic enzyme-linked click chemistry assay (cat-ELCCA) (**Figure 1-6**).[95] In this assay, biotin-labeled pre-miRNAs containing a click chemistry handle (e.g., trans-cyclooctene) within the loop-region are immobilized onto streptavidin-coated microtiter plates. To identify inhibitors of Dicer processing, these pre-miRNAs are treated with Dicer in presence of library of compounds. Covalent labelling with a horseradish peroxide (HRP)-tetrazine conjugate enables a robust readout via catalytic HRP-based chemiluminescence. The Garner lab utilized this methodology to a two-dimensional screen for identification of pre-miR-21 and pre-let-7d Dicer processing inhibitors.[96] Using this assay, two small molecules (**11** and **12**) were identified from a library of 127,007 small molecules (**Figure 1-5**).[97]

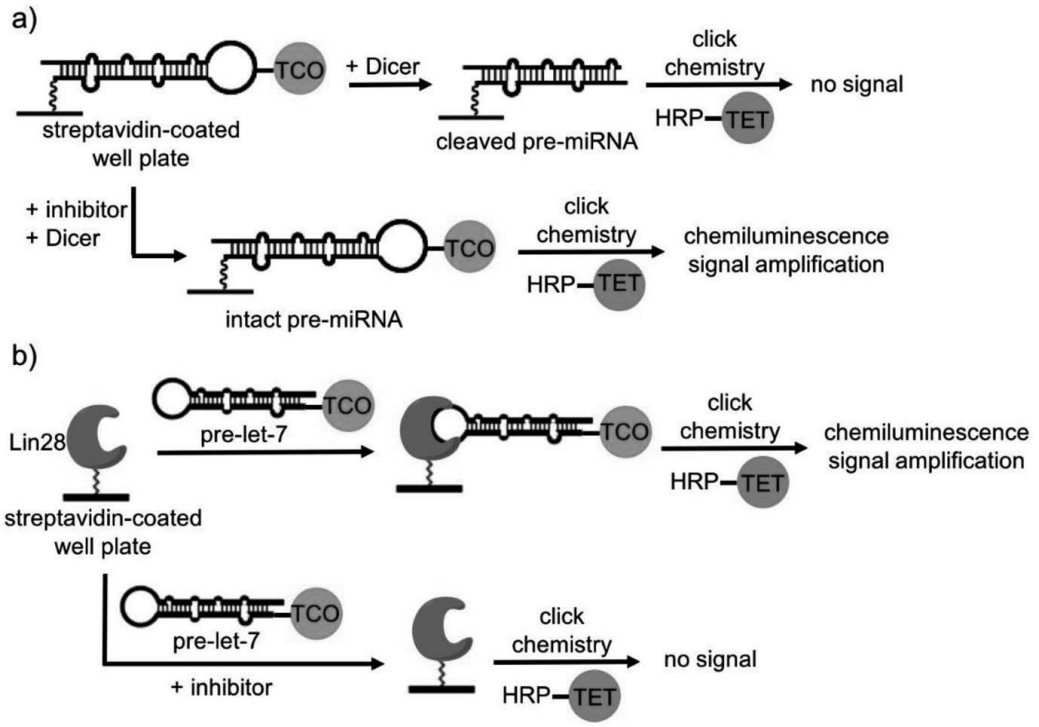

Figure 1-6 Two different cat-ELCCA (catalytic enzyme-linked click chemistry assay) approaches for high-throughput screening.

(A) cat-ELCCA for Dicer-mediated pre-miRNA processing and the identification of inhibitors. (B) cat-ELCCA for identification of small molecule inhibitors of the LIN28–pre-let-7d interaction. Adapted from *MicroRNAs in Diseases and Disorders*, **2019**, 323.[76]

Cell-based assays have distinct advantages over the biochemical screens as biochemical assays do not account for factors that may impact the efficacy of a potential hit compound in cells, such as toxicity, cell permeability, and stability. Also, as the number of factors involved is limited in biochemical approaches, cell-based assays can target unknown factors inside the cells enabling the discovery of novel biological pathways. In a typical cell-based reporter assay, the miRNA binding sequence is cloned on the 3'-UTR of the reporter gene. Secondary assays are necessary for validation of potential hit compounds.[98-100] Jin and co-workers utilized a HEK293 cell line

expressing an enhanced green fluorescent protein (EGFP) reporter together with a stably expressed short hairpin RNA (shRNA) targeting the EGFP mRNA in order to identify small molecule modifiers of the RNA interference (RNAi) pathway (**Figure 1-7**).[101] Following a screen of 2000 compounds, **13** (EC_{50} = 30 μM) was selected and found to modulate TRBP in the RISC complex as a suggested mode of inhibition (**Figure 1-8**).[102] In 2008, the Deiters lab, in collaboration with the Huang lab, developed a cell-based reporter assay for the identification of miR-21 inhibitors.[103] Using this assay on a pilot screen of > 1000 small molecules, **14** (EC_{50} = 2 μM) was discovered to reduced mature miR-21 (78% reduction at 10 μM) as well as pri-miR-21 levels (87% reduction at 10 μM), indicating that **14** acts at a transcriptional level in the miR-21 biogenesis pathway (**Figure 1-8**). Further SAR studies on **14** by Lu and co-workers resulted in discovery of **15**, which elicited a 90% reduction in mature miR-21 levels at 10 μM concentration (**Figure 1-8**).[104] Another high-throughput screening of 333,519 compounds in the HeLa-miR-21 reporter cell line and a successful SAR study revealed **16** as a potent inhibitor (**Figure 1-8**). Further studies revealed **16** (10 μM) to sensitize A498 renal carcinoma cells to topotecan (1 μM) treatment by ~11-fold.[105] Another lead compound identified in this high-throughput screening led to the discovery of **17** (**Figure 1-8**).[106] Maiti and co-workers developed a similar luciferase-based reporter plasmid by cloning the 3′-UTR of programmed cell death protein 4 (PDCD4), a known target of miR-21, and utilized this assay to screen aminoglycosides in MCF-7 cells.[107] Compound **18** was selected from this screening and subsequent studies revealed **18** to inhibit Dicer processing of pre-miR-21 (**Figure 1-8**). Similar screening by cell-based assays were employed to identify small molecule inhibitors (**19** and **20**) and an activator (**21**) of miR-122;[108] an activator (**22**) of miR-34a;[109] inhibitors (**23** and **24**) of miR-4644;[110] an inhibitor (**25**) of miR-1;[111] and modulators (**26**, **27** and **28**) of *let-7* function (**Figure 1-8**).[112]

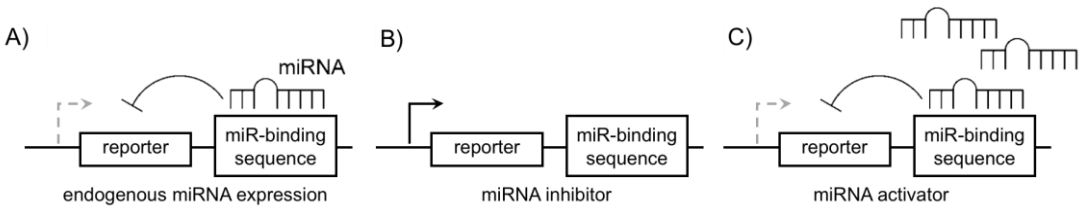

Figure 1-7 Cell-based reporter assay design.

A miRNA target sequence is cloned in the 3′ untranslated region of a luciferase or enhanced green fluorescent protein (EGFP) reporter gene. (A) Binding of a complementary miRNA to the target site results in repression of the reporter. (B) Treatment with a small molecule inhibitor of miRNA function leads to an increase in reporter expression. (C) Induction of miRNA expression or stabilization of miRNA function elicits further reduction in reporter expression. Adapted from *MicroRNAs in Diseases and Disorders*, **2019**, 323.[76]

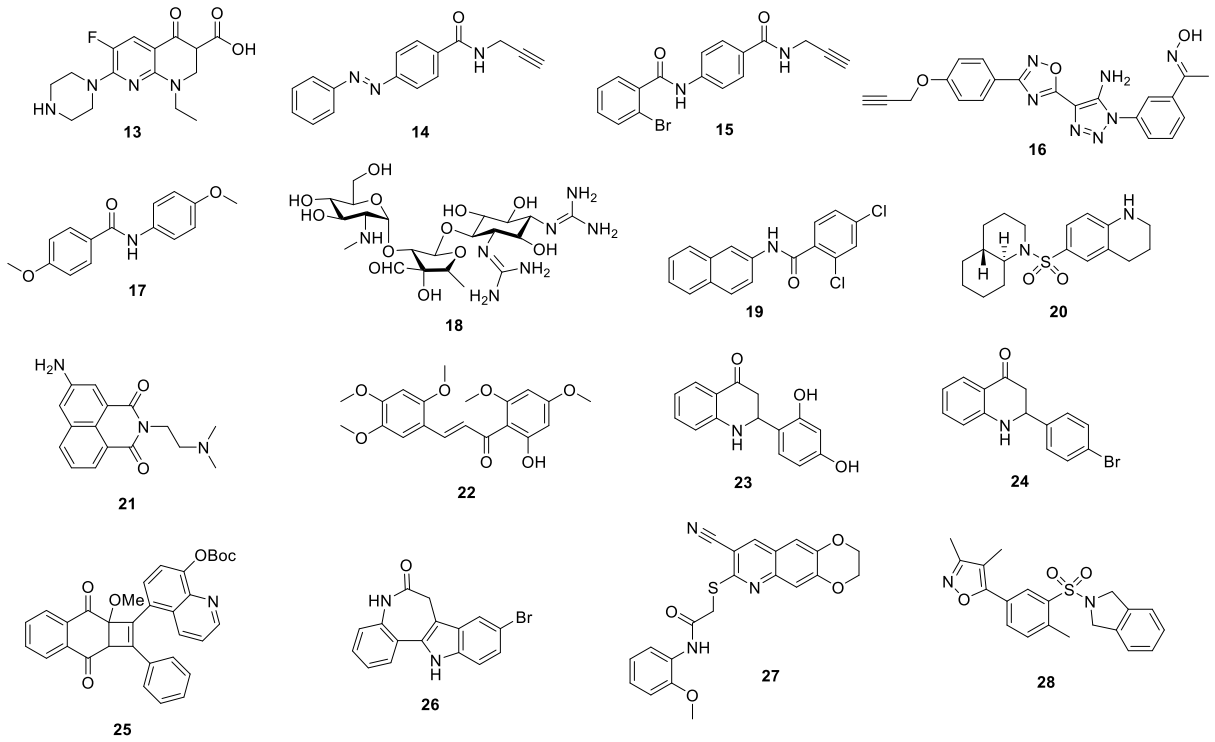

Figure 1-8 Structures of small molecule modifiers of miRNA function identified in cell-based reporter assays. Adapted from *MicroRNAs in Diseases and Disorders*, **2019**, 323.[76]

In rational design approaches, the ability to predict the RNA secondary structures and tertiary motifs accurately from sequences and guide the small molecule design can accelerate drug discovery efforts.[113] However, these approaches rely upon structural information for the target and the potential small molecules, in comparison to cell-based assays where the mode of action of the inhibitors is unknown at the time of screening.[114] With a view to overcome these limitations, the Disney lab developed a new approach of lead identification, called Inforna, which utilizes the RNA-small molecule binding information generated by 2DCS (explained above) and integrates it with a statistical approach that enables identification of RNA motifs and the rate of occurrence of specific RNA motifs in the entire RNA library, which is named SAR studies through sequencing (StARTS).[115] The Inforna platform can facilitate the identification of specific small molecule–miRNA pairs based upon tight binding interactions. The Inforna approach revealed that **29** (40 μM) binds to the Drosha cleavage site of pre-miR-96 and reduced mature miR-96 levels by 90% in MCF-7 cells and that **29** binds to the Dicer cleavage site on pre-miR-210 with a K_D of 200 nM (**Figure 1-9**). An additional bis-benzimidazole identified via Inforna that bind to the Drosha site of pre-miR-96 was conjugated to **29** through a peptoid backbone yielding the dimeric compound **30**, generating a more potent inhibitor (**Figure 1-9**).[116] With a spacer of 2 glycine residues, **30** was observed to reduce mature miR-96 levels by 50% at 50 nM concentration (K_D = 85 nM). In contrast to **29** and **30** binding the Drosha processing site of pre-miR-96, compound **31** was identified via Inforna to bind the Dicer cleavage site on pre-miR-210 with a K_D of 200 nM (**Figure 1-9**). Inforna was also utilized for identification of small molecules which bind to pre-miR-544 (**32**)[117] and pre-miR-525 (**33**) (**Figure 1-9**).[118] Other rational design and in silico screening methods included targeting bulges in double-stranded RNA in pre-miR-29a (**34**),[119] inhibiting Dicer processing in

miR-372/373 (**35**),[86] inhibitors (**36** and **37**) of AGO2-miR-122 complex,[120] and targeting Dicer binding site on pre-miR-21 (**38**) (**Figure 1-9**).[121]

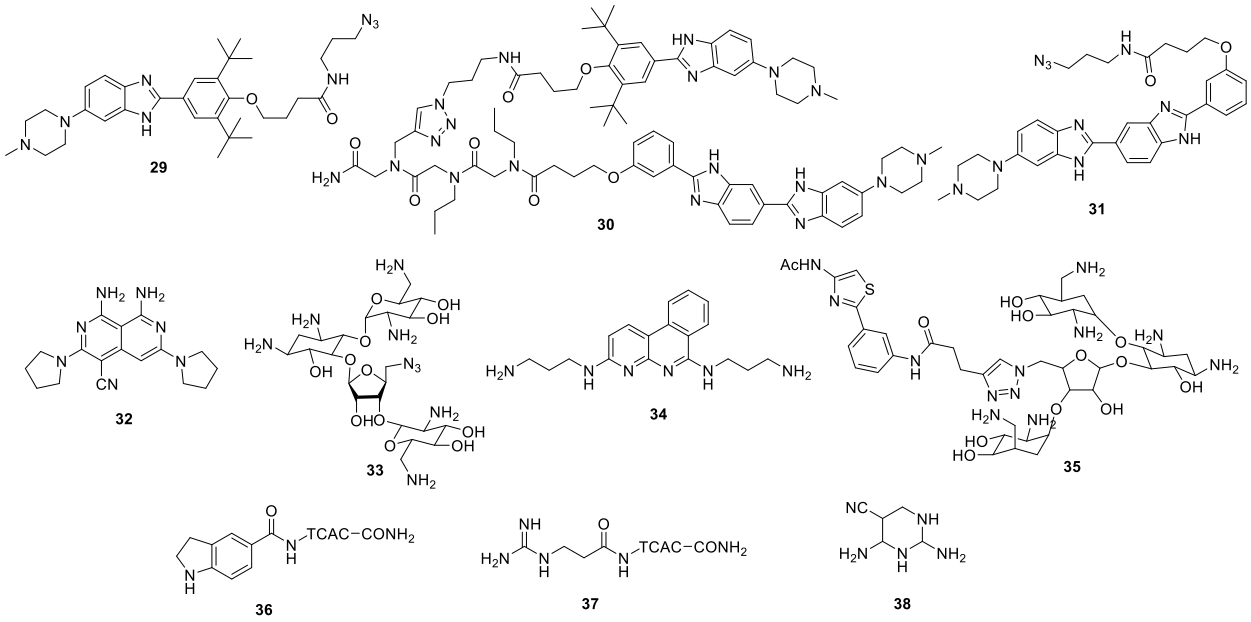

Figure 1-9 Structures of small molecules identified through rational design and computational approaches. Adapted from *MicroRNAs in Diseases and Disorders*, **2019**, 323.[76]

The approaches of *in vitro* biochemical assays, cellular assays and rational design for identification of small molecules targeting miRNAs each have their advantages and disadvantages. Future studies have been undertaken with an objective of identification of more potent small molecules and determination of new targets to achieve modulation of miRNAs of therapeutic value. Here, we chose to develop new specific miRNA small molecule regulators by cell-based assays for the following reasons: *(a) to develop new classes of molecules with specific miRNA modulation ability for therapeutic purposes, (b) to elucidate the gene pathways and to unravel role of miRNAs in disease development and progression, and (c) to study the role of different enzymes in miRNA biogenesis.*

1.4 Small molecule modifiers of microRNA-122

1.4.1 Introduction to microRNA-122

MicroRNA-122 (miR-122) is a 22-nucleotide long miRNA that is generally found in liver tissue and constitutes one of the most abundant miRNAs in liver;[122] it is conserved in all vertebrates.[123] Among other tissues, negligible expression of miR-122 in the human respiratory system was observed only by RNA-sequencing.[123] miR-122 was first discovered by cloning and sequencing tissues from mice and found to be highly specific to the murine liver.[124] It has been observed that miR-122 expression starts at the development of the liver bud and maximizes at birth.[125] In situ hybridization in zebrafish detected miR-122 expression only in the liver.[126]

Being the most abundant among hepatic miRNAs,[122] miR-122 plays a critical role in diverse liver functions and suppresses non-hepatic genes; its inhibition results in liver fibrosis[127] and dysregulation of iron homeostasis, differentiation of hepatocytes, and systemic and hepatic lipid metabolism.[128-129] Progeny of miR-122 germline knockout mice developed overt abnormalities in liver development.[130] Antisense-mediated inhibition of miR-122 results in delayed hepatic development in zebrafish[131] and downregulated expression of genes involved in fatty acid metabolism and cholesterol biosynthesis in mice.[66, 132] Restoration of miR-122 levels reversed liver inflammation in miR-122 KO mice.[130] In adult stem cells of human and mouse origin, multiple studies showed that ectopic expression of miR-122 promoted hepatocyte-like differentiation,[133-135] indicating that miR-122 expression is a crucial factor for maintaining a hepatic gene expression signature during development.

Consistent with its absence causing liver inflammation, miR-122 is classified as a tumor suppressor miRNA,[136] with decreased miR-122 levels associated with hepatocellular carcinoma

(HCC).[137] HCC is one of the five most common types of cancers, and accounts for around 75% of all cases of liver cancers. HCC is often detected at later stages, and decreased miR-122 levels are associated with metastasis and poor prognosis.[130] Interestingly, long-term loss-of-function of miR-122 or reduced miR-122 expression have been associated with hepatosteatosis, hepatitis, and the development of tumors resembling HCC in miR-122 knockout mice. These pathologic manifestations were associated with hyperactivity of oncogenic pathways and hepatic infiltration of inflammatory cells that produce pro-tumorigenic cytokines, including IL-6 and TNF. Additionally, delivery of miR-122 to a MYC-driven mouse model of HCC strongly inhibited tumorigenesis, further supporting miR-122's classification as a tumor suppressor. Interestingly, high endogenous levels of miR-122 are observed in Huh7 cells in comparison to other HCC-derived cell lines such as Hep3B and HepG2 as determined by RT-qPCR analysis.[138]

The biogenesis of miR-122 follows the canonical pathway,[128-129] with a huge variability observed in the pri-miR-122 sequence, while the mature miR-122 sequence is conserved.[139] In the livers of developing mouse embryos and in human HCC cell lines, miR-122 gene expression is activated by several liver-enriched transcription factors (LETFs), e.g. CCAAT/enhancer-binding protein (C/EBPα), and hepatocyte nuclear factors (HNFs) — HNF1α, HNF3β, HNF4α[140-141] and HNF6.[131] One of the first identified miR-122 targets was the cationic amino acid transporter 1 (CAT-1) or *Slc7a1*.[125] CAT-1 is expressed in many adult tissue types and strongly expressed in fetal liver, but under normal (unstressed) circumstances, is repressed in adult hepatocytes.[125, 142] miR-122 binds to the 3'-UTR to repress CAT-1 expression and the CAT-1 mRNA is targeted to P-bodies for mRNA decay.[142] In humans, this repression can be relieved by the protein HuR which is released by the nucleus under cellular stress. HuR releases the CAT-1 mRNA from P-bodies by binding to the 3'-UTR leading to the resumption of the protein translation. Interestingly, an

important indirect miR-122 target, c-MYC mRNA, exhibits reciprocal regulation with miR-122 in HCC.[143] miR-122 suppresses c-MYC transcription by regulating transcriptional activators E2f1 and Tfdp2, while c-MYC suppresses miR-122 by directly binding to the miR-122 promoter region and indirectly affecting binding of LETFs.[144] Another miR-122 target, CUTL1,[141] is a key transcriptional regulator of factors like WNT5A, which positively regulates tumor cell motility and tumor progression.[145] In HCC cells, the oncogene cyclin G1 is silenced by miR-122, resulting in the modulation of p53 protein stability and increased sensitivity to doxorubicin-induced apoptosis.[146] A number of other targets of miR-122 have also been identified, including anti-apoptotic and carcinogenic genes *Bcl-w*, ADAM10, IGF1R, SRF (which promotes tumorigenesis), and proto-oncogene Wnt1; all these genes are shown to be involved in hepatocarcinogenesis and angiogenesis.[136, 147]

miR-122 plays a crucial role in the replication of hepatitis C virus (HCV) RNA.[148] About 170 million people are affected by hepatitis C worldwide, resulting in chronic liver disease, cirrhosis, and even death. There are six genotypes of HCV known with individual subtypes and the current treatments depend upon identification of the HCV genotype.[149] Contrary to the role of miRNAs in downregulating gene expression by binding to 3'-UTR of mRNAs, miR-122 directly pairs with two adjacent binding sites in the 5'-UTR of the viral RNA, thus enhancing viral replication.[150] Studies have shown that binding of miR-122 to the 5'-UTR enhances the association of ribosomes with HCV genome,[151] and the binding of AGO proteins with RISC complex protects the genome from exonucleases.[152] In turn, HCV sequesters miR-122 binding to cognate mRNAs, creating a 'sponge' effect.[153] Such sequestration of miR-122 plays a role in the development of steatosis, followed by fibrosis, subsequent cirrhosis of the liver and finally, leading to HCC.[154] The first proof-of-concept study with a modified LNA anti-miR-122 SPC3649 (Miravirsen) was

carried out on chronically-infected chimpanzees. The inhibitor reduced HCV levels with no evidence of viral resistance or side effects in the treated animals during the treatment phase of 10 days at 5 mg/kg dose.[149] Furthermore, the miR-122 seed sites in the HCV genotypes are conserved in all genotypes. So, this treatment is expected to be genotype-independent. In phase 2a clinical trials, several patients were injected with Miravirsen up to a maximum dose of 7 mg/kg in human trials.[155] These patients showed almost undetectable HCV infection after 5 weeks.

Development of small molecule modifiers of miR-122 activity is of considerable interest. As upregulation and downregulation of miR-122 levels have therapeutic potential, small molecules capable of precisely modulating miR-122 levels have great potential as new treatments. Small molecule activators can be employed to elucidate the gene pathways that miR-122 regulates, and to develop new treatments for HCC. Ultimately, small molecule inhibitors will enable us to develop new therapies for HCV.

In 2010, our lab published two specific small molecule inhibitors of miR-122 (**19** and **20**) and one specific small molecule activator of miR-122 (**21**).[108] We developed an assay for screening small molecules based on the psiCHECK-2 reporter plasmid (**Figure 1-10**). This reporter plasmid expresses both *Renilla* luciferase and firefly luciferase. This allows for normalization to account for variable transfection efficiency and cell viability. The reported values are normalized as relative luciferase units (RLU). The plasmid consists of the miR-122 target sequence inserted downstream of the *Renilla* luciferase gene. Just as miRNAs are known to bind to the 3'-UTR to downregulate target genes, mature miR-122 downregulates luciferase expression upon binding the 3'-UTR. Thus, an increase in luciferase signal or RLU indicates miR-122 inhibition, while decreased luciferase signal indicates miR-122 activation. The ability of this reporter construct to detect endogenous miR-122 levels was confirmed by transfecting this psiCHECK-miR122

construct into HeLa and Huh7 cells. Huh7 cells express high levels of miR-122,[132] while miR-122 is not expressed in HeLa cells.[156] Upon assaying the cells with a Dual Luciferase Assay kit after 24 h, the construct elicited a > 15-fold reduced luciferase activity (RLU) in Huh7 cells compared to HeLa cells. Also, luciferase activity was recovered by co-transfecting Huh7 cells with the reporter and a miR-122 antagomir, further confirming that this reporter is a functional cellular screen for miR-122 levels. Another construct, psiCHECK-control, which contains an empty multicloning site, showed no change in RLU.

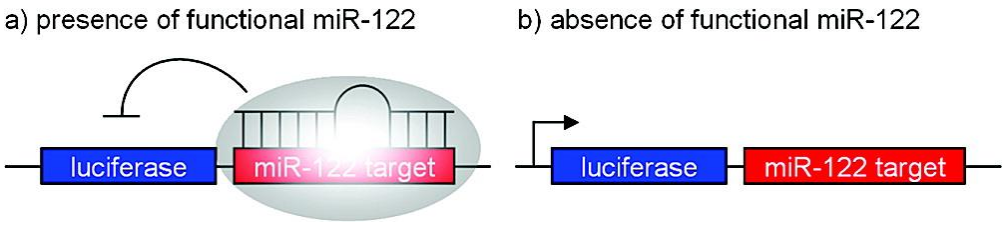

Figure 1-10 miR-122 assay.

(A) Binding of mature miR-122 represses luciferase expression in this reporter construct. (B) miR-122 inhibitors lead to repression of miR-122 inhibition, thereby increasing luciferase signal. Adapted from *J. Am. Chem. Soc.*, **2010**, 132 (23), 7976.[108]

psiCHECK-miR122 was further used for screening small molecules in Huh7 cells to discover miR-122 inhibitors and activators. Initially, a set of 1,364 compounds from Diversity Set II, NCI Development Therapeutics Program was screened in 96-well format using psiCHECK-miR122-Huh7 cells. These cells were exposed to each compound (10 µM) and assayed using a Dual Luciferase Assay Kit after 48 h. Two compounds (**19** and **20**) showed 773% and 1,251% increases in luciferase activity, respectively (**Figure 1-11A**). The data were confirmed by replicating this assay and treating Huh7 cells containing psiCHECK-control vector with **19** and **20** to test for non-miRNA specific activity. Negligible luciferase activity was observed in this assay.

These small molecules were also assayed using a miR-21 reporter construct[103] in HeLa cells; they did not induce luciferase expression reported, indicating that **19** and **20** specifically inhibit miR-122 (**Figure 1-11B**). A structure-activity relationship (SAR) analysis was undertaken for both these compounds (**Figure 1-12**).

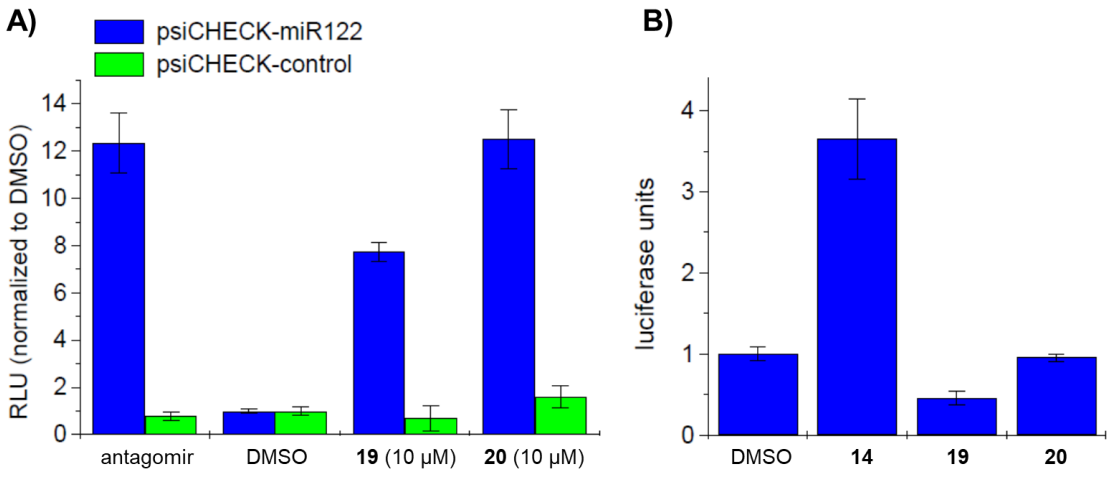

Figure 1-11 Validation of hits **19** and **20**.

(A) Validation of hits **19** and **20** (10 µM) in the NCI Diversity Set screen in Huh7 cells. (B) Specificity of **19** and **20** (10 µM) in miR-21 assay compared to specific miR-21 inhibitor **14** (10 µM) in HeLa cells. Adapted from *J. Am. Chem. Soc.*, **2010**, 132 (23), 7976.[108]

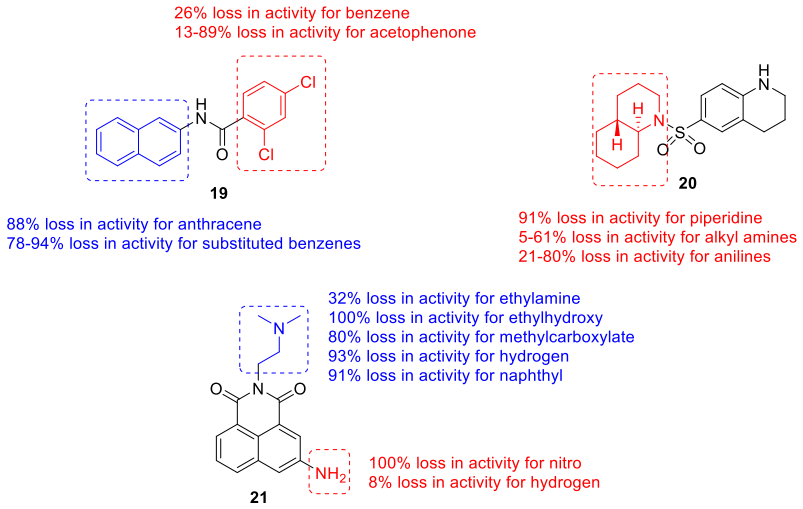

Figure 1-12 SAR data for compounds **19**, **20** and **21**.

SAR data for compounds **19**, **20** and **21** shows the various structural modifications performed on **19**, **20** and **21** and the resulting changes in activity. Adapted from *J. Am. Chem. Soc.*, **2010**, 132 (23), 7976.[108]

With these two miR-122 inhibitors, the screening results were also analyzed for reductions in luciferase activity. Several compounds were selected and re-assayed in psiCHECK-miR122-Huh7 and psiCHECK-empty-Huh7 cells to identify miR-122 activators. Compound **21** induced a 7-fold reduction in luciferase activity (RLU). As control experiments established the specific activity of **21** towards miR-122 activation (as mentioned in the previous paragraph), this compound was also taken up for SAR analysis (**Figure 1-12**).

A dose-response curve for these compounds revealed EC_{50} values for miR-122 inhibitors, **19** and **20,** to be 3 µM and 0.6 µM, respectively, while for miR-122 activator **21**, EC_{50} was 3 µM. The effects of the small molecule modifiers on miR-122 levels was quantified by RT-qPCR. The psiCHECK-miR122-Huh7 cells were exposed to these three small molecule modifiers for 48 h, followed by RNA isolation and RT-qPCR analysis. Consistent with the chemiluminescence data, the miR-122 inhibitor **20** induced a 72% knock-down of mature miR-122 levels, while **19** induced a 45% knock-down compared to DMSO-treated control cells. The miR-122 activator **21** elicited a

438% increase in miR-122 levels. Similarly, RT-qPCR analysis of HeLa cells containing miR-21 plasmid was performed, and no change in miR-21 levels was observed upon treatment with the compounds. This further confirmed the high specificity of these small molecules for miR-122.

Preliminary studies were conducted to further assess the mode of action of these compounds. Melting experiments with a miR-122 oligonucleotide revealed that these molecules do not interact directly with pre-miR-122. RT-qPCR analysis to quantify pri-miR-122 levels was performed (using primers unique to the pri-miR-122 sequence), showing a significant downregulation of pri-miR-122 levels to 22% and 3% of baseline levels for **19** and **20**, respectively. Thus, miR-122 inhibitors **19** and **20** are targeting miRNA-122 biogenesis at the transcriptional level. Interestingly, pri-miR-122 levels reduced further than mature miR-122 levels. A possible explanation for this result could be faster processing of pri-miRNA to mature miRNA compared to transcription of miRNA gene in presence of these molecules. Also, miR-122 activator **12** upregulated pri-miR-122 levels, suggesting transcriptional-level regulation by these compounds. An interesting study by the Yao group showed a combination inhibition achieved by a miR-122 antagomir and small molecule **20**.[157] The two mechanistically distinct inhibitors, a miR-122 antagomir (inhibition at mature miRNA level) and **20** (inhibition at transcriptional level on miRNA synthesis pathway) were delivered to psiCHECK-miR122-Huh7 cells by mesoporous silica nanoparticles (MSN) with surfaces modified by PEG-linker-RGD peptide. RGD peptide with PEG linker increases cellular uptake.[158] On simultaneous delivery of miR-122 antagomir (200 nM) and **20** (2 μM), an additive effect was observed as monitored by luciferase activity and RT-qPCR experiments (**Figure 1-13**).[157]

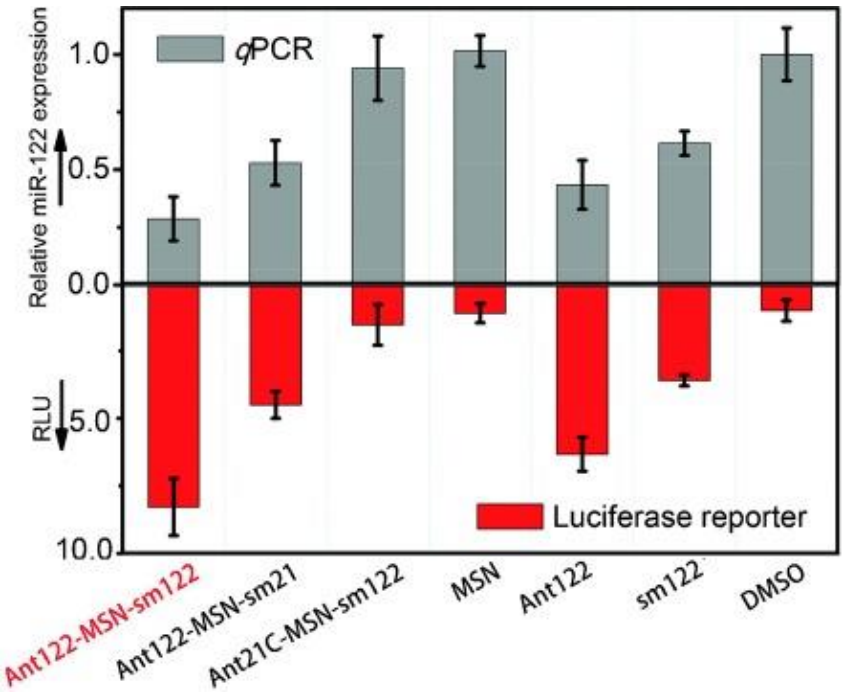

Figure 1-13 Combination effect of miR-122 antagomir and small molecule **20**.

Luciferase activity and RT-qPCR analysis shows an additive effect of two mechanistically distinct miR-122 inhibitors (Ant = antagomir, MSN = mesoporous silica nanoparticles, sm = small molecule). Adapted from *Angew. Chem. Int. Ed.*, **2015**, 127 (36), 10720.[157]

As explained earlier, HCV replication is highly dependent on miR-122 levels in hepatocytes, and decreased miR-122 impedes HCV replication. A LNA anti-miR-122 antagomir, SPC3649, induced significant reductions in HCV levels in animal and human studies.[149, 155] Thus, **19** and **20** were tested for their ability to inhibit HCV replication. Huh7 cells were transfected with pHtat2Neo/QR/KR/FV/SI plasmid (used to generate genotype 1a H77c RNA) for this study. These cells were also transfected with miR-122 antagomir (positive control), while DMSO-treated cells constituted the negative control. As reported in the literature, HCV RNA levels dropped by 80% in presence of miR-122 antagomir.[148] The small molecule inhibitors **19** and **20** induced a 52% and 53% decrease in HCV RNA levels, respectively.

Hepatocellular carcinoma (HCC) is characterized by low levels of miR-122 compared to normal liver tissue, as discussed above. In particular, in Hep3B and HepG2 cell lines, the anti-apoptotic gene and miR-122 target *Bcl-w* is abnormally upregulated when of miR-122 is decreased. In HepG2 cells, introducing the miR-122 duplex downregulated *Bcl-w* and — as a consequence — caspase-3 activity was restored, resulting in the induction of apoptosis in these diseased cells.[147] Treatment of HepG2 cells with miR-122 activator **21** (10 μM) led to a 20-fold increase in caspase-3 and caspase-7 activity. This suggests the ability of these cells to undergo apoptosis upon the introduction of **21**. In comparison, in Huh7 cells, which express significantly higher levels of miR-122 at baseline, only a slight decrease in cell viability was observed. Thus, compound **21** was successful in inducing apoptosis in cells with aberrantly low levels of miR-122. Taken together, these results suggest the therapeutic potential of specific small molecule modifiers of miR-122 expression.

After the encouraging discovery of small molecules **19** and **20** as specific miR-122 inhibitors and of **21** as an activator, attempts to discover new modifiers of miR-122 expression were undertaken. Using the same luciferase reporter psiCHECK-miR122-Huh7 stable cell line, a primary screen of 336,006 compounds from by combining the Broad Institute's Diversity Oriented Synthesis (DOS) collection (71,424 compounds) with the NIH's Molecular Libraries Probe Production Center Network (MLPCN) library (264,582 compounds) was conducted. The primary screen yielded 1,023 compounds as active inhibitors (0.3% hit rate). Active compounds were further screened through pan-assay interference (PAIN) analysis to identify compounds as potential false-positives for their promiscuous behavior in biological assays. Compounds with functional groups that were chemically reactive, metabolically unstable, pH sensitive, hydrolytically labile, or otherwise not amenable to SAR studies were eliminated as well. The

remaining 825 compounds were further tested in a dose-response assay in the stable cell line, and only 406 compounds, eliciting EC_{50} values less than 10 μM, were shortlisted. Next, these compounds were cross-referenced with active compounds obtained from a high-throughput screen (HTS) for miR-21 inhibitors using the MLCPN library (PubChem AID 2289), and analogs found active in both assays were disregarded. Then, solid samples of the remaining 65 compounds were re-tested in the stable cell line. Compound **39** was identified as one of the promising hits among 34 hits that also passed the powder re-test.

1.4.2 Synthesis and SAR studies of a sulfonamide series of miR-122 inhibitors

Following the identification of the parent compound **39**, an SAR study was initiated to improve the potency of **39** and to better understand the chemical functionalities required for its activity. Compound **39** was resynthesized in 3 steps from a commercially available precursor (4-isopropyl-3-methylphenol). 4-Isopropyl-3-methylphenol (**39a**) was methylated by dimethyl carbonate ($(MeO)_2CO$) in the presence of potassium carbonate (K_2CO_3) and tetrabutylammonium bromide (TBAB) under reflux conditions for 24 h, affording the corresponding methylated phenol **39b** in quantitative yields (**Figure 1-14**). This procedure was optimized by Meryl Thomas and the analytical data is in agreement with the literature reports.[159] Sulfonylation using chlorosulfonic acid (HSO_3Cl) in $CHCl_3$ at 0 °C for 1.5 h delivered the corresponding sulfonyl chloride **39c** in good yields (74%). The sulfonyl chloride **39c** was used as a reactant for the synthesis of a number of analogs with the same benzenesulfonyl part. The sulfonyl chloride **39c** was reacted with 4-methylimidazole in DCM to yield the parent compound **39** in 72% yield. Compound **39** was formed exclusively while the formation of other isomer, 1-((5-isopropyl-2-methoxy-4-

methylphenyl)sulfonyl)-5-methyl-1*H*-imidazole, was not observed. This result can be attributed to the formation of the sulfonamide **39** with the methyl group positioned farther from the sulfonyl end to minimize steric interactions.[160] For preparing the analogs, a modular approach was adopted and two parts of **39** were altered: the benzenesulfonyl and the imidazole. Substituting the 4-methylimidazole with a dimethylamine (**40**) or an ethylamine group (**41**) resulted in a significant loss in activity (**Table 1-1**). Drastic reductions in activity were also observed when replacing the 4-methylimidazole with a structurally-similar pyrrole (**42**), 3-methylpyrrole (**43**), 4-methylpyrazole (**44**), or 3-methylpyrazole (**45**), indicating the importance of the imidazole motif. Compounds **42**, **43**, **44** and **45** were synthesized using NaH in THF conditions in 72%, 37%, 48% and 78% yields, respectively.[161-162]

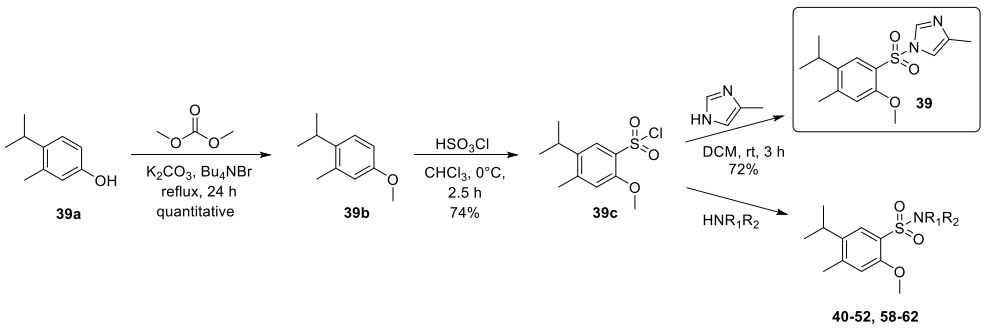

Figure 1-14 Synthetic route to the initial hit compound **39**.

Synthetic route to the initial hit compound **39** starting from commercially available phenol **39a** in three steps with an overall yield of 53%. Other sulfonamides were synthesized from the sulfonyl chloride **39c**.

Table 1-1 Structures and activity of derivatives **39**-**45**.

[a]RLU values represent *Renilla* luciferase luminescence signal in the Huh7-miR122 stable cell line and are first normalized to firefly luciferase (dual reporter system) and then normalized to the activity of the original hit **39**.

[b]*In vitro Renilla* luciferase data are normalized to DMSO.

[c]psiCHECK-empty assay data are normalized to DMSO. Data for all assays represents the average ± standard deviation from at least three independent experiments.

Data generated by Dr. Nicholas Ankenbruck.

Compounds **40** (PubChem CID 16644736) and **41** (PubChem CID 20105566) were used directly from the Broad Institute compound library without resynthesis.

compound	chemical structure	primary screen (RLU)[a]	*Renilla* luciferase assay[b]	psiCHECK-empty assay[c]
39	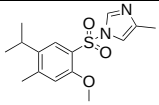	100 ± 3%	80%	127%
40	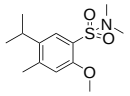	42 ± 3%	--	--
41	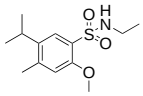	42 ± 3%	--	--
42	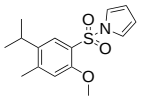	29 ± 1%	--	--
43	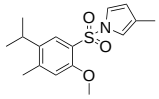	57 ± 4%	87%	--
44	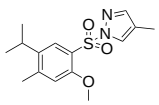	32 ± 1%	--	--
45	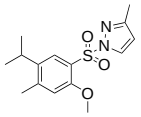	44 ± 1%	--	--

We next studied the requirement for the methyl group itself through substitution of 4-methylimidazole with an imidazole (**46**), 4-phenylimidazole (**47**), or 4-nitroimidazole (**48**) (**Table 1-2**). Removal of the methyl group or replacement with a phenyl moiety resulted in a large decrease in activity, while the nitro group elicited a more modest reduction. Analog **46** was synthesized with similar conditions as **39**, while compounds **47** and **48** were synthesized by refluxing the sulfonyl chloride with 4-nitroimidazole in DCM overnight.[163] Virtually complete loss of activity was also observed for 2-ethyl- (**49**) or 4,5-dichloro-imidazole (**50**) modifications. Further substitutions of the imidazole by more sterically demanding benzimidazole (**51**) and indole (**52**) motifs also led to a decrease in activity compared to **39**, again indicating the importance of the small 4-methylimidazole (**Table 1-2**). Both of these compounds (**49** and **50**) were synthesized by treating the sulfonyl chloride with corresponding imidazoles in DCM with triethylamine as base.[163] The indole analog (**52**) was prepared in a reaction of the sulfonyl chloride **39c** with indole in the presence of NaOH and TBAB in DCM.[164]

Table 1-2 Structures and activity of derivatives **46**-**52**.

[a]RLU values represent *Renilla* luciferase luminescence signal in the Huh7-miR122 stable cell line and are first normalized to firefly luciferase (dual reporter system) and then normalized to the activity of the original hit **39**.

[b]*In vitro Renilla* luciferase data are normalized to DMSO.

[c]psiCHECK-empty assay data are normalized to DMSO. Data for all assays represents the average ± standard deviation from at least three independent experiments.

Data generated by Dr. Nicholas Ankenbruck.

Compound **51** (PubChem CID 4175330) was used directly from the Broad Institute compound library without resynthesis, and **46**, and **47** were synthesized by Dr. Meryl Thomas.

compound	chemical structure	primary screen (RLU)[a]	*Renilla* luciferase assay[b]	psiCHECK-empty assay[c]
46	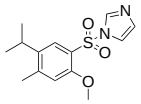	33 ± 4%	--	--
47	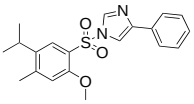	35 ± 1%	--	--
48	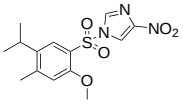	61.1 ± 0.4%	67%	--
49	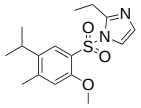	40 ± 1%	--	--
50	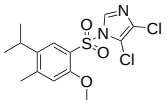	4 ± 1%	--	--
51	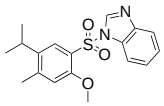	75 ± 3%	45%	--
52	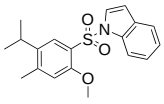	55 ± 1%	94%	--

Focusing our attention on the benzenesulfonyl moiety, a series of analogs were synthesized while keeping the 4-methylimidazole constant. Replacing the isopropyl group with a hydrogen

(**53**) or a methyl group (**54**) reduced activity. The rotationally-restricted 1,2,3,4-tetrahydronaphthamidyl analog (**55**) also showed a significant loss in activity**.** Furthermore, *O*-ethyl (**56**) and *O*-propargyl (**57**) analogs elicited reduced activity (**Table 1-3**). Analogs **53** and **54** were synthesized using a similar synthetic route as is reported for **55** (**Figure 1-14**). Thus, changes to the benzenesulfonyl part reduced activity, with the initial hit **39** still being the best analog.[163]

Table 1-3 Structures and activity of derivatives **53**-**57**.

[a]RLU values represent *Renilla* luciferase luminescence signal in the Huh7-miR122 stable cell line and are first normalized to firefly luciferase (dual reporter system) and then normalized to the activity of the original hit **39**.

[b]*In vitro Renilla* luciferase data are normalized to DMSO.

[c]psiCHECK-empty assay data are normalized to DMSO. Data for all assays represents the average ± standard deviation from at least three independent experiments.

Data generated by Dr. Nicholas Ankenbruck.

Compounds **54** (PubChem CID 20105692) and **56** (PubChem CID 163831221) were used directly from the Broad Institute compound library without resynthesis, and **53** was synthesized by Dr. Meryl Thomas.

compound	chemical structure	primary screen (RLU)[a]	*Renilla* luciferase assay[b]	psiCHECK-empty assay[c]
53	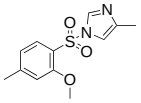	24 ± 3%	80%	--
54	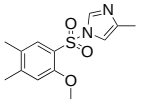	32 ± 5%	--	--
55	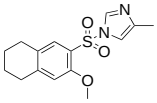	33.3 ± 0.5%	--	--
56	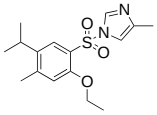	74 ± 10%	70%	--
57	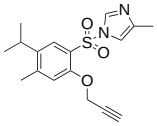	50 ± 3%	97%	--

It was recently reported that sulfonamide derivatives and many other small molecule inhibitors may be prone to increasing *Renilla* luciferase concentration in cells via ligand-based stabilization, possibly creating false-positive hits in high-throughput screens.[165] Conversely, biochemical evaluation of the same inhibitors causes a significant decrease in luciferase signal. Thus, the analogs that elicited ≥ 50% activity of the parent compound **39** in the initial screen were

tested in a biochemical *Renilla* luciferase (Rluc) assay. Here, **48**, **51**, and **56** induced ≥ 30% decrease in *Renilla* luminescence, while analogs **49**, **53**, and **57** only showed modest enzyme inhibition. To further validate the specificity of these inhibitors for acting through the miRNA pathway, Huh7 cells were transfected with a psiCHECK-empty reporter (where the miR-122 binding site was replaced with a linker not targeted by any known miRNAs) and exposed to each analog at 10 μM for 48 h. The parent compound **39** induced a 27% increase in the psiCHECK-empty assay, consistent with Rluc inhibition observed in the *in vitro* assay (**Table 1-1**).

A complete scaffold change of the imidazole motif was also investigated. A series of analogs with pyridin-2-amines and anilines were synthesized. Both the unsubstituted pyridine ring (**58**) and methylation at the 2-position (**59**) showed 89% activity relative to the parent compound, while 3-methyl-pyridin-2-amine (**60**) elicited a significant increase in activity (**Table 1-4**). Aniline (**61**) and 2-methylaniline (**62**) analogs showed a reduction in activity. Unfortunately, when assessed in the *in vitro* Rluc assay, **58-60** induced significant reductions in luminescence signal indicating they did not display enhanced miRNA-122 inhibition activity (**Table 1-4**). The sulfonyl chloride, upon treatment with pyridine-2-amines with pyridine as a base, in DCM or THF at reflux yielded the corresponding analogs,[166] while aniline analogs were prepared by stirring the sulfonyl chloride with the corresponding anilines in trimethylamine and THF at a variety of temperatures.[167]

Table 1-4 Structures and activity of derivatives **58**-**62**.

[a]RLU values represent *Renilla* luciferase luminescence signal in the Huh7-miR122 stable cell line and are first normalized to firefly luciferase (dual reporter system) and then normalized to the activity of the original hit **39**.

[b]*In vitro Renilla* luciferase data are normalized to DMSO.

[c]psiCHECK-empty assay data are normalized to DMSO. Data for all assays represents the average ± standard deviation from at least three independent experiments.

Data generated by Dr. Nicholas Ankenbruck.

compound	chemical structure	primary screen (RLU)[a]	*Renilla* luciferase assay[b]	psiCHECK-empty assay[c]
58	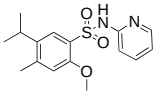	88 ± 1%	8%	--
59	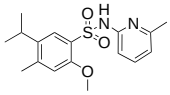	89 ± 11%	2%	--
60	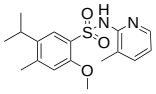	135 ± 4%	17%	--
61	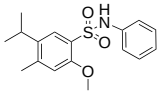	47 ± 3%	--	--
62	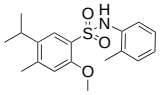	32 ± 3%	--	--

The next modification made was methylation of the secondary amine in the sulfonamide. On inspecting *in vitro Renilla* luciferase assay data and analogs bearing imidazole and pyrazole motifs, we hypothesized that a tertiary sulfonamide would minimize Rluc inhibition, because secondary sulfonamides comprise a subset of known Rluc inhibitors.[168] In order to convert **58**-**60** to the tertiary sulfonamides **63**-**65**, these analogs were *N*-methylated; a methyl substituent was chosen as it was the smallest possible change, minimizing further steric perturbation that might have had a negative impact on miR-122 inhibition. The analogs **58**-**60** were treated with methyl

iodide in the presence of NaH in THF or DMF with overnight stirring at room temperature to yield compounds **63-65**.[169] Compound **63** showed a modest reduction in activity, while **64** elicited a 7% increase compared to the parent compound. Unfortunately, **65** induced a disappointing 64% activity relative to **39**, but all three compounds showed no Rluc inhibition, supporting our hypothesis (**Table 1-5**). Gratifyingly, replacement of the pyridine moeity in **64** and **65** with a benzene ring in compounds **66** and **67** yielded 104% and 122% activity, respectively. Compound **66** showed no Rluc inhibition, while 20% inhibition was observed with **67**. Methylation of the aniline ring at the *para* position (**68**) yielded a modest decrease in activity compared to **39**, while 2,3-dimethyl- (**69**) and 2,5-dimethyl- (**70**) aniline derivatives showed 80% activity relative to the parent compound. Unfortunately, while **68-70** showed no inhibition in the *in vitro* assay, all three compounds displayed > 200% activity in the psiCHECK-empty assay, indicating that they increase luciferase activity by non-miRNA dependent mechanisms in cells. Furthermore, compounds **64** and **66** showed little to no inhibition in the psiCHECK-empty assay, consistent with Rluc inhibition observed in the *in vitro* assay (**Table 1-5**).

Table 1-5 Structures and activity of derivatives **63-70**.

[a]RLU values represent *Renilla* luciferase luminescence signal in the Huh7-miR122 stable cell line and are first normalized to firefly luciferase (dual reporter system) and then normalized to the activity of the original hit **39**.

[b]*In vitro Renilla* luciferase data are normalized to DMSO.

[c]psiCHECK-empty assay data are normalized to DMSO. Data for all assays represents the average ± standard deviation from at least three independent experiments.

Data generated by Dr. Nicholas Ankenbruck.

compound	chemical structure	primary screen (RLU)[a]	*Renilla* luciferase assay[b]	psiCHECK-empty assay[c]
63	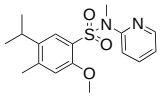	89 ± 4%	100%	88%
64	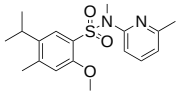	107 ± 1%	100%	117%
65	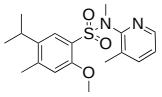	64 ± 12%	100%	87%
66	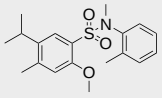	104 ± 7%	100%	90%
67	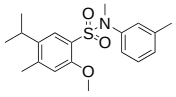	122 ± 1%	78%	103%
68	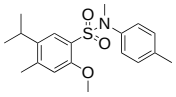	82 ± 1%	100%	218%
69	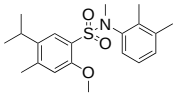	80 ± 4%	93%	225%
70	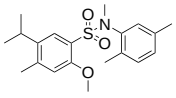	77 ± 1%	100%	245%

While **64** and **66** exhibited an excellent activity profile, poor solubility of the inhibitors presented a limitation of potential applications in animal studies. Because compound **66** elicited

less of a response in the psiCHECK-empty assay, further modifications were pursued on the *N*-methyl part of **66** (**Table 1-6**). Compound **71** containing an epoxide showed comparable activity to **66**, however, **71** exhibited water solubility similar to **66**. Installation of a carboxylic acid or corresponding isostere, such as tetrazole,[170] has been shown to enhance the water solubility of small molecules.[171] An introduction of the carboxy group in **72** significantly increased the water solubility. But **72** showed a 61% reduction in luminescence signal compared to **66**. Various tetrazoles were investigated and compound **73**, bearing a methyl tetrazole, yielded a higher luminescence signal compared to **66**. However, **73** showed a significant reduction in *Renilla* luminescence upon assessing in the *in vitro* Rluc assay. Analogs **74** and **75**, bearing a phenyl-tetrazole and pyrimidyl-tetrazole respectively, exhibited a 23% and 25% decrease in activity while no decrease in luciferase signal was observed in the *in vitro* Rluc assay. Surprisingly, analog **76**, containing a pyridyl-tetrazole moiety, induced an unexpected increase in luciferase signal compared to compounds **39** and **66**. Compound **76** elicited no inhibition in the *in vitro* Rluc assay. However, **76** induced an 80% increase in luminescence in the psiCHECK-empty assay compared to DMSO suggesting it is capable of activating luciferase in cells through an unknown mechanism (**Table 1-6**). Unfortunately, water solubility of compound **76** was not significantly improved compared to **66**.

Table 1-6 Structures and activity of derivatives **71-76**.

[a]RLU values represent *Renilla* luciferase luminescence signal in the Huh7-miR122 stable cell line and are first normalized to firefly luciferase (dual reporter system) and then normalized to the activity of the original hit **39**.

[b]*In vitro Renilla* luciferase data are normalized to DMSO.

[c]psiCHECK-empty assay data are normalized to DMSO. Data for all assays represents the average ± standard deviation from at least three independent experiments.

Data generated by Dr. Nicholas Ankenbruck.

compound	chemical structure	primary screen (RLU)[a]	*Renilla* luciferase assay[b]	psiCHECK-empty assay[c]
71	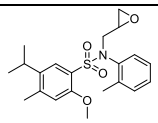	98 ± 9%		
72	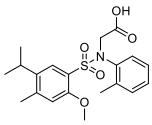	39 ± 1%	100%	
73	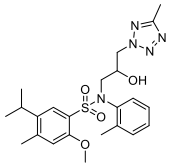	121 ± 10%	62%	
74	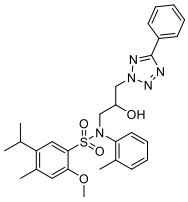	77 ± 4%	106%	
75	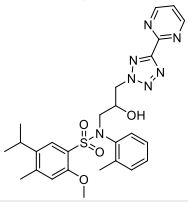	75 ± 2%	103%	
76	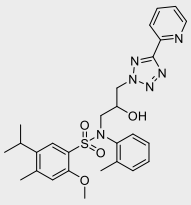	580 ± 25%	102%	178%

Compound **76** was synthesized from epoxide **71** and 2-(1*H*-tetrazol-5-yl)pyridine in DMF with K_2CO_3 as a base. This reaction can potentially yield two isomers (**A** and **B**; **Figure 1-15**).[172] To determine the exact structure of **76**, ^{1}H and ^{13}C NMR spectra were recorded (**Figure 1-21**). A primary analysis of the ^{1}H NMR spectrum indicates the presence of two conformers (or rotamers), or a mixture of two isomers as evidenced by fractional integral values of peaks at 5.3 – 5.4 ppm (ratio: 0.54:0.46, total: 1 H) and peaks at 2.23 ppm and 2.45 ppm (ratio: 1.54:1.46, total: 3 H). However, one-dimensional (1D) spectroscopy (^{1}H and ^{13}C NMRs) were unable to distinguish between both isomers **A** and **B** and a structure elucidation was carried out by two-dimensional (2D) correlation spectroscopy. Initially, a ^{1}H-^{1}H COSY spectrum was recorded (**Figure 1-22**). The COSY spectrum was used to determine the *J*-coupled protons within each ring system. The presence of cross peaks showed the identities of protons separated by 3 chemical bonds. Using this information, a scalar (*J*) coupling correlation network was identified based on the structures under investigation. The COSY spectrum revealed the location of H35, H36, H37, and H38 individually. In addition to COSY, a ^{1}H-^{1}H TOCSY spectrum yields through bond correlations with multiple bonds and was used to determine the different spin systems present in these structures. The different spin systems are highlighted in the TOCSY spectrum (**Figure 1-23**). However, aromatic protons H3, H6, H19, H20, H21, H21', H22, and H22' and aliphatic protons H24 and H25 were difficult to recognize due to resonance overlap, multiple couplings, and merging of peaks. To help further identify these peaks, ^{1}H-^{13}C HSQC and HMBC spectra were recorded (**Figures 1-24** and **1.25B**). The ^{1}H-^{13}C HSQC spectrum provides correlation between carbon and its attached protons ($^{1}J_{CH}$ couplings), while the ^{1}H-^{13}C HMBC spectrum shows long-range correlation between carbon and protons separated by 2 or 3 chemical bonds (in some cases, four bond correlations are also observed). First, carbon and its attached protons were pointed out from the ^{1}H-^{13}C HSQC spectrum

and finally, the ^{1}H-^{13}C HMBC spectrum was used for recognition of the ambiguous protons and carbons. In particular, H3 correlates to C1, C5, C10, and C4 (two bond correlation). H6 correlates to C2, C4, C7, and C1 (two bond correlation). H19 correlates to C11, C17, and C21. Upon identification of H19, protons H20, H21, and H22 were recognized by analysis of the COSY spectrum. Aliphatic proton H24 correlates to C26 and C25 (two-bond correlation), while H25 does not correlate to any carbon.

Furthermore, a ^{1}H-^{1}H ROESY spectrum was recorded (**Figure 1-26B**). The ROESY spectrum (^{1}H-^{1}H correlation) was utilized to ascertain the through space correlation between different protons. Upon analyzing the ROESY spectrum, the cross peaks for H26, H26', and H26'' are all in the same phase (opposite phase to the diagonal). This analysis indicates that the ROE cross peaks arise from direct dipole interactions and not from spin diffusion or chemical exchange over the NMR time scale. Thus, the cross peaks correlate the resonance frequencies of H26 and H26' in two different conformers (ratio: 54:46) and not a mixture of two different isomers.

To differentiate between isomers **A** and **B**, ^{1}H-^{13}C HMBC spectrum and ROESY spectrum were utilized. Upon analyzing the chemical structures of isomer **A**, protons H26, H26', and H26'' were anticipated to show three correlation peaks in ^{1}H-^{13}C HMBC spectrum – H26 ↔ C24 (three-bond correlation), H26 ↔ C31 (δ 142.74 ppm) (three-bond correlation), and H26 ↔ C25 (two-bond correlation) (**Figure 1-25A**). In comparison, only two correlation peaks in ^{1}H-^{13}C HMBC spectrum were expected in isomer **B** – H26 ↔ C24 (three-bond correlation) and H26 ↔ C25 (two-bond correlation). The ^{1}H-^{13}C HMBC spectrum revealed only two correlation peaks between H26 ↔ C24 and H26 ↔ C25 suggesting the presence of isomer **B** (**Figure 1-25B**). The isomers can also be distinguished by the analyzing the chemical structures of **A** and **B** for spatially close protons. Protons H8 (or H9) and H10 are spatially close to each other and are expected to show a

cross peak in the ROESY spectrum (**Figure 1-26A**). For reference, such a cross peak for H8 ↔ H10 (or H9 ↔ H10) is observed in the ROESY spectrum (**Figure 1-26B**). Upon inspection of chemical structures of isomers **A** and **B**, H26 and H38 appear to be spatially close in isomer **B**, whereas H26 and H38 are far apart from each other in isomer **B**. In the ROESY spectrum, no cross peak between H26 ↔ H38 was observed strongly indicating the presence of isomer **B** (**Figure 1-26B**). Compound **76** possibly exists as a mixture of two rotamers with a hindered rotation around the N16 – C24 bond at room temperature. Additional studies are required to determine the exact structures of these rotamers. In the future, X-ray crystallography will be utilized for further confirmation of the chemical structure and possible rotamers of **76**.

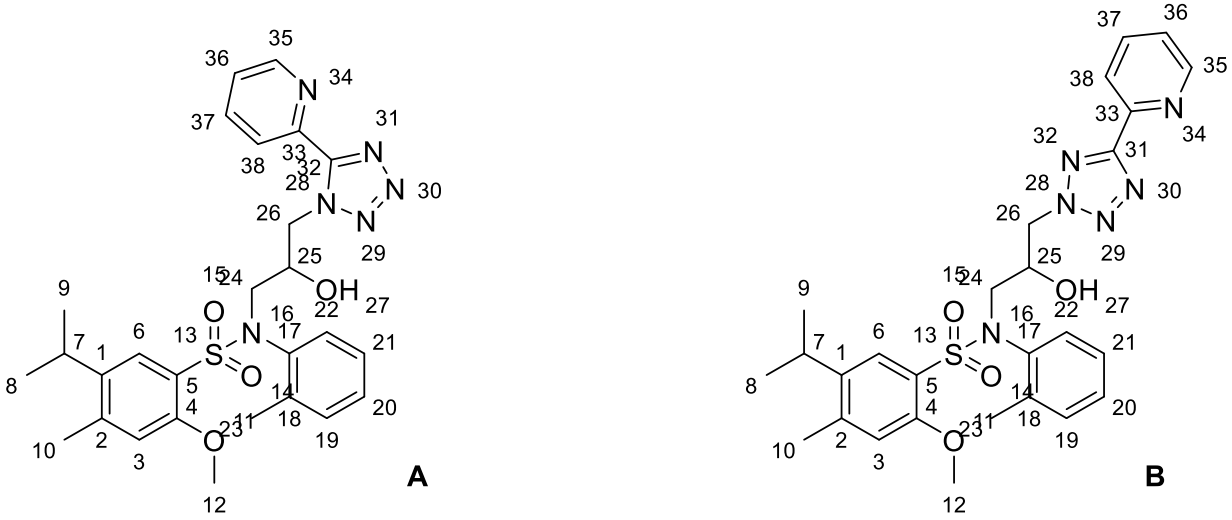

Figure 1-15 Chemical structures of isomers **A** and **B** of **76** with atom numbers.

These structures are zoomed for the atom numbers to be visible. 1D spectroscopy and 2D correlation spectroscopy experiments were conducted for the identification of structure of **76**.

The best analogs identified through structural modifications of **39** were tested in a dose-response assay in Huh7-miR122 cells (**Figure 1-16**). The inhibitor **66** had an EC_{50} of ~12.5 µM, while analog **76** showed an improved EC_{50} value of ~3.8 µM. The inhibitors, **66** and **76**, were

further investigated in RT-qPCR experiments measuring mature miRNA levels. Huh7 cells were exposed to a DMSO control (0.1%) or to the inhibitors at 25 µM for 48 h, total RNA was isolated using the miRNeasy kit (Qiagen), and RT-qPCR was performed in triplicate using TaqMan probes for miR-122 and RNU19 (control). The data were then normalized to the DMSO and RNU19 controls using the $2^{-\Delta\Delta Ct}$ method.[173] Compound **66** exhibited a 38% decrease in miR-122 levels while analog **76** elicited an 87% reduction in miR-122 expression, concomitant with their relative activity in the primary screen (**Figure 1-17A**).

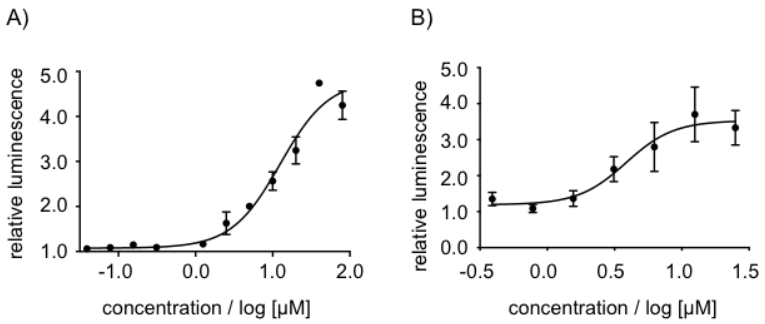

Figure 1-16 Luciferase dose-response curves for inhibitors **66** and **76** in the Huh7-psiCHECK-miR122 stable cell line.

(A) An EC_{50} of ~12.5 µM was observed for inhibitor **66**. (B) Compound **76** elicited an EC_{50} of ~3.8 µM. All data is normalized to DMSO and error bars represent standard deviations from three independent experiments. Data generated by Dr. Nicholas Ankenbruck.

In order to begin elucidating the mode of action of inhibitors **66** and **76**, several preliminary experiments were performed. A HeLa cell line that stably expresses a miR-21 reporter (HeLa-miR21)[174] was used to further confirm that the compounds are not general inhibitors of the miRNA pathway, since no increase in luciferase signal was observed (**Figure 1-17B**). To investigate cellular effects of these inhibitors, expression of E-cadherin was monitored in Huh7 cells following

treatment with **66** and **76.** E-cadherin is regulated by Wnt1, a known target of miR-122.[175] Endogenous E-cadherin levels are high in Huh7 cells due to Wnt1 repression by miR-122. Thus, treatment with a small molecule inhibitor was expected to lead to a reduction in E-cadherin protein levels. Treatment with DMSO alone elicited no inhibition of E-cadherin expression as expected, whereas reductions in E-cadherin levels were observed upon treatment with **66** and **76**, indicating suppression of the protein via miR-122-mediated induction of Wnt1 (**Figure 1-17C**). Pri-miR-122 expression was assessed by RT-qPCR to determine if these compounds inhibited miR-122 transcription. The miR-122 inhibitor **66** (25 μM) elicited up to a ~59% decrease in pri-miR-122 expression (**Figure 1-17D**), while **76** induced a more potent ~80% reduction, suggesting that both small molecules affect transcriptional or pre-transcriptional regulation, rather than downstream steps of the miRNA pathway.

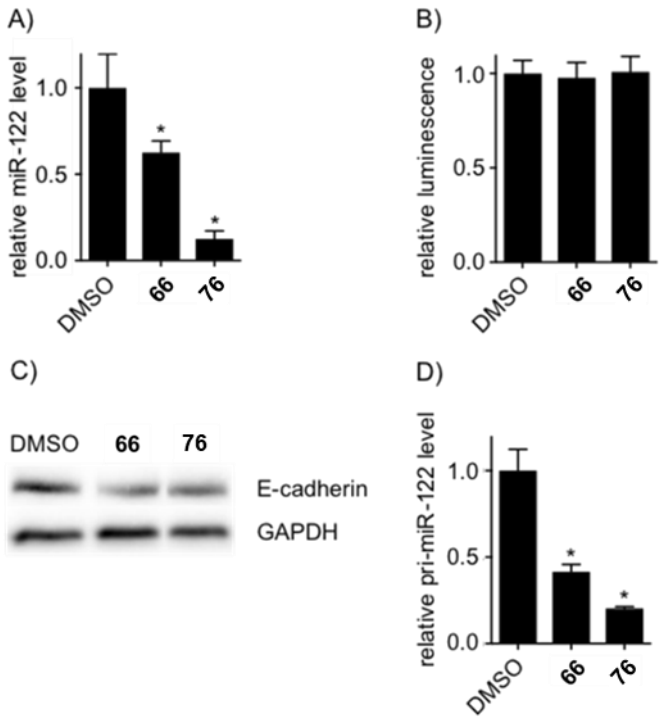

Figure 1-17 Effect of compounds **66** and **76** on different targets.

(A) Mature miR-122 levels in Huh7 cells were evaluated via RT-qPCR following 48 h treatment with compounds **66** and **76** (25 µM). Expression of miR-122 was normalized to a DMSO control. RNU19 expression was used as an internal control to account for variation between experiments. (B) HeLa-miR21 reporter cells were treated with **66** and **76** at 10 µM. After 48 h, luminescence was measured and normalized to a DMSO control. (C) E-cadherin expression was assessed in Huh7 cells via Western blot following treatment with **66** (25 µM) or **76** (10 µM) for 48 h. GAPDH expression was monitored as a loading control. (D) Primary miR-122 levels were evaluated via RT-qPCR in Huh7 cells following 48 h treatment with compounds **66** and **76** (25 µM). Expression of pri-miR-122 following small molecule treatment was normalized to a DMSO control. GAPDH expression was used as an internal control to account for variation between experiments. Data represent the averages ± standard deviations from three independent experiments. Data generated by Dr. Nicholas Ankenbruck.

To investigate the possibility of targeting miR-122 transcription and related proteins, a reporter plasmid in which a firefly luciferase gene was placed under the control of the miR-122 promoter was developed (**Figure 1-18A**).[176] Briefly, the miR-122 promoter sequence was PCR

amplified from Huh7 genomic DNA and ligated into a multi-cloning site upstream of the firefly luciferase gene in the pGL3-basic plasmid. As expected, almost no luminescence was observed for the control pGL3-basic reporter, while a significant level of luciferase expression was detected in Huh7 cells transfected with the pGL3-miR122promoter construct (**Figure 1-19A**). Treatment with the small molecule inhibitors **66** and **76** led to a reduction in miR-122 promoter activity (**Figure 1-18B**), consistent with the observed decrease in pri-miR-122 levels.

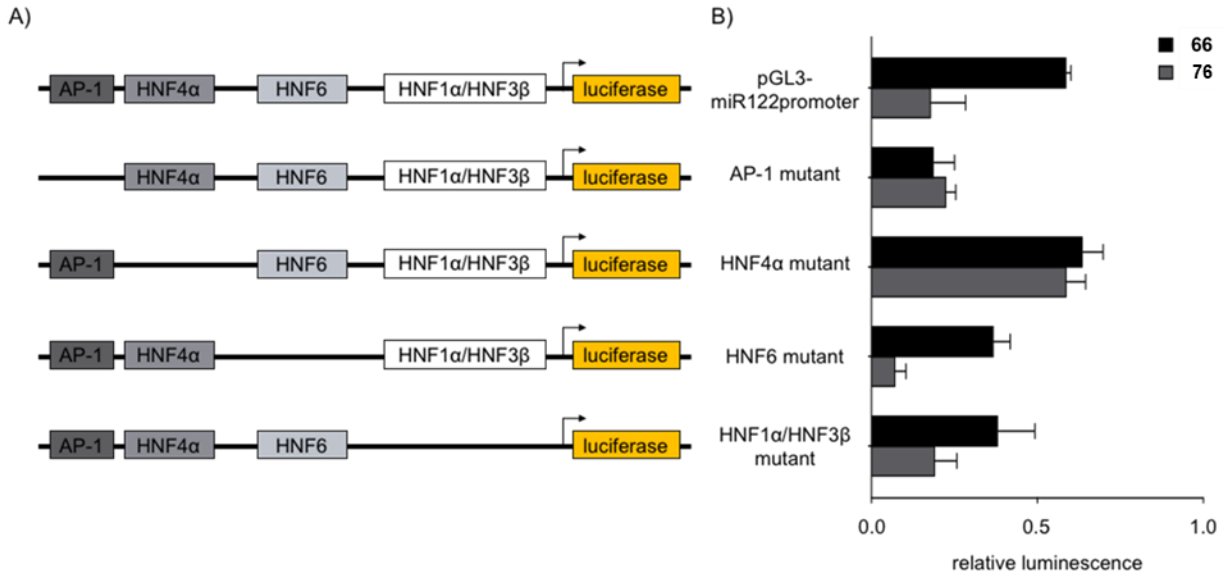

Figure 1-18 miR-122 promoter assay.

(A) Individual transcription factor binding sites within the miR-122 promoter sequence were mutated or deleted to attempt to identify the potential transcription factor target of **66** and **76**. Huh7 cells were treated with **66** and **76** at 25 µM following transfection with the pGL3-miR122 promoter plasmid. (B) Huh7 cells were transfected with the parent reporter plasmid or reporter plasmids in which transcription factor binding sites were mutated/deleted, then treated with compounds **66** and **76** at 25 µM. After 48 h, a Bright-Glo assay was performed. Luciferase expression was normalized to cell viability and the DMSO control. Data represent the averages ± standard deviations from three independent experiments. Data generated by Dr. Nicholas Ankenbruck.

After confirming that **66** and **76** inhibited the activity of the miR-122 promoter, a more detailed study was performed to identify the primary upstream transcription factor that is being influenced. Liver-enriched transcription factors, HNF1α, HNF3β, HNF4α, and HNF6 have been reported to regulate miR-122 transcription.[141, 176-177] Additionally, the AP-1 transcription factor was predicted to bind to the miR-122 promoter.[178-179] In order to study the effect of **66** and **76** on each individual transcription factor, reporter plasmids were developed in which a single transcription factor binding site in the natural miR-122 promoter sequence was mutated or deleted while the remaining binding sites were maintained (**Figure 1-18B**). Because there is overlap between the HNF1α and HNF3β binding sequences,[141] only a single mutant plasmid was generated for both. The mutated miR-122 promoter constructs were individually tested in Huh7 cells. All mutated constructs showed significant reductions in luciferase activity compared to the parent reporter (**Figure 1-18B**), suggesting that the interactions between the transcription factors and their corresponding promoters were diminished by the introduction of mutations. As expected, mutation of the HNF1α/HNF3β and HNF4α binding sites led to a 70% and 60% decrease in promoter activity respectively, indicating these transcription factors significantly contribute to miR-122 expression.[141] AP-1 and HNF6 mutants elicited only 30% reductions in activity. While the modest impact of HNF6 on miR-122 promoter activity reflects previous results,[177] we have found no reports demonstrating the effect of AP-1 on miR-122. Following transfection of HNF1α/HNF3β, HNF6, and AP-1 mutant reporters and subsequent treatment with **66** and **76**, up to 40% further reduction in luciferase activity was observed, indicating that the compounds are still able to inhibit transcription and thus must impact transcriptional activation independently of the mutated promoter (**Figure 1-18B**). However, in combination with the HNF4α mutant, **66** and **76** elicited ~6% and 41% less inhibition, respectively, compared with the parent construct, indicating that the

inhibitors may have an effect on the function of HNF4α-driven transcription of the miR-122 gene. Furthermore, small molecules bearing a similar sulfonamide scaffold have been reported to bind HNF4α and inhibit its function, providing further support for this hypothesis.[180-181]

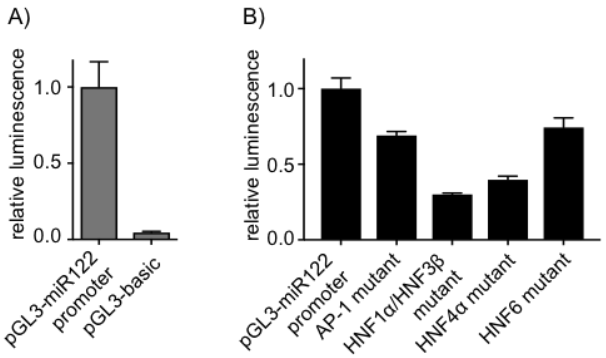

Figure 1-19 miR-122 promoter assay.

(A) Huh7 cells were transfected with pGL3-basic or pGL3-miR122promoter, then a Bright-Glo luciferase assay was performed after 48 h. (B) Transcription factor binding sites were deleted within the miR-122 promoter sequence. The resulting reporter plasmids were transfected into Huh7 cells. Luciferase activity was evaluated after 48 h using a Bright-Glo Assay. All data is normalized to DMSO and error bars represents standard deviations of three independent experiments. Data generated by Dr. Nicholas Ankenbruck.

Antisense oligonucleotide-mediated knockdown of miR-122 has previously been shown to inhibit HCV replication.[155, 182] Additionally, combination treatment of human liver cells stably expressing HCV replicons with an anti-miR-122 oligonucleotide and interferon-α2b resulted in additive antiviral activity.[183] Binding of miR-122 to the 5' terminus protects the HCV viral genome from degradation by the exonuclease XRN1, thereby stabilizing HCV RNA (**Figure 1-20A**).[184-185] Several additional mechanisms for miR-122-mediated promotion of HCV replication have also been proposed. For example, the 48S ribosomal complex association is enhanced in the presence

of miR-122 in rabbit reticulocyte lysate suggesting a potential mechanism for miR-122-mediated regulation of translation;[186] however, conflicting results support an alternative mechanism whereby miR-122 promotes translation via binding to the IRES independently of ribosome binding.[187] Furthermore, it has been hypothesized that miR-122 disrupts binding of cellular factors essential for viral translation, enhancing viral replication[188] and suggesting that miR-122 may promote or inhibit interactions with additional RNA-binding proteins. Additionally, miR-122 was proposed to augment positive-strand RNA synthesis by displacing the positive strand from the 3' terminus of the negative strand to be used as a template.[189] Finally, miR-122 been shown to enhance HCV RNA synthesis in association with Ago2,[190] potentially through recruitment of viral RNA to replication complexes;[191] however, this mechanism is not completely understood.

Because compounds **66** and **76** were able to inhibit miR-122 function, both compounds were investigated for their effect on HCV replication. Huh7.5 cells, which have a RIG-1 mutation for enhanced HCV replication, were pre-treated with **66** and **76** (10 μM) or DMSO (negative control) for one hour, then infected with HCV. After 48 h, total RNA was extracted and HCV RNA was analyzed via RT-qPCR. Inhibitors **66** and **76** elicited an 88% and 90% reduction in viral RNA expression, respectively (**Figure 1-20B**), suggesting that they may be promising candidates for HCV therapies. Furthermore, Huh7 cells treated with **66** and **76** for 48 h showed no reduction in cell viability at 10 or 25 μM, indicating they are capable of inhibiting miR-122 without toxicity (**Figure 1-20C**).

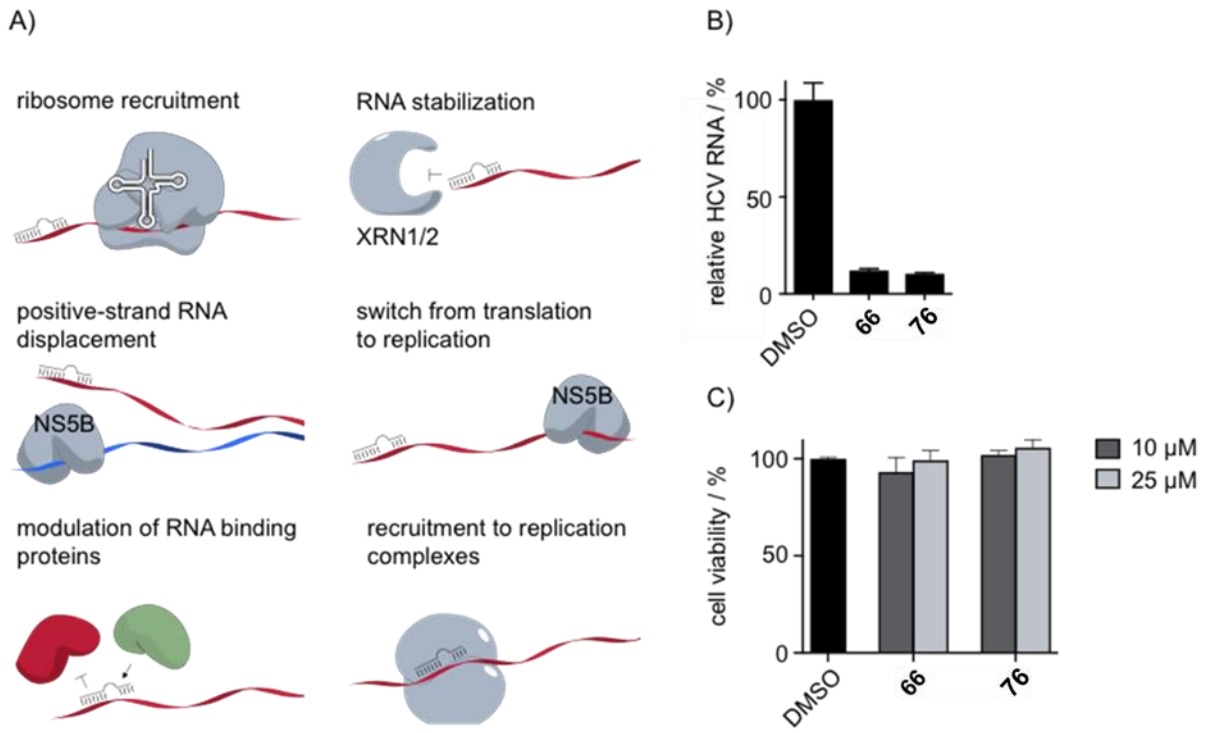

Figure 1-20 Effect of **66** and **76** on HCV RNA replication.

(A) Ago2-mediated miR-122 binding (green) to the 5-UTR of the HCV genome protects the viral RNA from Xrn1 (blue) degradation and PCBP2 (gray) binding, resulting in HCV RNA stabilization and enhanced replication. (B) Huh7.5 cells were pre-treated with **66** and **76** at 10 µM, then infected with HCV. After 48 h, RT-qPCR was performed to evaluate HCV replication. Relative expression of HCV RNA for small molecule treated cells was normalized to a DMSO control and 18S ribosomal RNA expression. (C) Huh7 cells were treated with **66** and **76** for 48 h, then an XTT assay was performed to evaluate cell viability. All data are normalized to DMSO and represents the averages ± standard deviations from three independent experiments. Data generated by Dr. Nicholas Ankenbruck.

1.4.2.1 Summary and future work

In summary, a new bis-arylsulfonamide class of small molecule miR-122 inhibitors was identified from a high-throughput screen of > 300,000 compounds. Several analogs were evaluated

in comprehensive structure-activity relationship studies, demonstrating that 5-isopropyl, 2-methoxy, and 4-methyl groups on the central benzene ring were important for miR-122 inhibitory activity. Replacement of the imidazole moiety led to the identification of several pyridine and aniline derivatives with excellent activity. Unfortunately, many of these compounds were also identified as false-positives through ligand-based stabilization of the *Renilla* luciferase (Rluc) enzyme in cells. By implementing a series of secondary assays to evaluate Rluc activity in the presence of potential hit compounds, we established that a tertiary sulfonamide moiety was required to prevent luciferase inhibition — a concept that may be generally applicable to other sulfonamides identified in screens using Rluc reporters. The miRNA inhibitor **66** was found to selectively induce downregulation of miR-122 in the Huh7-miR122 reporter cell line, while having no effect on Rluc activity in biochemical and cell-based control experiments. Furthermore, **66** did not inhibit miR-21 in the HeLa-miR21 reporter cell line, indicating that it is not a general inhibitor of the miRNA pathway. In an attempt to improve aqueous solubility of **66**, we synthesized the analog **76**. While **76** and several other analogs that we synthesized, did not improve water solubility significantly, the inhibitor displayed increased activity. Western blot analysis confirmed that the inhibitors were capable of reducing expression of E-cadherin by relieving translational repression of Wnt1 via miR-122 inhibition. Compounds **66** and **76** were shown to reduce cellular miR-122 levels to 62% and 13% at 25 μM as a result of inhibiting pri-miR-122 transcription, since pri-miR-122 levels were reduced as well. This is further supported by the observed inhibitory effects of the both compounds in a miR-122 native promoter assay. Moreover, deletion of individual transcription factor recognition sites within the miR-122 gene promoter sequence led to the discovery that compounds **66** and **76** decrease miR-122 expression presumably by inhibiting HNF4α-driven promoter activity. Since these small molecule inhibitors act at the transcriptional

level, they may be useful probes for the regulation of miR-122 expression. Most importantly, both miR-122 inhibitors **66** and **76** blocked viral HCV RNA replication in human liver cells by ~90%, indicating they may have therapeutic potential for treating HCV infection. miR-122 presents an attractive target for treatment of HCV infections because as a host component, it is much less susceptible to induction of drug resistance, and a corresponding therapeutic should be effective against all HCV genotypes,[192] in contrast to agents that directly target viral components.[193-194] Beyond applications in viral infection, small molecule-mediated inhibition of miR-122 could help further elucidate its role in metabolism and may present novel opportunities for the treatment of metabolic disorders.[195]

In the future, additional studies such as electrophoretic mobility shift assay (EMSA) or fluorescence polarization to monitor the direct binding of inhibitors **66** and **76** to HNF4α will be important. Moreover, further modifications to **76** to increase the water solubility should be attempted. A number of prodrugs approaches to increase water solubility are reported,[196] which utilize activation by selective enzymes such as esterases, phosphatases, and amidases to generate the active compound inside cells, can be pursued.

1.4.2.2 Experimentals

All reactions were performed in flame-dried glassware under a nitrogen atmosphere and stirred magnetically. Reactions were followed by thin layer chromatography (TLC) using glass-backed silica gel plates (Sorbent technologies, 250 μm thickness). Anhydrous THF and acetonitrile were purchased from Acros and anhydrous DMF was purchased from Alfa Aesar. Triethylamine was purchased from Fisher. Yields refer to pure compounds unless otherwise stated. Silica gel

flash column chromatography was performed on silica gel (60 Å, 40-63 μm, 230 × 400 mesh, Sorbtech) as a stationary phase. High resolution mass spectral analysis (HRMS) was performed on a Q-Exactive (Thermo Scientific) mass spectrometer. The ^{1}H NMR and ^{13}C NMR spectra were recorded on a 300 MHz, 400 MHz, or a 500 MHz Varian NMR spectroscope. Chemical shifts are given in δ units (ppm) for ^{1}H NMR spectra and ^{13}C NMR spectra relative to the respective solvent residual peaks ($CDCl_3$: 7.26 ppm for ^{1}H NMR and 77.16 ppm for ^{13}C NMR; CD_3OD: 3.31 ppm for ^{1}H NMR and 49.00 ppm for ^{13}C NMR; $(CD_3)_2SO$: 2.50 ppm for ^{1}H NMR and 39.52 ppm for ^{13}C NMR).[197]

Compounds **40** (PubChem CID 16644736), **41** (PubChem CID 20105566), **51** (PubChem CID 4175330), **54** (PubChem CID 20105692), and **56** (PubChem CID 163831221) were used directly from the Broad Institute compound library without re-synthesis.

1-Isopropyl-4-methoxy-2-methylbenzene (39b). To a solution of **39a** (2.0 g, 13.31 mmol, 1.0 eq) in dimethyl carbonate (11 mL, 0.133 mol, 10 eq), potassium carbonate (1.4 g, 10.13 mmol, 0.8 eq) and tetrabutylammonium bromide (2.2 g, 6.82 mmol, 0.5 eq) were added at room temperature. This suspension was refluxed for 36 h. Water (20 mL) was added to the reaction mixture and dimethyl carbonate was evaporated under reduced pressure. The aqueous layer was washed with ethyl acetate (3 × 20 mL). The combined ethyl acetate layers were washed with brine (20 mL), dried over sodium sulfate (5 g), filtered, and concentrated under reduced pressure to afford **39b** as a pale-yellow clear oil (2.2 g, quantitative yield). ^{1}H NMR (300 MHz, $CDCl_3$) δ 7.19 (d, *J*=8.31 Hz, 1 H), 6.71 – 6.81 (m, 2 H), 3.81 (s, 3 H), 3.12 (sep, *J*=6.82 Hz, 1 H), 2.36 (s, 3 H), 1.24 (d, *J*=6.80 Hz, 6 H); ^{13}C NMR (75 MHz, $CDCl_3$) δ 157.37, 139.22, 136.42, 125.74, 115.92, 111.37, 55.26, 28.76, 23.57, 19.61; HRMS (ESI) calcd. for $C_{11}H_{17}O$ $(M+H)^+$ 165.1274, found: 165.1275.

5-Isopropyl-2-methoxy-4-methylbenzenesulfonyl chloride (39c). 1-Isopropyl-4-methoxy-2-methylbenzene (1.0 g, 6.09 mmol, 1.0 eq) was dissolved in chloroform (6 mL) and the solution was cooled to 0 °C. Chlorosulfonic acid (1.2 mL, 18.02 mmol, 3.0 eq) was added dropwise to the reaction mixture and the reaction was stirred at 0 °C for 2.5 h. The reaction was poured into ice-water mixture (50 mL) and the chloroform layer was separated. The aqueous layer was washed with chloroform (3 × 20 mL). The combined chloroform layers were washed with brine (20 mL), dried over sodium sulfate (2 g), filtered, and concentrated under reduced pressure to yield **39c** as a white solid (1.2 g, 74% yield). ^{1}H NMR (400 MHz, $CDCl_3$) δ 7.76 (s, 1 H), 6.87 (s, 1 H), 4.01 (s, 3 H), 3.10 (sep, *J*=6.85 Hz, 1 H), 2.43 (s, 3 H), 1.23 (d, *J*=6.85 Hz, 6 H); ^{13}C NMR (101 MHz, $CDCl_3$) δ 154.94, 146.31, 139.54, 129.71, 126.22, 115.02, 56.66, 29.03, 23.21, 20.31.

1-((5-Isopropyl-2-methoxy-4-methylphenyl)sulfonyl)-4-methyl-1*H*-imidazole (39). To a solution of **A** (50 mg, 0.19 mmol, 1.0 eq) in anhydrous DCM (3 mL), 4-methylimidazole (47 mg, 0.57 mmol, 3.0 eq) was added at room temperature and the reaction was stirred at room temperature for 3 h. The reaction mixture was concentrated under reduced pressure. The product was purified from the crude residue by silica gel flash column chromatography (elution with 2:5 ethyl acetate/hexanes) to yield **39** as a white solid (42 mg, 72%). ^{1}H NMR (400 MHz, $CDCl_3$) δ 7.99 (s, 1 H), 7.83 (s, 1 H), 6.93 (s, 1 H), 6.73 (s, 1 H), 3.82 (s, 3 H), 3.09 (sep, *J*=6.89 Hz, 1 H), 2.38 (s, 3 H), 2.17 (s, 3 H), 1.23 (d, *J*=6.90 Hz, 6 H); ^{13}C NMR (101 MHz, $CDCl_3$) δ 154.94, 145.62, 139.94, 139.79, 137.63, 126.75, 123.18, 114.59, 113.70, 56.25, 28.99, 23.28, 20.18, 13.73; HRMS (ESI) calcd. for $C_{15}H_{21}O_3N_2S$ $(M+H)^+$ 309.1267, found: 309.1282.

1-((5-Isopropyl-2-methoxy-4-methylphenyl)sulfonyl)-1*H*-pyrrole (42). Pyrrole (10 μL, 0.13 mmol, 1.1 eq) was dissolved in anhydrous THF (3 mL) and this solution was cooled to 0 °C. NaH (5 mg, 0.13 mmol, 1.1 eq, 60% dispersion in mineral oil) was added to the solution at 0 °C and the resulting suspension was stirred at 0 °C for 15 min. Compound **39c** (30 mg, 0.11 mmol, 1.0 eq) was added to this suspension at 0 °C and the reaction mixture was stirred overnight while allowing the reaction to warm to room temperature. Water (3 mL) was slowly added to the reaction mixture while stirring at room temperature and THF was evaporated under reduced pressure. The aqueous layer was washed with ethyl acetate (3 × 5 mL) and the combined ethyl acetate layers were washed with brine (3 mL), dried over sodium sulfate (500 mg), filtered, and concentrated under reduced pressure. The product was purified from the residual solid by silica gel flash column chromatography (elution with 1:9 ethyl acetate/hexanes) to yield **42** as a white solid (24 mg, 72%). ^{1}H NMR (400 MHz, $CDCl_3$) δ 7.67 (s, 1 H), 7.19 (d, *J*=1.00 Hz, 2 H), 6.71 (s, 1 H), 6.24 (d, *J*=1.00 Hz, 2 H), 3.80 (s, 3 H), 3.06 (sep, *J*=6.89 Hz, 1 H), 2.35 (s, 3 H), 1.20 (d, *J*=6.78 Hz, 6 H); ^{13}C NMR (101 MHz, $CDCl_3$) δ 154.84, 144.46, 139.60, 126.30, 124.56, 121.50, 114.62, 111.87, 56.19, 28.92, 23.26, 20.02; HRMS (ESI) calcd. for $C_{15}H_{20}O_3NS$ $(M+H)^+$ 294.1158, found: 294.1173.

1-((5-Isopropyl-2-methoxy-4-methylphenyl)sulfonyl)-3-methyl-1*H*-pyrrole (43). 3-Methylpyrrole (11 μL, 0.13 mmol, 1.1 eq) was dissolved in anhydrous THF (3 mL) and this solution was cooled to 0 °C. NaH (5 mg, 0.13 mmol, 1.1 eq, 60% dispersion in mineral oil) was added to the solution at 0 °C and the resulting suspension was stirred at 0 °C for 15 min. Compound **39c** (30 mg, 0.11 mmol, 1.0 eq) was added to this suspension at 0 °C and the reaction mixture was stirred overnight while allowing the reaction to warm to room temperature. Water (3 mL) was slowly added to the reaction mixture while stirring at room temperature and THF was evaporated

under reduced pressure. The aqueous layer was washed with ethyl acetate (3 × 5 mL) and the combined ethyl acetate layers were washed with brine (3 mL), dried over sodium sulfate (500 mg), filtered, and concentrated under reduced pressure. The product was purified from the residual solid by silica gel flash column chromatography (elution with 1:9 ethyl acetate/hexanes) to yield **43** as a white solid (13 mg, 37%). ^{1}H NMR (400 MHz, $CDCl_3$) δ 7.62 (s, 1 H), 7.12 (br s, 1 H), 6.89 (s, 1 H), 6.71 (s, 1 H), 6.04 – 6.10 (m, 1 H), 3.81 (s, 3 H), 3.06 (sep, *J*=6.84 Hz, 1 H), 2.35 (s, 3 H), 2.04 (s, 3 H), 1.20 (d, *J*=6.90 Hz, 6 H); ^{13}C NMR (101 MHz, $CDCl_3$) δ 154.82, 144.15, 139.54, 126.26, 124.87, 122.91, 121.83, 118.34, 114.64, 113.97, 56.22, 28.94, 23.27, 20.02, 11.99; HRMS (ESI) calcd. for $C_{16}H_{22}O_3NS$ $(M+H)^+$ 308.1315, found: 308.1331.

1-((5-Isopropyl-2-methoxy-4-methylphenyl)sulfonyl)-4-methyl-1*H*-pyrazole (44). 4-Methyl-1*H*-pyrazole (11 μL, 0.13 mmol, 1.1 eq) was dissolved in anhydrous THF (3 mL) and this solution was cooled to 0 °C. NaH (5 mg, 0.13 mmol, 1.1 eq, 60% dispersion in mineral oil) was added to the solution at 0 °C and the resulting suspension was stirred at 0 °C for 15 min. Compound **39c** (30 mg, 0.11 mmol, 1.0 eq) was added to this suspension at 0 °C and the reaction mixture was stirred overnight while allowing the reaction to warm to room temperature. Water (3 mL) was slowly added to the reaction mixture while stirring at room temperature and THF was evaporated under reduced pressure. The aqueous layer was washed with ethyl acetate (3 × 5 mL) and the combined ethyl acetate layers were washed with brine (3 mL), dried over sodium sulfate (500 mg), filtered, and concentrated under reduced pressure. The product was purified from the residual solid by silica gel flash column chromatography (elution with 1:9 ethyl acetate/hexanes) to yield **44** as a white solid (17 mg, 48%). ^{1}H NMR (400 MHz, $CDCl_3$) δ 7.94 – 7.99 (m, 1 H), 7.92 (s, 1 H), 7.51 (s, 1 H), 6.69 (s, 1 H), 3.74 (s, 3 H), 3.07 (sep, *J*=6.81 Hz, 1 H), 2.36 (s, 3 H), 2.10 (s, 3 H),

1.23 (d, *J*=6.90 Hz, 6 H); ^{13}C NMR (101 MHz, $CDCl_3$) δ 155.03, 145.91, 145.30, 139.77, 130.52, 127.80, 122.43, 117.89, 114.54, 56.23, 29.07, 23.18, 20.16, 8.88; HRMS (ESI) calcd. for $C_{15}H_{21}O_3N_2S$ $(M+H)^+$ 309.1267, found: 309.1282.

1-((5-Isopropyl-2-methoxy-4-methylphenyl)sulfonyl)-3-methyl-1*H*-pyrazole (45). 3-Methyl-1*H*-pyrazole (46 μL, 0.57 mmol, 1.5 eq) was dissolved in anhydrous DMF (3 mL) and this solution was cooled to 0 °C. NaH (23 mg, 0.57 mmol, 1.5 eq, 60% dispersion in mineral oil) was added to the solution at 0 °C and the resulting suspension was stirred at 0 °C for 15 min. Compound **39c** (100 mg, 0.38 mmol, 1.0 eq) was added to this suspension at 0 °C and the reaction mixture was stirred overnight while allowing the reaction to warm to room temperature. Water (30 mL) was slowly added to the reaction mixture while stirring at room temperature and THF was evaporated under reduced pressure. The aqueous layer was washed with ethyl acetate (3 × 10 mL) and the combined ethyl acetate layers were washed with brine (10 mL), dried over sodium sulfate (1 g), filtered, and concentrated under reduced pressure. The product was purified from the residual solid by silica gel flash column chromatography (elution with 1:4 ethyl acetate/hexanes) to yield **45** as a white solid (86 mg, 73%). ^{1}H NMR (400 MHz, $CDCl_3$) δ 8.04 (d, *J*=2.69 Hz, 1 H), 7.85 (s, 1 H), 6.63 (s, 1 H), 6.09 (d, *J*=2.69 Hz, 1 H), 3.67 (s, 3 H), 3.00 (sep, *J*=6.89 Hz, 1 H), 2.29 (s, 3 H), 2.18 (s, 3 H), 1.16 (d, *J*=6.85 Hz, 6 H); ^{13}C NMR (101 MHz, $CDCl_3$) δ 154.82, 154.41, 145.09, 139.59, 133.67, 127.65, 122.40, 114.36, 107.79, 56.02, 28.96, 23.04, 20.04, 14.01; HRMS (ESI) calcd. for $C_{15}H_{21}O_3N_2S$ $(M+H)^+$ 309.1267, found: 309.1277.

1-((5-Isopropyl-2-methoxy-4-methylphenyl)sulfonyl)-4-nitro-1*H*-imidazole (48). To a solution of **39c** (30 mg, 0.11 mmol, 1.0 eq) in anhydrous THF (5 mL), 4-nitroimidazole (26 mg,

0.23 mmol, 2.0 eq), and triethylamine (64 μL, 0.46 mmol, 4.0 eq) were added at room temperature. The reaction was heated to 60 °C and stirred overnight at 60 °C. The reaction mixture was concentrated under reduced pressure. The product was purified from the residual solid by silica gel flash column chromatography (elution with 1:1 ethyl acetate/hexanes) to yield **48** as a white solid (38 mg, 98%). ^{1}H NMR (400 MHz, $CDCl_3$) δ 8.81 (s, 1 H), 8.01 (d, *J*=0.8 Hz, 1 H), 7.87 (s, 1 H), 6.794 (s, 1 H), 3.88 (s, 3 H), 3.12 (sep, *J*=6.8 Hz, 1 H), 2.42 (s, 3 H), 1.26 (d, *J*=6.8 Hz, 6 H); ^{13}C NMR (100 MHz, $CDCl_3$) δ 154.96, 147.64, 140.63, 136.25, 126.90, 121.06, 117.76, 114.73, 76.71, 56.39, 28.93, 23.12, 20.27; HRMS (ESI) calcd. for $C_{14}H_{18}O_5N_3S$ $(M+H)^+$ 340.0967, found: 340.0976.

2-Ethyl-1-((5-isopropyl-2-methoxy-4-methylphenyl)sulfonyl)-1*H*-imidazole (49). To a solution of **39c** (30 mg, 0.11 mmol, 1.0 eq) in anhydrous DCM (3 mL), 2-ethylimidazole (33 mg, 0.34 mmol, 3.0 eq) was added and the solution was cooled to 0 °C. Triethylamine (32 μL, 0.23 mmol, 2.0 eq) was added to this solution at 0 °C and the reaction was stirred for 4 h while allowing the reaction to warm to room temperature. The reaction mixture was concentrated under reduced pressure. The product was purified from the residual solid by silica gel flash column chromatography (elution with 1:1 ethyl acetate/hexanes) to yield **49** as a clear gum (39 mg, quantitative). ^{1}H NMR (400 MHz, $CDCl_3$) δ 7.82 (s, 1 H), 7.40 (d, *J*=1.6 Hz, 1 H), 6.85 (d, *J*=1.6 Hz, 1 H), 6.71 (s, 1 H), 3.74 (s, 3 H), 3.09 (sep, *J*=6.8 Hz, 1 H), 2.76 (q, *J*=7.6 Hz, 2 H), 2.37 (s, 3 H), 1.16 – 1.23 (m, 9 H); ^{13}C NMR (100 MHz, $CDCl_3$) δ 154.93, 150.69, 145.54, 139.70, 126.93, 126.35, 123.06, 120.79, 114.55, 56.13, 28.85, 23.27, 21.66, 20.13, 11.57; HRMS (ESI) calcd. for $C_{16}H_{23}O_3N_2S$ $(M+H)^+$ 323.1429, found: 323.1442.

4,5-Dichloro-1-((5-isopropyl-2-methoxy-4-methylphenyl)sulfonyl)-1*H*-imidazole (50). To a solution of **39c** (30 mg, 0.11 mmol, 1.0 eq) in anhydrous DCM (3 mL), 4,5-dichloro-1*H*-imidazole (33 mg, 0.34 mmol, 3.0 eq) was added and the solution was cooled to 0 °C. Triethylamine (32 µL, 0.23 mmol, 2.0 eq) was added to this solution at 0 °C and the reaction was stirred for 6 h while allowing the reaction to warm to room temperature. The reaction mixture was concentrated under reduced pressure. The product was purified from the residual solid by silica gel flash column chromatography (elution with 1:4 ethyl acetate/hexanes) to yield **50** as a yellow gum (41 mg, 99%). ^{1}H NMR (400 MHz, $CDCl_3$) δ 8.10 (s, 1 H), 7.93 (s, 1 H), 6.75 (s, 1 H), 3.79 (s, 3 H), 3.11 (sep, *J*=6.84 Hz, 1 H), 2.41 (s, 3 H), 1.24 (d, *J*=6.78 Hz, 6 H); ^{13}C NMR (101 MHz, $CDCl_3$) δ 155.06, 147.02, 140.06, 137.21, 129.22, 128.61, 120.64, 114.47, 112.35, 56.39, 28.93, 23.28, 20.36; HRMS (ESI) calcd. for $C_{14}H_{17}O_3N_2Cl_2S$ $(M+H)^+$ 363.0332, found: 363.0350.

1-((5-Isopropyl-2-methoxy-4-methylphenyl)sulfonyl)-1*H*-indole (52). To a suspension of indole (22 mg, 0.19 mmol, 1.0 eq) and NaOH (23 mg, 0.57 mmol, 3.0 eq) in anhydrous DCM (5 mL), tetrabutylammonium bromide (15 mg, 0.05 mmol, 0.25 eq) was added and the resulting suspension was cooled to 0 °C. Compound **39c** (50 mg, 0.19 mmol, 1.0 eq) was added to the reaction mixture at 0 °C and the reaction was stirred for 36 h while allowing the reaction mixture to warm to room temperature. Water (10 mL) was added to the reaction mixture and the DCM layer was separated. The aqueous layer was washed with DCM (3 × 5 mL) and the combined DCM layers were washed with brine (10 mL), dried over sodium sulfate (500 mg), filtered, and concentrated under reduced pressure. The product was purified from the residual solid by silica gel flash column chromatography (elution with 1:9 ethyl acetate/hexanes) to yield **52** as a white solid (35 mg, 54%). ^{1}H NMR (400 MHz, $CDCl_3$) δ 7.92 (s, 1 H), 7.75 (d, *J*=7.91 Hz, 1 H), 7.66

(d, *J*=3.76 Hz, 1 H), 7.49 – 7.58 (m, 1 H), 7.19 (m, 2 H), 6.56 – 6.63 (m, 2 H), 3.65 (s, 3 H), 3.06 (sep, *J*=6.81 Hz, 1 H), 2.30 (s, 3 H), 1.23 (d, *J*=6.90 Hz, 6 H); ^{13}C NMR (101 MHz, $CDCl_3$) δ 154.90, 144.37, 139.35, 134.81, 130.56, 128.19, 127.19, 123.85, 123.75, 122.77, 121.18, 114.46, 113.36, 106.31, 55.96, 28.86, 23.31, 19.99; HRMS (ESI) calcd. for $C_{19}H_{22}O_3NS$ $(M+H)^+$ 344.1315, found: 344.1332.

1-((3-Methoxy-5,6,7,8-tetrahydronaphthalen-2-yl)sulfonyl)-4-methyl-1*H*-imidazole (55). To a solution of 5,6,7,8-tetrahydronaphthalen-2-ol (500 mg, 3.4 mmol, 1.0 eq) in anhydrous acetonitrile (10 mL), iodomethane (252 µL, 4.1 mmol, 1.2 eq) was added at room temperature. Cesium carbonate (1.3 g, 4.1 mmol, 1.2 eq) was added to this solution at room temperature and the reaction mixture was stirred overnight at room temperature. Water (20 mL) was added to the reaction mixture and acetonitrile was evaporated under reduced pressure. The aqueous layer was washed with ethyl acetate (3 × 15 mL). The combined ethyl acetate layers were washed with brine (15 mL), dried over sodium sulfate (2 g), filtered, and concentrated under reduced pressure. The product was purified from the residual oil by silica gel flash column chromatography (elution with 1:20 ethyl acetate/hexanes) to afford 6-methoxy-1,2,3,4-tetrahydronaphthalene as a clear yellow oil (521 mg, 95% yield). ^{1}H NMR (400 MHz, $CDCl_3$) δ 6.98 (d, *J*=8.41 Hz, 1 H), 6.59 – 6.70 (m, 2 H), 3.78 (s, 3 H), 2.73 (br d, *J*=18.95 Hz, 4 H), 1.74 – 1.82 (m, 4 H); ^{13}C NMR (101 MHz, $CDCl_3$) δ 157.50, 138.30, 130.06, 129.40, 113.81, 111.90, 55.38, 29.86, 28.69, 23.58, 23.31; HRMS (ESI) calcd. for $C_{11}H_{15}O$ $(M+H)^+$ 163.1117, found: 163.1119.

6-Methoxy-1,2,3,4-tetrahydronaphthalene (50 mg, 0.31 mmol, 1.0 eq) was dissolved in chloroform (5 mL) and the solution was cooled to 0 °C. Chlorosulfonic acid (60 µL, 0.93 mmol, 3.0 eq) was added dropwise to the reaction mixture and the reaction was stirred at 0 °C for 2 h.

The reaction mixture was poured into ice-water mixture (20 mL) and the chloroform layer was separated. The aqueous layer was washed with chloroform (3 × 5 mL). The combined chloroform layers were washed with brine (10 mL), dried over sodium sulfate (500 mg), filtered, and concentrated under reduced pressure to yield 3-methoxy-5,6,7,8-tetrahydronaphthalene-2-sulfonyl chloride as a white solid (80 mg, quantitative). ^{1}H NMR (400 MHz, $CDCl_3$) δ 7.64 (s, 1 H), 6.78 (s, 1 H), 3.99 (s, 3 H), 2.71 – 2.87 (m, 4 H), 1.81 (dt, *J*=6.39, 3.35 Hz, 4 H); ^{13}C NMR (101 MHz, $CDCl_3$) δ 154.90, 148.12, 130.17, 129.64, 129.36, 113.53, 56.64, 30.36, 28.43, 22.87, 22.50.

To a solution of 3-methoxy-5,6,7,8-tetrahydronaphthalene-2-sulfonyl chloride (30 mg, 0.11 mmol, 1.0 eq) in anhydrous DCM (3 mL), 4-methylimidazole (29 mg, 0.34 mmol, 3.0 eq) was added at room temperature and the reaction was stirred at room temperature for 3 h. The reaction mixture was concentrated under reduced pressure. The product was purified from the crude residue by silica gel flash column chromatography (elution with 1:1 ethyl acetate/hexanes) to yield **55** as a white solid (23 mg, 65%). ^{1}H NMR (300 MHz, $CDCl_3$) δ 8.01 (s, 1 H), 7.73 (s, 1 H), 6.96 (s, 1 H), 6.67 (s, 1 H), 3.84 (s, 3 H), 2.73 – 2.84 (m, 4 H), 2.18 – 2.21 (m, 3 H), 1.82 (dt, *J*=6.47, 3.28 Hz, 4 H); ^{13}C NMR (75 MHz, $CDCl_3$) δ 154.83, 147.27, 137.47, 130.67, 129.90, 122.81, 113.58, 112.99, 56.09, 30.11, 28.33, 22.77, 22.39, 13.56; HRMS (ESI) calcd. for $C_{15}H_{19}O_3N_2S$ $(M+H)^+$ 307.1129, found: 307.1127.

1-((5-Isopropyl-4-methyl-2-(prop-2-yn-1-yloxy)phenyl)sulfonyl) 4-methyl-1*H*-imidazole (57). To a solution of **39a** (300 mg, 2.0 mmol, 1.0 eq) in anhydrous acetonitrile (10 mL), propargyl bromide (358 µL, 2.4 mmol, 1.2 eq, 80 wt% solution in toluene) and cesium carbonate (782 mg, 2.4 mmol, 1.2 eq) were added at room temperature. The resultant suspension was stirred overnight at room temperature. Water (20 mL) was added to the reaction mixture and acetonitrile was

evaporated under reduced pressure. The aqueous layer was washed with ethyl acetate (3 × 15 mL) and the combined ethyl acetate layers were washed with brine (20 mL), filtered, and concentrated under reduced pressure. The product was purified from the residual oil by silica gel flash column chromatography (elution with 1:20 ethyl acetate/hexanes) to afford 1-isopropyl-2-methyl-4-(prop-2-yn-1-yloxy)benzene as a pale-yellow oil (330 mg, 88% yield). ^{1}H NMR (400 MHz, $CDCl_3$) δ 7.17 (d, *J*=8.53 Hz, 1 H), 6.76 – 6.84 (m, 2 H), 4.67 (d, *J*=2.38 Hz, 2 H), 3.09 (sep, *J*=6.86 Hz, 1 H), 2.52 (t, *J*=2.38 Hz, 1 H), 2.33 (s, 3 H), 1.21 (d, *J*=6.90 Hz, 6 H) ^{13}C NMR (101 MHz, $CDCl_3$) δ 155.36, 140.19, 136.58, 125.78, 116.87, 112.25, 79.10, 75.35, 55.88, 28.80, 23.53, 19.65.

1-Isopropyl-2-methyl-4-(prop-2-yn-1-yloxy)benzene (250 mg, 1.33 mmol, 1.0 eq) was dissolved in chloroform (5 mL) and the solution was cooled to 0 °C. Chlorosulfonic acid (265 µL, 4.0 mmol, 3.0 eq) was slowly added to the reaction mixture and the reaction was stirred at 0 °C for 45 min. The reaction mixture was poured into ice-water mixture (20 mL) and the chloroform layer was separated. The aqueous layer was washed with chloroform (3 × 10 mL). The combined chloroform layers were washed with brine (20 mL), dried over sodium sulfate (2 g), filtered, and concentrated under reduced pressure to yield 5-isopropyl-4-methyl-2-(prop-2-yn-1-yloxy)benzenesulfonyl chloride as a white solid (253 mg, 66% yield). ^{1}H NMR (400 MHz, $CDCl_3$) δ 7.78 (s, 1 H), 7.04 (s, 1 H), 4.91 (d, *J*=2.26 Hz, 2 H), 3.11 (dt, *J*=13.68, 6.84 Hz, 1 H), 2.59 (t, *J*=2.32 Hz, 1 H), 2.39 – 2.48 (m, 3 H), 1.24 (d, *J*=6.90 Hz, 6 H); ^{13}C NMR (101 MHz, $CDCl_3$) δ 152.78, 146.06, 140.56, 130.53, 126.34, 116.52, 57.11, 29.12, 23.18, 20.33.

To a solution of 5-isopropyl-4-methyl-2-(prop-2-yn-1-yloxy)benzenesulfonyl chloride (30 mg, 0.10 mmol, 1.0 eq) in anhydrous DCM (3 mL), 4-methylimidazole (26 mg, 0.32 mmol, 3.0 eq) was added at room temperature and the reaction was stirred at room temperature for 3 h. The reaction mixture was concentrated under reduced pressure. The product was purified from the

crude residue by silica gel flash column chromatography (elution with 1:1 ethyl acetate/hexanes) to yield **57** as a white solid (15 mg, 43%). ^{1}H NMR (400 MHz, $CDCl_3$) δ 8.01 (s, 1 H), 7.85 (s, 1 H), 6.98 (s, 1 H), 6.83 (s, 1 H), 4.70 (d, *J*=2.26 Hz, 2 H), 3.09 (sep, *J*=6.86 Hz, 1 H), 2.57 (t, *J*=2.13 Hz, 1 H), 2.38 (s, 3 H), 2.17 (s, 3 H), 1.24 (d, *J*=6.90 Hz, 6 H); ^{13}C NMR (101 MHz, $CDCl_3$) δ 152.82, 145.45, 140.94, 139.78, 137.60, 126.89, 124.06, 115.80, 113.91, 56.90, 29.06, 23.23, 20.19, 13.71; HRMS (ESI) calcd. for $C_{17}H_{21}O_3N_2S$ $(M+H)^+$ 333.1267, found: 333.1278.

5-Isopropyl-2-methoxy-4-methyl-*N*-(pyridin-2-yl)benzenesulfonamide (58). 2-Aminopyridine (12 mg, 0.12 mmol, 1.1 eq) was dissolved in anhydrous pyridine (1 mL) and the solution was cooled to 0 °C. Compound **39c** (30 mg, 0.11 mmol, 1.0 eq) was added to this solution at 0 °C and the reaction was stirred overnight while allowing the reaction mixture to warm to room temperature. The reaction mixture was concentrated under reduced pressure. The product was purified from the crude residue by silica gel flash column chromatography (elution with 1:1 ethyl acetate/hexanes) to yield **58** as a white solid (8 mg, 22%). ^{1}H NMR (300 MHz, $CDCl_3$) δ 10.82 (br s, 1 H), 8.20 (br d, *J*=4.72 Hz, 1 H), 7.76 (s, 1 H), 7.45 – 7.52 (m, 1 H), 7.29 (d, *J*=8.69 Hz, 1 H), 6.76 (t, *J*=6.42 Hz, 1 H), 6.60 (s, 1 H), 3.60 (s, 3 H), 2.98 (sep, *J*=6.89 Hz, 1 H), 2.25 (s, 3 H), 1.13 (d, *J*=6.80 Hz, 6 H); ^{13}C NMR (101 MHz, $CDCl_3$) δ 159.47, 154.23, 153.14, 143.00, 139.04, 126.94, 124.83, 117.39, 114.10, 89.97, 56.06, 29.72, 28.74, 23.20, 19.88; HRMS (ESI) calcd. for $C_{16}H_{19}O_3N_2S$ $(M-H)^-$ 319.1111, found: 319.1116.

5-Isopropyl-2-methoxy-4-methyl-*N*-(6-methylpyridin-2-yl)benzenesulfonamide (59). To a solution of 2-amino-6-picoline (25 mg, 0.12 mmol, 1.1 eq) and pyridine (18 μL, 0.23 mmol, 2.0 eq) in anhydrous DCM (5 mL), **39c** (30 mg, 0.11 mmol, 1.0 eq) was added at room temperature.

The reaction was heated to reflux and stirred overnight. The reaction mixture was concentrated under reduced pressure. The product was purified from the crude residue by silica gel flash column chromatography (elution with 1:1 ethyl acetate/hexanes) to yield **59** as a white solid (23 mg, 60%). ^{1}H NMR (400 MHz, $CDCl_3$) δ 7.79 (s, 1 H), 7.39 – 7.44 (m, 1 H), 7.01 (br d, *J*=8.41 Hz, 1 H), 6.63 – 6.70 (m, 2 H), 3.82 (s, 3 H), 3.04 (sep, *J*=6.89 Hz, 1 H), 2.38 (s, 3 H), 2.32 (s, 3 H), 1.19 (d, *J*=6.90 Hz, 6 H); ^{13}C NMR (101 MHz, $CDCl_3$) δ 154.28, 142.67, 139.25, 126.94, 114.14, 56.30, 28.88, 23.29, 23.08, 19.98; HRMS (ESI) calcd. for $C_{17}H_{21}O_3N_2S$ $(M-H)^-$ 333.1267, found: 333.1274.

5-Isopropyl-2-methoxy-4-methyl-*N*-(3-methylpyridin-2-yl)benzenesulfonamide (60). Compound **39c** (30 mg, 0.11 mmol, 1.0 eq) and 2-amino-3-methylpyridine (23 μL, 0.23 mmol, 2.0 eq) were dissolved in anhydrous DCM (5 mL) and the solution was cooled to 0 °C. Pyridine (18 μL, 0.23 mmol, 2.0 eq) was added to this solution at 0 °C and the reaction was stirred overnight while allowing the reaction mixture to warm to room temperature. The reaction mixture was concentrated under reduced pressure. The product was purified from the crude residue by silica gel flash column chromatography (elution with 1:1 ethyl acetate/hexanes) to yield **60** as a white solid (23 mg, 60%). ^{1}H NMR (400 MHz, $CDCl_3$) δ 7.91 (s, 1 H), 7.37 – 7.52 (m, 2 H), 6.65 (s, 1 H), 6.52 (br t, *J*=6.53 Hz, 1 H), 3.58 (s, 3 H), 3.06 (sep, *J*=6.86 Hz, 1 H), 2.33 (s, 3 H), 2.14 (s, 3 H), 1.22 (d, *J*=6.90 Hz, 6 H); ^{13}C NMR (101 MHz, $CDCl_3$) δ 154.63, 140.99, 139.48, 139.00, 125.84, 113.73, 55.64, 29.02, 23.29, 19.87, 18.03; HRMS (ESI) calcd. for $C_{17}H_{21}O_3N_2S$ $(M-H)^-$ 333.1267, found: 333.1279.

5-Isopropyl-2-methoxy-4-methyl-*N*-phenylbenzenesulfonamide (61). Compound **39c** (30 mg, 0.11 mmol, 1.0 eq) and aniline (13 μL, 0.14 mmol, 1.2 eq) were dissolved in anhydrous DCM (5 mL) and the solution was cooled to 0 °C. Triethylamine (24 μL, 0.17 mmol, 1.5 eq) was added to this solution at 0 °C and the reaction was stirred overnight while allowing the reaction mixture to warm to room temperature. The reaction mixture was concentrated under reduced pressure. The product was purified from the crude residue by silica gel flash column chromatography (elution with 1:4 ethyl acetate/hexanes) to yield **61** as a white solid (26 mg, 71%). ^{1}H NMR (300 MHz, $CDCl_3$) δ 7.56 (s, 1 H), 7.06 – 7.16 (m, 2 H), 6.93 – 7.03 (m, 3 H), 6.85 (s, 1 H), 6.65 (s, 1 H), 3.90 (s, 3 H), 2.92 (sep, *J*=6.80 Hz, 1 H), 2.25 (s, 3 H), 1.06 (d, *J*=6.80 Hz, 6 H); HRMS (ESI) calcd. for $C_{17}H_{22}O_3NS$ $(M+H)^+$ 320.1315, found: 320.1335.

5-Isopropyl-2-methoxy-4-methyl-*N*-(*o*-tolyl)benzenesulfonamide (62). To a solution of **39c** (200 mg, 0.76 mmol, 1.0 eq) and *o*-toluidine (100 μL, 0.91 mmol, 1.2 eq) in anhydrous THF (5 mL), triethylamine (160 μL, 1.15 mmol, 1.5 eq) was added at room temperature. The reaction was heated to reflux and stirred overnight. The reaction mixture was concentrated under reduced pressure. The product was purified from the crude residue by silica gel flash column chromatography (elution with 1:4 ethyl acetate/hexanes) to yield **62** as a white solid (207 mg, 82%). ^{1}H NMR (300 MHz, $CDCl_3$) δ 7.66 (s, 1 H), 7.17 – 7.24 (m, 1 H), 6.92 – 7.13 (m, 3 H), 6.74 (s, 2 H), 3.94 (s, 3 H), 3.02 (sep, *J*=6.87 Hz, 1 H), 2.34 (s, 3 H), 2.25 (s, 3 H), 1.15 (d, *J*=6.80 Hz, 6 H); ^{13}C NMR (75 MHz, $CDCl_3$) δ 153.71, 142.95, 139.64, 135.48, 130.85, 130.12, 127.43, 126.87, 125.22, 124.93, 121.76, 114.13, 56.37, 28.91, 23.20, 20.00, 17.69; HRMS (ESI) calcd. for $C_{18}H_{24}O_3NS$ $(M+H)^+$ 334.1471, found: 334.1491.

5-Isopropyl-2-methoxy-*N*,4-dimethyl-*N*-(pyridin-2-yl)benzenesulfonamide (63). Compound **39c** (50 mg, 0.19 mmol, 1.0 eq) and 2-(methylamino)pyridine (39 μL, 0.38 mmol, 2.0 eq) were dissolved in anhydrous DCM (5 mL) and the solution was cooled to 0 °C. Pyridine (31 μL, 0.38 mmol, 2.0 eq) was added to this solution at 0 °C and the reaction was stirred overnight while allowing the reaction mixture to warm to room temperature. The reaction mixture was concentrated under reduced pressure. The product was purified from the crude residue by silica gel flash column chromatography (elution with 1:9 ethyl acetate/hexanes) to yield **63** as a white solid (55 mg, 86%). ^{1}H NMR (300 MHz, $CDCl_3$) δ 8.28 (d, *J*=4.72 Hz, 1 H), 7.77 (s, 1 H), 7.56 – 7.66 (m, 2 H), 6.95 – 7.04 (m, 1 H), 6.62 (s, 1 H), 3.47 (s, 3 H), 3.35 (s, 3 H), 3.06 (sep, *J*=6.82 Hz, 1 H), 2.33 (s, 3 H), 1.20 (d, *J*=6.99 Hz, 6 H); ^{13}C NMR (75 MHz, $CDCl_3$) δ 154.56, 154.38, 147.30, 143.11, 139.09, 137.15, 128.42, 123.39, 119.54, 118.45, 114.08, 55.82, 35.03, 28.87, 23.33, 19.95; HRMS (ESI) calcd. for $C_{17}H_{23}O_3N_2S$ $(M+H)^+$ 335.1424, found: 335.1436.

5-Isopropyl-2-methoxy-*N*,4-dimethyl-*N*-(6-methylpyridin-2-yl)benzenesulfonamide (64). Compound **59** (15 mg, 0.04 mmol, 1.0 eq) was dissolved in anhydrous THF (1 mL) and this solution was cooled to 0 °C. NaH (5 mg, 0.09 mmol, 2.0 eq, 60% dispersion in mineral oil) was added to the reaction mixture at 0 °C and the resulting suspension was stirred for 15 min at 0 °C. Iodomethane (15 μL, 0.23 mmol, 5.0 eq) was added to the reaction at 0 °C and the reaction was stirred overnight while allowing the reaction mixture to warm to room temperature. Water (3 mL) was added to the reaction at room temperature and THF was evaporated under reduced pressure. The aqueous layer was washed with ethyl acetate (3 × 5 mL) and the combined ethyl acetate layers were washed with brine (5 mL), dried over sodium sulfate (500 mg), filtered, and concentrated under reduced pressure. The product was purified from the crude residue by silica gel flash column

chromatography (elution with 1:9 ethyl acetate/hexanes) to yield **64** as a white solid (5 mg, 32%). ^{1}H NMR (400 MHz, $CDCl_3$) δ 7.79 (s, 1 H), 7.43 – 7.50 (m, 1 H), 7.33 (d, *J*=8.19 Hz, 1 H), 6.83 (d, *J*=7.34 Hz, 1 H), 6.63 (s, 1 H), 3.52 (s, 3 H), 3.38 (s, 3 H), 3.06 (sep, *J*=6.85 Hz, 1 H), 2.41 (s, 3 H), 2.33 (s, 3 H), 1.21 (d, *J*=6.85 Hz, 6 H); ^{13}C NMR (101 MHz, $CDCl_3$) δ 156.37, 154.54, 153.56, 142.82, 138.98, 137.46, 128.31, 124.04, 118.75, 114.64, 114.00, 55.77, 37.79, 35.06, 28.88, 24.28, 23.36, 19.98; HRMS (ESI) calcd. for $C_{18}H_{25}O_3N_2S$ $(M+H)^+$ 349.1580, found: 349.1598.

5-Isopropyl-2-methoxy-*N*,4-dimethyl-*N*-(3-methylpyridin-2-yl)benzenesulfonamide (65). Compound **60** (15 mg, 0.04 mmol, 1.0 eq) was dissolved in anhydrous THF (1 mL) and this solution was cooled to 0 °C. NaH (5 mg, 0.09 mmol, 2.0 eq, 60% dispersion in mineral oil) was added to the reaction mixture at 0 °C and the resulting suspension was stirred for 15 min at 0 °C. Iodomethane (15 μL, 0.23 mmol, 5.0 eq) was added to the reaction at 0 °C and the reaction was stirred overnight while allowing the reaction mixture to warm to room temperature. Water (3 mL) was added to the reaction at room temperature and THF was evaporated under reduced pressure. The aqueous layer was washed with ethyl acetate (3 × 5 mL) and the combined ethyl acetate layers were washed with brine (5 mL), dried over sodium sulfate (500 mg), filtered, and concentrated under reduced pressure. The product was purified from the crude residue by silica gel flash column chromatography (elution with 1:9 ethyl acetate/hexanes) to yield **65** as a white solid (11 mg, 70%). ^{1}H NMR (400 MHz, $CDCl_3$) δ 8.08 (br d, *J*=3.55 Hz, 1 H), 7.52 – 7.58 (m, 2 H), 7.05 (dd, *J*=7.46, 4.77 Hz, 1 H), 6.66 (s, 1 H), 3.57 (s, 3 H), 3.12 (s, 3 H), 2.99 (sep, *J*=6.85 Hz, 1 H), 2.47 (s, 3 H), 2.30 (s, 3 H), 1.09 (d, *J*=6.85 Hz, 6 H); ^{13}C NMR (101 MHz, $CDCl_3$) δ 154.79, 149.89, 142.61,

138.66, 128.55, 123.14, 122.75, 114.17, 55.79, 37.20, 29.72, 28.73, 23.20, 19.88, 18.69; HRMS (ESI) calcd. for $C_{18}H_{25}O_3N_2S$ $(M+H)^+$ 349.1580, found: 349.1599.

5-Isopropyl-2-methoxy-*N*,4-dimethyl-*N*-(*o*-tolyl)benzenesulfonamide (66). Compound **62** (150 mg, 0.45 mmol, 1.0 eq) was dissolved in anhydrous DMF (5 mL) and this solution was cooled to 0 °C. NaH (20 mg, 0.50 mmol, 1.1 eq, 60% dispersion in mineral oil) was added to the reaction mixture at 0 °C and the resulting suspension was stirred for 15 min at 0 °C. Iodomethane (40 μL, 0.64 mmol, 1.4 eq) was added to the reaction at 0 °C and the reaction was stirred overnight while allowing the reaction mixture to warm to room temperature. Water (50 mL) was added to the reaction at room temperature and the aqueous layer was washed with ethyl acetate (3 × 15 mL). The combined ethyl acetate layers were washed with brine (10 mL), dried over sodium sulfate (2 g), filtered, and concentrated under reduced pressure. The product was purified from the crude residue by silica gel flash column chromatography (elution with 1:9 ethyl acetate/hexanes) to yield **66** as a white solid (133 mg, 85%). ^{1}H NMR (400 MHz, $CDCl_3$) δ 7.49 (s, 1 H), 7.22 – 7.25 (m, 1 H), 7.15 (td, *J*=7.46, 1.22 Hz, 1 H), 6.94 – 7.02 (m, 1 H), 6.80 (s, 1 H), 6.68 – 6.72 (m, 1 H), 3.91 (s, 3 H), 3.28 (s, 3 H), 2.96 – 3.09 (m, 1 H), 2.38 (m, 6 H), 1.09 (d, *J*=6.85 Hz, 6 H); ^{13}C NMR (101 MHz, $CDCl_3$) δ 154.41, 142.31, 140.48, 139.17, 138.94, 131.42, 128.57, 128.24, 128.20, 126.42, 125.58, 114.14, 56.04, 39.72, 28.85, 23.20, 19.98, 18.20; HRMS (ESI) calcd. for $C_{19}H_{26}O_3NS$ $(M+H)^+$ 348.1628, found: 348.1649.

5-Isopropyl-2-methoxy-*N*,4-dimethyl-*N*-(*m*-tolyl)benzenesulfonamide (67). To a solution of **39c** (200 mg, 0.76 mmol, 1.0 eq) in anhydrous THF (10 mL), *m*-toluidine (98 μL, 0.91 mmol, 1.2 eq) and triethylamine (160 μL, 1.14 mmol, 1.5 eq) were added at room temperature. The reaction

was heated to 60 °C and stirred overnight at 60 °C. The reaction mixture was concentrated under reduced pressure. The product was purified from the residual solid by silica gel flash column chromatography (elution with 1:1 ethyl acetate/hexanes) to yield 5-isopropyl-2-methoxy-4-methyl-*N*-(*m*-tolyl)benzenesulfonamide as a white solid (159 mg, 63% yield). ^{1}H NMR (300 MHz, $CDCl_3$) δ 10.49 (br s, 1 H), 7.66 (s, 1 H), 7.02 – 7.08 (m, 1 H), 6.91 (s, 1 H), 6.79 – 6.86 (m, 2 H), 6.71 (s, 1 H), 3.96 (s, 3 H), 3.00 (sep, *J*=6.80 Hz, 1 H), 2.31 (s, 3 H), 2.23 (s, 3 H), 1.14 (d, *J*=6.88 Hz, 6 H); HRMS (ESI) calcd. for $C_{18}H_{24}O_3NS$ $(M+H)^+$ 334.14714, found: 334.14644.

5-Isopropyl-2-methoxy-4-methyl-*N*-(*m*-tolyl)benzenesulfonamide (100 mg, 0.30 mmol, 1.0 eq) was dissolved in anhydrous DMF (5 mL) and this solution was cooled to 0 °C. NaH (18 mg, 0.45 mmol, 1.5 eq, 60% dispersion in mineral oil) was added to the reaction mixture at 0 °C and the resulting suspension was stirred for 15 min at 0 °C. Iodomethane (28 μL, 0.45 mmol, 1.5 eq) was added to the reaction at 0 °C and the reaction was stirred overnight while allowing the reaction mixture to warm to room temperature. Water (50 mL) was added to the reaction at room temperature and the aqueous layer was washed with ethyl acetate (3 × 15 mL). The combined ethyl acetate layers were washed with brine (10 mL), dried over sodium sulfate (2 g), filtered, and concentrated under reduced pressure. The product was purified from the crude residue by silica gel flash column chromatography (elution with 1:9 ethyl acetate/hexanes) to yield **67** as a white solid (86 mg, 83%). ^{1}H NMR (300 MHz, $CDCl_3$) δ 7.57 (s, 1 H), 6.91 – 7.15 (m, 4 H), 6.71 (s, 1 H), 3.74 (s, 3 H), 3.31 (s, 3 H), 3.02 (sep, *J*=6.82 Hz, 1 H), 2.35 (s, 3 H), 2.27 (s, 3 H), 1.12 (d, *J*=6.80 Hz, 6 H); ^{13}C NMR (75 MHz, $CDCl_3$) δ 154.52, 142.50, 142.13, 139.05, 138.58, 128.59, 128.53, 127.08, 126.51, 124.26, 122.46, 114.03, 55.92, 38.45, 28.80, 23.23, 21.45, 19.90; HRMS (ESI) calcd. for $C_{19}H_{26}O_3NS$ $(M+H)^+$ 348.1628, found: 348.1643.

5-Isopropyl-2-methoxy-*N*,4-dimethyl-*N*-(*p*-tolyl)benzenesulfonamide (68). To a solution of **39c** (200 mg, 0.76 mmol, 1.0 eq) in anhydrous THF (10 mL), *p*-toluidine (98 mg, 0.91 mmol, 1.2 eq) and triethylamine (160 μL, 1.14 mmol, 1.5 eq) were added at room temperature. The reaction was heated to 60 °C and stirred overnight at 60 °C. The reaction mixture was concentrated under reduced pressure. The product was purified from the residual solid by silica gel flash column chromatography (elution with 1:1 ethyl acetate/hexanes) to yield 5-isopropyl-2-methoxy-4-methyl-*N*-(*p*-tolyl)benzenesulfonamide as a white solid (164 mg, 65% yield). ^{1}H NMR (300 MHz, $CDCl_3$) δ 7.60 (s, 1 H), 6.91 – 6.99 (m, 4 H), 6.73 (s, 1 H), 3.98 (s, 3 H), 2.91 – 3.07 (m, 1 H), 2.32 (s, 3 H), 2.22 (s, 3 H), 1.12 (d, *J*=6.79 Hz, 6 H); HRMS (ESI) calcd. for $C_{18}H_{24}O_3NS$ $(M+H)^+$ 334.14714, found: 334.14633.

5-Isopropyl-2-methoxy-4-methyl-*N*-(*p*-tolyl)benzenesulfonamide (100 mg, 0.30 mmol, 1.0 eq) was dissolved in anhydrous DMF (5 mL) and this solution was cooled to 0 °C. NaH (18 mg, 0.45 mmol, 1.5 eq, 60% dispersion in mineral oil) was added to the reaction mixture at 0 °C and the resulting suspension was stirred for 15 min at 0 °C. Iodomethane (28 μL, 0.45 mmol, 1.5 eq) was added to the reaction at 0 °C and the reaction was stirred overnight while allowing the reaction mixture to warm to room temperature. Water (50 mL) was added to the reaction at room temperature and the aqueous layer was washed with ethyl acetate (3 × 15 mL). The combined ethyl acetate layers were washed with brine (10 mL), dried over sodium sulfate (2 g), filtered, and concentrated under reduced pressure. The product was purified from the crude residue by silica gel flash column chromatography (elution with 1:9 ethyl acetate/hexanes) to yield **68** as a white solid (82 mg, 79%). ^{1}H NMR (400 MHz, $CDCl_3$) δ 7.54 (s, 1 H), 7.00 – 7.10 (m, 4 H), 6.71 (s, 1 H), 3.75 (s, 3 H), 3.30 (s, 3 H), 3.01 (sep, *J*=6.85 Hz, 1 H), 2.35 (s, 3 H), 2.28 (s, 3 H), 1.11 (d, *J*=6.85 Hz, 6 H); ^{13}C NMR (101 MHz, $CDCl_3$) δ 154.49, 142.45, 139.54, 139.02, 136.33, 129.42,

128.61, 126.00, 124.18, 113.99, 55.93, 38.71, 29.83, 28.80, 23.20, 21.05, 19.94, 14.26; HRMS (ESI) calcd. for $C_{19}H_{26}O_3NS$ $(M+H)^+$ 348.1628, found: 348.1639.

***N*-(2,3-dimethylphenyl)-5-isopropyl-2-methoxy-*N*,4-dimethylbenzenesulfonamide (69).** To a solution of **39c** (200 mg, 0.76 mmol, 1.0 eq) in anhydrous THF (10 mL), 2,3-dimethylaniline (113 μL, 0.91 mmol, 1.2 eq) and triethylamine (160 μL, 1.14 mmol, 1.5 eq) were added at room temperature. The reaction was heated to 60 °C and stirred overnight at 60 °C. The reaction mixture was concentrated under reduced pressure. The product was purified from the residual solid by silica gel flash column chromatography (elution with 1:2 ethyl acetate/hexanes) to yield *N*-(2,3-dimethylphenyl)-5-isopropyl-2-methoxy-4-methylbenzenesulfonamide as a white solid (143 mg, 54% yield). ^{1}H NMR (300 MHz, $CDCl_3$) δ 10.53 (br s, 1 H), 7.61 (s, 1 H), 6.85 – 6.94 (m, 3 H), 6.77 (s, 1 H), 3.97 (s, 3 H), 3.02 (sep, *J*=6.83 Hz, 1 H), 2.36 (s, 3 H), 2.24 (s, 3 H), 2.19 – 2.22 (m, 3 H), 1.13 (d, *J*=6.88 Hz, 6 H); HRMS (ESI) calcd. for $C_{19}H_{26}O_3NS$ $(M+H)^+$ 348.16279, found: 348.16206.

N-(2,3-dimethylphenyl)-5-isopropyl-2-methoxy-4-methylbenzenesulfonamide (50 mg, 0.14 mmol, 1.0 eq) was dissolved in anhydrous DMF (5 mL) and this solution was cooled to 0 °C. NaH (9 mg, 0.22 mmol, 1.5 eq, 60% dispersion in mineral oil) was added to the reaction mixture at 0 °C and the resulting suspension was stirred for 15 min at 0 °C. Iodomethane (14 μL, 0.22 mmol, 1.5 eq) was added to the reaction at 0 °C and the reaction was stirred overnight while allowing the reaction mixture to warm to room temperature. Water (50 mL) was added to the reaction at room temperature and the aqueous layer was washed with ethyl acetate (3 × 15 mL). The combined ethyl acetate layers were washed with brine (10 mL), dried over sodium sulfate (2 g), filtered, and concentrated under reduced pressure. The product was purified from the crude

residue by silica gel flash column chromatography (elution with 1:9 ethyl acetate/hexanes) to yield **39** as a white solid (47 mg, 90%). ^{1}H NMR (400 MHz, $CDCl_3$) δ 7.52 (s, 1 H), 7.11 (d, *J*=7.70 Hz, 1 H), 6.94 – 7.00 (m, 1 H), 6.81 (s, 1 H), 6.52 (s, 1 H), 3.91 (s, 3 H), 3.27 (s, 3 H), 3.04 (sep, *J*=6.80 Hz, 1 H), 2.39 (s, 3 H), 2.27 (m, 6 H), 1.11 (m, 6 H); ^{13}C NMR (101 MHz, $CDCl_3$) δ 154.42, 142.20, 140.29, 139.13, 135.97, 135.39, 131.12, 128.96, 128.73, 128.48, 125.72, 114.14, 56.01, 39.51, 28.82, 23.22, 20.80, 19.95, 17.66; HRMS (ESI) calcd. for $C_{20}H_{28}O_3NS$ $(M+H)^+$ 362.1784, found: 362.1792.

***N*-(2,5-dimethylphenyl)-5-isopropyl-2-methoxy-*N*,4-dimethylbenzenesulfonamide (70).** To a solution of **39c** (200 mg, 0.76 mmol, 1.0 eq) in anhydrous THF (10 mL), 2,5-dimethylaniline (115 μL, 0.91 mmol, 1.2 eq) and triethylamine (160 μL, 1.14 mmol, 1.5 eq) were added at room temperature. The reaction was heated to 60 °C and stirred overnight at 60 °C. The reaction mixture was concentrated under reduced pressure. The product was purified from the residual solid by silica gel flash column chromatography (elution with 1:2 ethyl acetate/hexanes) to yield *N*-(2,5-dimethylphenyl)-5-isopropyl-2-methoxy-4-methylbenzenesulfonamide as a white solid (157 mg, 59% yield). ^{1}H NMR (300 MHz, $CDCl_3$) δ 7.71 (s, 1 H), 7.06 (s, 1 H), 6.95 (d, *J*=7.70 Hz, 1 H), 6.72 – 6.77 (m, 2 H), 3.93 (s, 3 H), 3.03 (sep, *J*=6.83 Hz, 1 H), 2.34 (s, 3 H), 2.17 (s, 6 H), 1.16 (d, *J*=6.88 Hz, 6 H); HRMS (ESI) calcd. for $C_{19}H_{26}O_3NS$ $(M+H)^+$ 348.16279, found: 348.16225.

N-(2,5-dimethylphenyl)-5-isopropyl-2-methoxy-4-methylbenzenesulfonamide (50 mg, 0.14 mmol, 1.0 eq) was dissolved in anhydrous DMF (5 mL) and this solution was cooled to 0 °C. NaH (9 mg, 0.22 mmol, 1.5 eq, 60% dispersion in mineral oil) was added to the reaction mixture at 0 °C and the resulting suspension was stirred for 15 min at 0 °C. Iodomethane (14 μL, 0.22 mmol, 1.5 eq) was added to the reaction at 0 °C and the reaction was stirred overnight while

allowing the reaction mixture to warm to room temperature. Water (50 mL) was added to the reaction at room temperature and the aqueous layer was washed with ethyl acetate (3 × 15 mL). The combined ethyl acetate layers were washed with brine (10 mL), dried over sodium sulfate (2 g), filtered, and concentrated under reduced pressure. The product was purified from the crude residue by silica gel flash column chromatography (elution with 1:9 ethyl acetate/hexanes) to yield **70** as a white solid (48 mg, 92%). ^{1}H NMR (400 MHz, $CDCl_3$) δ 7.49 (s, 1 H), 7.04 (d, *J*=7.46 Hz, 1 H), 6.87 (t, *J*=7.70 Hz, 1 H), 6.81 (s, 1 H), 6.54 (d, *J*=7.82 Hz, 1 H), 3.91 (s, 3 H), 3.25 (s, 3 H), 3.03 (sep, *J*=6.85 Hz, 1 H), 2.39 (s, 3 H), 2.30 (s, 3 H), 2.12 (s, 3 H), 1.11 (d, *J*=6.90 Hz, 6 H); ^{13}C NMR (101 MHz, $CDCl_3$) δ 154.26, 142.10, 140.24, 139.03, 138.53, 137.46, 129.57, 128.43, 125.58, 125.42, 114.01, 55.93, 39.89, 28.73, 23.15, 23.02, 20.58, 19.85, 14.52; HRMS (ESI) calcd. for $C_{20}H_{28}O_3NS$ $(M+H)^+$ 362.1784, found: 362.1794.

5-Isopropyl-2-methoxy-4-methyl-*N*-(oxiran-2-ylmethyl)-*N*-(*o*-tolyl)benzene sulfonamide (71). To a stirred suspension of **62** (250 mg, 0.75 mmol, 1.0 eq) and potassium carbonate (210 mg, 1.52 mmol, 2.0 eq) in anhydrous acetonitrile (10 mL), (±)-epichlorohydrin (90 µL, 1.15 mmol, 1.5 eq) was added at room temperature. The resulting suspension is heated to 60 °C and stirred overnight. Water (30 mL) was added to the reaction and acetonitrile was evaporated under reduced pressure. The aqueous layer was washed with ethyl acetate (3 × 20 mL). The combined ethyl acetate layers were washed with brine (20 mL), dried over sodium sulfate (5 g), filtered, and concentrated under reduced pressure. The product was purified from the residual solid by silica gel flash column chromatography (elution with 1:3 ethyl acetate/hexanes) to obtain **71** as a white solid (181 mg, 0.45 mmol, 62% yield). ^{1}H NMR (500 MHz, $CDCl_3$) δ 7.43 (s, 1 H), 7.23 – 7.24 (m, 1 H), 7.15 – 7.18 (m, 1 H), 6.99 (br s, 1 H), 6.71 – 6.81 (m, 2 H), 4.01 – 4.19 (m, 1 H), 3.93

(s, 3 H), 3.52 – 3.68 (m, 1 H), 3.18 – 3.19 (m, 1 H), 3.01 (sep, *J*=6.84 Hz, 1 H), 2.65 – 2.70 (m, 1 H), 2.23 – 2.38 (m, 7 H), 1.05 – 1.09 (m, 6 H); ^{13}C NMR (126 MHz, $CDCl_3$) δ 154.14, 142.47, 139.52, 139.21, 131.27, 129.47, 128.60, 128.39, 126.31, 125.30, 114.14, 56.00, 55.23, 50.71, 49.97, 45.94, 28.70, 23.03, 19.81, 18.19; HRMS (ESI) calcd. for $C_{21}H_{28}O_4NS$ $(M+H)^+$ 390.1734, found: 390.1744.

***N*-((5-Isopropyl-2-methoxy-4-methylphenyl)sulfonyl)-*N*-(*o*-tolyl)glycine (72).** Compound **66** (50 mg, 0.15 mmol, 1.0 eq) was dissolved in anhydrous DMF (2 mL) and this solution was cooled to 0 °C. NaH (9 mg, 0.22 mmol, 1.5 eq, 60% dispersion in mineral oil) was added to the reaction at 0 °C and the resulting suspension was stirred at 0 °C for 15 min. Ethyl bromoacetate (50 μL, 0.45 mmol, 3.0 eq) was added to the reaction at 0 °C while stirring. The reaction was stirred overnight while allowing the reaction mixture to warm to room temperature. Water (20 mL) was added to the reaction mixture and the aqueous layer was washed with ethyl acetate (3 × 10 mL). The combined ethyl acetate layers were washed with brine (10 mL), dried over sodium sulfate (1 g), filtered, and concentrated under reduced pressure. The product was purified from the residual oil by silica gel flash column chromatography (elution with 1:4 ethyl acetate/hexanes) to afford ethyl *N*-((5-isopropyl-2-methoxy-4-methylphenyl)sulfonyl)-*N*-(*o*-tolyl)glycinate as a white solid (51 mg, 81%). ^{1}H NMR (400 MHz, $CDCl_3$) δ 7.44 (s, 1 H), 7.09 − 7.20 (m, 3 H), 6.97 − 7.08 (m, 1 H), 6.77 (s, 1 H), 4.23 − 4.91 (m, 2 H), 4.12 (q, *J*=7.13 Hz, 2 H), 3.88 (s, 3 H), 3.01 (sep, *J*=6.87 Hz, 1 H), 2.37 (s, 3 H), 2.28 (s, 3 H), 1.22 (t, *J*=7.15 Hz, 3 H), 1.07 (d, *J*=6.85 Hz, 6 H); ^{13}C NMR (101 MHz, $CDCl_3$) δ 169.41, 154.24, 142.55, 139.17, 138.92, 138.49, 131.24, 130.81, 128.54, 128.26, 126.24, 125.81, 114.06, 61.18, 55.99, 52.92, 28.80, 23.18, 19.99, 17.97, 14.21; HRMS (ESI) calcd. for $C_{22}H_{30}NO_5S$ $(M+H)^+$ 420.18392, found: 420.18379.

To a solution of *N*-((5-isopropyl-2-methoxy-4-methylphenyl)sulfonyl)-*N*-(*o*-tolyl)glycinate (20 mg, 0.05 mmol, 1.0 eq) in THF (1 mL), 2 N aqueous LiOH solution (1 mL) was added at room temperature. The resulting mixture was vigorously stirred at room temperature for 2 h. THF layer was separated and the aqueous layer was washed with ethyl acetate (2 × 2 mL). The ethyl acetate layers were discarded. The aqueous layer was then acidified with 1 M dilute HCl solution (3 mL) to a pH of 2. The aqueous layer was washed with ethyl acetate (3 × 5 mL). The combined ethyl acetate layers were dried over sodium sulfate (500 mg), filtered, and concentrated under reduced pressure to yield **72** as a yellow solid (12 mg, 64%). ^{1}H NMR (400 MHz, CD_3OD) δ 7.34 (s, 1 H), 7.10 − 7.21 (m, 3 H), 6.99 − 7.05 (m, 2 H), 4.48 (br s, 2 H), 3.93 (s, 3 H), 3.07 (sep, *J*=6.85 Hz, 1 H), 2.40 (s, 3 H), 2.22 (s, 3 H), 1.07 (d, *J*=6.85 Hz, 6 H); ^{13}C NMR (101 MHz, CD_3OD) δ 155.98, 144.57, 115.56, 56.53, 29.85, 23.63, 19.86, 18.27; HRMS (ESI) calcd. for $C_{20}H_{26}O_5NS$ $(M+H)^+$ 392.15262, found: 392.15261.

***N*-(2-hydroxy-3-(5-methyl-2*H*-tetrazol-2-yl)propyl)-5-isopropyl-2-methoxy-4-methyl-*N*-(*o*-tolyl)benzenesulfonamide (73).** To a solution of **71** (60 mg, 0.15 mmol, 1.0 eq) in anhydrous DMF (2 mL), 5-methyl-1*H*-tetrazole (19 mg, 0.23 mmol, 1.5 eq), synthesized by a reported procedure,[198] and potassium carbonate (43 mg, 0.31 mmol, 2.0 eq) were added at room temperature. The reaction was heated to 100 °C and stirred overnight at 100 °C. The reaction was cooled to room temperature and water (30 mL) was added to the reaction mixture. The aqueous layer was washed with ethyl acetate (3 × 10 mL). The combined ethyl acetate layers were washed with brine (10 mL), dried over sodium sulfate (1 g), filtered, and concentrated under reduced pressure. The product was purified from the residual oil by silica gel flash column chromatography (elution with 2:1 ethyl acetate/hexanes) to yield **73** as a white solid (26 mg, 36%). ^{1}H NMR (400

MHz, $CDCl_3$) δ 7.36 (s, 1 H), 7.13 − 7.24 (m, 2 H), 7.01 (br t, *J*=7.46 Hz, 1 H), 6.73 − 6.86 (m, 2 H), 4.66 − 5.02 (m, 1 H), 4.59 (dd, *J*=14.00, 7.03 Hz, 1 H), 4.01 − 4.21 (m, 2 H), 3.91 (d, *J*=6.72 Hz, 3 H), 3.61 − 3.82 (m, 1 H), 2.99 (sep, *J*=6.77 Hz, 1 H), 2.77 (br s, 1 H), 2.51 (s, 3 H), 2.26 − 2.39 (m, 6 H), 1.00 − 1.09 (m, 6 H); ^{13}C NMR (101 MHz, $CDCl_3$) δ 163.15, 154.18, 143.15, 139.65, 138.15, 131.66, 129.96, 129.28, 128.95, 128.69, 126.68, 124.35, 114.47, 68.37, 56.73, 56.41, 56.23, 55.47, 28.80, 23.13, 20.00, 18.44, 11.00; HRMS (ESI) calcd. for $C_{23}H_{32}N_5O_4S$ $(M+H)^+$ 474.21695, found: 474.21621.

***N*-(2-hydroxy-3-(5-phenyl-2*H*-tetrazol-2-yl)propyl)-5-isopropyl-2-methoxy-4-methyl- *N*-(*o*-tolyl)benzenesulfonamide (74).** To a solution of **71** (125 mg, 0.32 mmol, 1.0 eq) in anhydrous DMF (3 mL), 5-phenyl-1*H*-tetrazole (55 mg, 0.38 mmol, 1.2 eq), synthesized by a reported procedure,[198] and potassium carbonate (67 mg, 0.49 mmol, 1.5 eq) were added at room temperature. The reaction was heated to 100 °C and stirred overnight at 100 °C. The reaction was cooled to room temperature and water (30 mL) was added to the reaction mixture. The aqueous layer was washed with ethyl acetate (3 × 15 mL). The combined ethyl acetate layers were washed with brine (10 mL), dried over sodium sulfate (2 g), filtered, and concentrated under reduced pressure. The product was purified from the residual oil by silica gel flash column chromatography (elution with 1:1 ethyl acetate/hexanes) to yield **74** as a white solid (112 mg, 65%). ^{1}H NMR (400 MHz, $CDCl_3$) δ 8.09 (br d, *J*=3.67 Hz, 2 H), 7.99 (s, 1 H), 7.44 − 7.49 (m, 2 H), 7.36 (s, 1 H), 7.13 − 7.24 (m, 2 H), 7.00 (br t, *J*=6.72 Hz, 1 H), 6.75 − 6.86 (m, 2 H), 5.08 (dd, *J*=14.06, 3.18 Hz, 1 H), 4.77 − 5.14 (m, 1 H), 4.68 − 4.76 (m, 1 H), 4.21 − 4.33 (m, 1 H), 4.08 − 4.18 (m, 1 H), 3.90 (d, *J*=11.86 Hz, 3 H), 3.68 − 3.84 (m, 1 H), 2.95 − 3.04 (m, 2 H), 2.31 − 2.39 (m, 6 H), 0.98 − 1.10 (m, 6 H); ^{13}C NMR (101 MHz, $CDCl_3$) δ 165.26, 162.75, 154.20, 143.15, 139.45, 138.88, 138.33,

131.66, 130.51, 129.85, 129.34, 128.76, 128.66, 127.31, 127.26, 126.98, 126.68, 124.31, 114.47, 68.45, 57.25, 56.36, 55.51, 36.71, 31.63, 28.78, 23.11, 19.98, 18.47; HRMS (ESI) calcd. for $C_{28}H_{34}N_5O_4S$ $(M+H)^+$ 536.23260, found: 536.23278.

***N*-(2-hydroxy-3-(5-(pyrimidin-2-yl)-2*H*-tetrazol-2-yl)propyl)-5-isopropyl-2-methoxy-4-methyl-*N*-(*o*-tolyl)benzenesulfonamide (75).** To a solution of **71** (62 mg, 0.16 mmol, 1.0 eq) in anhydrous DMF (3 mL), 2-(1*H*-tetrazol-5-yl)pyrimidine (29 mg, 0.19 mmol, 1.2 eq), synthesized by a reported procedure,[198] and potassium carbonate (35 mg, 0.25 mmol, 1.5 eq) were added at room temperature. The reaction was heated to 100 °C and stirred overnight at 100 °C. The reaction was cooled to room temperature and water (30 mL) was added to the reaction mixture. The aqueous layer was washed with ethyl acetate (3 × 15 mL). The combined ethyl acetate layers were washed with brine (10 mL), dried over sodium sulfate (2 g), filtered, and concentrated under reduced pressure. The product was purified from the residual oil by silica gel flash column chromatography (elution with 2:1 ethyl acetate/hexanes) to yield **75** as a white solid (30 mg, 95%). ^{1}H NMR (400 MHz, $CDCl_3$) δ 8.87 (br s, 2 H), 7.24 − 7.47 (m, 2 H), 7.04 − 7.17 (m, 2 H), 6.93 (q, *J*=7.50 Hz, 1 H), 6.65 − 6.84 (m, 2 H), 4.87 − 5.38 (m, 1 H), 4.68 − 4.85 (m, 1 H), 3.58 − 4.37 (m, 6 H), 2.85 − 2.96 (m, 2 H), 2.16 − 2.32 (m, 6 H), 0.97 (br dd, *J*=15.89, 6.72 Hz, 6 H); ^{13}C NMR (101 MHz, $CDCl_3$) δ 158.07, 153.89, 143.15, 139.30, 138.54, 138.01, 131.14, 129.55, 129.07, 128.81, 128.68, 128.60, 126.70, 124.34, 121.78, 114.10, 68.24, 60.51, 57.38, 56.52, 56.28, 55.43, 28.77, 23.11, 19.97, 18.43; HRMS (ESI) calcd. for $C_{26}H_{32}N_7O_4S$ $(M+H)^+$ 538.22310, found: 538.22288.

***N*-(2-hydroxy-3-(5-(pyridin-2-yl)-2*H*-tetrazol-2-yl)propyl)-5-isopropyl-2-methoxy-4-methyl-*N*-(*o*-tolyl)benzenesulfonamide (76).** Compound **71** (124 mg, 0.32 mmol, 1.0 eq) was added to a

stirred suspension of 2-(1*H*-tetrazol-5-yl)pyridine (56 mg, 0.38 mmol, 1.2 eq), synthesized by a reported procedure,[198] and potassium carbonate (66 mg, 0.48 mmol, 1.5 eq) in anhydrous DMF (5 mL) at room temperature. The resulting suspension was heated to 100 °C and stirred overnight. Water (50 mL) was added to the reaction mixture and the aqueous layer was washed with ethyl acetate (3 × 15 mL). The combined ethyl acetate layers were washed with brine (15 mL), dried over sodium sulfate (2 g), filtered, and concentrated under reduced pressure. The product was purified from the residual solid by silica gel flash column chromatography (elution with 1:1 ethyl acetate/hexanes) to yield **76** as a white solid (99 mg, 58% yield). ^{1}H NMR (500 MHz, $CDCl_3$) δ 8.68 (br s, 1 H), 8.26 – 8.33 (m, 1 H), 7.96 (dt, *J*=15.14, 7.76 Hz, 1 H), 7.48 – 7.55 (m, 1 H), 7.34 (br d, *J*=7.63 Hz, 1 H), 7.09 – 7.24 (m, 2 H), 6.74 – 7.07 (m, 3 H), 5.20 – 5.43 (m, 1 H), 4.90 – 5.02 (m, 1 H), 3.67 – 4.34 (m, 7 H), 2.98 (sep, *J*=6.79 Hz, 1 H), 2.20 – 2.47 (m, 6 H), 0.98 – 1.08 (m, 6 H); ^{13}C NMR (126 MHz, $CDCl_3$) δ 154.19, 148.95, 144.11, 139.27, 138.45, 131.47, 131.40, 129.31, 128.91, 128.70, 128.36, 126.52, 126.40, 125.32, 114.22, 69.71, 69.25, 56.77, 56.33, 56.13, 52.76, 52.52, 28.67, 23.03, 19.83, 18.59, 18.05; HRMS (ESI) calcd. for $C_{27}H_{33}O_4N_6S$ $(M+H)^+$ 537.2278, found: 537.2265.

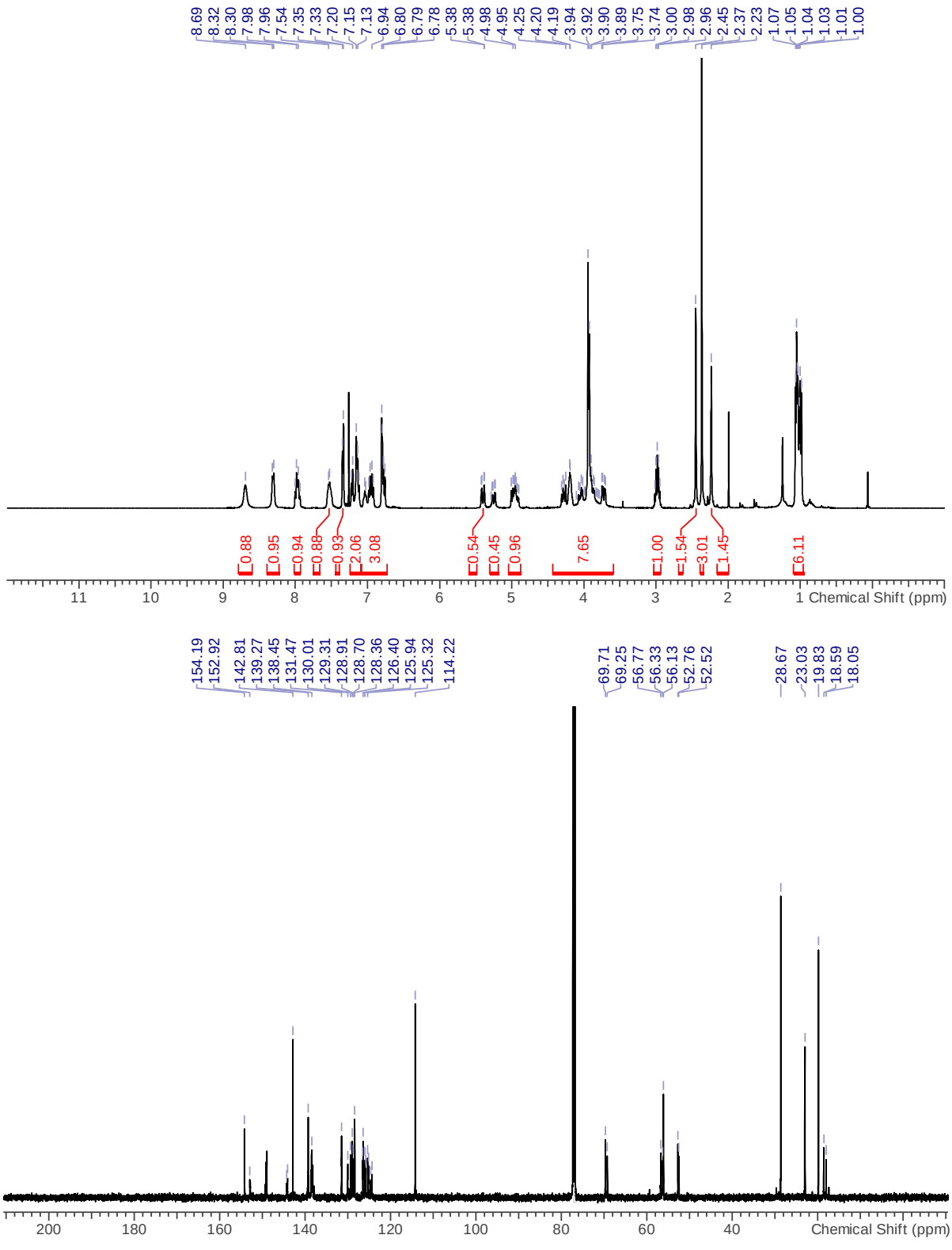

Figure 1-21 ^{1}H and ^{13}C (1D NMR) spectra of **76**.

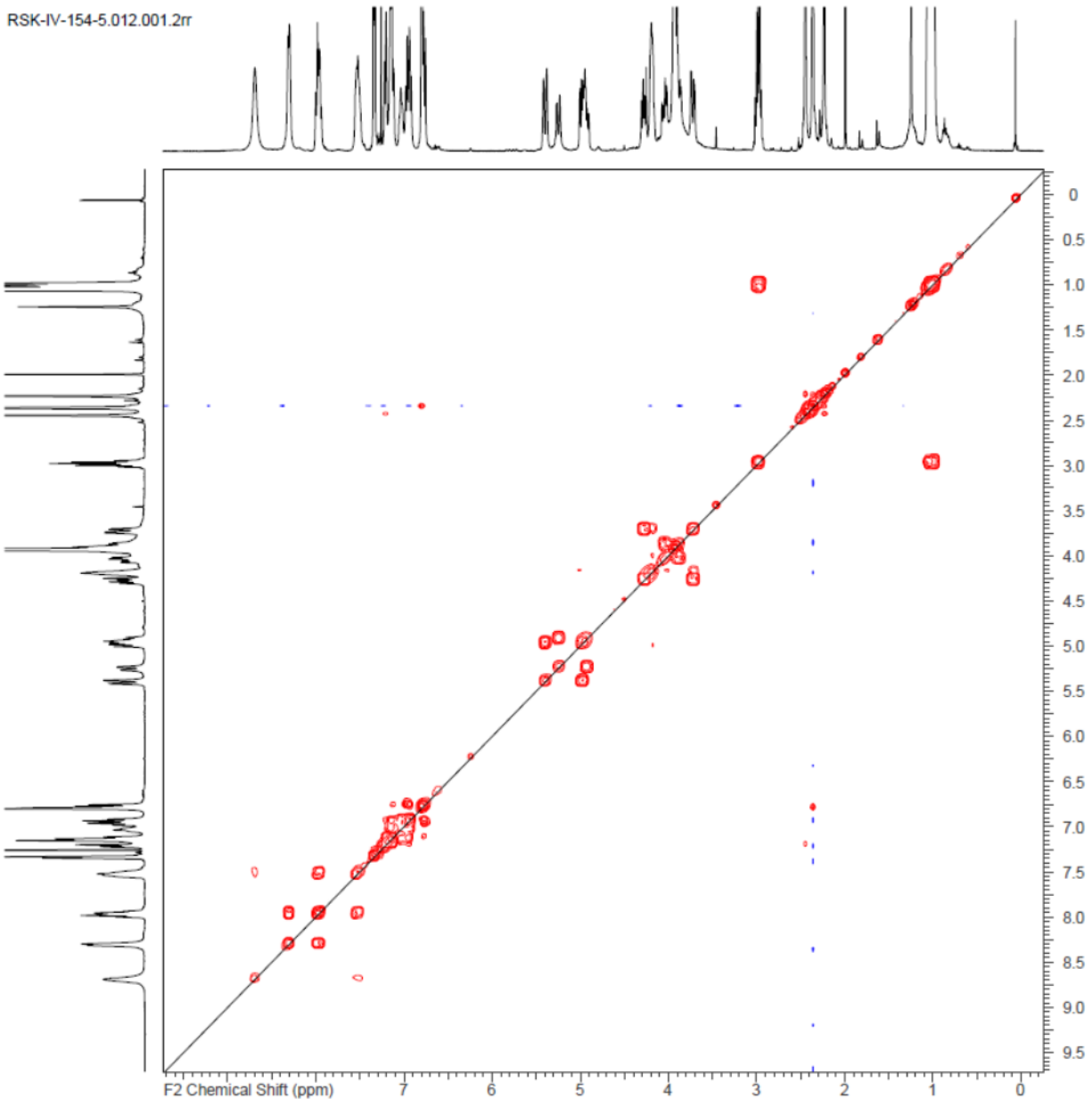

Figure 1-22 ^{1}H-^{1}H correlation spectroscopy (COSY) spectrum of **76**.

The cross peaks represent ^{1}H-^{1}H three-bond correlation between different protons.

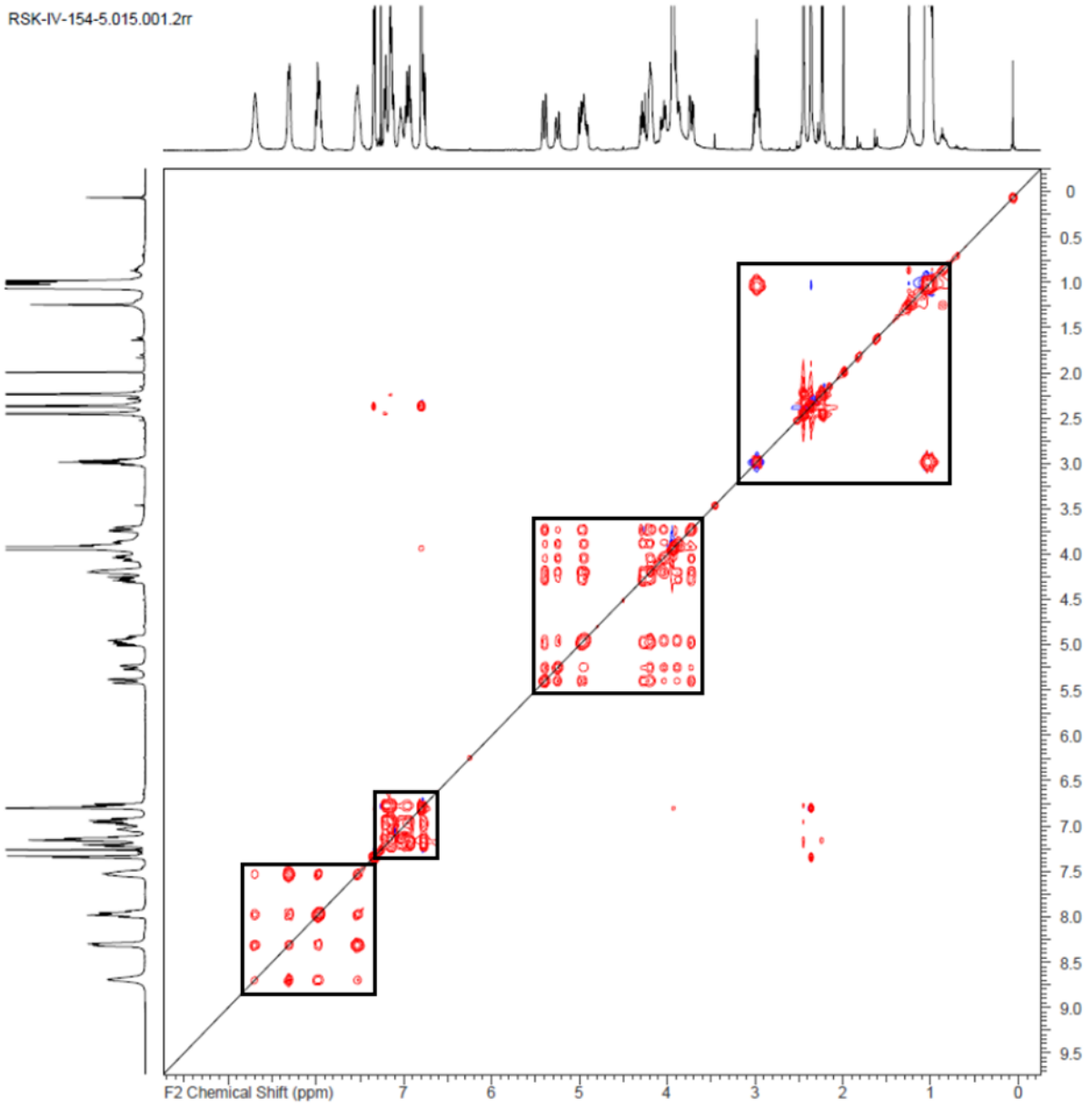

Figure 1-23 ^{1}H-^{1}H total correlation spectroscopy (TOCSY) spectrum of **76**.

TOCSY spectrum shows correlations between all protons within a given spin system. The spin systems are highlighted by boxes.

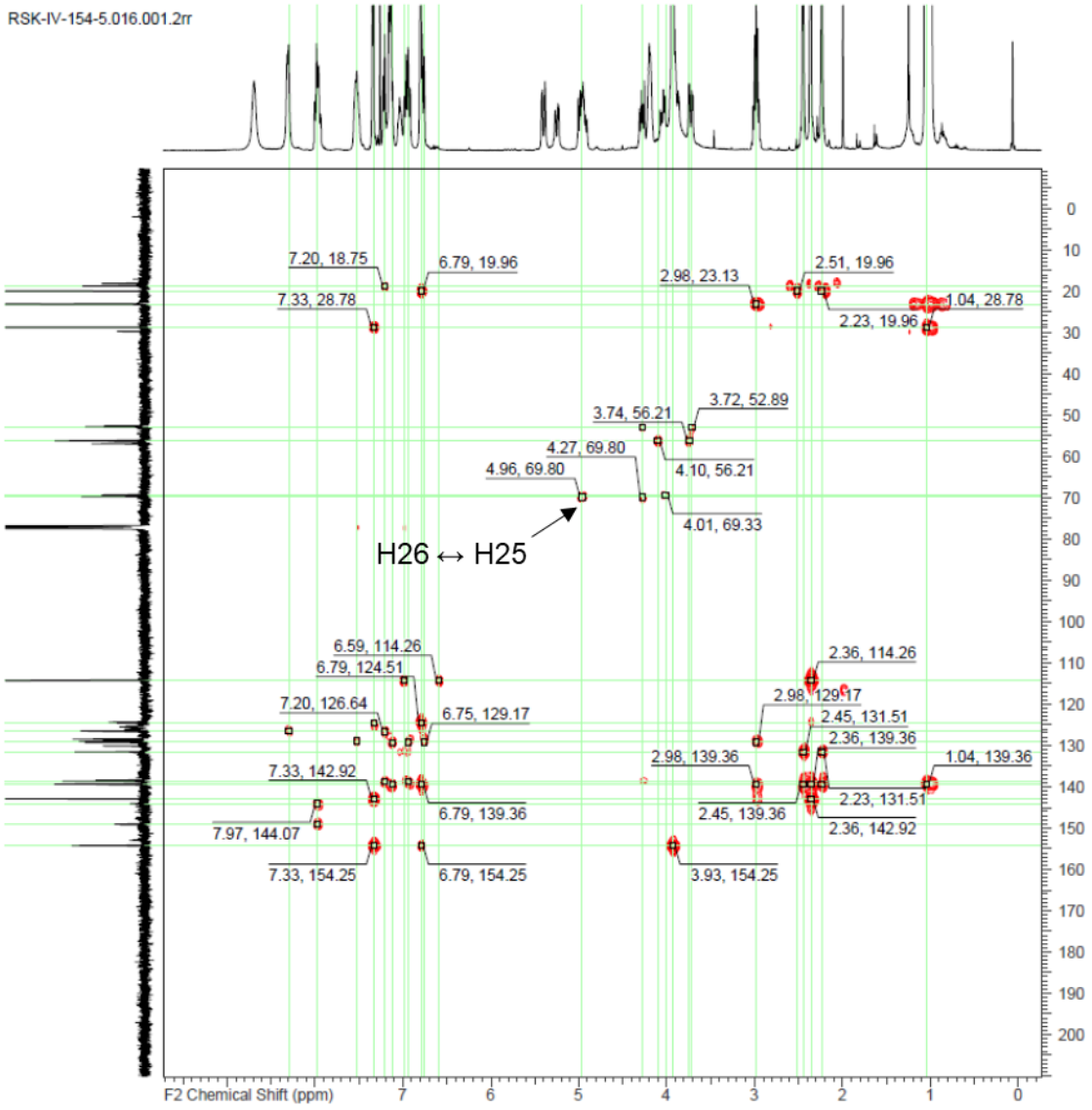

Figure 1-24 ^{1}H-^{13}C heteronuclear single quantum correlation (HSQC) spectrum of **76**.

HSQC spectrum shows correlations between carbons and its attached protons ($^{1}J_{CH}$ couplings). The ^{1}H-^{13}C correlations are identified and highlighted by corresponding ppm values with ^{1}H spectrum on the horizontal axis and ^{13}C spectrum on the vertical axis.

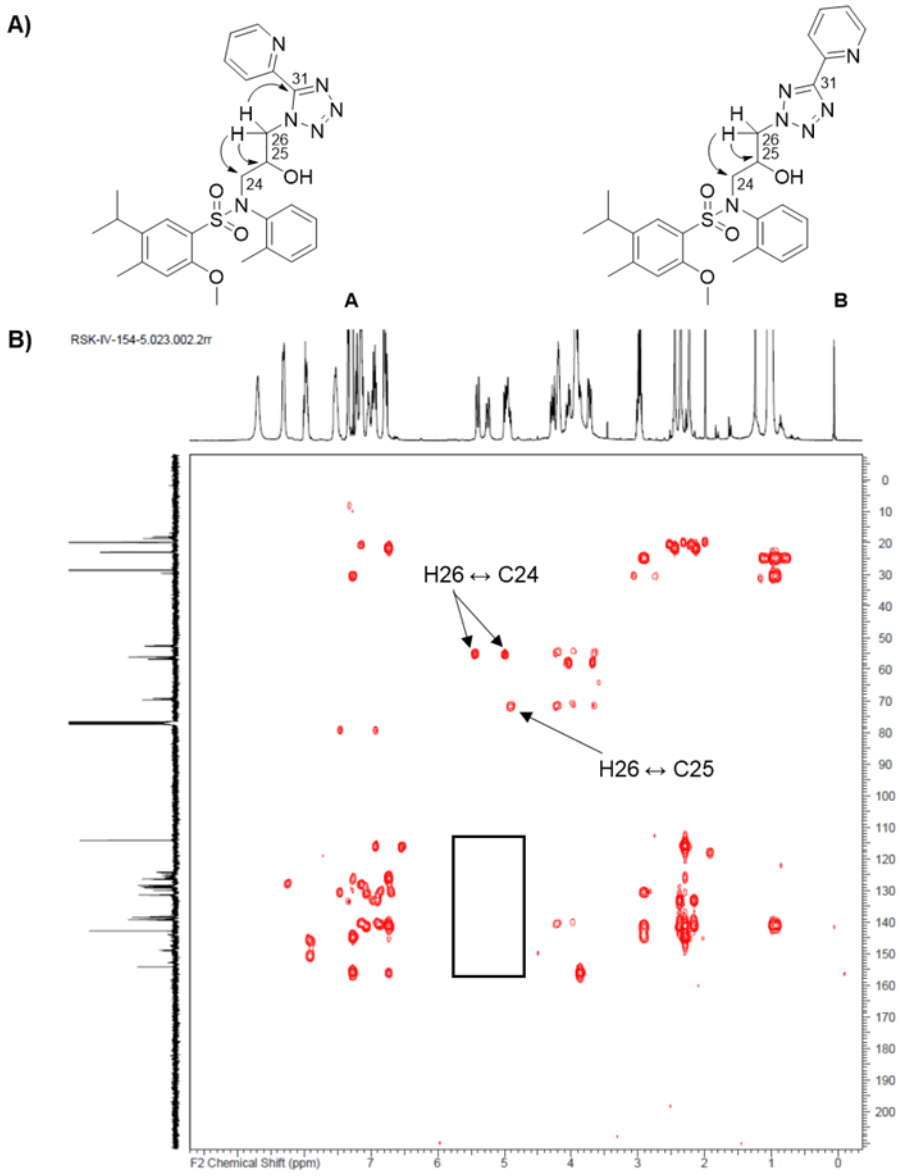

Figure 1-25 ^{1}H-^{13}C heteronuclear multiple bond correlation (HMBC) spectrum of **76**.

(A) Chemical structures of isomers **A** and **B** with the expected correlation peaks in the ^{1}H-^{13}C heteronuclear multiple bond correlation (HMBC) spectrum shown by arrows. (B) HMBC spectrum of **76**. HMBC spectrum gives long-range correlations between carbons and protons that are two or three chemical bonds apart. The ^{1}H-^{13}C correlations between H26 ↔ C24 (three-bond correlation) and H26 ↔ C24 (two-bond correlation) are pointed out, while no H26 ↔ C31 (three-bond correlation) was observed in the spectrum (region highlighted by box) indicating the presence of isomer **B**. The ^{1}H spectrum is on the horizontal axis and ^{13}C spectrum on the vertical axis with corresponding scales (ppm).

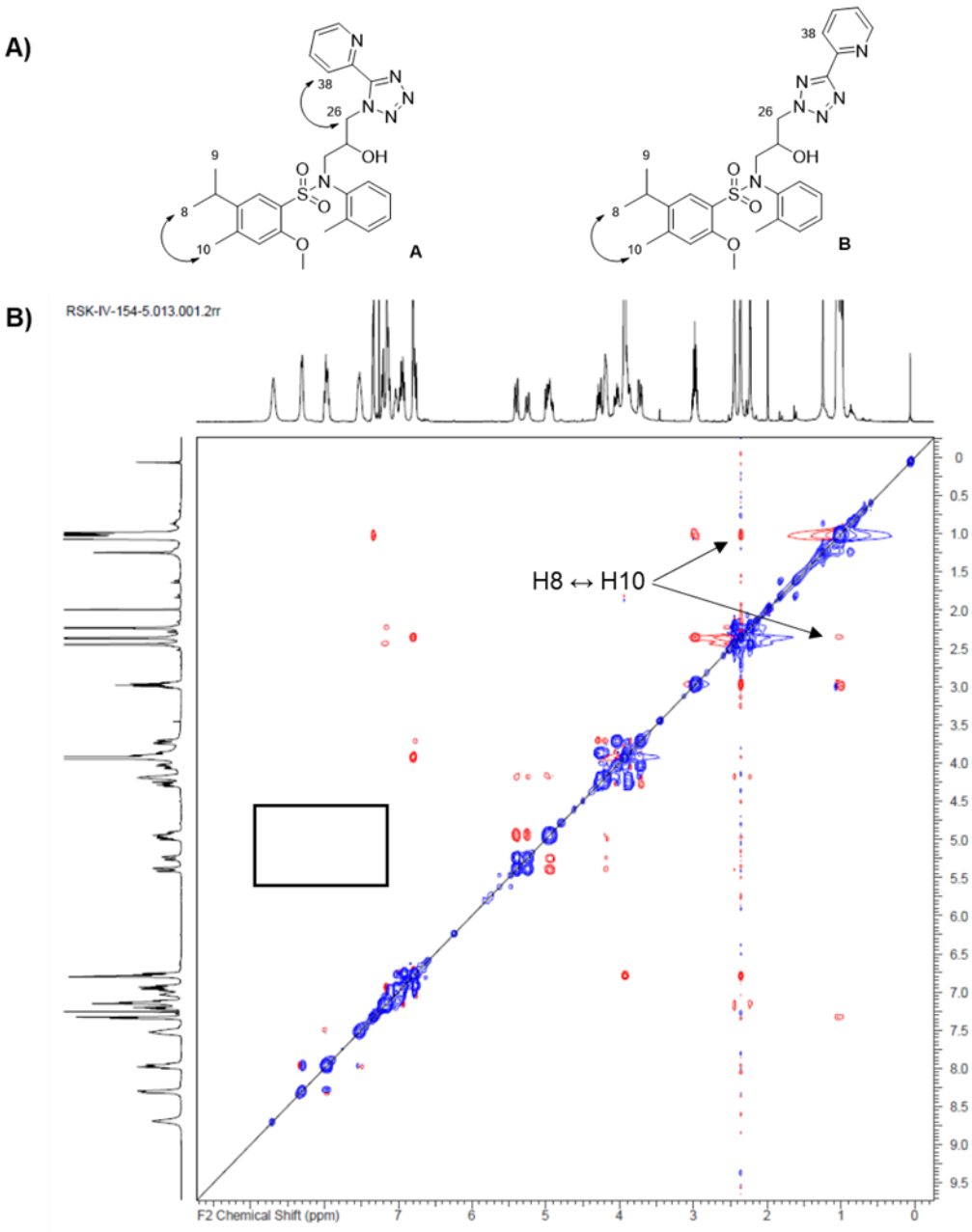

Figure 1-26 2D rotational frame nuclear Overhauser effect spectroscopy (ROESY) spectrum of **76**.

(A) Chemical structures of isomers **A** and **B** with the spatially close protons highlighted by left right arrows. (B) 2D rotational frame nuclear Overhauser effect spectroscopy (ROESY) spectrum of **76**. The red and blue colors represent opposite phases of the peaks. For reference, H8 ↔ H10 cross peak was observed in the spectrum. (highlighted by arrows). No such cross peaks were observed between H26 ↔ H38 (highlighted by box) suggesting the presence of isomer **B**.

1.4.3 Synthesis and SAR studies of non-sulfonamide series of miR-122 inhibitors

Among the final 34 shortlisted compounds from the high-throughput screening of small molecules in the miR-122 assay,[108] many with sulfonamide scaffolds were found to be *Renilla* luciferase inhibitors. A powder re-test of these 34 compounds from the Broad Institute was conducted by Dr. Meryl Thomas and revealed **77** to be a potent miR-122 inhibitor without a sulfonamide scaffold. The lead compound **77** exhibited a 423% increase in luciferase activity compared to DMSO-treated control cells (Huh7-miR122 stable cell line), but unfortunately elicited a ~2-fold increase in luciferase signal in the psiCHECK-empty assay, suggesting that **77** can induce non-specific inhibition. In dose-response studies, **77** exhibited an EC_{50} value of 196 nM. An *in vitro Renilla* luciferase (Rluc) assay revealed that **77** decreased *Renilla* luciferase activity by 31%, indicating some degree of Rluc inhibition shown by **77** (**Table 1-5**). A RT-qPCR analysis showed that miR-122 levels decreased by 15% after treatment with **77** (10 μM), suggesting that **77** is a potential miR-122 inhibitor and a good candidate to conduct SAR studies with a view to increase the miR-122 inhibition and reduce the extent of Rluc binding.

To elucidate the SAR, the piperazine ring was kept constant and changes to either end of the ring — the ethoxybenzene part and the biphenyl part — were made. The small molecule inhibitor **77** was synthesized by direct amide coupling between piperazine **77c** and carboxylic acid **77b** with 1-ethyl-3-(3-dimethylaminopropyl)carbodiimide (EDC) as a coupling agent, in the presence of triethylamine and 4-dimethylaminopyridine (DMAP) in DCM (**Figure 1-27**).[199] The pure product was obtained only by HPLC purification on a portion of the reaction mixture in 46% yield. Otherwise, the general synthetic route was to activate the carboxylic acid **78a** on the biphenyl part by formation of acid chloride using oxalyl chloride and catalytic DMF in DCM solvent. This reaction mixture was concentrated under reduced pressure to obtain the acid chloride

78b.[200] This acid chloride was directly used in the next reaction with different phenylpiperazines **78c** in the presence of triethylamine as a base in DCM as the solvent to yield analogs of compound **77** (compounds **78–99, Figure 1-27**).[201]

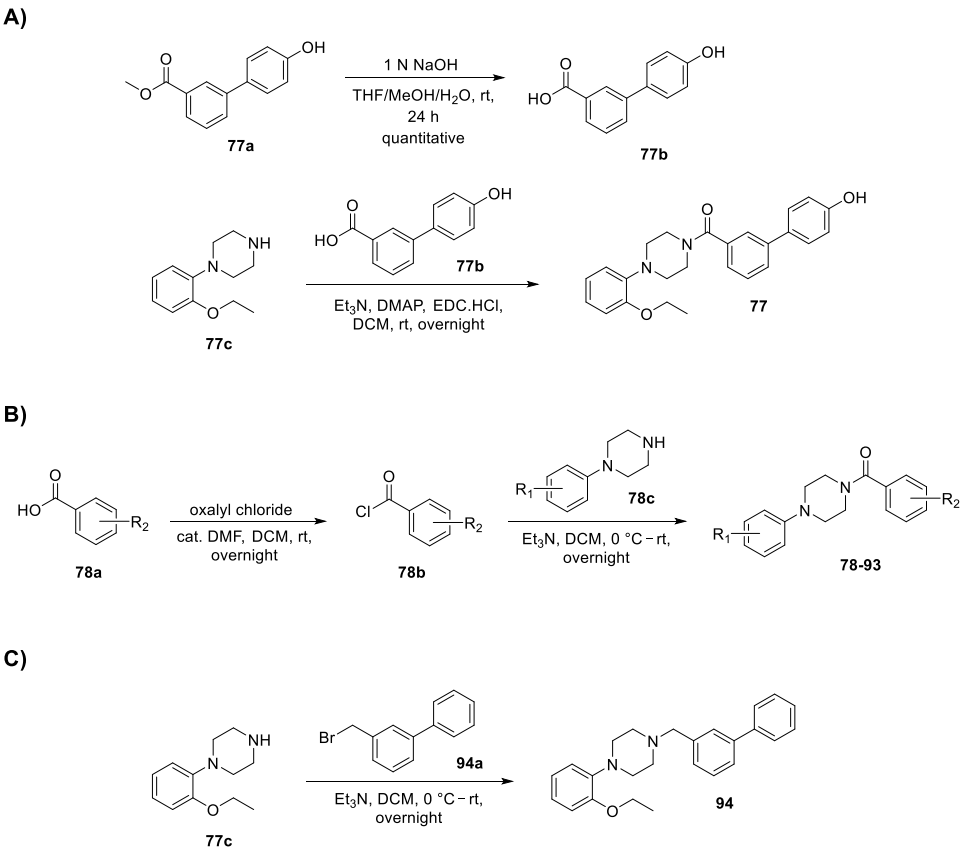

Figure 1-27 Synthetic route for synthesis of non-sulfonamide series of miR-122 inhibitors.

(A) The ester **77a** was hydrolyzed to obtain carboxylic acid **77b**, which was then coupled to piperazine **77c** to yield initial hit **77**. (B) Analogs for SAR studies were synthesized by activating the carboxylic acids **78a** with oxalyl chloride to obtain the acid chlorides **78b**, and then addition to piperazines **78c**. (C) Compound **94** was synthesized by substitution reaction between **77c** and **94a**.

In the first set of analogs (**78** and **79**), the hydroxy group on the biphenyl part was replaced with trifluoromethyl and methyl groups (**Table 1-7**). The methyl group constitutes a space-filling,

non-H-bonding substitute for hydroxy group, while the CF_3 group substitutes for the hydroxyl group with polar F-bonding (similar to H-bonding) capabilities with similar spatial constraints. Both the substitutions resulted in significant loss of activity – the activity decreased to 59% and 29% for methyl and CF_3 analog in the primary screen, respectively. The omission of the hydroxyl group (replacement of OH by H) in compound **80** gave the second-best analog in this series, with 80% activity compared to initial hit **77**. Next, a series of analogs were made by altering the substitutions of the biphenyl group. The different orientations for the biphenyl group in compounds **81** and **82** imparted 20% and 18% activity compared to **77**. Thus, the 1,3-isomer of the biphenyl group in **77** is important for activity. A diphenyl ether modification at the place of biphenyl group (**83**) is tolerable, with comparable activity to **80**. Gratifyingly, *in vitro* Rluc activity of **83** was observed to be 99%, indicating no undesired *Renilla* luciferase inhibition.

Table 1-7 Structures and activity of derivatives **77-83**.

RLU values represent *Renilla* luciferase luminescence signal in the Huh7-psiCHECK-miR122 stable cell line normalized to firefly luciferase and relative to **77**.

In vitro Renilla luciferase and psiCHECK-empty assay data are normalized to DMSO.

Data represents the average ± standard deviation from at least three independent experiments.

Data generated by Dr. Nicholas Ankenbruck.

compound	chemical structure	primary screen (RLU)	*Renilla* luciferase assay	psiCHECK-empty assay
77	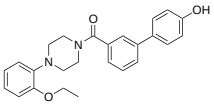	100 ± 9%	69%	1.8-fold
78	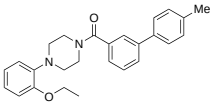	59 ± 12%	--	--
79	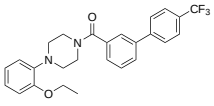	29 ± 4%	--	--
80	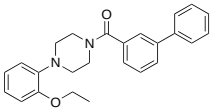	80 ± 7%	--	--
81	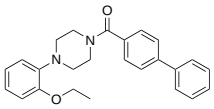	20.4 ± 0.9%	--	--
82	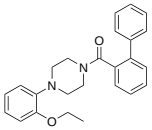	18 ± 1%	--	--
83	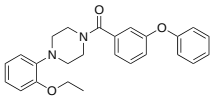	72 ± 8%	99%	--

Compounds **84-87** were synthesized and tested to measure the effect of changes on the ethoxybenzene part (**Table 1-8**). The removal of the ethoxy group in **84** resulted in significant reduction in activity. Analogs **85**, **86**, **87** and **88** exhibited lower activity (55%, 61%, 48% and 50%, respectively) than **77** and **80.** Further, modifying the ethyl part of the ethoxy group to methyl

(**89**) resulted in loss of the activity compared to **80**, indicating the importance of ethoxy group. To study the orientation of ethoxy group, compounds **89** and **90** were synthesized and tested with a methoxy group as a substitute for ethoxy group. Both analogs **89** and **90** elicited an activity of 26% and 36% respectively, compared to 55% activity by **85**. Thus, 1,2-orientation of methoxy (or ethoxy) group relative to the piperazine core is beneficial to maintain potency.

Table 1-8 Structures and activity of derivatives **84**-**90**.

RLU values represent *Renilla* luciferase luminescence signal in the Huh7-psiCHECK-miR122 stable cell line normalized to firefly luciferase and relative to **77**.

In vitro Renilla luciferase and psiCHECK-empty assay data are normalized to DMSO.

Data represents the average ± standard deviation from at least three independent experiments.

Data generated by Dr. Nicholas Ankenbruck.

Compound	chemical structure	primary screen (RLU)
84	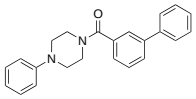	45 ± 3%
85	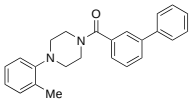	55 ± 4%
86	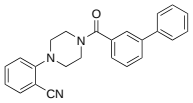	61.1 ± 0.5%
87	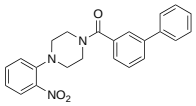	48 ± 2%
88	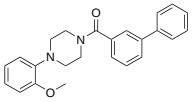	50 ± 2%
89	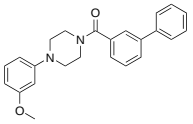	26 ± 2%
90	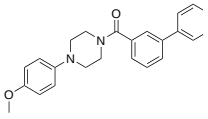	36.0 ± 0.3%

Another set of analogs was synthesized and tested to study the importance of the biphenyl substituent. Analog **91**, having a hydroxyphenyl group, exhibited a huge loss of activity, reduced to 29% of the activity showed by **77** (**Table 1-9**). Moreover, substitution of the biphenyl group with a phenyl group in **92** reduced activity to levels comparable with **91**. Modifying the biphenyl

moiety with a fused naphthalene ring in compound **93** elicited a deleterious effect, with 26% activity. Finally, a non-amide analog **94** with an alkyl amine modification elicited a 36% activity compared to **77**. Compound **94** was synthesized by piperazine **77c** substitution with alkyl bromide **94a** (**Scheme 1.2C**).

Table 1-9 Structures and activity of derivatives **91-97**.

RLU values represent *Renilla* luciferase luminescence signal in the Huh7-psiCHECK-miR122 stable cell line normalized to firefly luciferase and relative to **77**.

In vitro Renilla luciferase and psiCHECK-empty assay data are normalized to DMSO.

Data represents the average ± standard deviation from at least three independent experiments.

Data generated by Dr. Nicholas Ankenbruck.

Compound	chemical structure	primary screen (RLU)
91	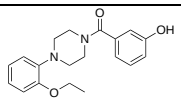	29 ± 2%
92	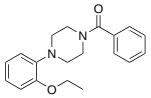	28 ± 5%
93	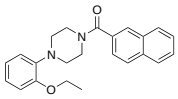	26 ± 2%
94	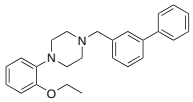	36 ± 3%

Two of the top analogs, **77** and **83**, were further studied for miR-122 inhibitory activity, A dose-response study showed EC_{50} values of compounds **77** and **83** to be 2.0 µM and 9.6 µM, respectively in the Huh7-psiCHECK-miR122 stable cell line.

1.4.3.1 Summary and future work

In summary, a high-throughput screening and powder re-test revealed **77** as a lead compound for miR-122 inhibition. The SAR studies were conducted with the objective of improving the potency of the lead compound for miR-122 inhibition and reducing off-target Rluc inhibition. The SAR studies targeted various moieties in compound **77** while keeping the piperazine core as a constant. It was established that the hydroxy group in **77** and the 1,3-position of the biphenyl group are important to maintain activity. Furthermore, the presence and position of the ethoxy group was crucial for miR-122 inhibition. Replacement of biphenyl group with substituted phenols and fused ring systems resulted in loss of miR-122 inhibitory activity. Moreover, non-amide linkages also diminished activity. Unfortunately, none of the analogs synthesized were better than the lead compound, and further modifications will be necessary for lead optimization.

Upon close investigation of the current SAR and analysis of the top three inhibitors, **83** shows that a diphenyl ether is tolerable in comparison to biphenyl group and this can be the path forward to pursue for the further analog synthesis. Importantly, **83** showed minimum Rluc inhibition as observed by *Renilla* luciferase assay indicating that this modification holds promise for further SAR analysis. In addition, *in vitro Renilla* luciferase and psiCHECK-empty assay data of some of the best analogs like **80** and **83** needs to be recorded.

1.4.3.2 Experimentals

All reactions were performed in flame-dried glassware under a nitrogen atmosphere and

stirred magnetically. Reactions were followed by thin layer chromatography (TLC) using glass-backed silica gel plates (Sorbent Technologies, 250 μm thickness). Anhydrous acetonitrile and tetrahydrofuran (THF) were purchased from Acros and anhydrous toluene and dimethylformamide (DMF) were purchased from Alfa Aesar. Silica gel flash column chromatography was performed on silica gel (60 Å, 40–63 μm, 230 × 400 mesh, Sorbtech) as a stationary phase. High resolution mass spectral analysis (HRMS) was performed on a Q-Exactive (Thermo Scientific) mass spectrometer. The ^{1}H NMR and ^{13}C NMR spectra were recorded on a 300 MHz or 400 MHz Varian NMR spectroscope. Chemical shifts are given in δ units (ppm) for ^{1}H NMR spectra and ^{13}C NMR spectra relative to the respective solvent residual peaks ($CDCl_3$: 7.26 ppm for ^{1}H NMR and 77.16 ppm for ^{13}C NMR; CD_3OD: 3.31 ppm for ^{1}H NMR and 49.00 ppm for ^{13}C NMR; $(CD_3)_2SO$: 2.50 ppm for ^{1}H NMR and 39.52 ppm for ^{13}C NMR).[197]

(4-(2-Ethoxyphenyl)piperazin-1-yl)(4'-hydroxy-[1,1'-biphenyl]-3-yl)methanone (77). 1-Ethyl-3-(3-dimethylaminopropyl)carbodiimide hydrochloride (70 mg, 0.36 mmol, 1.5 eq) was added to a stirred solution of **77c** (50 mg, 0.24 mmol, 1.0 eq) and **77b** (52 mg, 0.24 mmol, 1.0 eq) in anhydrous DCM (5 mL) at room temperature. Triethylamine (100 μL, 0.73 mmol, 3.0 eq) and DMAP (3 mg, 0.02 mmol, 0.1 eq) were subsequently added at room temperature and the reaction mixture was stirred overnight at room temperature. Water (10 mL) was added to the reaction mixture and the DCM layer was separated. The aqueous layer was washed with ethyl acetate (3 × 5 mL). The combined ethyl acetate layers were washed with brine (5 mL), dried over sodium sulfate (2 g), filtered, and concentrated under reduced pressure. Purification of the product by silica gel column chromatography was unsuccessful. So, product **77** (2.3 mg) was purified by reverse-

phase HPLC from a portion (5.0 mg) of crude **77** (46% yield). ^{1}H NMR (300 MHz, $CDCl_3$) δ 7.48 − 7.56 (m, 2 H), 7.23 − 7.43 (m, 1 H), 7.21 − 7.44 (m, 3 H), 6.72 − 7.11 (m, 6 H), 5.99 − 6.29 (m, 1 H), 4.02 (q, *J*=6.92 Hz, 4 H), 3.47 − 3.83 (m, 2 H), 2.81 − 3.33 (m, 4 H), 1.39 (br t, *J*=6.89 Hz, 4 H). LRMS (ESI) calcd. for $C_{25}H_{27}O_3N_2$ $(M+H)^+$ 403.20, found: 403.00.

General procedure for synthesis of compounds 78-97.

Oxalyl chloride (0.36 – 0.44 mmol, 2.0 eq) was added dropwise to a solution of carboxylic acids **78a** (0.18 – 0.22 mmol, 1.0 eq) in anhydrous DCM (5 mL) at room temperature. DMF (0.04 mmol, 0.1 eq) was added to this solution and the reaction mixture was stirred overnight at room temperature. The reaction mixture was concentrated under reduced pressure. The residual acid chloride **78b** was confirmed by NMR and used in the next reaction without any purification. Compounds **78b** were dissolved in anhydrous DCM (5 mL) and this solution was cooled to 0 °C. Piperazines **78c** (0.22 – 0.26 mmol, 1.2 eq) and triethylamine (0.27 – 0.33 mmol, 1.5 eq) were added dropwise to this solution at 0 °C, and the reaction mixture was warmed to room temperature, and stirred overnight at room temperature. On complete consumption of **78b** as confirmed by TLC, the reaction mixture was concentrated under reduced pressure and the residual mass was loaded onto silica gel column. Compounds **78-97** were purified by elution with 1:5 ethyl acetate/hexanes in 25-95% yields.

(4-(2-Ethoxyphenyl)piperazin-1-yl)(4'-methyl-[1,1'-biphenyl]-3-yl)methanone (78). 84 mg, 87% yield; ^{1}H NMR (400 MHz, $CDCl_3$) δ 7.61 − 7.68 (m, 2 H), 7.46 − 7.54 (m, 3 H), 7.37 − 7.42 (m, 1 H), 7.25 − 7.30 (m, 3 H), 7.02 (br s, 1 H), 6.84 − 6.97 (m, 3 H), 3.94 − 4.13 (m, 4 H), 3.66

(br s, 2 H), 3.19 (br s, 2 H), 2.93 − 3.12 (m, 2 H), 2.41 (s, 3 H), 1.46 (t, *J*=6.91 Hz, 3 H); ^{13}C NMR (101 MHz, $CDCl_3$) δ 170.56, 151.68, 141.65, 137.74, 137.57, 137.51, 136.45, 129.76, 129.09, 128.33, 127.10, 125.68, 121.18, 112.60, 63.78, 21.25, 15.05; HRMS (ESI) calcd. for $C_{26}H_{29}O_2N_2$ $(M+H)^+$ 401.2224, found: 401.2219.

(4-(2-Ethoxyphenyl)piperazin-1-yl)(4'-(trifluoromethyl)-[1,1'-biphenyl]-3-yl) methanone (79). 79 mg, 72% yield; ^{1}H NMR (300 MHz, $CDCl_3$) δ 7.58 − 7.82 (m, 6 H), 7.42 − 7.58 (m, 2 H), 6.83 − 7.05 (m, 4 H), 3.93 − 4.17 (m, 4 H), 3.65 (br s, 2 H), 3.19 (br s, 2 H), 2.95 − 3.13 (m, 2 H), 1.45 (t, *J*=6.89 Hz, 3 H); ^{13}C NMR (75 MHz, $CDCl_3$) δ 170.00, 151.61, 143.80, 140.26, 136.77, 130.06, 129.63, 129.20, 128.49, 127.48, 126.72, 126.04, 125.87, 123.51, 121.08, 118.58, 118.52, 112.60, 63.68, 14.94; HRMS (ESI) calcd. for $C_{26}H_{26}O_2N_2F_3$ $(M+H)^+$ 455.1941, found: 455.1935.

[1,1'-Biphenyl]-3-yl(4-(2-ethoxyphenyl)piperazin-1-yl)methanone (80). 78 mg, 83% yield; ^{1}H NMR (400 MHz, $CDCl_3$) δ 7.51 − 7.60 (m, 4 H), 7.28 − 7.45 (m, 5 H), 6.77 − 6.96 (m, 4 H), 3.88 − 4.04 (m, 4 H), 3.57 (br s, 2 H), 3.11 (br s, 2 H), 2.89 − 3.04 (m, 2 H), 1.37 (t, *J*=6.97 Hz, 3 H); ^{13}C NMR (101 MHz, $CDCl_3$) δ 170.37, 151.58, 141.62, 140.64, 140.31, 136.45, 129.03, 128.93, 128.90, 128.41, 127.75, 127.18, 125.88, 125.80, 123.45, 121.05, 118.48, 112.48, 77.27, 63.64, 51.26, 50.54, 48.16, 42.46, 42.38, 14.96; HRMS (ESI) calcd. for $C_{25}H_{27}O_2N_2$ $(M+H)^+$ 387.2067, found: 387.2073.

[1,1'-Biphenyl]-4-yl(4-(2-ethoxyphenyl)piperazin-1-yl)methanone (81). 49 mg, 52% yield; ^{1}H NMR (400 MHz, $CDCl_3$) δ 7.57 − 7.68 (m, 4 H), 7.50 − 7.57 (m, 2 H), 7.43 − 7.50 (m, 2 H), 7.35 − 7.42 (m, 1 H), 6.79 − 7.13 (m, 4 H), 4.09 (q, *J*=6.97 Hz, 2 H), 3.80 − 4.03 (m, 2 H), 3.56 − 3.80

(m, 2 H), 3.18 (br s, 2 H), 2.94 − 3.13 (m, 2 H), 1.46 (t, *J*=6.91 Hz, 3 H); ^{13}C NMR (101 MHz, $CDCl_3$) δ 170.43, 151.69, 142.79, 140.75, 140.38, 134.67, 130.71, 129.02, 127.92, 127.86, 127.43, 127.35, 127.29, 127.19, 123.55, 121.16, 118.56, 112.60, 63.76, 15.05; HRMS (ESI) calcd. for $C_{25}H_{27}O_2N_2$ $(M+H)^+$ 387.2067, found: 387.2070.

[1,1'-Biphenyl]-2-yl(4-(2-ethoxyphenyl)piperazin-1-yl)methanone (82). 26 mg, 28% yield; ^{1}H NMR (400 MHz, $CDCl_3$) δ 7.37 (br s, 1 H), 7.30 − 7.56 (m, 10 H), 6.90 − 7.02 (m, 1 H), 6.77 − 6.90 (m, 2 H), 6.64 (br d, *J*=6.85 Hz, 1 H), 4.00 (q, *J*=6.93 Hz, 2 H), 3.87 (br s, 1 H), 3.53 − 3.77 (m, 1 H), 3.10 − 3.20 (m, 1 H), 3.00 − 3.09 (m, 1 H), 2.90 − 3.00 (m, 1 H), 2.64 − 2.74 (m, 1 H), 2.52 − 2.64 (m, 1 H), 1.87 (br s, 1 H), 1.38 (t, *J*=6.97 Hz, 3 H); HRMS (ESI) calcd. for $C_{25}H_{27}O_2N_2$ $(M+H)^+$ 387.2067, found: 387.2071.

(4-(2-Ethoxyphenyl)piperazin-1-yl)(3-phenoxyphenyl)methanone (83). 33 mg, 34% yield; ^{1}H NMR (400 MHz, $CDCl_3$) δ 7.32 − 7.39 (m, 3 H), 7.32 − 7.39 (m, 1 H), 7.10 − 7.18 (m, 3 H), 6.98 − 7.08 (m, 6 H), 6.84 − 6.96 (m, 3 H), 4.07 (q, *J*=6.97 Hz, 2 H), 3.94 (br s, 2 H), 3.56 − 3.69 (m, 2 H), 3.14 (br s, 2 H), 3.01 (br s, 2 H), 1.45 (t, *J*=6.97 Hz, 3 H); HRMS (ESI) calcd. for $C_{25}H_{27}O_3N_2$ $(M+H)^+$ 403.2016, found: 403.2016.

[1,1'-Biphenyl]-3-yl(4-phenylpiperazin-1-yl)methanone (84). 69 mg, 83% yield; ^{1}H NMR (300 MHz, $CDCl_3$) δ 7.25 − 7.72 (m, 10 H), 6.89 − 7.04 (m, 2 H), 3.99 (br s, 1 H), 3.48 − 3.83 (m, 2 H), 3.22 (br s, 3 H); ^{13}C NMR (75 MHz, $CDCl_3$) δ 170.59, 170.44, 150.71, 141.70, 141.61, 140.23, 140.02, 136.09, 132.19, 130.05, 129.32, 129.05, 128.93, 128.82, 128.59, 127.81, 127.78, 127.18,

127.16, 125.88, 125.84, 120.98, 116.92, 50.05; HRMS (ESI) calcd. for $C_{23}H_{23}ON_2$ $(M+H)^+$ 343.1805, found: 343.1812.

[1,1'-Biphenyl]-3-yl(4-(*o*-tolyl)piperazin-1-yl)methanone (85). 83 mg, 93% yield; ^{1}H NMR (400 MHz, $CDCl_3$) δ 7.58 − 7.70 (m, 4 H), 7.36 − 7.53 (m, 5 H), 7.16 − 7.23 (m, 2 H), 7.00 − 7.05 (m, 2 H), 3.98 (br s, 2 H), 3.56 − 3.81 (m, 2 H), 3.01 (br s, 2 H), 2.88 (br s, 2 H), 2.34 (s, 3 H); ^{13}C NMR (101 MHz, $CDCl_3$) δ 170.51, 150.84, 141.72, 140.39, 136.51, 132.82, 131.34, 129.13, 129.03, 128.52, 127.85, 127.27, 126.83, 125.96, 125.89, 123.97, 119.35, 17.95; HRMS (ESI) calcd. for $C_{24}H_{25}ON_2$ $(M+H)^+$ 357.1961, found: 357.1969.

2-(4-([1,1'-Biphenyl]-3-carbonyl)piperazin-1-yl)benzonitrile (86). 68 mg, 76% yield; ^{1}H NMR (300 MHz, $CDCl_3$) δ 7.35 − 7.70 (m, 11 H), 6.95 − 7.14 (m, 2 H), 3.88 − 4.10 (m, 2 H), 3.73 (br s, 2 H), 3.24 (br s, 4 H); ^{13}C NMR (75 MHz, $CDCl_3$) δ 170.44, 155.12, 141.74, 140.23, 136.12, 134.35, 133.90, 128.91, 128.58, 127.77, 127.15, 125.83, 125.86, 119.07, 118.02, 106.80, 77.76, 76.79; HRMS (ESI) calcd. for $C_{24}H_{22}ON_3$ $(M+H)^+$ 368.1757, found: 368.1761.

[1,1'-Biphenyl]-3-yl(4-(2-nitrophenyl)piperazin-1-yl)methanone (87). 41 mg, 44% yield; ^{1}H NMR (300 MHz, $CDCl_3$) δ 7.79 (dd, *J*=8.12, 1.51 Hz, 1 H), 7.37 − 7.67 (m, 10 H), 7.09 − 7.21 (m, 2 H), 3.97 (br s, 2 H), 3.50 − 3.81 (m, 2 H), 2.84 − 3.32 (m, 4 H); ^{13}C NMR (75 MHz, $CDCl_3$) δ 170.58, 145.69, 144.40, 141.82, 140.32, 136.20, 133.72, 129.17, 129.04, 128.94, 128.70, 127.90, 127.27, 125.94, 123.25, 121.80; HRMS (ESI) calcd. for $C_{23}H_{22}O_3N_3$ $(M+H)^+$ 388.1656, found: 388.1659.

[1,1'-Biphenyl]-3-yl(4-(2-methoxyphenyl)piperazin-1-yl)methanone (88). 78 mg, 81% yield; ^{1}H NMR (400 MHz, $CDCl_3$) δ 7.58 − 7.68 (m, 4 H), 7.35 − 7.52 (m, 5 H), 6.87 − 6.97 (m, 1 H), 6.86 − 7.08 (m, 1 H), 6.85 − 7.09 (m, 1 H), 6.79 − 7.14 (m, 1 H), 6.76 − 7.17 (m, 1 H), 3.58 − 4.11 (m, 7 H), 2.91 − 3.26 (m, 4 H); ^{13}C NMR (101 MHz, $CDCl_3$) δ 170.42, 152.36, 141.73, 140.69, 140.41, 136.48, 129.13, 129.04, 128.53, 127.86, 127.29, 125.99, 125.91, 123.77, 121.21, 118.63, 111.46, 55.56, 53.57, 51.39, 50.79; HRMS (ESI) calcd. for $C_{20}H_{28}O_3NS$ $(M+H)^+$ 362.1784, found: 362.1792.

[1,1'-Biphenyl]-3-yl(4-(4-methoxyphenyl)piperazin-1-yl)methanone (90). 19 mg, 20% yield; ^{1}H NMR (300 MHz, $CDCl_3$) δ 7.56 − 7.73 (m, 4 H), 7.33 − 7.55 (m, 5 H), 6.81 − 7.06 (m, 4 H), 3.44 − 4.26 (m, 7 H), 2.88 − 3.33 (m, 4 H); ^{13}C NMR (75 MHz, $CDCl_3$) δ 170.47, 141.85, 140.36, 129.19, 129.07, 128.73, 127.92, 127.30, 126.02, 125.97, 119.48, 114.81, 55.73; HRMS (ESI) calcd. for $C_{24}H_{25}O_2N_2$ $(M+H)^+$ 373.1911, found: 373.1926.

(4-(2-Ethoxyphenyl)piperazin-1-yl)(3-hydroxyphenyl)methanone (91). 62 mg, 64% yield; ^{1}H NMR (400 MHz, $CDCl_3$) δ 7.78 (br s, 1 H), 7.17 − 7.24 (m, 1 H), 6.76 − 7.12 (m, 7 H), 4.08 (q, *J*=6.89 Hz, 2 H), 3.98 (br s, 2 H), 3.63 (br s, 2 H), 3.17 (br s, 2 H), 2.90 − 3.10 (m, 2 H), 1.45 (t, *J*=6.97 Hz, 3 H); ^{13}C NMR (101 MHz, $CDCl_3$) δ 170.94, 157.08, 151.67, 136.26, 129.82, 121.21, 118.25, 117.65, 114.80, 76.99, 63.82, 15.05; HRMS (ESI) calcd. for $C_{19}H_{23}O_3N_2$ $(M+H)^+$ 327.1703, found: 327.1713.

(4-(2-Ethoxyphenyl)piperazin-1-yl)(naphthalen-2-yl)methanone (93). 63 mg, 70% yield; ^{1}H NMR (300 MHz, $CDCl_3$) δ 7.83 − 7.94 (m, 5 H), 7.51 − 7.60 (m, 4 H), 6.84 − 6.96 (m, 3 H), 4.08

(q, *J*=6.92 Hz, 4 H), 3.70 (br s, 2 H), 3.20 (br s, 2 H), 2.93 − 3.14 (m, 2 H), 1.45 (t, *J*=6.99 Hz, 3 H); HRMS (ESI) calcd. for $C_{23}H_{25}O_2N_2$ $(M+H)^+$ 361.1911, found: 361.1917.

(4-(2-Ethoxyphenyl)piperazin-1-yl)(phenyl)methanone (92). Benzoyl chloride (34 µL, 0.29 mmol, 1.2 eq) was added to a stirred solution of **77c** (50 mg, 0.24 mmol, 1.0 eq) in anhydrous DCM (5 mL) at 0 °C. Triethylamine (51 µL, 0.36 mmol, 1.5 eq) was added dropwise to this solution at 0 °C and the resulting reaction mixture was stirred overnight while allowing to warm to room temperature. On complete consumption of **77c** as confirmed by TLC, the reaction mixture was concentrated under reduced pressure and the residual mass was loaded onto a silica gel column. Compound **92** was purified as a white solid by elution with 1:4 ethyl acetate/hexanes (61 mg, 79% yield). ^{1}H NMR (300 MHz, $CDCl_3$) δ 7.32 − 7.54 (m, 5 H), 6.83 − 7.05 (m, 4 H), 3.91 − 4.13 (m, 4 H), 3.62 (br s, 2 H), 3.16 (br s, 2 H), 2.91 − 3.11 (m, 2 H), 1.45 (t, *J*=6.89 Hz, 3 H); ^{13}C NMR (75 MHz, $CDCl_3$) δ 170.59, 151.74, 135.99, 129.82, 128.64, 127.25, 123.60, 121.20, 112.72, 63.81, 15.06; HRMS (ESI) calcd. for $C_{19}H_{23}O_2N_2$ $(M+H)^+$ 311.1754, found: 311.1760.

1-([1,1'-Biphenyl]-3-ylmethyl)-4-(2-ethoxyphenyl)piperazine (94). Compound **94a** (90 mg, 0.364 mmol, 1.5 eq) was added to a stirred solution of **77c** (50 mg, 0.242 mmol, 1.0 eq) in anhydrous DCM (5 mL) at 0 °C. Triethylamine (70 µL, 0.48 mmol, 2.0 eq) was added dropwise to this solution at 0 °C and the resulting reaction mixture was stirred overnight while allowing to warm to room temperature. On complete consumption of **77c** as confirmed by TLC, the reaction mixture was concentrated under reduced pressure and the residual mass was loaded onto a silica gel column. Compound **94** was purified as a white solid by elution in 1:5 ethyl acetate/hexanes (89 mg, 99% yield). ^{1}H NMR (400 MHz, $CDCl_3$) δ 7.60 − 7.66 (m, 3 H), 7.34 − 7.54 (m, 6 H), 6.84 −

7.00 (m, 4 H), 4.07 (q, *J*=6.97 Hz, 2 H), 3.67 (s, 2 H), 3.16 (br s, 4 H), 2.72 (br s, 4 H), 1.46 (t, *J*=6.97 Hz, 3 H); ^{13}C NMR (101 MHz, $CDCl_3$) δ 151.58, 141.46, 141.22, 138.70, 128.76, 128.72, 128.28, 128.09, 127.28, 127.26, 125.96, 122.68, 120.99, 118.19, 112.39, 63.54, 63.28, 53.47, 50.59, 14.98; HRMS (ESI) calcd. for $C_{25}H_{29}ON_2$ $(M+H)^+$ 373.2274, found: 373.2279.

1.5 Small molecule modifiers of microRNA-21

1.5.1 Introduction to microRNA-21

MicroRNA-21 (miR-21) is a 22-nucleotide long miRNA and was one of the first microRNAs to be discovered in humans.[10] The role of miR-21 in cardiovascular biology is well-studied, and dysregulation of miR-21 is found to be involved in proliferative vascular disease, cardiac hypertrophy, ischemic heart disease, and human cardiovascular diseases.[202] Along with its role as an anti-apoptotic and pro-survival factors, high expression levels of miR-21 are a common feature of pathological cell growth or cell stress.[203] Upregulation of miR-21 may be a characteristic of cancer cells and is commonly found in breast,[204] colon,[205] lung,[206] pancreas,[207] prostate,[208] and gastric cancer.[209] In a large-scale miRNA profiling study on solid tumors of 540 human samples derived from 363 specimens, miR-21 was the only miRNA found to be upregulated.[210]

Human miR-21 was mapped to chromosome 17q23.2, where the gene overlaps with Vacuole Membrane Protein 1 (VMP1 or TMEM49), a human homolog of rat vacuole 42 membrane protein.[10] However, these overlapping genes are transcribed independently, with pri-miR-21 transcription facilitated by a promoter in the intron of the overlapping gene codon. In the

human genome, the Activator Protein 1 (AP-1) transcription factor, comprising c-Fos and c-Jun proteins, interacts with the miR-21 promoter region for miR-21 gene expression.[211] A well-known target of miR-21 is a tumor suppressor gene, programmed cell death protein 4 (PCPD4), which contains the target binding site of miR-21.[212] PCPD4 is implicated in the progression of glioma,[213] breast,[107] and colorectal cancers.[214] A consequence of miR-21 overexpression in cancer cells is the downregulation of PCPD4 (miR-21 binds directly to the 3'-UTR of PCPD4 at 228-249 nt[215]). Interestingly, PCPD4 inhibits transcription of AP-1,[216] which further results in downregulation of miR-21. Thus, miR-21 is capable of auto-regulation and maintaining its own levels through a miR-21, PCPD4, and AP-1 feedback loop.[217] One of the targets of miR-21 is the reversion-inducing cysteine-rich protein with Kazal motifs (RECK). RECK is a tumor suppressor gene and a negative regulator for matrix metalloproteinase-9, a key enzyme involved in tumor invasion and metastasis.[218] RECK is downregulated in gastric cancer cells with upregulation of miR-21.[219] Another miR-21 target, Sprouty2 (SPRY2) is a protein that affects cellular outgrowths, branching, and migration and is downregulated as a result of higher miR-21 expression in SW480 colon cancer cells.[220] Additionally, phosphatase and tensin (PTEN) homolog, which is a tumor suppressor, is also downregulated by miR-21 in colorectal cancer cells.[221] Silencing of PTEN can lead to chemoresistance via activation of the Akt and ERK pathways.

A study by Shi, et al. showed the involvement of miR-21 in mediating chemoresistance towards docetaxel in prostate cancer PC3 cells.[222] Ectopic expression of miR-21 was observed to increase the docetaxel resistance of these cancer cells. However, ASO-mediated silencing of miR-21 led to sensitization of PC3 cells to docetaxel treatment. Here, chemoresistance towards docetaxel was also attributed to low expression of PDCD4.[222] Si, et al. reported growth inhibition of breast cancer MCF-7 cells, injected into mice, by anti-miR-21 ASOs.[223] These mice showed

slow tumor growth for 2 weeks following anti-miR-21 treatment. In 2010, Slack's group demonstrated for the first time the *in vivo* importance of miR-21 in cancer.[224] With the help of Cre and Tet-off technologies, they generated mice conditionally expressing miR-21 (doxycycline-induced miR-21 expression). miR-21 levels were normal for mice fed with doxycycline, whereas high expression of miR-21 was observed in mice fed normal chow. However, on withdrawal of doxycycline, a ten-fold increase in the level of miR-21 was observed, which led to development of lymphoma. Retreatment with doxycycline returned miR-21 levels back to normal and surprisingly, tumors completely regressed within a week. Also, knockdown of miR-21 by anti-miR-21 ASOs led to the activation of caspase 3/7, further leading to induction of apoptosis in A172, LN229, LN428, LN308, U87, and U373 glioblastoma cells.[203] Taken together, these data indicate the importance and dependency of tumor initiation and maintenance of malignancies on miR-21.[224] Thus, small molecule inhibitors of miR-21 present a unique opportunity for therapeutic use, and can provide effective means for elucidating genetic networks involving miR-21 in targeted cancer therapy.

In 2008, our lab (in collaboration with Prof. Qihong Huang at the Wistar Institute) reported the first small molecule modifier of miR-21 activity.[103] For screening small molecules, a lentiviral reporter construct was assembled using sequences complementary to mature miR-21 (**Figure 1-28**). Additionally, two constructs, one with mature miR-30 as a specificity control, and another with a negative-control linker sequence (a sequence with no detectable natural miRNA binding) were built, and plasmids were transfected into HeLa cells. HeLa cells express high levels of miR-21 but relatively low levels of miR-30.[225] Similar to the aforementioned miR-122 reporter construct, these mature miRNA binding sequences were present downstream of a luciferase reporter gene. In the case of high mature miR-21 levels, reduction of luciferase signal is be

observed, while in the case of low miR-21 levels, high luciferase activity would be present. To study the miRNA specificity of these reporter plasmids, cells containing the luciferase miR-30A (Luc-miR-30A) reporter plasmid and a construct encoding exogenous primary miR-30 were assayed (**Figure 1-28**). These cells showed a diminished luciferase signal compared to cells containing a mismatched combination of Luc-miR-30A reporter and miR-21. These results study indicate that Luc-miR-21 and Luc-miR-30A reporter plasmids are specific and only respond to the complementary miRNAs. These constructs detected endogenous miRNAs as expected. HeLa cells containing the Luc-miR-21 plasmid exhibited almost 90% decrease in the intensity of luciferase signal, confirming the ability of these constructs to detect endogenous miR-21. Cells containing the Luc-miR-30A reporter construct showed a slight decrease in luciferase signal, indicating low levels of miR-30 in HeLa cells.

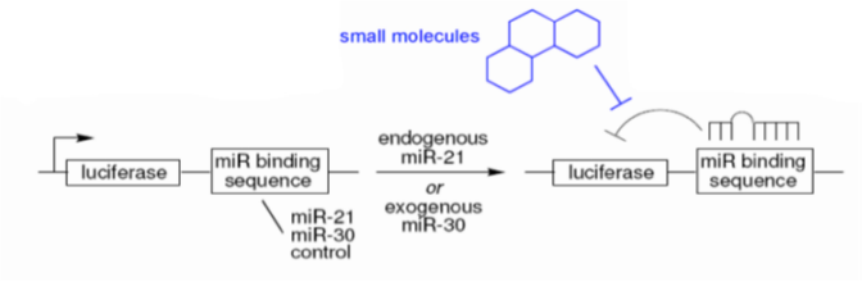

Figure 1-28 miR-21 assay.

The reporter construct consists of a miR-21 binding site downstream of the luciferase gene. In the presence of high levels of miR-21, luciferase transcription is downregulated, reducing chemiluminescence. Small molecules which increase luciferase activity are selected. The reporter plasmid with the miR-30 binding sequence constitutes the negative control for determining the specificity of inhibitors for miR-21. Adapted from *Angew. Chem. Int. Ed.*, **2008**, 47 (39), 7482.[103]

Subsequently, a primary screen of more than 1,000 compounds from the Deiters Lab compound collection and from the Library of Pharmacologically Active Compounds (LOPAC, Sigma-Aldrich) were conducted at a compound concentration of 10 µM. Compound **95** was initially identified as a hit compound with a 251% increase in luciferase signal compared to DMSO-treated control cells. Further, an SAR analysis was undertaken (**Figure 1-29**), revealing compound **14** to be the most active compound. Compound **14** elicited a 485% increase in luciferase signal at a concentration of 10 µM. Furthermore, compound **14** did not display cytotoxic effects at the EC_{50} value of 2 µM.

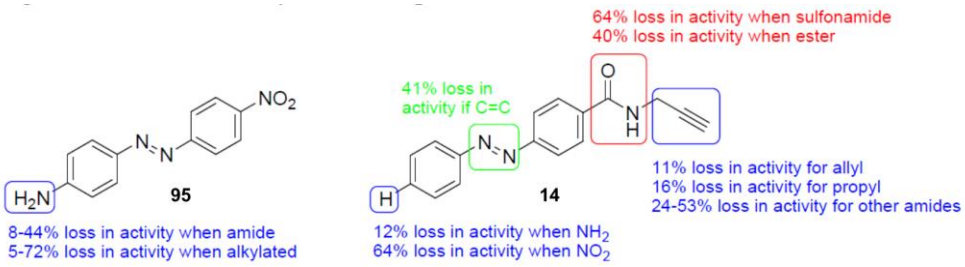

Figure 1-29 Discovered miR-21 inhibitor **95** and SAR investigation of **95** and **14**.

Modifications on compounds **95** and **14** are highlighted along with the outcome. Adapted from *Angew. Chem. Int. Ed.*, **2008**, 47 (39), 7482.[103]

As a control experiment, HeLa cells transfected with the Luc-linker (control) did not show any alterations in luciferase signal upon exposure to compound **14**. Also, small molecule **14** did not elicit any increase in luciferase signal in cells co-transfected with both the Luc-miR-30A reporter plasmid and the miR-30 plasmid. These data confirm the action of compound **14** as a specific miR-21 inhibitor, and not as a general inhibitor of miRNAs. A RT-qPCR analysis revealed miR-21 expression in HeLa cells is reduced by 78% compared to DMSO-treated cells. Mode of action studies were carried out similarly to the aforementioned work in miR-122 reporter cells.

RT-qPCR experiments with primers specific for the primary miR-21 (pri-miR-21) sequence revealed pri-miR-21 levels to be decreased by 87% in cells treated with **14**. This strongly suggests that compound **14** acts on the transcriptional level in the miRNA biogenesis pathway. The role of small molecule **14** as a robust miR-21 inhibitor was further confirmed by successful reduction of miR-21 levels on exposing **14** to three other cell lines — MCF-7, A172 and MDA-MB-231, which expresses high levels of miR-21.

This study was followed up by Jiang, et al.[104] For simplifying modifications and SAR development, the (*E*)-1,2-diphenylazene scaffold was replaced by *N*-phenylbenzamide. Thus, compound **14** can be envisioned as structurally similar 4-benzyolamino-*N*-(prop-2-yn-1-yl)-benzamides (**96**) and 4-phenylaminocanbonyl-*N*-(prop-2-yn-1-yl)benzamides (**97**). These two classes of small molecules were independently modified to produce individual SARs (**Figure 1-30**). All of these compounds were used for stem-loop RT-qPCR analysis and analogs of **96** were found to be more active than **97**. Compound **15** was one of the analogs more potent than compound **14**, and was selected for further analysis (**Figure 1-30**).

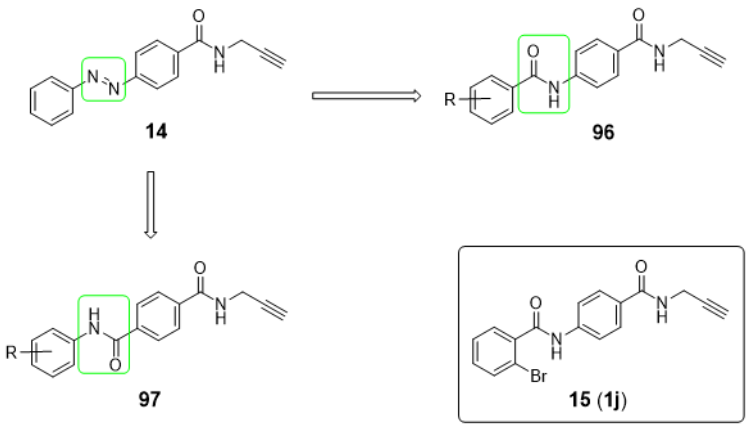

Figure 1-30 Design strategy of compounds **96** and **97**.

miR-21 inhibitor **14** was modified to compounds with a similar geometric configuration (**96** and **97**). Compound **15** (**1j**) was selected as the most promising analog for miR-21 inhibition. Adapted from *Bioorg. Med. Chem.*, **2015**, 23, 6510.[104]

Subsequently, functional studies were carried out comparing compounds **15** and **14**. **15** showed a higher enhancement in rescuing PCPD4, a tumor suppressor protein and direct target of miR-21, compared to **14**. The compound **15** induced increased apoptosis in HeLa and U-87 MG cells compared to DMSO-treated control cells, and induced much higher apoptosis in 50 μM H_2O_2-treated cells. A study by Cheng, et al. demonstrated the role of miR-21 in protecting cardiac myocytes against H_2O_2-induced injury.[226] Downregulation of miR-21 in H_2O_2-treated cells led to higher cell death, while upregulation of miR-21 levels by transfection with pre-miR-21 led to protective effect on cardiac myocyte injury. In addition, proliferation tests performed on HeLa cells (and on 50 μM H_2O_2-treated HeLa cells), using CFSE staining with detection by FACS, revealed a slower decrease in mean fluorescence intensity (MFI) on treatment of HeLa cells with **15**, indicating a decreased proliferation with miR-21 inhibition by **15**. Here, an enhanced anti-proliferative effect was observed on H_2O_2-treated cells. Additionally, cell doubling time was also increased in HeLa cells and H_2O_2-treated HeLa cells by 0.5 h and 1 h, respectively, on exposing

to **15**. There is increasing evidence about higher intracellular H_2O_2 concentration in providing a conducive environment for apoptotic cell death in tumor cells.[227] Thus, the effect of **15** as miR-21 inhibitor that is more effective in conjunction with H_2O_2 treatment suggested its potential for synergistic use with chemotherapeutic agents in future.

To determine the specificity of **15**, a detailed miRNA profile comprising 11 inflammatory miRNAs (let-7a, miR-25, miR-26, miR-126, miR-133, miR-143, miR-145, miR-146, miR-148, miR-152 and miR-195) showed no significant difference in miRNA levels on treatment with **15** (10 μM) for 24 h (**Figure 1-31A**). In addition, the key genes in the miRNA biogenesis pathway, including DROSHA, TARBP2, DGCR8, XPO5, DICER1 and AGO2, were quantified using RT-qPCR and showed no significant difference upon exposure to **15**, indicating the specificity of small molecule **15** (**Figure 1-31B**).

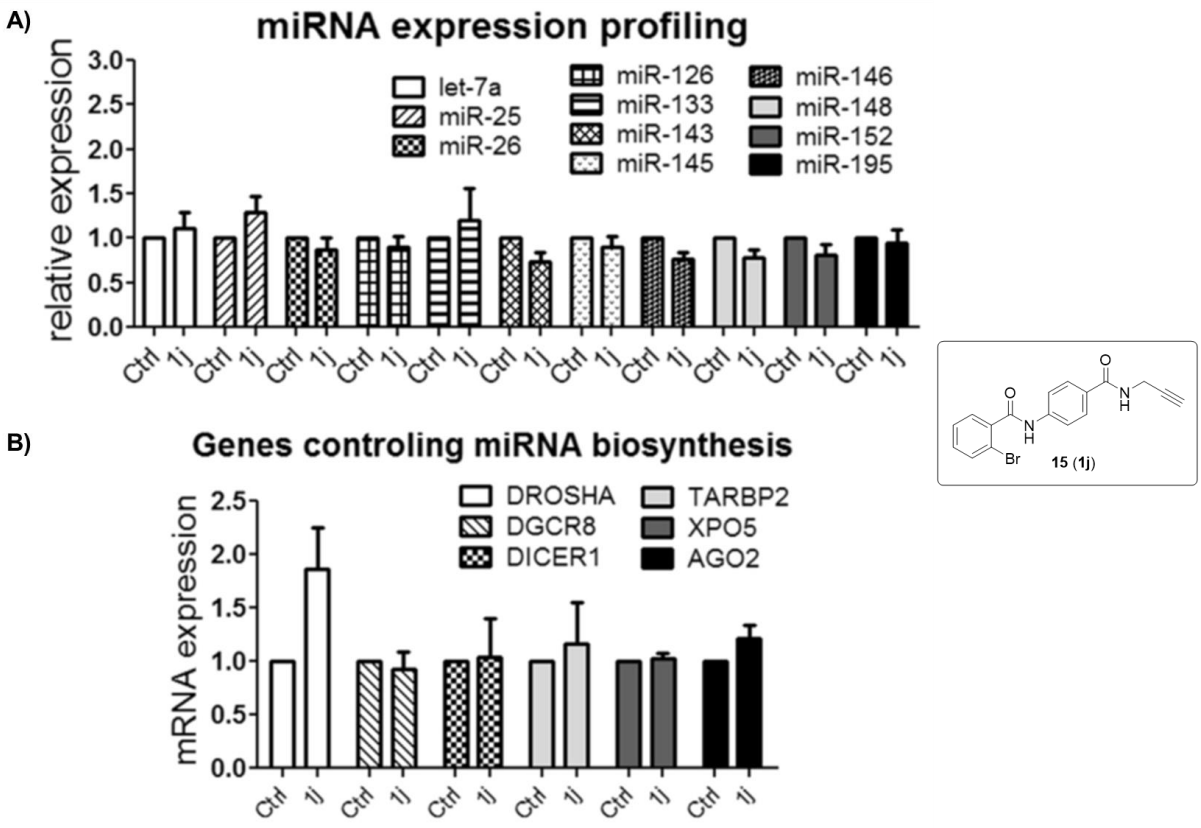

Figure 1-31 Mode of action studies of inhibitor **15**.

(A) Compound **15** did not elicit any activity against all the 11 miRNAs tested, indicating specificity of **15** towards miR-21. (B) Genes controlling miRNA biosynthesis did not show any significant transcriptional changes upon exposure to **15**, indicating that **15** is a specific miR-21 inhibitor and does not influence the whole miRNA synthesis pathway. Adapted from *Bioorg. Med. Chem.*, **2015**, 23, 6510.[104]

In 2015, our lab published a series of aryl amides as a new class of specific miR-21 inhibitors.[106] Similar to previous studies, an initial hit compound was identified with the aforementioned luciferase-based reporter assay. The hit compound was further subjected to SAR analysis, through which 4 analogs (**98**, **99**, **100**, and **17)** were selected (**Figure 1-32A**). Subsequently, these compounds were scrutinized for specific miR-21 activity. When the Huh7-psiCHECK-miR122 cell line was treated with **98**, **99**, **100**, and **17**, no effect on luciferase signal was observed, while these compounds exhibited more than doubled luciferase signal in a HeLa-

miR21-Luc cell line (**Figure 1-32B**). A RT-qPCR analysis showed that HeLa cells treated with these compounds at 10 µM for 48 hours did not show altered miR-21, miR-125b, miR-17-5p and miR-222 levels. Compounds **98**, **99**, **100**, and **17** showed EC_{50} values of 10.8 µM, 6.1 µM, 2.3 µM and 0.86 µM, respectively (**Figure 1-32C**). Moreover, a RT-qPCR analysis of primary miR-21 revealed almost no effect on pri-miR-21 levels, thus indicating a mode of action downstream of transcription of miR-21 gene (i.e., in miRNA maturation or effector function). This mode of action is novel compared to extant inhibitors. To confirm this further, a reporter construct with an endogenous miR-21 promoter was cloned upstream of luciferase gene in pGL4 vector in such a way that luciferase reporter was placed under the control of the miR-21 promoter. No effect was seen on luciferase signal in this pGL4-miR21P construct in HeLa cells on exposure to **98**, **99**, **100**, and **17**, thereby supporting the role of these compounds in the miRNA maturation pathway.

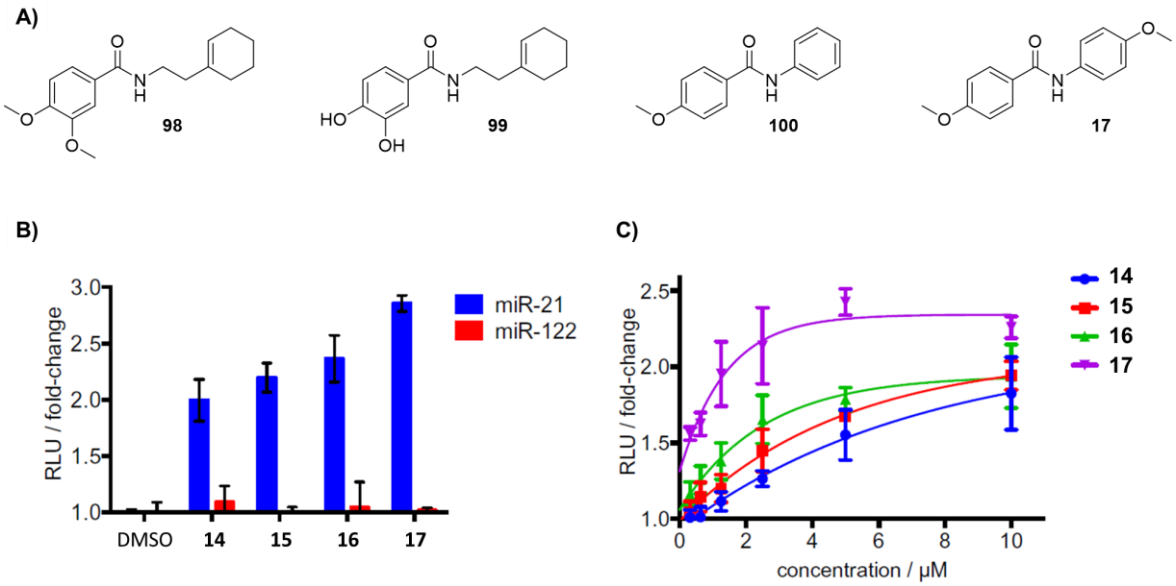

Figure 1-32 Specificity and dose-response characteristics of inhibitors **98**, **99**, **100**, and **17**.

(A) Chemical structures of inhibitors **98**, **99**, **100**, and **17**. (B) Luciferase activity elicited by inhibitors **98**, **99**, **100**, and **17** in HeLa-miR21-Luc and Huh7-psiCHECK-miR122 stable cell lines indicates the specificity of these inhibitors towards miR-21 activity. (C) Luciferase dose-response curves for inhibitors **98**, **99**, **100**, and **17** in HeLa-miR21-Luc cells. Adapted *from Bio. Med. Chem. Lett.*, **2015**, 25 (21), 4793.[106]

Building from the foundation of the few classes of specific miR-21 inhibitors reported in the literature, studies to identify and develop new structurally diverse miR-21 inhibitors were undertaken. A pilot screen using the same luciferase-based reporter assay under the regulation of miR-21 was used to identify small molecule inhibitors. An extensive high-throughput screen (HTS) of 333,519 compounds was performed (PubChem AID 2289), which identified 3,282 hits (1% hit rate). Subsequently, 124 of the top-ranking compounds were identified and assayed in secondary screens for their specificity and selectivity. These compounds were subjected to a cell-based reporter assay with the miR-30A reporter (PubChem AID 2507); compounds active in both the assays were not considered to be specific miR-21 inhibitors, but instead were considered to be general miRNA inhibitors and were discarded. Another cell-based assay with the luciferase gene

construct was conducted on the remaining compounds to identify luciferase inhibitors considered to be false-positives (PubChem AID 493175). Finally, 58 small molecules were confirmed as miR-21-specific inhibitors and subjected to dose-dependent studies.

In 2018, our lab published the development of oxadiazole series of miR-21 inhibitors.[105] From these 58 hit molecules, 2 small molecules were selected with similar structural features and lead compound **16** was selected as the optimized miR-21 inhibitor after a detailed SAR study. A dose-dependent inhibition study of **16** in a HeLa-miR-21-Luc assay revealed an EC_{50} value of 5.3 µM. However, upon RT-qPCR analysis, **16** showed no significant decrease in mature miR-21 and pri-miR-21 levels in HeLa cells, as well as mature miR-21 levels in A498, SKOV3, and A549 cells at 10 µM concentration after 48 h. Treatment of **16** in HeLa cells transfected with luciferase reporter construct pGL4-miR21P which monitors miR-21 promoter activity revealed no changes in the reporter gene expression. Furthermore, no change in melting temperature was observed with mature miR-21 in presence of **16**, thereby establishing no direct binding of miR-21 with **16**. Although mode of action studies is still under investigation, **16** (10 µM) exhibited sensitization of A498 cells (renal cell carcinoma) towards topotecan exposure in a concentration-dependent treatment (IC_{50} of topotecan alone is 1 µM, IC_{50} of topotecan+**16** is 90 nM – a ~11-fold increase in potency). In addition, this effect of **16** was specific towards A498 cells.[105]

From these 58 hit small molecules, benzoxazole **101** (PubChem CID 71233585) was selected for further investigation based on its promising activity and synthetic accessibility.

1.5.2 Synthesis and SAR studies of miR-21 inhibitors

This material was reprinted in its entirety from N. Ankenbruck, R. Kumbhare, Y. Naro, M. Thomas, L. Gardner, C. Emanuelson and A. Deiters, *Bioorg. Med. Chem.*, **2019**, *27*, 3735-3743.[228]

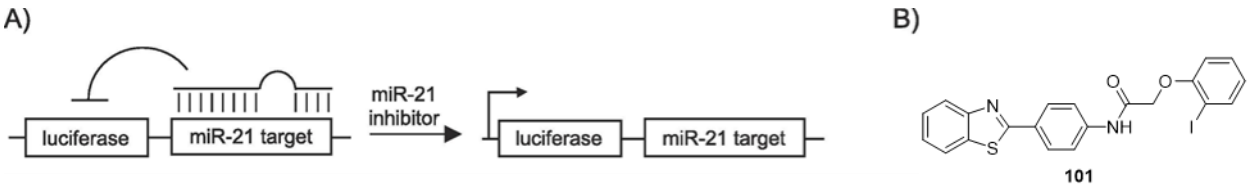

Figure 1-33 miR-21 assay and hit compound **101**.

(A) Design of a luciferase-based live-cell reporter for high-throughput screening of small molecule modulators of miR-21 function. miR-21 binds to a complementary sequence in the 3′-UTR of the luciferase gene, inhibiting translation and resulting in a decrease in luciferase expression. The presence of a small molecule inhibitor of miR-21 transcription relieves translational repression of the reporter, resulting in an increase in luciferase levels. (B) Chemical structure of hit compound **101** identified in the high-throughput screen.

Analogs of the initial hit **101** were synthesized using a synthetic route that allowed for facile functionalization of numerous positions across the structure (**Figure 1-34**). Commercially available *ortho*-substituted anilines **102** were readily reacted with **103** via a condensation reaction in polyphosphoric acid to obtain the resulting benzimidazoles, benzothiazoles, and benzoxazoles **104**. Subsequent reaction with chloroacetyl chloride provided the linker region in **105** which readily underwent nucleophilic substitution with phenols, thiols and anilines in the presence of cesium carbonate to yield the final products.

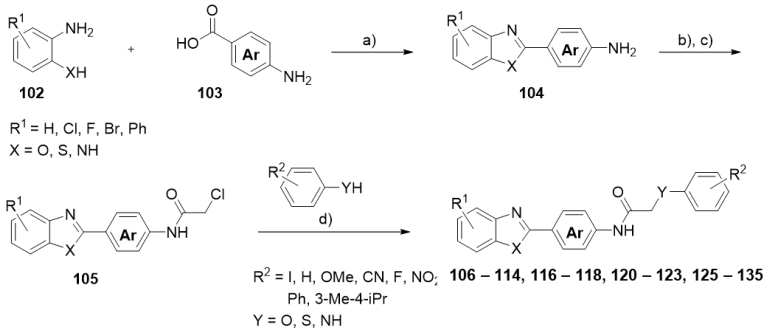

Figure 1-34 Synthetic route to ether-amide miR-21 inhibitors.

(a) polyphosphoric acid, 170 °C; (b) chloroacetyl chloride, toluene, 90 °C; (c) sat. $NaHCO_3$, rt; (d) Cs_2CO_3, CH_3CN, rt; Ar = phenyl, naphthyl, benzothiazolyl.

Using this synthetic route, a small panel of analogs was generated and their biological activity was evaluated using the HeLa-miR21-Luc cell line (**Figure 1-35**). The initial hit **101** demonstrated modest activity, inducing a 1.55-fold increase in luciferase signal following treatment at 10 μM for 48 h. Absence of the iodide in **106** resulted in only a very minor improvement in activity, while loss of the iodide along with introduction of a para-methoxy group in **107** had little to no effect on activity. Turning towards modifying the benzothiazole ring, the benzoxazole derivative of **101** yielded **108**, which maintained the same activity as the parent compound. Keeping the benzoxazole and removal of the iodide resulted in **109**, which showed no change in activity, while introduction of a para-methoxy to yield **110** abolished all activity. Expanding upon **109**, addition of a 5-chloro modification to the benzoxazole led to in **111**, which demonstrated an 85% enhancement in activity compared to the initial hit **101**. Furthermore, addition of a para-methoxy substitution to **111** to yield **112** further enhanced activity, eliciting a 314% improvement compared to **101**. Continuing from the promising results obtained from **111** and **112**, analogs containing benzimidazoles (**113** and **114**) were synthesized, however, only a loss in activity was observed in both cases.

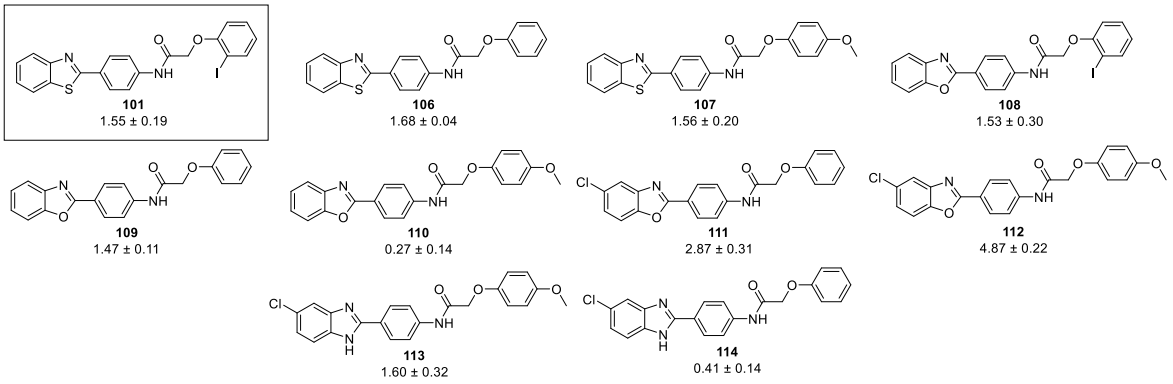

Figure 1-35 Activity of compounds **101** and **106–114** in the HeLa-miR21-Luc assay.

Values represent fold-changes in luminescence signal in the HeLa-miR21-Luc stable cell line normalized to cell viability and relative to a DMSO control. Data represent the averages ± standard deviations from at least three independent experiments. Luminescence data generated by Dr. Nicholas Ankenbruck.

To build upon the improvement in activity seen in **111** and **112**, an additional round of analogs was generated containing further modification to each respective compound. For **111**, moving the 5-chloride to the 6-position yielded **116**, which had only a minor impact on activity. Changing the ether-amide linker from the para- to the meta-position yielded analogs **117** and **118**, which resulted in a loss of activity. The importance of the ether-amide linker was investigated by synthesizing **119** bearing a shorter carbamate linker (**Figure 1-36**). Compound **119** elicited a 35% increase in activity relative to **111** and a 249% increase relative to the initial hit **101**. Analogous modifications were also made to **112** to produce **120**, **121**, **122**, and **123**, however, only reduced activity was observed in this set of analogs (**Figure 1-37**).

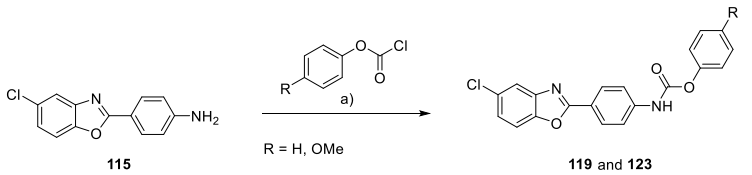

Figure 1-36 Synthetic route to miR-21 inhibitors **119** and **123**.

a) Et_3N, DCM, 0 °C – rt.

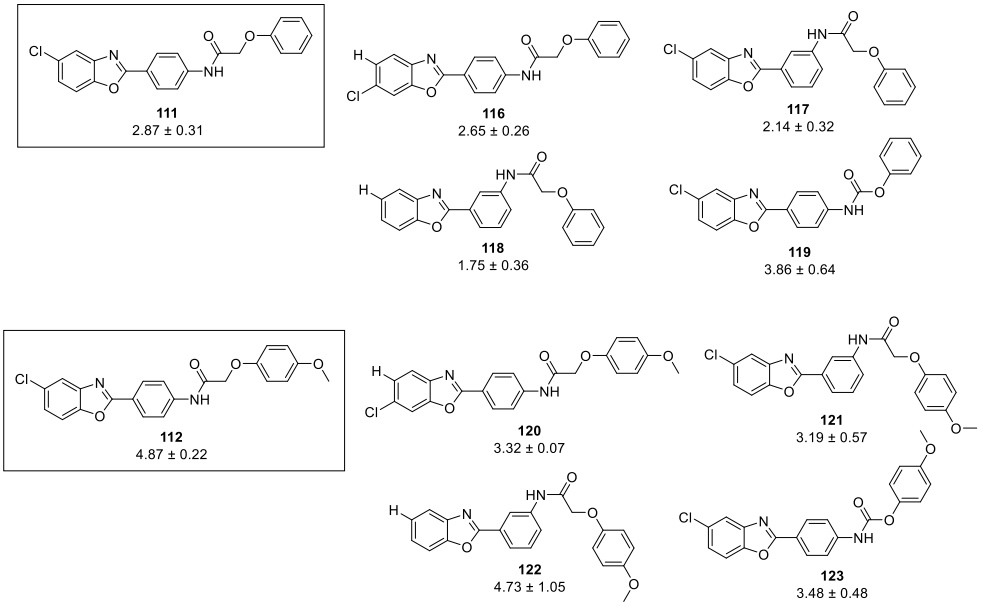

Figure 1-37 Activity of compounds **116–123** in the HeLa-miR21-Luc assay.

Values represent fold-changes in luminescence signal in the HeLa-miR21-Luc stable cell line normalized to cell viability and relative to a DMSO control. Data represent the averages ± standard deviations from at least three independent experiments. Luminescence data generated by Dr. Nicholas Ankenbruck.

With **112** remaining the most potent inhibitor identified thus far, we decided to investigate further modifications to its structure. To this end, analogs containing modifications to the ether-amide linker and the central aniline ring were synthesized and their activity was tested in the HeLa-miR21-Luc stable cell line (**Figure 1-34**). Replacement of the etheramide linker with a thioether amide linker produced analog **124** which exhibited a 54% decrease in activity relative to **112**

(**Figure 1-38**). Furthermore, incorporation of an amino-amide linker in place of the ether-amide linker resulted in **125** and completely abolished activity. Replacement of the central aniline ring with a naphthalene (**126**) or benzothiazole (**127**) was also detrimental to activity. Lastly, alkylation of the amide nitrogen in **112** with a methyl or propargyl group, **128** and **129** respectively (**Figure 1-39**), abolished activity compared to the parent compound **112**. Taken together, these results confirmed the importance of the ether-amide linker to activity and thus we decided to maintain this moiety moving forward with additional analogs.

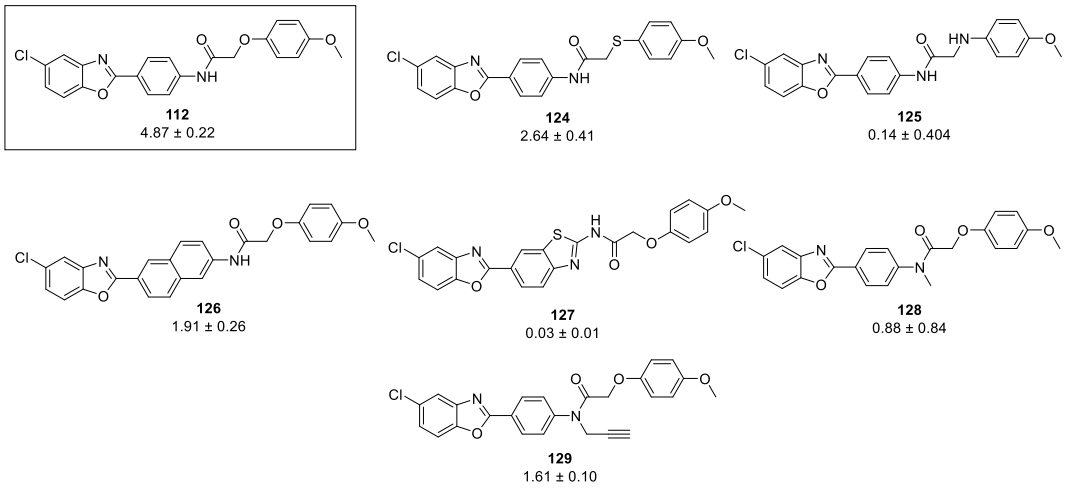

Figure 1-38 Activity of compounds **124–129** in the HeLa-miR21-Luc assay.

Values represent fold-changes in luminescence signal in the HeLa-miR21-Luc stable cell line normalized to cell viability and relative to a DMSO control. Data represent the averages ± standard deviations from at least three independent experiments. Luminescence data generated by Dr. Nicholas Ankenbruck.

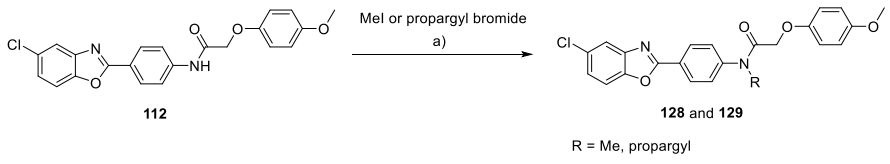

Figure 1-39 Synthetic route to ether-amide miR-21 inhibitors **128** and **129**.

(a) LiHMDS, MeI, THF, 0 °C – rt (for R = Me); NaH, propargyl bromide, DMF, 0 °C – rt (for R = propargyl).

Building upon the generated structure-activity information, we decided to synthesize an additional set of analogs based on **112**, but containing more diverse changes to the two distal ring systems while maintaining the structure of the central region of the scaffold. To this end, additional analogs were synthesized and tested in the miR-21 luciferase reporter (**Figure 1-40**). Moving the *para*-methoxy to the *meta*-position resulted in **130**, which displayed similar activity to **112**. Replacement of the *para*-methoxy with a nitrile (**131**), fluorine (**132**), nitro (**133**), or phenyl (**134**) group all resulted in losses of activity. Similarly, introduction of a *para*-isopropyl in conjunction with a *meta*-methyl group (**135**) led to a 46% decrease in activity. Interestingly, replacement of the 5-chloro with a 5-fluoro in conjunction with (**136**) or without (**137**) the *para*-methoxy group also reduced activity, providing evidence that the 5-position may be highly sensitive to modifications. To further support this, introduction of a bromine at the 5-position (**138**) resulted in a 27% increase in activity compared to the parent compound **112**. Surprisingly, introduction of a phenyl group at the 5-position (**139**) had an even greater impact on activity, demonstrating a 62% improvement in activity compared to **112**, and a 508% increase in activity relative to the initial hit **101**. Conversion of the benzoxazole to a pyridinyloxazole (**140**) led to a loss in activity compared to **101** and further supports the critical nature of the 5-position on the benzoxazole.

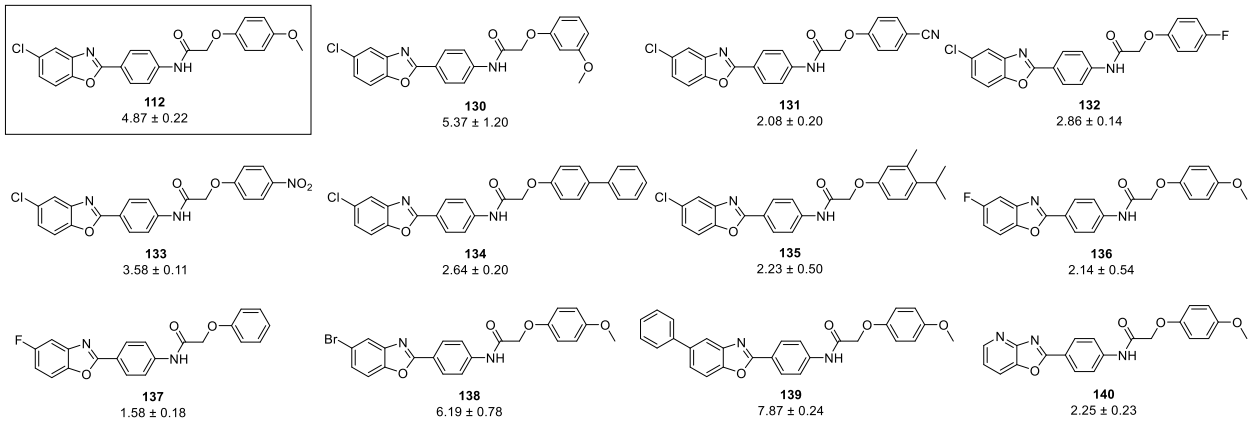

Figure 1-40 Activity of compounds **130–140** in the HeLa-miR21-Luc assay.

Values represent fold-changes in luminescence signal in the HeLa-miR21-Luc stable cell line normalized to cell viability and relative to a DMSO control. Data represent the averages ± standard deviations from at least three independent experiments. Luminescence data generated by Dr. Nicholas Ankenbruck.

Overall, the SAR studies suggest several key positions on the inhibitor that appear sensitive to modification, including the ether-amide linker core and the 5-position on the benzoxazole ring system. With the promising and improved candidates **112**, **130**, **138**, and **139** in hand, we next evaluated their biological activity and confirmed their function as miR-21 inhibitors.

1.5.2.1 Secondary assays to confirm activity of miR-21 inhibitors

Firstly, the HeLa-miR21-Luc reporter cell line was treated with a dilution series of the most promising analogs, and **112**, **130**, **138**, and **139** all demonstrated reporter activation in a dose-dependent fashion with EC_{50} values of 6.7 μM, 4.7 μM, 6.4 μM, and 3.5 μM, respectively (**Figure 1-41**).

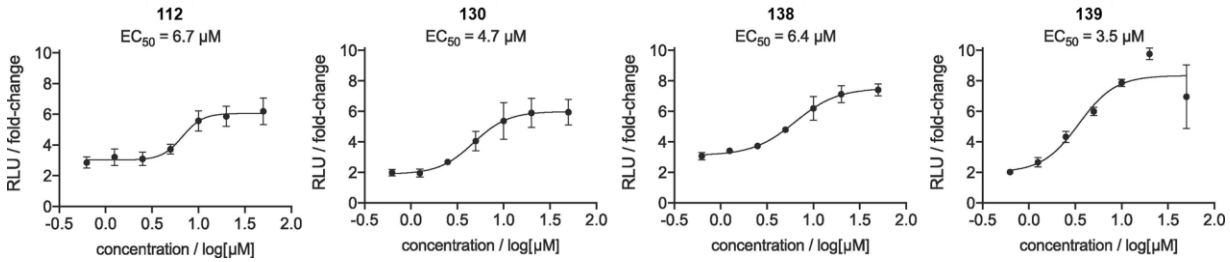

Figure 1-41 Treatment of HeLa-miR21-Luc stable reporter cells with varying concentrations of inhibitor **112**, **130**, **138**, and **139** followed by a Bright-Glo assay.

Luciferase signal was first normalized to cell viability and then to a DMSO control. Errors bars represent standard deviations from three independent experiments. EC_{50} values were determined by fitting data to a nonlinear regression analysis in GraphPad Prism software. Luminescence data generated by Dr. Yuta Naro.

Firefly luciferase inhibitors have been previously identified as false positive hits in high-throughput screens due to luciferase enzyme stabilization in cells.[98] Because this is a documented concern when using luciferase reporter assays,[229] we decided to evaluate the effect of **112**, **130**, **138**, and **139** on luciferase activity in a biochemical assay. Treatment with the positive control firefly luciferase inhibitor PTC-124[206] led to a 94% reduction in enzyme activity. While treatment with **112** elicited no significant reduction in luciferase activity, treatment with **130**, **138**, and **139** all led to 44%, 38%, and 27% reductions in luminescence signal, respectively (**Figure 1-42A**). To further validate whether these inhibitors act on the miRNA pathway, we transfected HeLa cells with a psiCHECK-empty reporter (containing a sequence not targeted by any known miRNA) followed by treatment with the compounds at 10 µM for 48 h. The positive control PTC-124 and compounds **130**, **138**, and **139** induced an increase in luminescence signal ranging from 1.5 to 1.8-fold, while compound **112** only showed a minor increase in luciferase activity (**Figure 1-42B**). These biochemical and cell-based results indicate that **130**, **138**, and **139** may have inflated activity profiles in the HeLa-miR21-Luc assay due to off-target binding to the firefly luciferase enzyme.

Taking both the dose-response and *in vitro* firefly luciferase data into account, we decided to carry **112** forward as the primary candidate for further biological testing.

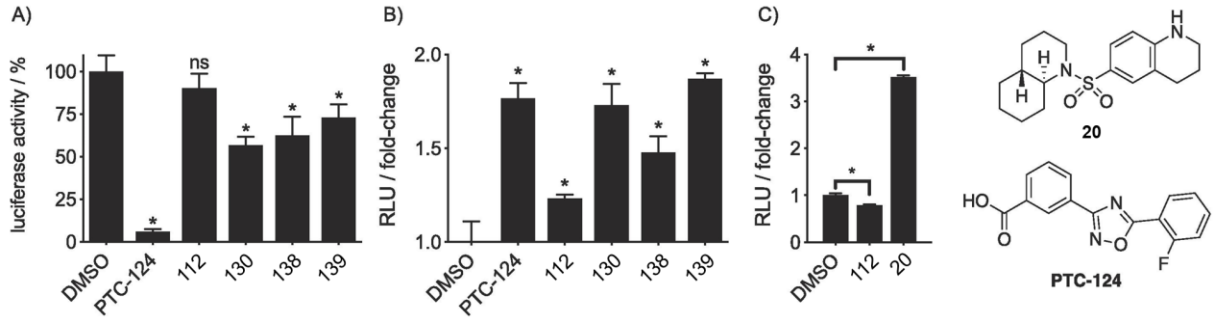

Figure 1-42 Evaluation of selectivity of lead compounds.

(A) Incubation of recombinant firefly luciferase with inhibitors **112**, **130**, **138**, and **139** at 10 μM, followed by a Bright-Glo assay. PTC-124, a known firefly luciferase inhibitor, was included as a positive control. (B) Transfection of HeLa cells with the psiCHECK-empty plasmid followed by treatment with compounds **112**, **130**, **138**, and **139** or the positive control at 10 μM. A dual luciferase assay was performed after 48 h. RLU values represent firefly luciferase luminescence signal normalized to *Renilla* luciferase luminescence signal. (C) Treatment of Huh7-miR122 stable cells with **112** (10 μM) or positive control **20** (10 μM). A dual luciferase assay was performed after 48 h. RLU values represent *Renilla* luciferase luminescence signal normalized to firefly luciferase luminescence signal. All data were normalized to DMSO treatment (negative control) and errors bars represent standard deviations from three independent experiments. Statistical significance was determined using an unpaired t-test, $*P < 0.05$, ns $P \geq 0.05$. Luminescence data in A and C generated by Dr. Yuta Naro and in B generated by Dr. Nicholas Ankenbruck.

Next, we tested if **112** is a general miRNA pathway inhibitor or if it has selectivity for miR-21. To this end, we employed an additional stable reporter cell line, Huh7-miR122, which places *Renilla* luciferase expression under the control of miR-122 activity.[108] Treatment with **112** (10 μM) elicited only a minor 0.2-fold reduction in *Renilla* luciferase signal, demonstrating that **112** does not inhibit miR-122 activity (**Figure 1-42C**). As a positive control, cells were also treated

with **20**, a known miR-122 inhibitor,[108] which induced a > 3.5-fold increase in luminescence, confirming functionality of the assay. Taken together, these results indicate that **112** shows some level of selectivity for miR-21 and is not a general miRNA pathway inhibitor.

1.5.2.2 Identification of preliminary mode of action

To explore the mechanism by which **112** inhibits miR-21 function, levels of mature miR-21 were measured via reverse transcription quantitative PCR (RT-qPCR) after treatment with **112**. To ensure that the effects were not cell line dependent, three different cancer cell lines were tested. These cell lines included the parental line of the HeLa-miR21-Luc stable reporter cell line, HeLa cervical carcinoma cells, along with A549 non-small cell lung carcinoma cells, and SKOV3 ovarian cancer cells. Each cell line was treated with **112** (10 μM) or DMSO (0.1%) for 48 h, followed by miRNA isolation and RT-qPCR analysis. In HeLa cells, a 57% reduction was observed (**Figure 1-43A**), while in A549 and SKOV3 cells, 33% and 31% reductions were detected, respectively (**Figure 1-44**). These results support a mechanism by which treatment with **112** results in depletion of mature miR-21 and subsequent reduction of miR-21 regulatory functions. To determine if **112** inhibits miR-21 maturation via binding directly to pre-miR-21, melting curve analyses were carried out in the presence of DMSO or **112**. The melting temperature of pre-miR-21 in the presence of DMSO control was measured to be 56.0 °C. The presence of **112** (10 μM) had no effect on melting temperature yielding a T_m of 56.2 °C (**Figure 1-45**). These results indicate that **112** does not directly interact with miR-21 RNA and that miR-21 levels are likely impacted via an alternative mechanism.

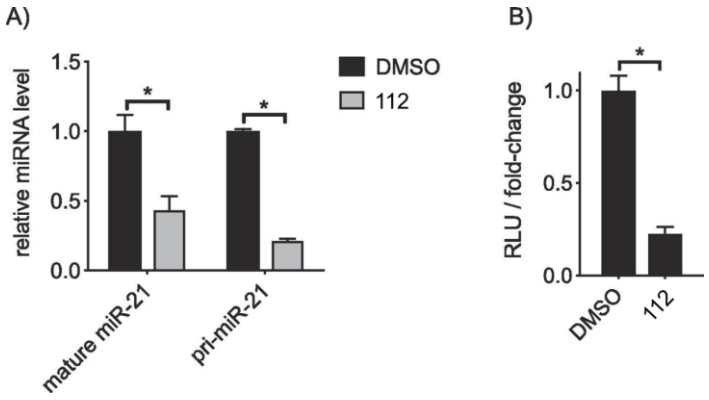

Figure 1-43 Effect of **112** on different targets.

(A) Treatment of HeLa cells with **112** (10 μM) for 48 h, followed by RT-qPCR analysis of mature miR-21 or primary miR-21 (pri-miR-21). (B) Transfection of HeLa cells with a miR-21 promoter gene expression reporter followed by treatment with **112** (10 μM). A Bright-Glo assay was performed after 48 h. Data were normalized to DMSO treatment (negative control) and errors bars represent standard deviations from three independent experiments. Statistical significance was determined using an unpaired t-test, *P < 0.05. Data in A generated by Dr. Nicholas Ankenbruck and in B generated by Dr. Yuta Naro.

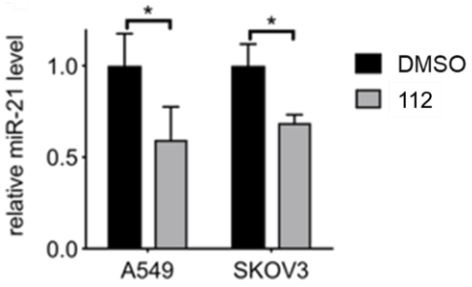

Figure 1-44 Effect of **112** on different cell lines.

Treatment of A549 (NSCLC) or SKOV3 (ovarian carcinoma) with DMSO or **112** (10 μM), followed by qPCR analysis of mature miR-21 RNA levels elicited a 33 and 31% decrease, respectively. All data was normalized to DMSO treatment (negative control) and errors bars represent standard deviations from three independent experiments. Statistical significance was determined using an unpaired t-test, * P < 0.05, ns P ≥ 0.05.

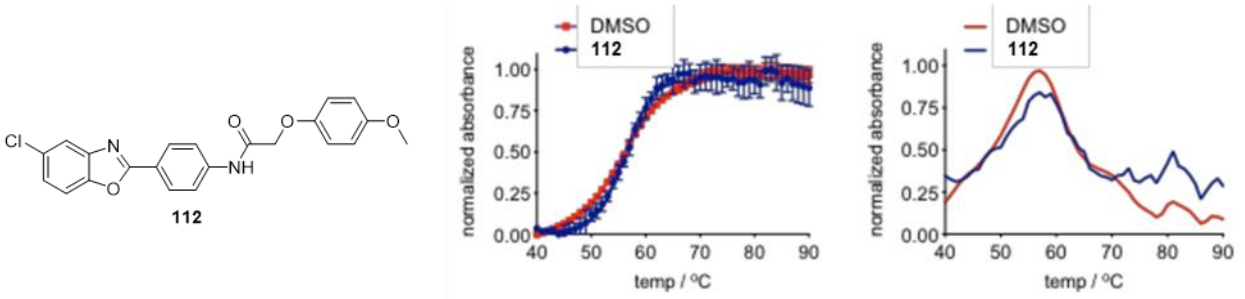

Figure 1-45 Melting curves for pre-miR-21 in the absence and presence of **112**.

Differentiation of the melting curves (right) reveals no change in melting temperatures in the presence (T_m = 56.2 °C) or absence (T_m = 56.0 °C) of **112**. Errors bars represent standard deviations from three independent experiments. Data generated by Dr. Nicholas Ankenbruck.

To further investigate what step of the miR-21 biogenesis pathway our inhibitor may be targeting, primary miR-21 levels were analyzed via RT-qPCR in HeLa cells after treatment with **112** (10 µM) for 48 h. Interestingly, a marked 79% decrease in primary miR-21 levels was observed following treatment (**Figure 1-43A**). This result supports a mechanism by which **112** inhibits transcription of the miR-21 gene, resulting in depletion of primary miR-21 levels. To confirm that compound **112** inhibits miR-21 transcription, HeLa cells were transfected with a previously described luciferase reporter construct that monitors miR-21 promoter activity, pGL4-miR21P,[106] and were treated with DMSO or **112** (10 µM) for 48 h. As expected, treatment with **112** resulted in a 78% decrease in miR-21 promoter activity compared to DMSO control (**Figure 1-43B**). This result directly supports the drastic reduction in primary miR-21 levels observed via RT-qPCR and further suggests a mechanism of action by which **112** inhibits transcription of the miR-21 gene.

1.5.2.3 Functional studies of 112

Next, we evaluated whether **112**-mediated inhibition of miR-21 could elicit a therapeutic response in HeLa cells by subjecting them to a cell viability study using an XTT assay.[230] Following treatment with the compound for 72 h, **112** demonstrated a disappointing IC_{50} > 50 μM (**Figure 1-46A**). Additionally, treatment of HEK293T cells, which do not express miR-21, with a serial dilution of compound **112** did not inhibit cell viability, supporting our hypothesis that the compound reduces HeLa cell viability in a miR-21-dependent manner (**Figure 1-47**). To further explore this response and determine if **112**-induced limited cell death was due to triggering of apoptosis, we examined caspase-3/7 activation in HeLa cells. Antisense oligonucleotide-mediated inhibition of miR-21 has been previously shown to inhibit cell proliferation and increase apoptosis of HeLa cells.33 Treatment of HeLa cells with **112** (10 μM) for 24 h elicited a modest 50% increase in caspase-3/7 activity, while a 2-fold increase was observed at an increased concentration of 50 μM (**Figure 1-46B**). This suggests that knockdown of miR-21 by **112** leads to a reduction in cell viability by inducing apoptosis, consistent with previous reports.[231-234]

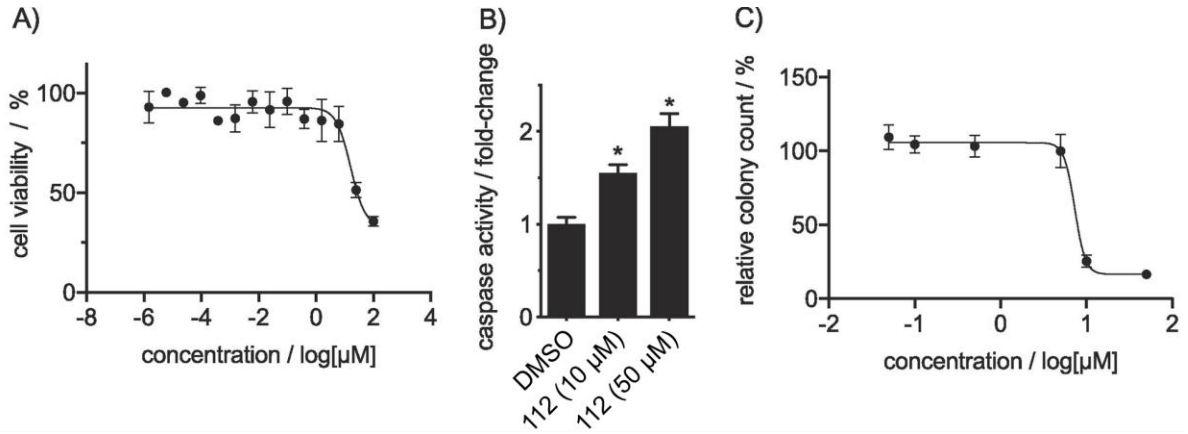

Figure 1-46 Functional studies of **112** in HeLa cells.

(A) Treatment of HeLa cells with **112** for 72 h, followed by a cell viability assay. (B) Treatment of HeLa cells with **112** for 24 h, followed by a caspase-3/7 activity assay. (C) Treatment of HeLa cells with **112** in a two-week clonogenic assay. Data were normalized to DMSO treatment (negative control) and errors bars represent standard deviations from three independent experiments. Data in A and C were generated by Dr. Nicholas Ankenbruck and in B generated by Cole Emanuelson.

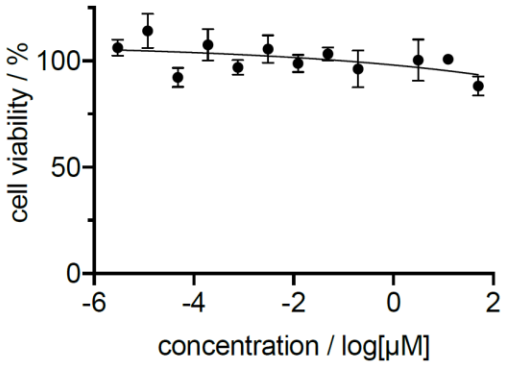

Figure 1-47 Treatment of HEK293T cells with a dilution series of **112**.

Treatment of HEK293T cells with a dilution series of **112** for 72 h, followed by a cell viability assay. Data was normalized to DMSO treatment (negative control) and errors bars represent standard deviations from three independent experiments. Data generated by Dr. Nicholas Ankenbruck.

We further explored the therapeutic potential of **112** by investigating the ability of the small molecule to elicit long-term effects in reducing microtumor formation in a clonogenic assay. Oligonucleotide silencing of miR-21 has been shown to inhibit clonogenicity in several cancer cell models[235-237] including cervical cancer.[231, 238] Briefly, HeLa cells were suspended in low melt agarose and exposed to a dilution series of **112** for two weeks at 37 °C prior to imaging (**Figure 1-48**). Interestingly, while treatment with **112** only inhibited cell viability at high concentrations, the compound was capable of reducing colony formation of HeLa cells with an EC_{50} of 7.3 µM (**Figure 1-46C**). This inhibition of microtumor formation is in good agreement with previous reports that have shown similar results using antisense oligonucleotide-mediated knockdown of miR-21.[231, 235, 239-240] Furthermore, it was also reported that inhibition or knockout of miR-21 with genetic tools had limited or no effect on cell viability, depending on the cell line,[241-242] while connections between miR-21 and metastasis and tumorigenesis have been observed in a variety of cancers.[224, 243-245]

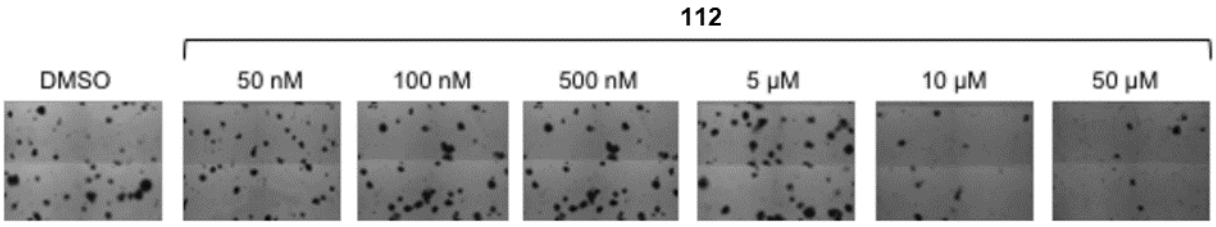

Figure 1-48 Representative images from clonogenic assays following 2-week treatment of HeLa cells with a dilution series of **112**.

Images were cropped to 4 tiles each in the center of the well from the extended depth of focus image. Data generated by Dr. Nicholas Ankenbruck.

1.5.2.4 Summary

In summary, a high-throughput screen for small molecule modulators of miR-21 function led to the identification of a new ether-amide scaffold, and a subsequent structure-activity relationship study of the initial hit compound **101** resulted in the identification of the improved miR-21 inhibitor **112**. Through a biochemical and cell-based firefly luciferase assays as well as a miR-122 reporter cell line, we determined that compound **116** showed selectivity for inhibiting miR-21 function. Furthermore, **112** was found to inhibit transcription of the miR-21 gene resulting in significant reductions in primary and mature miR-21 levels. This mechanism of action is in contrast to other classes of miR-21 inhibitors which appear to inhibit maturation of pre-miR-21[80, 83, 106, 246] as well as oxadiazole-based inhibitors which appear to inhibit the function of mature miR-21 without affecting miR-21 levels.[105] However, the ether-amide class does appear to follow a similar mechanism to a previously reported azobenzene-based miR-21 inhibitor.[103] Pre-therapeutic evaluation of the lead compound using toxicity and caspase activation assays showed that miR-21 inhibition mediated by **112** reduces cell viability in HeLa cells by inducing apoptosis, although high concentrations are required. However, treatment of HeLa cells with **112** in a long-term clonogenic assay effectively inhibited microtumor formation at low micromolar doses, suggesting that the inhibitor **112** may have potential as a therapeutic for treating miR-21-related diseases.

1.5.2.5 Experimentals

All reactions were performed in flame-dried glassware under a nitrogen atmosphere and stirred magnetically. Reactions were followed by thin layer chromatography (TLC) using glass-

backed silica gel plates (Sorbent Technologies, 250 μm thickness). Anhydrous acetonitrile and tetrahydrofuran (THF) were purchased from Acros and anhydrous toluene and dimethylformamide (DMF) were purchased from Alfa Aesar. Silica gel column chromatography was performed on silica gel (60 Å, 40–63 μm, 230 × 400 mesh, Sorbtech) as a stationary phase. High resolution mass spectral analysis (HRMS) was performed on a Q-Exactive (Thermo Scientific) mass spectrometer. The ^{1}H NMR and ^{13}C NMR spectra were recorded on a 300 MHz or 400 MHz Varian NMR spectroscope. Chemical shifts are given in δ units (ppm) for ^{1}H NMR spectra and ^{13}C NMR spectra.

General procedure for synthesis of compounds 101, 106–114, 116–118, 120–123, 125–135.

Polyphosphoric acid (10 g) was added to a mixture of 2-aminophenols (or 2 aminothiols or 2-phenylenediamines) **102** (7–9 mmol, 1.0 eq) and carboxylic acids **103** (1.0 eq) at room temperature and heated to 170 °C (dissolution of the reactants and effective stirring was observed at elevated temperatures). The reaction mixture was stirred at 170 °C for 3 h and was then allowed to cool to room temperature. The viscous reaction mixture was slowly diluted with ice-water (200 mL), neutralized (to pH 7) by adding saturated $NaHCO_3$, and extracted with multiple portions of ethyl acetate (3 × 50 mL). The combined organic extracts were washed with brine (50 mL), dried over sodium sulfate (30 g), filtered, and concentrated to yield compounds **104** in 24–91% yields as colored solids.

Further, compounds **104** (0.35–0.50 mmol, 1.0 eq) were heated with chloroacetyl chloride (3.0 eq) in anhydrous toluene (10 mL) to 90 °C for 2 h. This reaction mixture was concentrated under reduced pressure and the residue was triturated with diethyl ether (10 mL). The product was filtered and subsequently washed with multiple portions of diethyl ether (3 × 5 mL) and dried to

recover colored solids. The solids were vigorously stirred in a saturated solution of $NaHCO_3$ (10 mL) for 30 min, acidified to neutral pH with aqueous 1 M HCl solution, and then extracted with multiple portions of ethyl acetate (5 × 10 mL) until the aqueous layer turned colorless. The combined organic extracts were washed with brine (10 mL), dried over sodium sulfate (10 g), were filtered and concentrated to yield pure amides **105** as colored solids in 70–90% yield.

To a solution of amides **105** (0.08–0.44 mmol, 1.0 eq) in anhydrous acetonitrile (5 mL), the indicated phenols, thiophenols, or anilines (1.2 eq) and Cs_2CO_3 (1.2 eq) were added and the reaction mixture was stirred overnight at room temperature. The reaction was quenched by adding water (10 mL) and extracted with ethyl acetate (5 × 10 mL). The combined ethyl acetate extracts were washed with brine (10 mL), dried over sodium sulfate (10 g), filtered, and concentrated under reduced pressure. The residual solid was purified by silica gel column chromatography eluted with 1:9–7:3 ethyl acetate/hexanes to yield compounds **101**, **106–114, 116–118, 120–123, 125–135** in 23% to quantitative yield.

Compounds **106** (PubChem CID 871321) and **107** (PubChem CID 82391) have been previously characterized.

***N*-(4-(Benzo[*d*]oxazol-2-yl)phenyl)-2-(2-iodophenoxy)acetamide (108).** 58 mg, 39% yield; ^{1}H NMR (300 MHz, $CHCl_3$-*d*) δ 9.07 (s, 1H), 8.28 (d, *J* = 8.8 Hz, 1H), 7.89–7.76 (m, 4H), 7.61–7.58 (m, 1H), 7.40–7.32 (m, 2H), 6.88 (t, *J* = 14.4 Hz, 2H), 6.83–6.76 (m, 2H), 4.69 (s, 2H). HRMS (ESI) calcd. for $C_{21}H_{15}N_2O_3I$ $(M+H)^+$ 471.0206, found: 471.0226.

***N*-(4-(Benzo[*d*]oxazol-2-yl)phenyl)-2-phenoxyacetamide (109).** 35 mg, 90% yield; ^{1}H NMR (300 MHz, $CHCl_3$-*d*) δ 8.47 (s, 1H), 8.26 (d, *J* = 8.7 Hz, 2H), 7.82–7.75 (m, 3H), 7.61–7.55 (m,

1H), 7.40–7.33 (m, 3H), 7.08–7.00 (dd, *J* = 15.6, 6.6 Hz, 3H), 4.66 (s, 2H). HRMS (ESI) calcd. for $C_{21}H_{16}N_2O_3$ $(M+H)^+$ 345.1239, found: 345.1269.

***N*-(4-(Benzo[*d*]oxazol-2-yl)phenyl)-2-(4-methoxyphenoxy)acetamide (110).** 16 mg, 52% yield; ^{1}H NMR (400 MHz, DMSO-d_6) δ 8.48 (s, 1H), 8.26 (d, *J* = 8.4 Hz, 2H), 7.76–7.80 (m, 3H), 7.57–7.58 (m, 1H), 7.34–7.36 (m, 2H), 6.80–6.96 (m, 4H), 4.59 (s, 2H), 3.79 (s, 3H); HRMS (ESI) calcd. for $C_{22}H_{17}O_4N_2$ $(M+H)^+$ 373.1183, found: 373.1187.

***N*-(4-(5-Chlorobenzo[*d*]oxazol-2-yl)phenyl)-2-phenoxyacetamide (111).** 21 mg, 56% yield; ^{1}H NMR (400 MHz, DMSO-d_6) δ 8.47 (s, 1H), 8.23 (d, *J* = 8.4 Hz, 2H), 7.80 (d, *J* = 8.8 Hz, 2H), 7.24 (d, *J* = 2.2 Hz, 1H), 7.49 (d, *J* = 8.2 Hz, 1H), 7.37–7.39 (m, 2H), 7.32–7.33 (m, 1H), 7.00–7.08, 3H), 4.65 (s, 2H); HRMS (ESI) calcd. for $C_{21}H_{16}O_3N_2Cl$ $(M+H)^+$ 379.0844, found: 379.0848.

***N*-(4-(5-Chlorobenzo[*d*]oxazol-2-yl)phenyl)-2-(4-methoxyphenoxy)acetamide (112).** 20 mg, 52% yield; ^{1}H NMR (400 MHz, $CHCl_3$-*d*) δ 8.48 (s, 1H), 8.23 (d, *J* = 8.2 Hz, 2H), 7.81–7.79 (m, 2H), 7.72 (d, *J* = 2.2 Hz, 1H), 7.50 (d, *J* = 8.8 Hz, 2H), 7.30–7.33 (m, 1H), 6.88–6.96 (m, 4H), 4.60 (s, 2H), 3.79 (s, 3H); ^{13}C NMR (100 MHz, $CHCl_3$-*d*) δ 166.73, 162.59, 155.14, 151.00, 150.74, 142.16, 139.80, 128.73, 125.03, 124.61, 123.37, 119.90, 119.86, 116.01, 115.02, 110.55, 68.56, 55.73; HRMS (ESI) calcd. for $C_{22}H_{16}O_4N_2Cl$ $(M+H)^+$ 407.0793, found: 407.0796.

***N*-(4-(5-Chloro-1*H*-benzo[*d*]imidazol-2-yl)phenyl)-2-(4-methoxyphenoxy)acetamide (113).** 22 mg, 58% yield; ^{1}H NMR (400 MHz, DMSO-d_6) δ 13.01 (br s, 1H), 10.29 (s, 1H), 8.08–8.15 (m, 2H), 7.80–7.87 (m, 2H), 7.47–7.69 (m, 2H), 7.21 (dd, *J* = 8.4, 1.8 Hz, 1H), 6.85–7.01 (m, 4H),

4.67 (s, 2H), 3.70 (s, 3H); HRMS (ESI) calcd. for $C_{22}H_{19}O_3N_3Cl$ $(M+H)^+$ 408.1109, found: 408.1120.

***N*-(4-(5-Chloro-1*H*-benzo[*d*]imidazol-2-yl)phenyl)-2-phenoxyacetamide (114).** 21 mg, 60% yield; ^{1}H NMR (400 MHz, DMSO-d_6) δ 13.01 (d, *J* = 12.4 Hz, 1H), 10.35 (s, 1H), 8.09–8.16 (m, 2H), 7.80–7.87 (m, 2H), 7.62–7.70 (m, 1H), 7.50–7.54 (m, 1H), 7.30–7.36 (m, 2H), 7.21 (ddd, *J* = 9.9, 8.3, 2.0 Hz, 1H), 6.96–7.04 (m, 3H), 4.75 (s, 2H); HRMS (ESI) calcd. for $C_{21}H_{17}O_2N_3Cl$ $(M+H)^+$ 378.1004, found: 378.1007.

***N*-(4-(6-Chlorobenzo[*d*]oxazol-2-yl)phenyl)-2-phenoxyacetamide (116).** 12 mg, 32% yield; ^{1}H NMR (300 MHz, DMSO-d_6) δ 10.41 (s, 1H), 8.15 (d, *J* = 8.6 Hz, 2H), 7.89–7.99 (m, 3H), 7.79 (d, *J* = 8.5 Hz, 1H), 7.45 (dd, *J* = 8.4, 2.0 Hz, 1H), 6.86–7.01 (m, 4H), 4.69 (s, 2H), 3.70 (s, 3H); HRMS (ESI) calcd. for $C_{21}H_{16}O_3N_2Cl$ $(M+H)^+$ 379.08440, found: 379.0862.

***N*-(3-(5-Chlorobenzo[*d*]oxazol-2-yl)phenyl)-2-phenoxyacetamide (117).** 23 mg, 62% yield; ^{1}H NMR (300 MHz, DMSO-d_6) δ ppm 8.35–8.52 (m, 1H), 8.31 (s, 1H), 7.90–8.03 (m, 2H), 7.71 (d, *J* = 1.7 Hz, 1H), 7.42–7.56 (m, 2H), 7.22–7.38 (m, 3H), 6.96–7.09 (m, 2H), 4.63 (s, 2H); HRMS (ESI) calcd. for $C_{21}H_{14}O_3N_2Cl$ $(M+H)^+$ 377.0688, found: 377.0697.

***N*-(3-(Benzo[*d*]oxazol-2-yl)phenyl)-2-phenoxyacetamide (118).** 38 mg, 97% yield; ^{1}H NMR (400 MHz, DMSO-d_6) δ 10.41 (s, 1H), 8.6 (t, *J* = 1.8 Hz, 1H), 7.9 (dt, *J* = 7.6, 1.3 Hz, 1H), 7.79–7.85 (m, 3H), 7.67–7.79 (m, 1H), 7.58 (t, *J* = 7.9 Hz, 1H), 7.41–7.47 (m, 2H), 7.30–7.37 (m, 2H),

6.97–7.07 (m, 3H), 4.76 (s, 2H); HRMS (ESI) calcd. for $C_{21}H_{17}O_3N_2$ $(M+H)^+$ 345.1233, found: 345.1249.

***N*-(4-(6-Chlorobenzo[*d*]oxazol-2-yl)phenyl)-2-(4-methoxyphenoxy)acetamide (120).** 25 mg, 65% yield; ^{1}H NMR (300 MHz, DMSO-d_6) δ 10.41 (s, 1H), 8.15 (d, *J* = 8.6 Hz, 2H), 7.89–7.99 (m, 3H), 7.79 (d, *J* = 8.5 Hz, 1H), 7.45 (dd, *J* = 8.4, 2.0 Hz, 1H), 6.86–7.01 (m, 4H), 4.69 (s, 2H), 3.70 (s, 3H); HRMS (ESI) calcd. for $C_{22}H_{18}O_4N_2Cl$ $(M+H)^+$ 409.0949, found: 409.0964.

***N*-(3-(5-Chlorobenzo[*d*]oxazol-2-yl)phenyl)-2-(4-methoxyphenoxy)acetamide (121).** 35 mg, 89% yield; ^{1}H NMR (300 MHz, DMSO-d_6) δ 10.36 (s, 1H), 8.68 (s, 1H), 7.81–7.98 (m, 4H), 7.45–7.62 (m, 2H), 6.86–7.03 (m, 4H), 4.68 (s, 2H), 3.70 (s, 3H); HRMS (ESI) calcd. for $C_{22}H_{18}O_4N_2Cl$ $(M+H)^+$ 409.0949, found: 409.0963.

***N*-(3-(Benzo[*d*]oxazol-2-yl)phenyl)-2-(4-methoxyphenoxy)acetamide (122).** 35 mg, 89% yield; ^{1}H NMR (400 MHz, DMSO-d_6) δ ppm 10.36 (s, 1H), 8.67 (t, *J* = 1.8 Hz, 1H), 7.93 (d, *J* = 7.7 Hz, 1H), 7.85 (br s, 1H), 7.79–7.88 (m, 2H), 7.58 (t, *J* = 8.0 Hz, 1H), 7.41–7.46 (m, 2H), 6.88–7.01 (m, 4H), 4.69 (s, 2H); HRMS (ESI) calcd. for $C_{22}H_{19}O_4N_2$ $(M+H)^+$ 375.1339, found: 375.1353.

***N*-(4-(5-Chlorobenzo[*d*]oxazol-2-yl)phenyl)-2-((4-methoxyphenyl)thio)acetamide (124).** 24 mg, 60% yield; ^{1}H NMR (400 MHz, DMSO-d_6) δ ppm 10.49 (s, 1H), 8.12–8.17 (m, 2H), 7.77–7.85 (m, 4H), 7.39–7.47 (m, 3H), 6.90–6.96 (m, 2H), 3.73–3.76 (m, 5H); HRMS (ESI) calcd. for $C_{22}H_{18}O_3N_2ClS$ $(M-H)^-$ 423.0576, found: 423.0565.

***N*-(4-(5-Chlorobenzo[*d*]oxazol-2-yl)phenyl)-2-((4-methoxyphenyl)amino)acetamide (125).** 11 mg, 29% yield; ^{1}H NMR (300 MHz, DMSO-d_6) δ ppm 10.60 (s, 1H), 8.16–8.22 (m, 3H), 7.80–7.95 (m, 4H), 7.44–7.46 (m, 2H), 6.89–7.06 (m, 2H), 4.38 (s, 1H), 4.09 (s, 2H), 3.70 (s, 3H); HRMS (ESI) calcd. for $C_{22}H_{19}O_3N_3Cl$ $(M+H)^+$ 408.1109, found: 408.1090.

***N*-(6-(5-Chlorobenzo[*d*]oxazol-2-yl)naphthalen-2-yl)-2-phenoxyacetamide (126).** 32 mg, 87% yield; ^{1}H NMR (300 MHz, DMSO-d_6) δ 10.48 (s, 1H), 8.76 (s, 1H), 8.45 (s, 1H), 8.10–8.28 (m, 2H), 8.04 (d, *J* = 8.7 Hz, 1H), 7.94 (d, *J* = 2.1 Hz, 1H), 7.69–7.90 (m, 2H), 7.49 (dd, *J* = 8.6, 2.1 Hz, 1H), 7.34 (dd, *J* = 8.6, 7.1 Hz, 2H), 6.93–7.10 (m, 3H), 4.79 (s, 2H); HRMS (ESI) calcd. for $C_{25}H_{18}O_3N_2Cl$ $(M+H)^+$ 429.1000, found: 429.1012.

***N*-(5-(5-Chlorobenzo[*d*]oxazol-2-yl)benzo[*d*]thiazol-2-yl)-2-(4-methoxyphenoxy) acetamide (127).** 29 mg, 78% yield; ^{1}H NMR (400 MHz, DMSO-d_6) δ 12.98 (s, 1H), 8.90 (d, *J* = 1.6 Hz, 1H), 8.25 (dd, *J* = 8.4, 1.6 Hz, 1H), 7.91–7.96 (m, 3H), 7.79–7.84 (m, 2H), 7.48–7.78 (m, 2H), 6.92 (m, 1H), 4.51 (s, 2H); HRMS (ESI) calcd. for $C_{23}H_{17}O_4N_3ClS$ $(M+H)^+$ 466.0623, found: 466.0615.

***N*-(4-(5-Chlorobenzo[*d*]oxazol-2-yl)phenyl)-2-(3-methoxyphenoxy)acetamide (130).** 23 mg, 60% yield; ^{1}H NMR (300 MHz, DMSO-d_6) δ 10.46 (s, 1H), 8.17 (br d, *J* = 8.4 Hz, 2H), 7.86–7.95 (m, 3H), 7.81 (d, *J* = 8.6 Hz, 1H), 7.45 (dd, *J* = 8.6, 2.1 Hz, 1H), 7.22 (t, *J* = 8.4 Hz, 1H), 6.53–6.65 (m, 3H), 4.75 (s, 2H), 3.74 (s, 3H); ^{13}C NMR (75 MHz, DMSO-d_6) δ 167.11, 163.63, 160.44, 158.93, 148.96, 142.94, 142.00, 130.01, 128.94, 128.44, 125.16, 120.79, 119.76, 119.23, 112.11,

106.93, 106.72, 101.15, 67.23, 55.12; HRMS (ESI) calcd. for $C_{20}H_{14}O_3N_2Cl$ $(M+H)^+$ 407.0793, found: 407.0790.

***N*-(4-(5-Chlorobenzo[*d*]oxazol-2-yl)phenyl)-2-(4-cyanophenoxy)acetamide (131).** 21 mg, 53% yield; ^{1}H NMR (300 MHz, DMSO-d_6) δ 10.56 (s, 1H), 8.17 (d, *J* = 8.7 Hz, 2H), 7.89–7.95 (m, 6H), 7.44 (dd, *J* = 8.7, 2.1 Hz, 1H), 7.18 (d, *J* = 8.7 Hz, 2H), 4.91 (s, 2H); HRMS (ESI) calcd. for $C_{22}H_{15}O_3N_3Cl$ $(M+H)^+$ 404.0797, found: 404.0803.

***N*-(4-(5-Chlorobenzo[*d*]oxazol-2-yl)phenyl)-2-(4-fluorophenoxy)acetamide (132).** 37 mg, 94% yield; ^{1}H NMR (300 MHz, DMSO-d_6) δ 10.47 (s, 1H), 8.17 (d, *J* = 8.6 Hz, 2H), 7.86–7.95 (m, 3H), 7.81 (d, *J* = 8.6 Hz, 1H), 7.45 (dd, *J* = 8.6, 2.1 Hz, 1H), 7.11–7.20 (m, 2H), 7.00–7.09 (m, 2H), 4.75 (s, 2H); HRMS (ESI) calcd. for $C_{21}H_{15}O_3N_2ClF$ $(M+H)^+$ 397.0750, found: 397.0769.

***N*-(4-(5-Chlorobenzo[*d*]oxazol-2-yl)phenyl)-2-(4-nitrophenoxy)acetamide (133).** 10 mg, 23% yield; ^{1}H NMR (300 MHz, DMSO-d_6) δ 10.43 (s, 1H), 8.13–8.20 (m, 3H), 7.88–7.99 (m, 4H), 7.79–7.82 (m, 2H), 7.25–7.49 (m, 2H), 4.36 (s, 2H); HRMS (ESI) calcd. for $C_{21}H_{15}O_5N_3Cl$ $(M+H)^+$ 424.0695, found: 424.0674.

2-([1,1′-Biphenyl]-4-yloxy)-*N*-(4-(5-chlorobenzo[*d*]oxazol-2-yl)phenyl)acetamide (134). 27 mg, 61% yield; ^{1}H NMR (400 MHz, DMSO-d_6) δ ppm 10.54 (s, 1H), 8.16–8.20 (m, 1H), 7.79–8.00 (m, 5H), 7.61–7.66 (m, 1H), 7.39–7.51 (m, 3H), 7.26–7.38 (m, 1H), 7.11 (d, *J* = 8.8 Hz, 2H), 4.83 (s, 1H); HRMS (ESI) calcd. for $C_{27}H_{20}O_3N_2Cl$ $(M+H)^+$ 455.1157, found: 455.1153.

***N*-(4-(5-Chlorobenzo[*d*]oxazol-2-yl)phenyl)-2-(4-isopropyl-3-methylphenoxy) acetamide (135).** 41 mg, 96% yield; ^{1}H NMR (400 MHz, DMSO-d_6) δ ppm 10.45 (s, 1H), 8.17 (d, *J* = 8.8 Hz, 2H), 7.79–7.98 (m, 4H), 7.45 (dd, *J* = 8.7, 2.1 Hz, 1H), 7.16 (d, *J* = 9.3 Hz, 1H), 6.77–6.83 (m, 2H), 4.71 (s, 2H), 3.03 (sep, J = 6.9 Hz, 1H), 2.27 (s, 3H), 1.14 (d, *J* = 6.9 Hz, 6H); HRMS (ESI) calcd. for $C_{25}H_{24}O_3N_2Cl$ $(M+H)^+$ 435.1470, found: 435.1462.

***N*-(4-(5-Fluorobenzo[*d*]oxazol-2-yl)phenyl)-2-(4-methoxyphenoxy)acetamide (136).** 37 mg, 96% yield; ^{1}H NMR (300 MHz, DMSO-d_6) δ 10.43 (s, 1H), 8.16 (d, *J* = 8.6 Hz, 2H), 7.91 (d, *J* = 8.6 Hz, 2H), 7.80 (dd, *J* = 8.9, 4.4 Hz, 1H), 7.66 (dd, *J* = 8.8, 2.6 Hz, 1H), 7.27 (td, *J* = 9.3, 2.6 Hz, 1H), 6.85–7.01 (m, 4H), 4.69 (s, 2H), 3.70 (s, 3H); HRMS (ESI) calcd. for $C_{22}H_{18}O_4N_2F$ $(M+H)^+$ 393.1245, found: 393.1264.

***N*-(4-(5-Fluorobenzo[*d*]oxazol-2-yl)phenyl)-2-phenoxyacetamide (137).** 39 mg, quantitative yield; ^{1}H NMR (300 MHz, DMSO-d_6) δ 10.48 (s, 1H), 8.17 (d, *J* = 8.5 Hz, 2H), 7.91 (d, *J* = 8.5 Hz, 2H), 7.80 (dd, *J* = 8.9, 4.4 Hz, 1H), 7.66 (dd, *J* = 8.8, 2.6 Hz, 1H), 7.22–7.39 (m, 3H), 6.95–7.07 (m, 3H), 4.76 (s, 2H); HRMS (ESI) calcd. for $C_{21}H_{16}O_3N_2F$ $(M+H)^+$ 363.1140, found: 363.1149.

***N*-(4-(5-Bromobenzo[*d*]oxazol-2-yl)phenyl)-2-(4-methoxyphenoxy)acetamide (138).** 31 mg, 81% yield; ^{1}H NMR (300 MHz, DMSO-d_6) δ 10.43 (s, 1H), 8.17 (d, *J* = 8.5 Hz, 2H), 8.02 (d, *J* = 1.9 Hz, 1H), 7.91 (d, *J* = 8.6 Hz, 2H), 7.76 (d, *J* = 8.6 Hz, 1H), 7.57 (dd, *J* = 8.6, 2.0 Hz, 1H), 6.86–7.00 (m, 4H), 4.69 (s, 2H), 3.70 (s, 3H); ^{13}C NMR (75 MHz, DMSO-d_6) δ 167.44, 163.42, 153.87, 151.74, 149.33, 143.42, 142.04, 128.44, 127.87, 122.14, 120.73, 119.76, 116.68, 115.72,

114.60, 112.60, 67.93, 55.35; HRMS (ESI) calcd. for $C_{22}H_{16}O_4N_2Br$ $(M-H)^-$ 451.0288, found: 451.0307.

2-(4-Methoxyphenoxy)-*N*-(4-(5-phenylbenzo[*d*]oxazol-2-yl)phenyl)acetamide (139). 28 mg, 70% yield; ^{1}H NMR (300 MHz, DMSO-d_6) δ 10.40–10.46 (m, 1H), 8.20 (br d, J = 8.5 Hz, 2H), 8.03 (d, J = 1.7 Hz, 1H), 7.89–7.97 (m, 2H), 7.84 (d, J = 8.6 Hz, 1H), 7.67–7.77 (m, 3H), 7.46–7.54 (m, 2H), 7.35–7.42 (m, 1H), 6.86–7.01 (m, 4H), 4.69 (s, 2H), 3.70 (s, 3H); ^{13}C NMR (75 MHz, DMSO-d_6) δ 167.40, 153.88, 151.76, 149.77, 142.40, 141.76, 140.02, 137.54, 128.94, 128.24, 127.34, 127.08, 124.34, 119.79, 117.53, 115.72, 114.61, 110.96, 67.95, 55.35, 40.22; HRMS (ESI) calcd. for $C_{22}H_{16}O_4N_2Cl$ $(M-H)^-$ 407.0793, found: 407.0790.

2-(4-Methoxyphenoxy)-*N*-(4-(oxazolo[4,5-*b*]pyridin-2-yl)phenyl)acetamide (140). 29 mg, 74% yield; ^{1}H NMR (300 MHz, DMSO-d_6) δ 10.48 (s, 1H), 8.54 (dd, J = 4.8, 1.4 Hz, 1H), 8.20–8.28 (m, 3H), 7.95 (d, J = 8.6 Hz, 2H), 7.45 (dd, J = 8.1, 4.8 Hz, 1H), 6.87–7.02 (m, 4H), 4.71 (s, 2H), 3.72 (s, 3H); HRMS (ESI) calcd. for $C_{21}H_{18}O_4N_3$ $(M+H)^+$ 376.1292, found: 376.1297.

Phenyl (4-(5-chlorobenzo[*d*]oxazol-2-yl)phenyl)carbamate (119). To a solution of 4-(5-chlorobenzo[*d*]oxazol-2-yl)aniline (50 mg, 1 eq) in anhydrous DCM (5 mL) at 0 °C, phenyl chloroformate (31 µL, 1.2 eq) and triethylamine (42 µL, 1.5 eq) was added. The reaction mixture was warmed to room temperature and stirred for 3 h. The reaction was quenched with water (10 mL) and extracted with multiple portions of ethyl acetate (3 × 5 mL). The combined organic extracts were combined, washed with a saturated solution of sodium bicarbonate (10 mL) followed by brine (10 mL), dried over sodium sulfate (10 g), filtered, and concentrated. Compound **123** was

purified by silica gel column chromatography in 50% ethyl acetate/hexanes to yield a white solid (62 mg, 83% yield). ^{1}H NMR (400 MHz, DMSO-d_6) δ ppm 10.72 (s, 1H), 8.15–8.20 (m, 2H), 7.89 (d, *J* = 2.1 Hz, 1H), 7.81 (d, *J* = 8.6 Hz, 1H), 7.74–7.78 (m, 2H), 7.42–7.48 (m, 3H), 7.25–7.34 (m, 3H); HRMS (ESI) calcd. for $C_{21}H_{16}ClO_4N_2$ $(M+H)^+$ 365.0688, found: 365.0694.

4-Methoxyphenyl (4-(5-chlorobenzo[*d*]oxazol-2-yl)phenyl) carbamate (123). To a solution of 4-(5-chlorobenzo[*d*]oxazol-2-yl) aniline (50 mg, 1 eq) in anhydrous DCM (5 mL) at 0 °C, 4-methoxyphenyl chloroformate (36 µL, 1.2 eq) and triethylamine (42 µL, 1.5 eq) was added. The reaction mixture was warmed to room temperature and stirred for 3 h. The reaction was quenched by water (10 mL) and extracted with multiple portions of ethyl acetate (3 × 5 mL). The combined organic extracts were combined, washed with saturated solution of sodium bicarbonate (10 mL) and brine (10 mL), dried over sodium sulfate (10 g), filtered, and concentrated. Compound **127** was purified by silica gel column chromatography in 50% ethyl acetate/hexanes to yield a white solid (81 mg, 79% yield). ^{1}H NMR (400 MHz, DMSO-d_6) δ 10.66 (s, 1H), 8.16 (s, 1H), 7.89 (d, *J* = 2.1 Hz, 1H), 7.82 (d, *J* = 8.6 Hz, 1H), 7.73–7.78 (m, 2H), 7.45 (dd, *J* = 8.6, 2.2 Hz, 1H), 7.16–7.22 (m, 2H), 6.96–7.01 (m, 2H), 3.78 (s, 3H); HRMS (ESI) calcd. for $C_{21}H_{16}ClO_4N_2$ $(M+H)^+$ 395.0793, found: 395.0792.

***N*-(4-(5-Chlorobenzo[*d*]oxazol-2-yl)phenyl)-2-(4-methoxyphenoxy)-*N*-methyl acetamide (128).** To a solution of **116** (10 mg, 1.0 eq) in anhydrous THF (1 mL) at 0 °C, LiHMDS (30 µL, 1.2 eq, 1 M in THF) was added the suspension was stirred for 30 min. Methyl iodide (5 µL, 3.3 eq) was added to this solution at 0 °C and the reaction mixture was warmed to room temperature and stirred overnight. Upon complete consumption of 12, the reaction mixture was concentrated.

Compound **132** was purified by silica gel column chromatography using 30% ethyl acetate/hexanes to yield a white solid (8.9 mg, 86% yield). ^{1}H NMR (400 MHz, DMSO-d_6) δ 8.23 (d, *J* = 8.4 Hz, 2H), 7.94 (d, *J* = 2.0 Hz, 1H), 7.84 (d, *J* = 8.4 Hz, 1H), 7.66 (d, *J* = 8.4 Hz, 2H), 7.48 (dd, *J* = 8.7, 2.4 Hz, 1H), 6.76–6.82 (m, 4H), 4.63 (br s, 3H), 3.66 (s, 3H), 3.30 (s, 3H); HRMS (ESI) calcd. for $C_{23}H_{20}O_4N_2Cl$ $(M+H)^+$ 423.1106, found: 423.1110.

***N*-(4-(5-Chlorobenzo[*d*]oxazol-2-yl)phenyl)-2-(4-methoxyphenoxy)-*N*-(prop-2-yn-1-yl)aceta mide (129).** To a solution of **116** (50 mg, 1.0 eq) in anhydrous DMF (3 mL) at 0 °C, sodium hydride (6 mg, 60% suspension in mineral oil, 1.2 eq) was added the suspension was stirred for 15 min. Propargyl bromide (22 µL, 1.2 eq, 80 wt% solution in toluene) was added dropwise to this solution at 0 °C and the reaction mixture was warmed to room temperature and stirred overnight. Upon complete consumption of **12**, the reaction mixture was quenched by ice-water mixture (5 mL) and extracted with multiple portions of ethyl acetate (3 × 5 mL). The combined organic extracts were combined, washed with brine (10 mL), dried over sodium sulfate (10 g), filtered and concentrated. Compound **133** was purified by silica gel column chromatography with 30% ethyl acetate/hexanes to yield a yellow solid (24 mg, 44% yield). ^{1}H NMR (300 MHz, DMSO-d_6) δ 8.07 (d, *J* = 8.9 Hz, 2H), 7.82 (d, *J* = 2.1 Hz, 1H), 7.76 (d, *J* = 8.7 Hz, 1H), 7.39 (dd, *J* = 8.6, 2.2 Hz, 1H), 7.08 (d, *J* = 9.1 Hz, 2H), 6.84–6.90 (m, 4H), 4.31 (d, *J* = 2.3 Hz, 3H), 3.57–3.65 (m, 1H), 3.23 (t, *J* = 2.1 Hz, 2H); HRMS (ESI) calcd. for $C_{25}H_{20}O_4N_2Cl$ $(M+H)^+$ 447.1106, found: 447.1105.

2.0 Introduction to caged morpholinos (cMO)

Over the years, gene knockdown tools have improved in terms of specificity and reduced off-target effects.[247] A reverse genetics approach of RNA silencing requires high sequence specificity without non-antisense-mediated interactions with other biomolecules. The introduction of first antisense agent was reported by Stephenson and Zamecnik in 1978. The authors utilized a 13-nucleotides long single-stranded DNA (ssDNA) complementary to the 3' and 5'-terminal sequences of Rous sarcoma virus 35S RNA in chick embryo fibroblast tissue culture infected with Rous sarcoma virus.[248] The ssDNA and modifications like phosphorothioate-DNA (PS-DNA) constitute the first generation of antisense agents. These antisense agents suffer from nuclease cleavage and potential cellular toxicity.[249-250] In additions, PS-DNAs have a high affinity for proteins because of the sulfur-containing backbone.[251] For example, these oligonucleotides interact with a number of proteins including laminin, protein kinase C, DNA polymerase, and telomerase, etc.[251] To address these issues, second generation antisense agents were developed. These antisense agents include DNAs and RNAs with 2'-*O*-alkyl modifications. These modifications provide resistance to nuclease cleavage and less toxicity, along with better binding affinity with the target mRNA compared to the first-generation agents. The third-generation of antisense agents comprises of oligonucleotides with a significant change in the structures of nucleobases from the first- and second-generation agents. The third generation of antisense agents include peptide nucleic acids (PNA), locked nucleic acids (LNA), and morpholino oligomers (MO). PNAs are oligomers with repeating *N*-(2-aminoethyl)-glycine units linked by peptide bonds and nucleobases are linked to the backbone as an amide linkage with a methylene bridge. PNAs have been utilized in a variety of applications like DNA decoys, antagomirs, PCR primers, and antisense agents.

PNAs are resistant to endogenous nucleases as well as peptidases, and exhibit higher binding affinity to the complementary target sequences. LNAs are oligomers with modifications to the ribose ring and provide a better affinity to the target mRNAs along with better cellular uptake than the first- and second-generation antisense agents.

Morpholino oligomers (MOs) are synthetic phosphorodiamidate morpholino oligomers used as antisense agents for silencing gene function and function by binding to RNA molecules following Watson-Crick base-pairing rules.[252] MOs have a backbone of methylenemorpholine bridges with phosphorodiamidate linkages (**Figure 33A**). These oligomers contain DNA nucleobases attached to individual morpholine units. MOs are usually characterized by their high specificity, resistance to nucleases, stability in biological systems, and predictable targeting.[247, 253] Due to the presence of non-charged phosphorodiamidate groups in the backbone, MOs are less likely to nonselectively bind to cellular proteins.[254] Additionally, the complex formed is a MO–RNA heteroduplex and is quite stable (more stable than DNA–RNA or PS-DNA–RNA duplex, but weaker than LNA–RNA duplex).[255] An MO with 25-bases long is generally used for antisense applications and a long MO provides high specificity towards target RNA sequences. MOs have been used to target mature miRNAs[256-257] and the miRNA maturation pathway[258].

Conventionally, MOs were utilized to target the translational start codon of mRNAs of genes of interest.[253] MOs targeted to the 5'-untranslated region (5'-UTR) of the start codon prevent binding of the translational machinery to mRNA. MOs have been used with great effect to understand genetic pathways in several vertebrates.[253] Effects of developmental signaling genes including no tail (*ntl*), chordin, one-eyed pinhead, and sonic hedgehog were studied with rapid 'knockdown' of these genes by MOs in zebrafish.[259] Erickson and colleagues used MOs directed against transcription factor FoxD3 in chick embryos.[260] Angerer and co-workers used MOs

designed to block SpKr1, a transcription factor for β-catenin regulation, in sea urchin embryos.[261] These examples point towards the precise targeting of MOs in producing mutant phenotypes with temporal control.[253] Moving beyond temporal control, spatiotemporal control with MOs was achieved by conditional gene silencing, first demonstrated by the Chen Lab.[262]

In 2007, the Chen lab from Stanford University reported a study on light-controlled MO-based gene silencing in zebrafish embryos.[262] To study conditional gene silencing using an MO caging strategy, they selected no tail (*ntl*) gene. The *Ntl* is zebrafish homologue of mouse Brachyury, a T-box transcription factor. The *Ntl* transcription factor is required for formation of the tail and notochord, and is expressed during gastrulation in the germ ring, shield, and chordamesoderm.[263-264] This gene is restricted to the notochord and tailbud during somitogenesis. Phenotypes associated with zebrafish *ntl* mutants include loss of notochord cells and posterior structures. Also, a rounded-off, U-shaped morphology is seen in *ntl* mutants and morphants, compared to the V-shaped wild-type morphology.[263-264]

Photocontrol was achieved by tethering a 3'-azide functionalized *ntl* MO to an 5'-alkyne-modified antisense inhibitor (a decamer MO) by Huisgen 1,3-dipolar cycloaddition (**Figure 2-1A**). The inhibitor-*ntl* MO structure forms a hairpin caged MO (hairpin cMO). The structure also contains a photocleavable dimethoxynitrobenzyl (DMNB) group on the 5'-tether side and a fluorescein moiety on the 3'-end for visualization by fluorescence microscopy (**Figure 2-1B**). Wild-type zebrafish embryos were injected with *ntl* cMO and were either globally irradiated with 360-nm UV light at 4 hours post-fertilization (4 hpf), or were cultured in dark. At 24 hpf, the non-irradiated embryos developed normally, while most of the irradiated embryos exhibited a loss in posterior structures, lack of notochord cells, and U-shaped morphology typical of *ntl* mutants. As

controls, non-injected embryos and 5’-DMNB-tethered decamer MO inhibitor injected embryos were not affected upon irradiation (**Figures 2-1C–2-1J**).

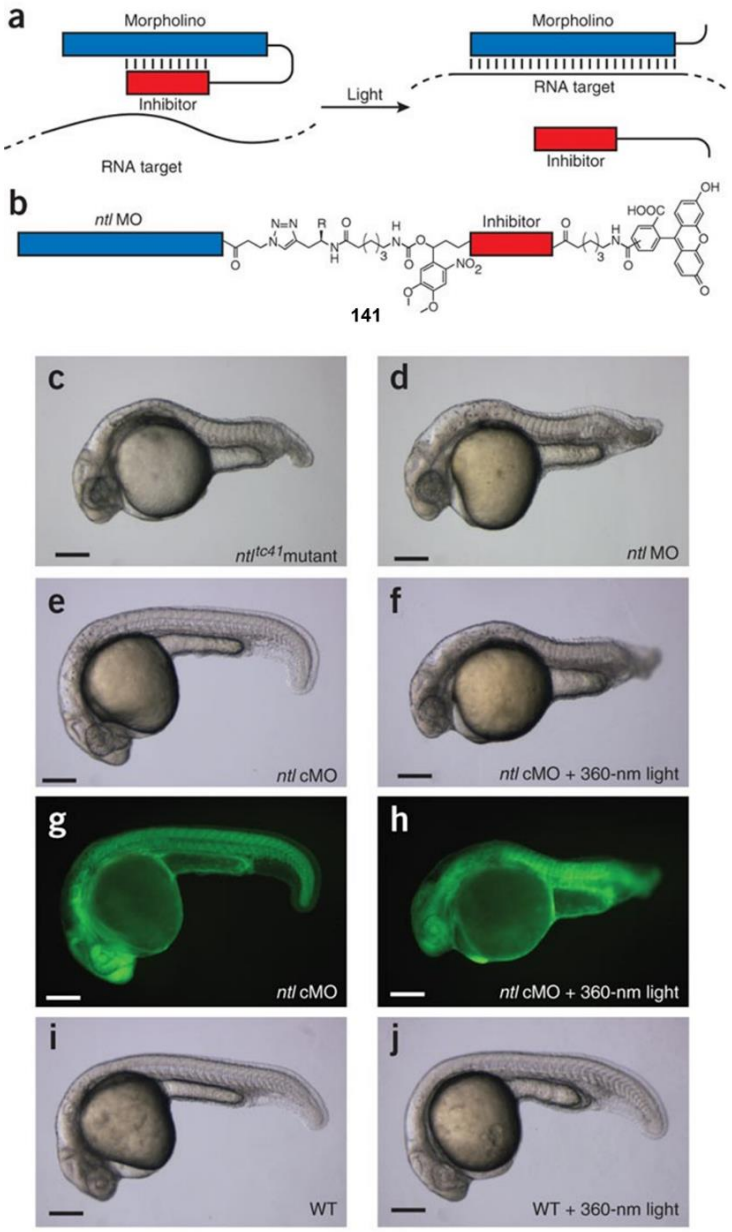

Figure 2-1 First example of caged MO targeting *ntl* gene in zebrafish embryos.

(A) Schematic diagram for light activation of hairpin cMO. (B) Structure of caged MO **141**. (C, D) Identical phenotypes of *ntl*^{tc41} mutant and *ntl* morphant. (E, F) Phenotypes observed with *ntl* cMO without and with 360-nm light irradiation. No particular phenotypic change compared to wild-type is observed in *ntl* cMO without light irradiation. (G, H) Fluorescence imaging confirms a uniform reagent distribution. (I, J) Light irradiation does not significantly affect wild-type embryos. Adapted from *Nat. Chem. Biol.*, **2007**, 3 (10), 650.[262]

Furthermore, *ntl* cMO was activated at various stages of embryo development. Irradiation at the 16-cell stage (1.5 hpf) produced a phenotype similar to the *ntl* mutant. Irradiation at the sphere stage (4 hpf) led to missing notochord cells and U-shaped somites, but a significant proportion of those embryos exhibited limited posterior development. This could be attributed to some *ntl* protein present even after *ntl* gene silencing. At 12 hpf, irradiation produced embryos with incompletely vacuolated notochord cells, V-shaped somites, and a shortened anterior-posterior axis. This study demonstrated a spatiotemporal control over gene silencing with photocontrollable MO construct.

In another approach, a sense RNA inhibitor strand consisting of two complementary RNA strands connected by a nitrobenzyl-based linker was utilized to supress antisense MO function.[265] The active antisense MO can be released from the MO–RNA inhibitor duplex by UV irradiation that cleaves and separates the sense inhibitor strand. Among various other targets studied, this technology was utilized to conditionally target *ras homolog enriched in brain* (*rheb*) gene. The time course of uncaging was monitored by RT-qPCR and the uncaging was monitored at 24 hpf, 48 hpf, and 72 hpf. At 72 hpf, the gene knockdown was less pronounced due to inefficient caging at later time points. Futhermore, a large excess (5-fold) of the caging strand was required to completely inactivate the antisense MO indicating weak base-pairing interactions of the MO–RNA inhibitor duplex.

In 2012, two photo-MO technologies were reported – sense-photo-MOs (S-photo-MOs) with a stable MO-MO inhibitor duplex (replacing the instable MO-RNA inhibitor duplex) and an antisense-photo-MO (AS-photo-MOs) containing a nitrobenzyl-based photocleavable group that can be cleaved by UV irradiation (**Figure 2-2**).[266] It was shown that to cleave and separate the MO inhibitor from the active antisense MO, either a MO inhibitor with a 21-nucleotides long or 25-

nucleotides long with 4 mismatches was necessary for a 25-nucleotides long antisense MO. Additionally, a strict stochiometric (1:1) ratio of the antisense MO and the MO-MO inhibitor duplex was important for optimal binding and dissociation properties. Using this technology, a number of genes were targeted including *ntla*, *gal4*, and *sox10*. An advantage of this methodology is the ease of synthesis of the MO–MO inhibitor duplex in comparison to the hairpin cMO.

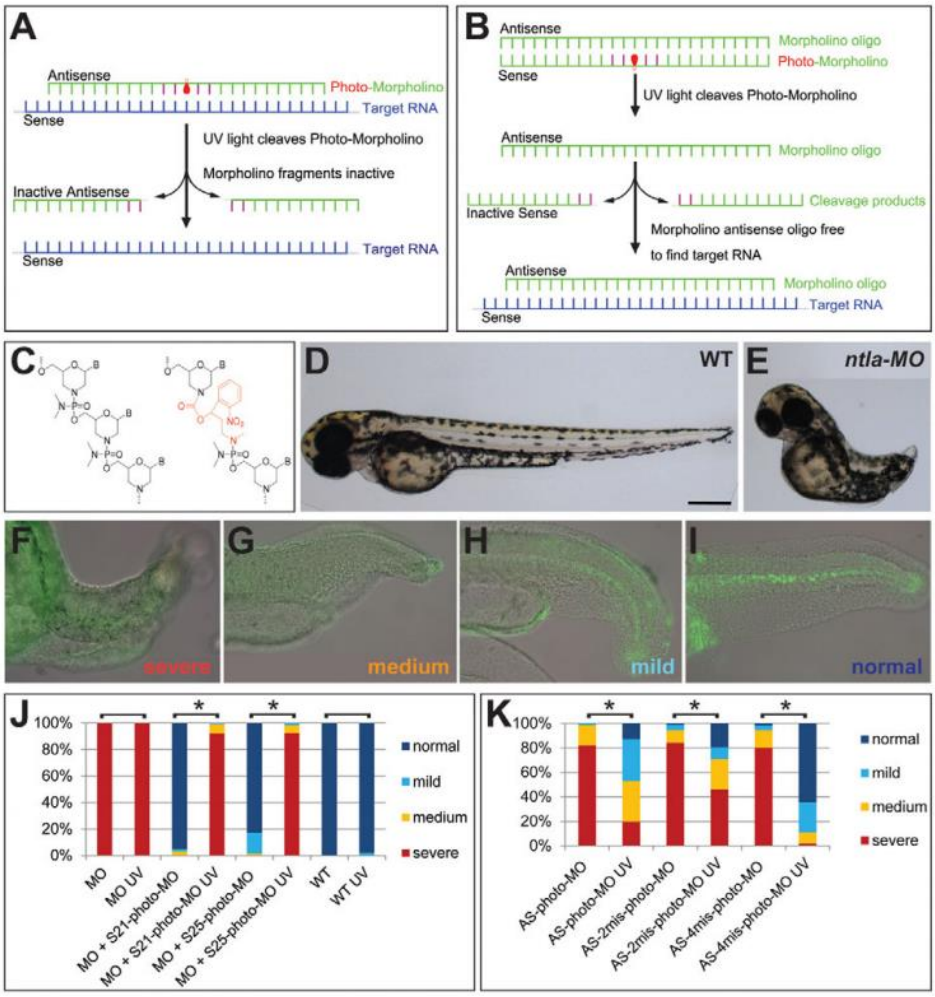

Figure 2-2 Photo-MOs for regulation of *ntla* gene function.

(A) Diagram detailing the mode of action of antisense-photo-MOs (AS-photo-MOs). (B) Diagram detailing the mode of action of sense-photo-MOs (S-photo-MOs). (C) Structures of MOs and nitrobenzyl-based photocleavable linker. (D, E) Wildtype and *ntla* morphant phenotype. (F, G, H, I) Overlays showing bright field and anti-Ntla labeling (green) in injected embryos at 26-28 hpf. Examples of severe (F), medium (G), mild (H) and normal (I) phenotypes. (J, K) Graphs showing percentage of embryos injected with MOs and photo-MOs and the phenotype observed with or without UV irradiation. S21-photo-MO: *ntla*-sense-photo-MOs of a length of 21 nucleotides, S25-photo-MO: *ntla*-sense-photo-MOs of a length of 25 nucleotides with 4 mismatches, AS-2mis-photo-MO: *ntla*-antisense-photo-MOs with 2 mismatches, AS-4mis-photo-MO: *ntla*-antisense-photo-MOs with 4 mismatches. Introducing 2 mismatches on either side of the photo-subunit (AS-4mis-photo-MO) significantly improved dissociation rate from the target sequence. Adapted from *Development*, **2012**, 139, 1691.[266]

In 2010, the Deiters Lab in collaboration with the Yoder Lab demonstrated a more direct approach to photoactivation of caged morpholino monomers in MOs to regain RNA-binding ability.[267] Here, 6-nitropiperonyloxymethyl (NPOM) caged morpholino monomers were incorporated into an MO sequence targeting the *chordin* gene in zebrafish and *Xenopus* embryos (**Figure 2-3A**). The presence of the NPOM group hinders the ability of the MO sequence to hybridize with the target gene. This was evident from the melting temperature experiments in which T_ms for RNA-MO duplexes were compared to T_ms for RNA-MO^4 duplexes with four NPOM-caged monomers. T_m for the EGFP-MO^4 duplex showed a 30 °C decrease in comparison to EGFP-MO^0 duplex with no caging groups, and T_m for the *chordin*-MO^4 duplex showed a 10 °C decrease compared to *chordin*-MO^0 duplex. Thus, this approach is unique as neither external inhibitors nor topological constraints are necessary to effect a light-activated regulation of gene function.[267]

Knockdown of the *chordin* gene is characterized by a shrunken head and a ventralized tail by 24-28 hpf when chordin-MO^0 is injected during 1-4-cell stage.[259] In embryos injected with *chordin*-MO^4, 365-nm UV-light activation resulted in > 90% embryos exhibiting the *chordin* knockdown phenotype (**Figures 2-3B–2-3I**). In the case of *Xenopus* frog embryos, a single cell at the 8-16-cell stage was co-injected with synthetic EGFP mRNA, EGFP-MO^4 and synthetic mCherry mRNA. It was observed that EGFP expression went down only after brief UV exposure, with mCherry expression unaffected. Thus, the authors successfully demonstrated gene regulation in this caging strategy.[267]

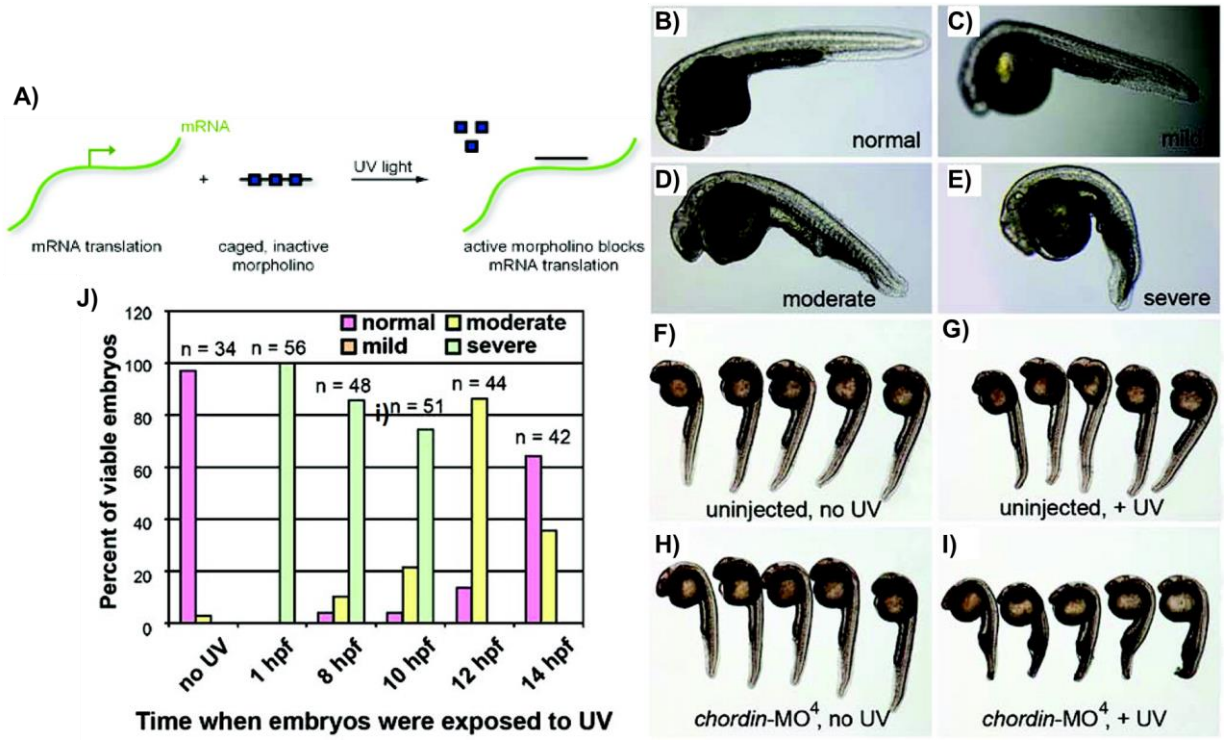

Figure 2-3 Effects of MO containing caged morpholino monomers on zebrafish embryos.

(A) Schematic representation of mode of action of MO containing caged morpholino monomers. NPOM caging group represented by box. (B, C, D, E) Classification of phenotypes in zebrafish embryos 24-28 hpf. (F, G) Zebrafish embryos are not affected by brief UV exposure in the absence of MO. (H, I) UV exposure on chordin-MO^4 injected embryos exhibit the reported aberrant phenotype, while the normal phenotype is observed in chordin-MO^4 injected embryos without UV exposure. Adapted from *J. Am. Chem. Soc.*, **2010**, 132 (44), 15644.[267]

Two years later, the Chen group published another report on caging techniques for MOs and introduced a new topology for cMOs: a cyclic structure for cMOs without the use of an inhibitor for hairpin cMOs.[268] The cyclic structure was attained by joining both the ends of the MO to a linker through orthogonal reactions. The photocleavable DMNB-linker contained an *N*-hydroxysuccinimide (NHS) ester on one end and a chloroacetamide group on the other, which would react specifically towards a 5'-amine and 3'-disulfide-containing MO. For testing the effectiveness of cyclic cMOs, again *ntl* gene in zebrafish embryos was targeted. The cyclic MOs

elicited similar response to hairpin MOs, with 90% of the embryos exhibiting the *ntl* morphant phenotype on irradiation 3 hpf (**Figure 2-4A–2-4C**). Another experiment comparing cyclic cMOs to hairpin cMOs was performed with pancreas exocrine-specific *pancreas transcription factor 1 alpha* (*ptf1a*) in zebrafish embryos as a target. Almost 95% of embryos injected with cyclic cMOs, upon irradiation, exhibited no formation of pancreatic exocrine cells after 72 hpf, whereas embryos injected with hairpin cMOs showed partial disruption of pancreatic exocrine cells possibly due to linker degradation or linearization of hairpin cMOs during 72 h, highlighting the advantages of the topology of cyclic cMOs over hairpin cMOs for conditional gene silencing studies. Additionally, cyclic cMOs eliminates the need of inhibitor strand, which, upon photocleavage, the inhibitor strand and the MO strand separates and the presence of the inhibitor strand can trigger off-target cytotoxic effects.[268]

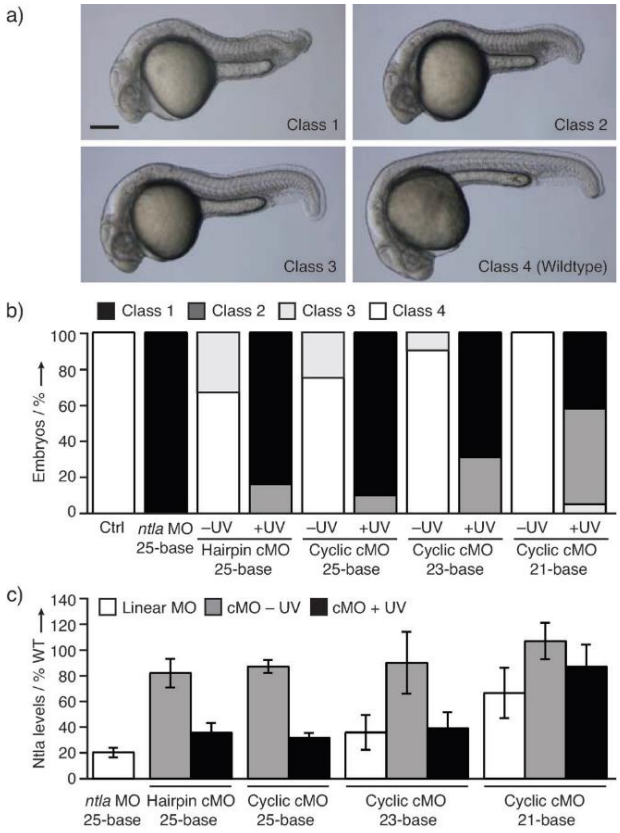

Figure 2-4 Comparative studies on hairpin cMO and cyclic cMO.

(A) Four classes of phenotypes observed on light activation of cMOs at 24 hpf. (B) Phenotypic distribution observed with or without UV irradiation upon injecting indicated cMOs. (C) Ntl protein levels at 10 hpf under indicated conditions. Adapted from *Angew. Chem. Int. Ed.*, **2012**, 51 (28), 6908.[268]

Later in 2014, the Deiters Lab in collaboration with the Chen Lab published a study on gene silencing by wavelength-selective light activated cyclic cMOs.[269] In this study, four wavelength-specific linkers containing DMNB, 2-nitrobenzyl (NB), 7-(diethylamino)coumarin (DEACM) and diethylaminocoumarylidenemalononitrilemethyl (DEACM-MN) groups were synthesized, and here as well, *ntl* MO was optically controlled with these linkers. These linkers are photocleaved specifically at 365 nm, 405 nm, and 470 nm, respectively. A wavelength-specific activity profile of these cMOs revealed NB and DMNB linkers to be quite selective towards 365

nm light, whereas DEACM and DEACM-MN linkers to be activated by both 405 nm and 470 nm light (**Figure 2-5**). Furthermore, NB and DEACM cyclic cMOs were employed in examining the timing of mesoderm patterning.[269]

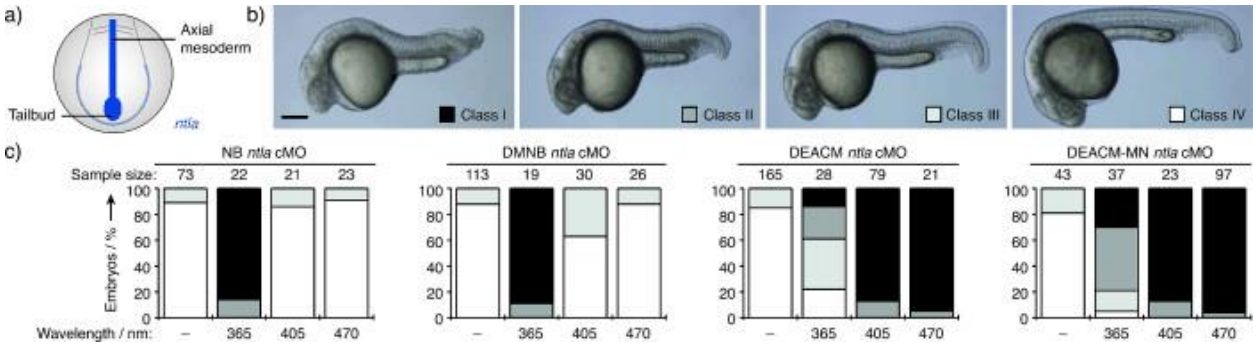

Figure 2-5 Studies on wavelength-selective activation of cMOs.

(A) Schematic diagram of *ntla*-expressing embryos highlighting axial mesoderm and tailbud. (B) Classification of phenotypes at 24 hpf upon irradiation of cMO. (C) Phenotypic distribution observed in wavelength-selective activation of *ntla* cMOs at 3.5 hpf. Adapted from *Angew. Chem. Int. Ed.*, **2014**, 126 (38), 10278.[269]

The same year, Chen lab reported a nitroreductase-activatable cyclic cMOs as a first example of enzyme trigger for activation.[270] Here as well, they targeted *ntl* gene as it is a well-studied gene with a known phenotype. A similar linker **142** (**Figure 2-12A**) was prepared, with a 4-nitrobenzyl group in place of the DMNB group, and a nitroreductase (nfsB-mCherry) mRNA construct was transfected into embryos. Subsequent studies established nitroreductase as an effective and an alternative trigger to light activation.

2.1 Small molecule-based activation of cMOs

2.1.1 Introduction

Photoactivatable linkers are limited to samples into which light can penetrate for effective spatial control. Tissues with complex 3D morphology and depth are almost inaccessible to light of any wavelength (**Figure 2-6**).[271] Most of the reported photoactivatable linkers can be uncaged by UV light, making deep tissues unaccessible. Two-photon uncaging with IR photons rather than the customary single UV photons helps to focus activation in the *z*-dimension improves penetration depth, but often requires elaborate instrumental setup. As another limiting factor, cells with rapid movements are challenging to target for spatial control using optical methods.[270]

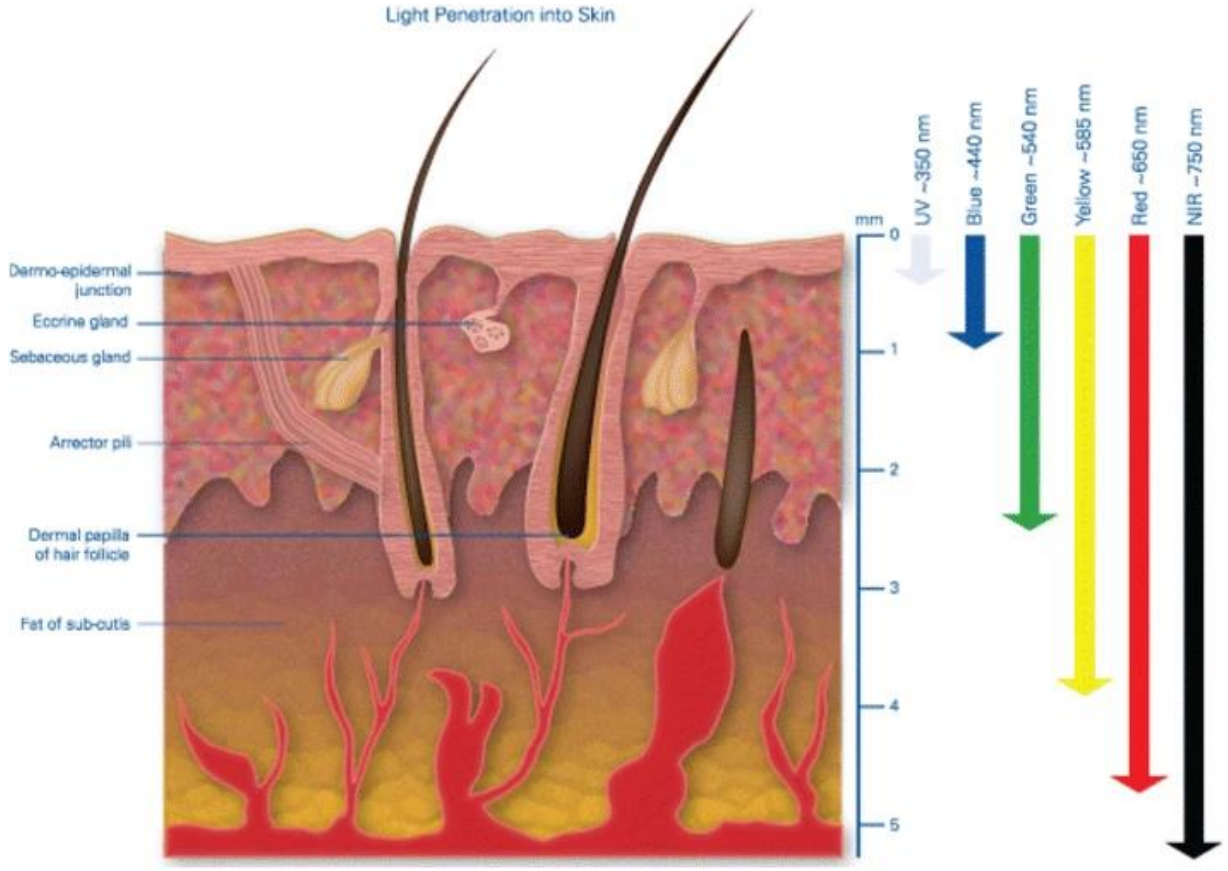

Figure 2-6 Penetration depth of different wavelengths of light into human skin.

UV light has the lowest penetrative depth (< 1 mm), while red and near-infrared light penetrates 5 mm.[271]

Small molecules and enzymes can also trigger cMO activation. These triggers solve the aforementioned problems with light activation. Small molecules may be modified easily for increased efficiency towards activating cMOs. Bioothogonal chemistry can be viewed as a promising technology towards this goal.

2.1.2 Tetrazine-*trans*-cyclooctene bioorthogonal reaction

"Bioorthogonal reaction" is a term coined by Prof. Carolyn Bertozzi and refers to any reaction which is mutually exclusive to other reactions and can occur within living systems without interfering with natural biochemical processes.[272] To date, a number of bioorthogonal pairs have been reported, including phosphine-azide,[273] isonitrile-tetrazine,[274] etc. The first bioorthogonal reaction to be developed was the phosphine-azide reaction.[273] In this study, Prescher et al. developed the century-old Staudinger reaction (phosphine-mediated reduction of azides to amines) to achieve ligation. Ligation was achieved by trapping of the 'aza-ylide' intermediate by a nearby electrophilic trap (methyl ester) to yield an amide, linking the two partners. Here, cells containing an azide-modified unnatural sugar effected remodelling of cell surface glycans and enabled cell identification and sorting by use of specific antibodies to study glycosylation patterning.[273] Although the Staudinger reduction exhibit high bioorthogonality, this reaction suffers from slow reaction kinetics (second-order rate constant in the low 10^{-3} $M^{-1}s^{-1}$ range) and potential for off-target redox chemistry.[275] In particular, the phosphines are prone to air oxidation or metabolic enzymes and react with disulfides (can be overcome by large excess of phosphines),[275] while azides undergo reduction with disulfides.[276]

Tetrazines' reaction with alkenes and alkynes has been exploited before for different bioorthogonal ligation approaches;[277] the tetrazine-*trans*-cyclooctene pair is of particular interest. The tetrazine-*trans*-cyclooctene pair is distinguished among the bioorthogonal pairs known by faster reaction kinetics and relative non-toxicity of the reactants and by-products.[278] The reaction of 1,2,4,5-tetrazine (hereafter referred to as "tetrazine") with *trans*-cyclooctene is an example of the inverse electron-demand Diels-Alder (iEDDA) reaction.[279] As opposed to the "normal" electron-demand Diels-Alder reactions involving an electron rich diene and an electron poor

dienophile, iEDDA reactions comprise an electron rich dienophile and electron deficient diene. Frontier molecular orbital analysis reveals "normal" electron-demand Diels-Alder reactions to be facile based on the small separation in energy between the $HOMO_{diene}$–$LUMO_{dienophile}$ orbitals (**Figure 2-7**). On the contrary, in iEDDA reactions, reactivity is dominated by $HOMO_{dienophile}$–$LUMO_{diene}$ orbital gap. Here, the tetrazines constitutes the electron deficient diene, and *trans*-cyclooctene constitutes the dienophile.[279] The particular reason for utilizing *trans*-cyclooctene is the inherent strain in the eight-membered ring. The ring strain in eight-embered rings has a precedence of solving problems for biooorthogonal chemistry. A class of reactions called copper(I)-catalysed Azide-Alkyne Cycloaddition (CuAAC) utilizes copper(I) catalysts to promote 1,3-dipolar azide-alkyne reactions (also known as the Huisgen 1,3-dipolar cycloaddition). CuAAC was employed for many ligation applications.[280] These reactions, however, were limited to *in vitro* applications due to the toxicity of the copper(I) catalyst (and its potential for oxidation in many conditions). These limitations were addressed by the development of Strain-Promoted Azide-Alkyne Cycloaddition (SPAAC) reactions. Azide-cyclooctyne forms a SPAAC pair, where the reaction is promoted by inherent strain in the cyclooctyne eight-membered ring, eliminating the need for copper(I) catalysts.[281] SPAACs have been used in many *in vivo* ligation applications, but the kinetics and biocompatibility often are suboptimal. Tetrazine-*trans*-cyclooctene chemistry employs similar principles with faster reaction kinetics, once again taking advantage of ring strain for use in bioorthogonal chemistry.

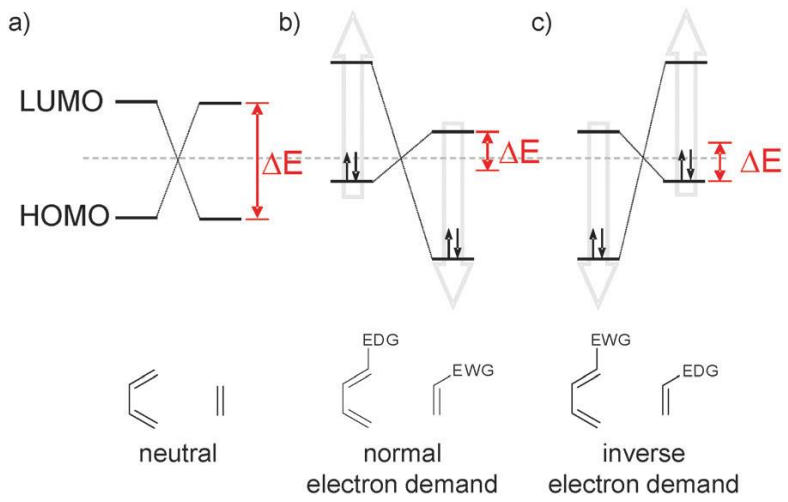

Figure 2-7 Frontier orbital model of Diels-Alder cycloadditions.

(A) neutral electron demand, (B) normal electron demand, and (C) inverse electron demand. (EDG = electon donating group, EWG = electron withdrawing group). LUMO: lowest unoccupied molecular orbital; HOMO: highest occupied molecular orbital. Adapted from *Chem. Soc. Rev.*, **2013**, 42 (12), 5131.[279]

Traditionally, these bioorthogonal reactions have been used to link molecules. However, these reactions may also be used for spatiotemporally-controlled release of bioactive substances — a "click-to-release" approach. In 2013, Versteegen et al. reported a nearly instantaneous release of caged doxorubicin on ligation of *trans*-cycloocten-2-ol with tetrazine.[282] Doxorubicin attached to *trans*-2-cyclooctenol through a carbamate linkage is specifically released on reaction and subsequent rearrangement and elimination with tetrazines (**Figure 2-8A**). As an example, doxorubicin conjugated to *trans*-cycloocten-2-ol (**143**) was released within minutes in 79% yield on reaction with 3,6-di(pyridin-2-yl)-1,2,4,5-tetrazine (**144**).[282] Subsequently, a year later, Chen's group published a detailed study of these reactions, demonstrating tetrazine-mediated release of the amino acid lysine (**Figure 2-8B**).[109] *Trans*-2-cyclooctene-conjugated lysine (**145**) was incorporated into firefly luciferase in HEK293T cells, and a 90% rescue of enzymatic activity was observed when treated with 3,6-dimethyl-1,2,4,5-tetrazine (**146**, 100 μM) for 60 min (**Figure 2-**

8C). They reported two isomers of *trans*-2-cyclooctenol-conjugated lysines (**Figure 2-15**), axial (**180a**) and equatorial (**180e**), with the axial isomer having faster reaction kinetics; specifically, the axial isomer reacted to completion with tetrazine **146** within 5 min, while the equatorial isomer required > 3 h to reach saturation. A number of tetrazines were screened, with dimethyl tetrazine **146** giving the best results – a 92% yield of lysine (**147**) released from the axial isomer **180a**, and 98% yield of lysine (**147**) released from the equatorial isomer **180e**.[109]

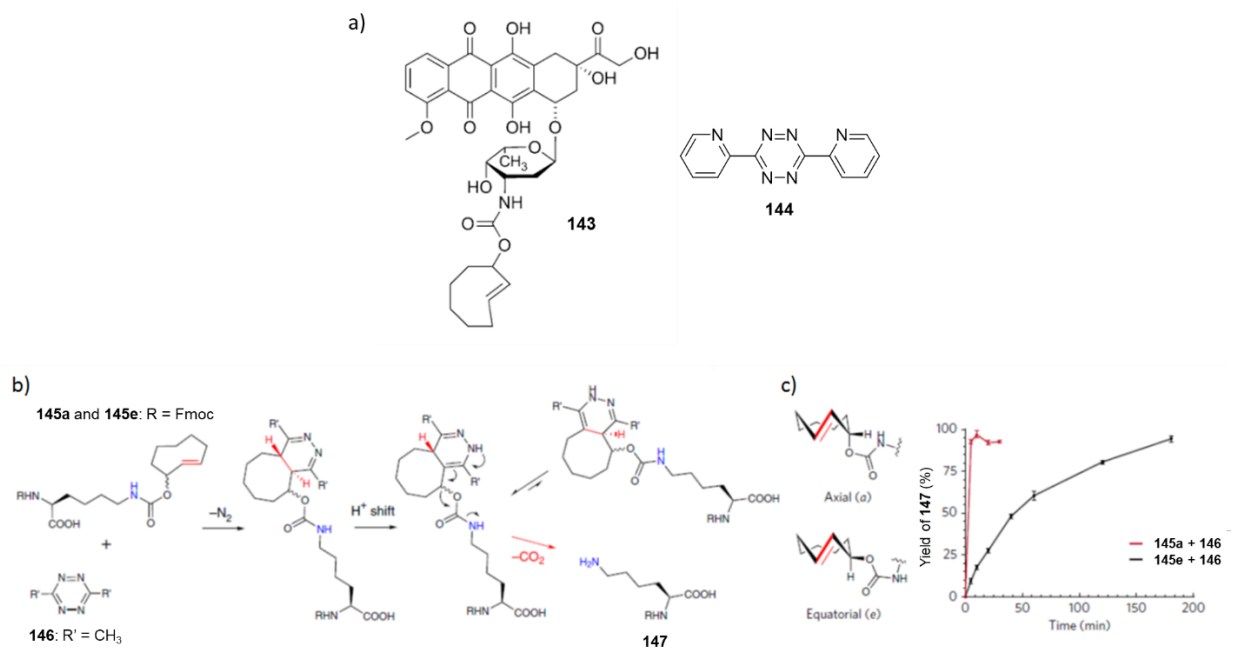

Figure 2-8 Tetrazine-mediated decaging strategy and proposed mechanism.

(A) First example of tetrazine-mediated decaging with trans-cycloocten-2-ol caged-doxorubicin **143** and tetrazine **144**. Adapted from *Angew. Chem. Int. Ed.*, **2013**, 52 (52), 14112.[282] (B) Possible mechanism of tetrazine (**146**)-mediated decaging of axial and equatorial isomer-lysine-conjugate (**145a** and **145e**). (C) Kinetics of **145a** and **145e** decaging by tetrazine **146**, demonstrating the superiority of the axial isomer. Adapted from *Nat. Chem. Biol.*, **2014**, 10, 12, 1003.[109]

After this initial work, a detailed study of tetrazine optimization for bioorthogonal decaging was reported by Chen and co-workers.[283] A library of tetrazines were screened against fluorogenic *trans*-cycloocten-2-ol-caged-coumarin (**148**) for coumarin (**149**) release (**Figure 2-9A**). From the screening data, the authors concluded that asymmetrical tetrazines showed enhanced decaging activities compared to symmetrical ones. The presence of an electron-withdrawing group (EWG) is necessary to accelerate the cycloaddition step, while a while the para position must not be electron deficient for efficient elimination (**Figure 2-9B**). Tetrazine **150** showed excellent decaging efficiency *in vitro*, whereas tetrazine **151** exhibited the highest decaging activity in HEK293T cells (> 90% coumarin recovery with 50 µM **151** within 4 min) (**Figure 2-9C**).

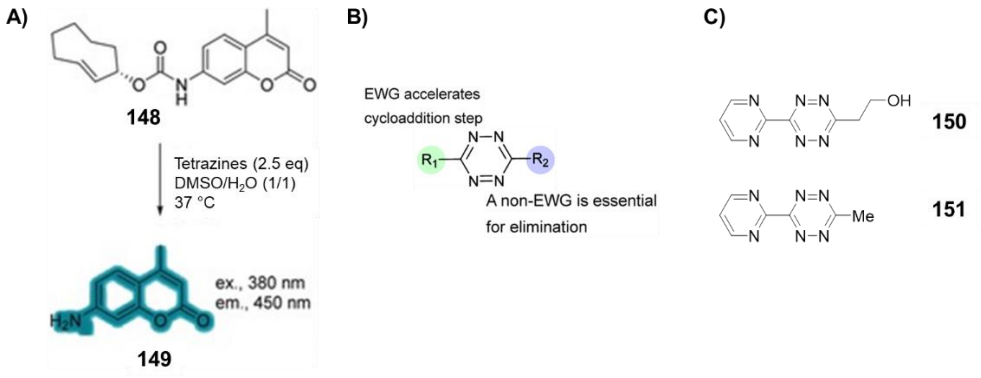

Figure 2-9 Optimization of tetrazines for "click-to-release" applications.

(A) *Trans*-cycloocten-2-ol-coumarin conjugate (**148**) releases coumarin (**149**) after tetrazine reaction. (B) Guidelines for tetrazine design for "click-to-release" applications. (C) Tetrazines **150** and **151**, which demonstrate faster kinetics and better efficiency of *trans*-cycloocten-2-ol decaging for *in vitro* and *in vivo* applications, respectively. (EDG = electon donating group, EWG = electron withdrawing group). Adapted from *Angew. Chem. Int. Ed.*, **2016**, *55*, 45, 14046.[283]

The Weissleder lab investigated the crucial features of this reaction with the goal of attaining higher efficiency.[284] The authors found that the release rate and kinetics are highly

sensitive to pH and to the functional groups present on the tetrazine, as well as the *trans*-cycloocten-2-ol linkage. For favorable release, rapid tautomerization to the pre-release intermediate was enhanced by acid-functionalized tetrazines. This is evident from a complete release of the fluorophore upon incubating diacid tetrazine **PA$_2$** with **152** (**Figure 2-10A**). The acid group is proposed to coordinate with the pre-release complex to facilitate elimination and release of the payload. However, the acid-functionalized tetrazines are dependent on pH, with higher rate of release of the payload observed at low pH owing to the feasibility of the formation of pre-release complex. In general, it was discovered that alkyl containing tetrazines are sensitive to pH; the payload release by tetrazine **146** was completed within an hour under acidic conditions (pH 5.0), whereas it takes several hours for complete release under physiological conditions (pH 7.0).[285] To optimize the *trans*-cycloocten-2-ol, undesirable cyclization with no release of the payload was minimized (**Figure 2-10B**).[284] Cargo linked via a *N*-methyl carbamate eliminates the formation of the "tricyclic" dead-end by intramolecular cyclization.

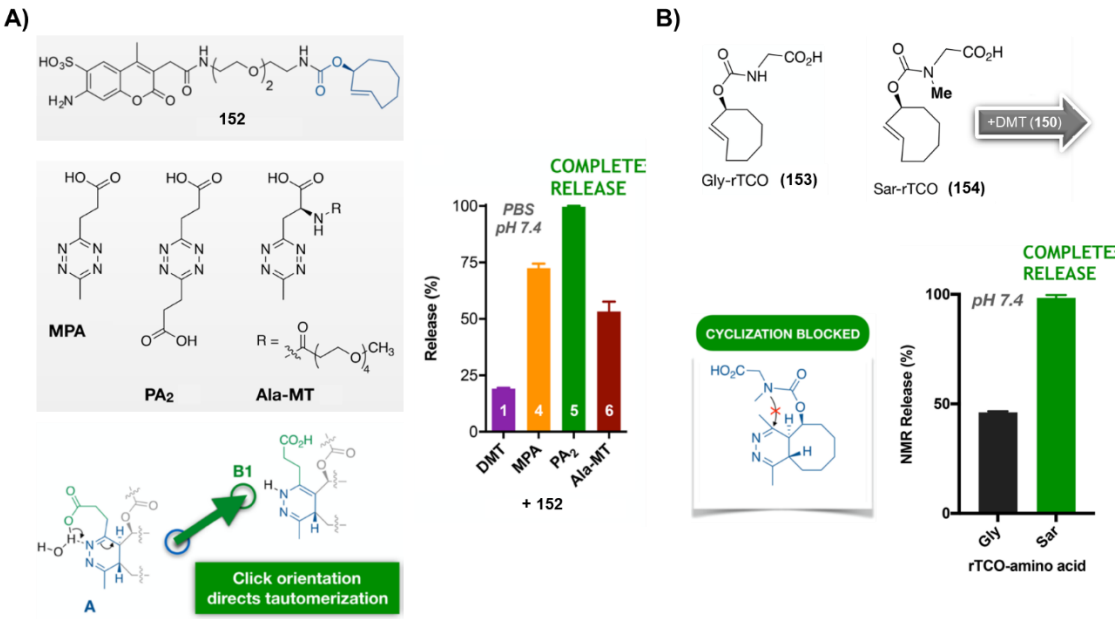

Figure 2-10 Mechanistic insights into the tetrazine—*trans*-cycloocten-2-ol ligation and elimination reaction. (A) A complete decaging and release of the fluorophore is observed upon treating **152** with acid-functionalized tetrazine PA_2. An acid group in PA_2 coordinates and directs tautomerization to the pre-release complex. (B) The undesirable cyclization and formation of the 'dead-end' complex is blocked by *N*-methylation in Sar-rTCO (**154**) as compared to Gly-rTCO (**153**), resulting in complete release of the amino acid. Adapted from *J. Am. Chem. Soc.*, **2018**, *140*, 3603.[284]

A follow-up study was undertaken to optimize tetrazine **150** to tolerate a wider pH range.[285] Amino-functionalized tetrazines **155** and **156** exhibit reaction kinetics independent of pH in the acidic to physiological range (3-7.4) (**Figure 2-11**). At pH values below the pK_a, protonation of the amino group is proposed to induce similar intramolecular coordination as with the acid-functionalized tetrazines. Moreover, the pH-independent tetrazine **156** exhibits a rate enhancement of 23-fold over the pH-dependent tetrazine **150** at pH = 7.4. Unfortunately, these amino-tetrazines could only release coumarin from *trans*-cyclooctenol-caged-coumarin in ~50% yields.

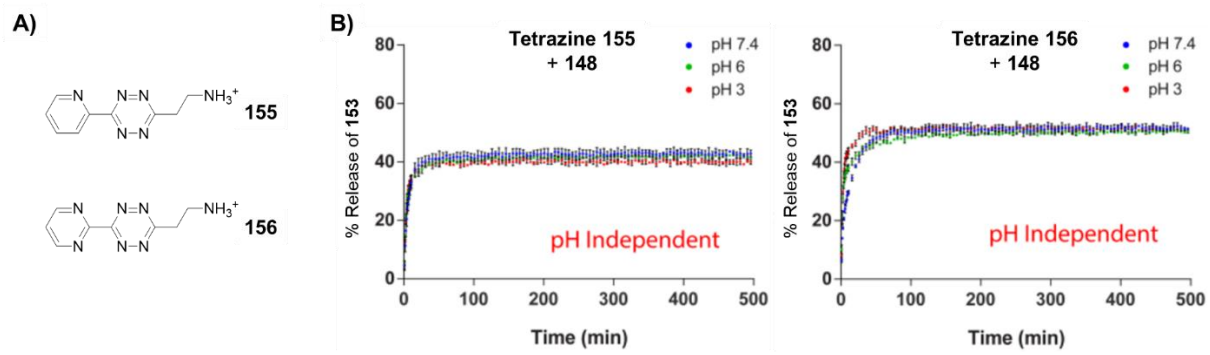

Figure 2-11 Amino-functionalized tetrazines for "click-to-release" applications with a wider pH range. (A) Chemical structures of amino-functionalized tetrazines **155** and **156**. (B) Coumarin 149 release proceeds rapidly, but incompletely, in a pH-independent manner, as monitored by the reaction of tetrazines **155** and **156** with *trans*-cycloocten-2-ol-coumarin conjugate (**148**). Adapted from *Chem. Eur.*, **2018**, *24*, 68, 18075.[285]

With all this information in hand, we proposed a linker conjugated to *trans*-cycloocten-2-ol for cyclizing MOs that is specifically activated by small molecules (tetrazines) as triggers for releasing an active, linear MO. The *ntla* MO will be cyclized with this linker and injected in zebrafish embryos to target *ntla* gene.

2.1.3 Synthesis of aryl-*trans*-cycloocten-2-ol linker for tetrazine-activated cMOs

Inspired by the nitroreductase-activated linker **142** for linearization of cyclic cMOs, linker **161** was envisioned to open a cMO using small molecule tetrazines as triggers (**Figure 2-12B**). As discussed previously, this linker contained two orthogonal reactive handles — an *N*-hydroxysuccinimide (NHS) ester and a chloroacetamide group — for selective reaction with 5'-amine and 3'-disulfide-modified ends of an MO. Linker **142** has been modified to have a *trans*-2-cyclooctene (or *trans*-cycloocten-2-ol) functionality via a carbamate linkage in place of the 4-

nitrobenzyl group. A schematic representation of the caged cMO and subsequent activation and linearization of MO in the presence of a tetrazine via iEDDA "click-to-release" chemistry is shown (**Figure 2-12C**).

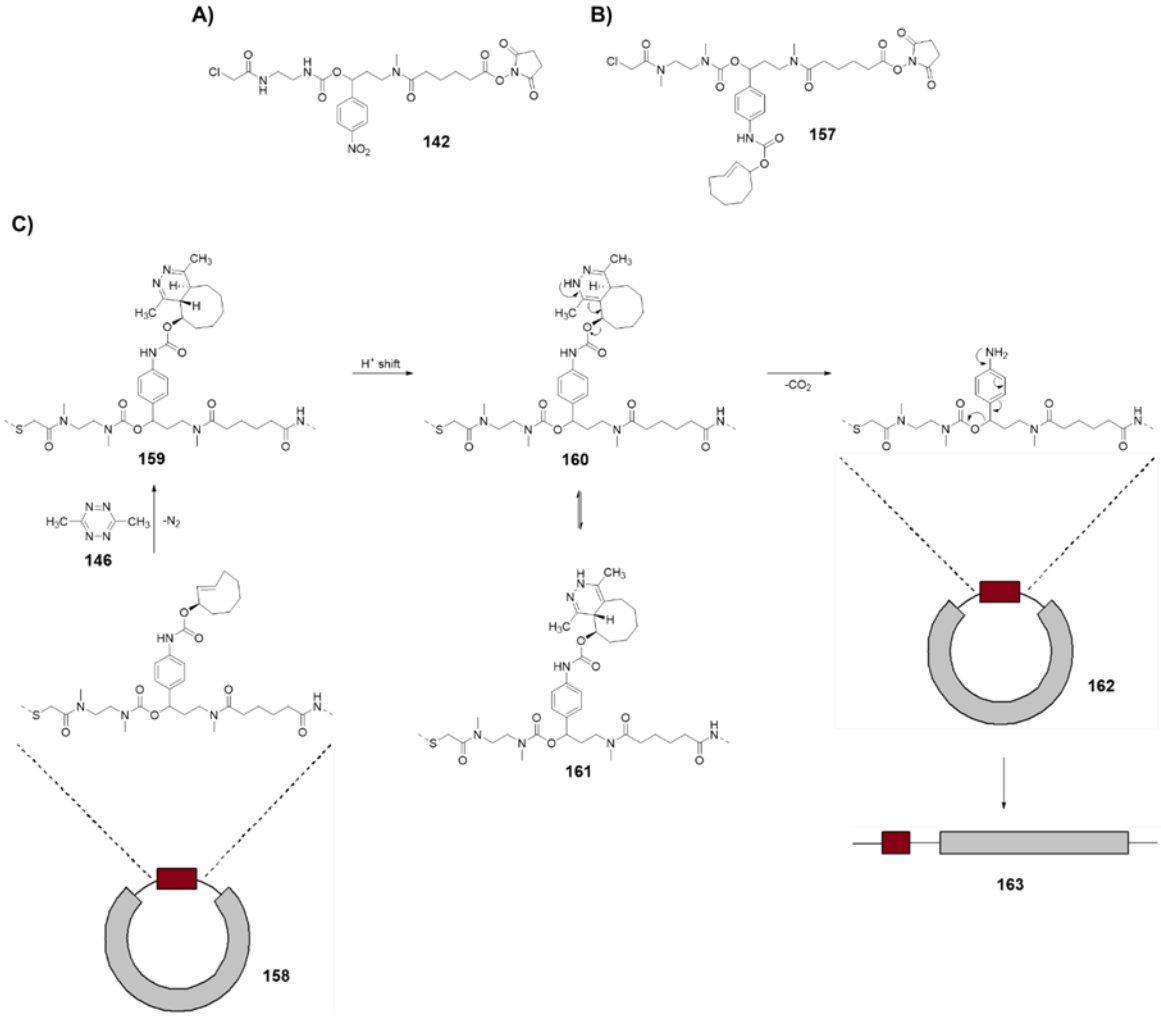

Figure 2-12 Schematic representation of tetrazine-mediated activation of *trans*-cycloocten-2-ol containing cMO **142**. (A) Structure of nitroreductase-activatable linker **142**. Adapted from *ACS Chem. Biol.*, **2014**, 9 (9), 1985.[270] (B) Structure of *trans*-cycloocten-2-ol-containing-linker **157**. (C) Proposed mechanism of activation of cMO **158** by tetrazine **146** to afford linear MO **163**.

Initially, synthesis of *cis*-cycloocten-2-ol was undertaken. First, diphenyl diselenide (**164**) was treated with sulfuryl chloride (SO_2Cl_2) to yield phenylselenyl chloride (**165**) (**Figure 2-13A**).[286] Commercially available *cis*-cyclooctene (**166**) was then reacted with **165** in CH_3CN/H_2O, and was stirred for 24 h at room temperature to furnish 2-(phenylselanyl)cyclooctan-1-ol (**167**) in 74% yield.[286] A *tert*-butyl hydroperoxide (TBHP)-mediated selenoxide elimination (Grieco elimination) yielded *cis*-cycloocten-2-ol (**168**) in 72% yield (**Figure 2-13B**).[287] A batch of *cis*-cycloocten-2-ol (**168**) was shipped to the Fox lab (Prof. Joseph Fox, Department of Chemistry, University of Delaware) for conversion to its *trans*-isomers.[288] Both the isomers, axial and equatorial *trans*-cycloocten-2-ol, were obtained in 33% and 32% yields, respectively and separated by silica gel flash column chromatography.

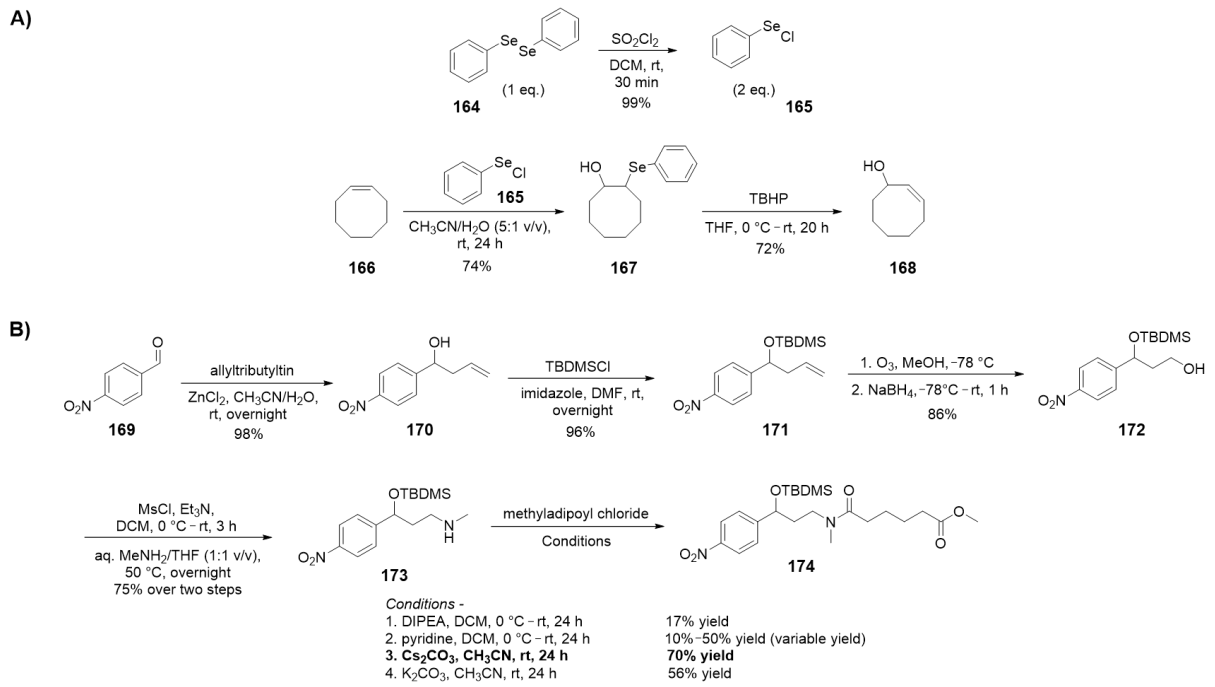

Figure 2-13 Synthesis of *cis*-cycloocten-2-ol **168** and compound **174** in the tetrazine-mediated activation strategy. (A) Synthesis of *cis*-cycloocten-2-ol (**168**) from *cis*-cyclooctene (**166**). (B) Synthesis of linker intermediate **174**.

Following the nitroreductase-activated linker synthesis,[270] 4-nitrobenzaldehyde (**169**) was treated with allyltributyltin and zinc chloride in CH_3CN/H_2O (4:1 v/v) conditions and stirred overnight at ambient temperature to obtain the homoallylic addition product **170** in 98% yield (**Figure 2-13B**), which was protected with TBDMSCl to deliver the alkene **171**. Compound **172** was obtained in 86% yield by ozonolysis and subsequent sodium borohydride reduction. Activation of terminal alcohol in **172** with mesyl chloride and subsequent substitution with methylamine yielded the amine **173**. A series of conditions were screened for the addition of methyl adipoyl chloride, with the use of cesium carbonate in acetonitrile delivering compound **174** in 70% yield (**Figure 2-13B**). Reduction of the nitro group in **174** to an amine group was challenging (**Figure 2-14**). A number of conditions were tested as product degradation was observed, making the reaction optimization difficult. A possible reason for the product degradation was the fragmentation of the linker intermediate similar to **162** (**Figure 2-12**). However, we were unable to characterize the fragmented product by NMR spectroscopy. Mild hydrogenation using ammonium formate as a heterogenous hydrogen source and Pd/C as the catalyst worked the best with 82-86% yields and minimal product degradation.[289] The product **175** was purified by flash chromatography and quickly used for further reactions (it was necessary to use **175** quickly in the next reaction as presence of fragmented product was observed by NMR spectroscopy after overnight storage (data not shown)).

A *cis*-cycloocten-2-ol substitute was used to generate **177** as a model compound. The synthesis of the isocyanate **176** was achieved by heating the the amine in a solution of triphosgene in toluene at 100 °C for 10 min. Without further purification of the isocyanate, carbamate formation with *cis*-cycloocten-2-ol (**168**) was attempted by screening a few conditions. We were unable to characterize the isocyanate product by NMR spectroscopy. Thus, to optimize the reaction

conditions for the synthesis of the desired carbamate, cyclohexanol was used as a commercially available substitute for *cis*-cycloocten-2-ol. After screening a few reaction conditions, the cyclohexanol carbamate was obtained in 50% yield with DIPEA as a base in toluene and heating the reaction at 80 °C for 2 h (data not shown). Unfortunately, these reaction conditions failed to produce **177**. After many optimization attempts with *cis*-cycloocten-2-ol, NaH in THF allowed for conversion of **175** to **177**, albeit with very low yields (< 10%) (**Figure 2-14**). Other attempts with *cis*-cycloocten-2-ol chloroformate failed to afford the desired carbamate (data not shown). The majority of the reactant was believed to be decomposed under these conditions and we were unable to characterize the decomposed reactant by NMR spectroscopy.

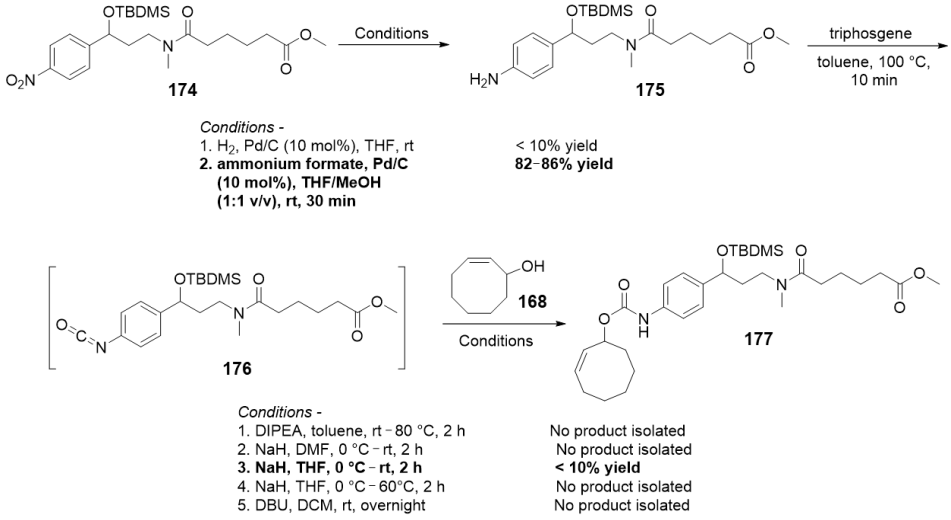

Figure 2-14 Synthesis of compound **177**.

Attempts at optimization of synthetic procedure for synthesis of compound **175** and **177** are listed; the condition in bold was found to be the best among the tested conditions.

Finally, a phenylcarbamate **179** was synthesized by treating aniline **175** with the commercially available phenylchloroformate (**178**) using pyridine as the base (**Figure 2-15A**). The

desired product **179** was synthesized in 67% yield by an alcohol-exchange between phenylcarbamate **179** and **168**, catalyzed by dibutyltin dilaurate at 100 °C for 2 h (data not shown). To translate these conditions for the use of *trans*-cycloocten-2-ol isomers, we needed to address the high reaction temperature and longer reaction times given the instability of *trans*-cyclooctenes.[290] For effective heating, the reactions were set up in a microwave reactor. A number of conditions were screened with varying temperatures and reaction times. No product was isolated in the reaction of **179** with the axial isomer (**180a**) in a number of conditions tested (**Figure 2-15B**). In some of the reaction conditions, the amine **175** was isolated from hydrolysis of the reactant **179**. Complete decomposition of **179** was observed at 100 °C with overnight stirring and the decomposed product was unable to be characterized by NMR spectroscopy. A proposed reason for the inability of **180a** to react with **179** was the conformational and steric interactions close to the hydoxyl group, similar to 1,3-diaxial interactions in substituted cyclohexanes (**Figure 2-15D**). Gratifyingly, the equatorial conformer was prepared in 78% yield by microwave-assisted heating of phenylcarbamate **179** and **180e** to 100 ºC in toluene for 20 min in the presence of dibutyltin dilaurate (**Figure 2-15C**). The selected conditions were utilized for the synthesis of the *trans*-cycloocten-2-ol-conjugated linkers.

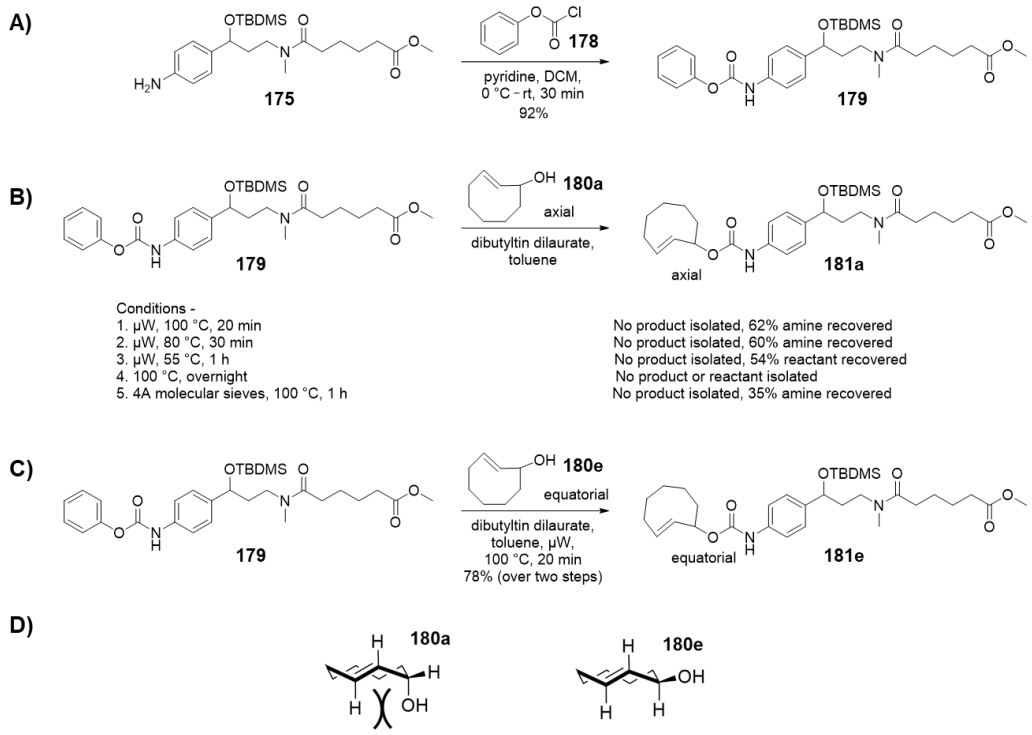

Figure 2-15 Screening of reaction conditions for the formation of carbamate linkage with *trans*-cycloocten-2-ol to the cMO linker scaffold.

(A) Synthesis of the phenylcarbamate **179**. (B) Unsuccessful attempts to synthesize **181a** with **179** and axial-*trans*-cycloocten-2-ol (**180a**). (C) The equatorial-*trans*-cycloocten-2-ol (**180e**) reacted with **179** to afford product **181e** in high yields. (D) The inability of axial-*trans*-cycloocten-2-ol (**180a**) was proposed to the presence of 1,3-diaxial interactions near the hydroxy group.

Since the linker intermediate **181a** was the desired product due to its faster reaction kinetics with tetrazines compared to the equatorial isomer **180e** (**Figure 2-15**), a sample of compound **177** was sent to the Fox lab for late-stage photoisomerization. However, the Fox lab reported only a 7% conversion to the *trans*-isomers **181a** and **181e**, with the inability to separate the *trans*-isomers from the starting material **177** (data not shown).

The Chen lab demonstrated the tetrazine-mediated decaging of axial and equatorial *trans*-cycloocten-2-ol caged-lysine (**145a** and **145e**) with the axial isomer showing faster decaging

kinetics.[109] In this case, although the synthesis of axial isomer (**181a**) with faster decaging kinetics was unsuccessful, we were able to synthesize the linker intermediate with the equatorial isomer (**181e**). We decided to complete the linker synthesis with linker intermediate (**181e**), as **181e** can undergo tetrazine-mediated decaging albeit with slower kinetics as compared to **181a**. The TBDMS group in **181e** was deprotected using TBAF (data not shown). However, the installation of the chloroacetamide handle for conjugation to a thiol-modified MO was unsuccessful. Here again, a number of reaction conditions were screened, but none of the conditions yielded the desired product (data not shown). A shorter length variant **182** of the original linker **157** was considered, with the position of the reactive handles switched (**Figure 2-16A**). The linker synthesis was successful up to the ultimate step of NHS activation. Synthesis of several variants (**183**–**187**) of the linker **157** were attempted with varying linker lengths and reactive groups. Here, *cis*-cycloocten-2-ol (**168**) was utilized instead of the *trans*-isomers (**180a** and **180e**) for optimization of linker design and synthesis. Unfortunately, the syntheses of all these linkers failed (**Figure 2-16A**). For the linkers **182**, **184**, and **185**, the final NHS activation of these linkers were unsuccessful. In this case, the NHS ester was found to be easily hydrolyzed to the acid and thus, purification and storage of **182**, **184**, and **185** was not successful. In the case of **183** and **186**, the installation of the arm containing the chloroacetamide and the maleimide proved difficult on the corresponding alcohol (**177a**, **Figure 2-16B**, obtained by TBDMS deprotection of **177** by TBAF). In particular, the synthesis of the chloroacetamide part in **183** was attempted by three-step one-pot synthesis, as reported for the synthesis of **146**.[270] Unfortunately, this procedure failed to yield the desired chloroacetamide. The reason for this failure could not be determined as we were unable to characterize the by-products formed by NMR spectroscopy. Additionally, for the synthesis of **183**, a two-step procedure was also attempted (**Figure 2-16B**). However, in this procedure, the desired

product **183b** was not formed and a possible reason for this failure is the intramolecular reaction of **183a** in presence of a base to form a cyclized amide (**Figure 2-16B**).[291] Similarly, the failure to synthesize the linker intermediate **186b** could be because of the intramolecular aza-Michael reaction in **186a** in presence of a base (**Figure 2-16C**).[292] In the case of linker **187**, the NHS carbonate in **187** was found to be easily hydrolyzed to the alcohol and thus, purification of **187** was not successful.

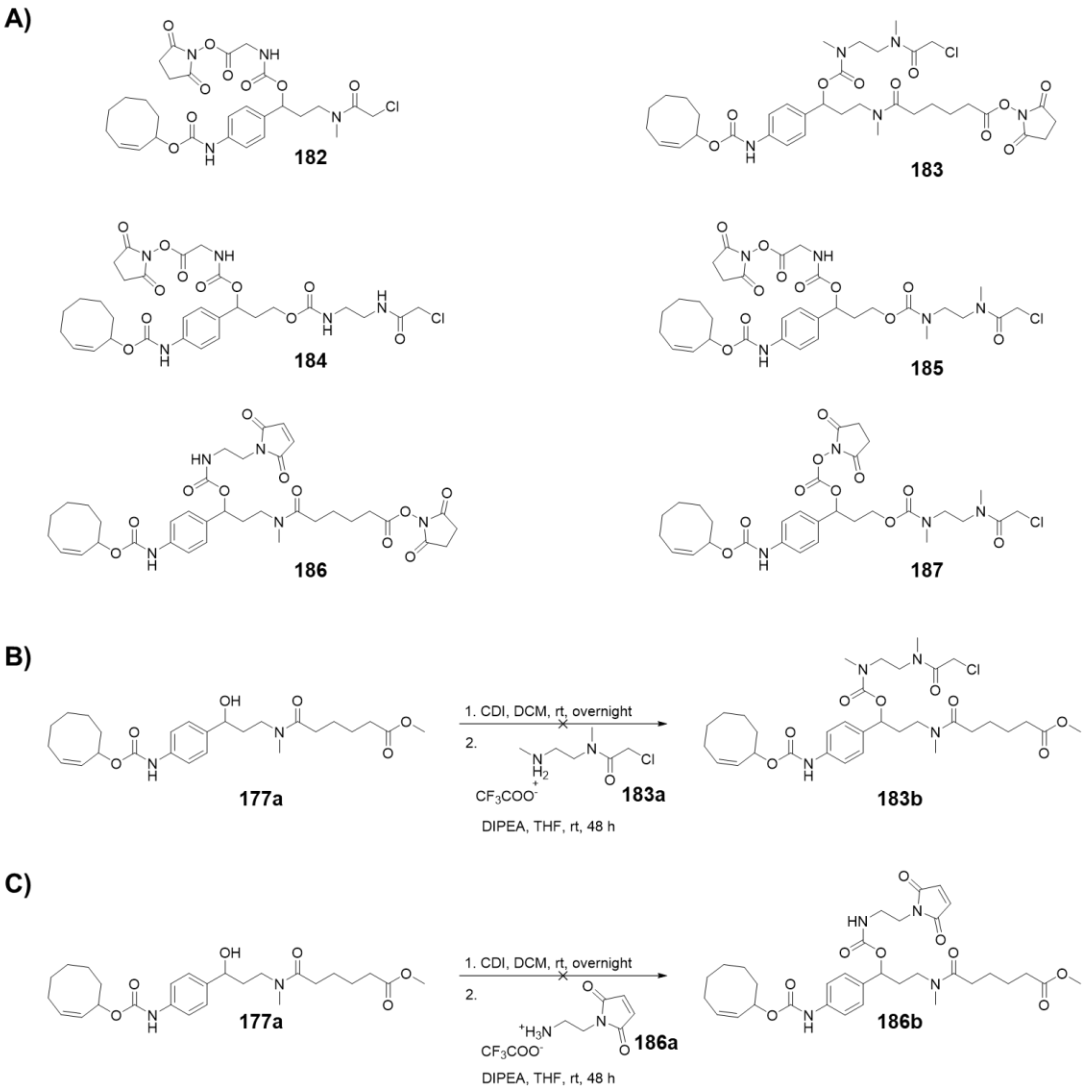

Figure 2-16 Different linkers with varying linker lengths and reactive groups attempted for linker design optimization.

(A) Structures of linkers **182–187**. (B) Unsuccessful attempt at the synthesis of **183a**, a precursor to linker **183**. (C) Unsuccessful attempt at the synthesis of **186a**, a precursor to linker **186**.

2.1.4 Synthesis of a bifunctional *trans*-bicyclo-nonene for 'click-to-release' applications

After the unsuccessful attempts to synthesize linker **157**, the design of this linker was reconsidered. As all the parts of the linker were optimized, it was important to eliminate the aryl-*trans*-cycloocten-2-ol carbamate linkage. Although other linkages like carbonate, ester, and ether are reported,[293] such linkages were not considered to connect *trans*-cycloocten-2-ol and aryl part of the linker as the failure to synthesize the axial-*trans*-cycloocten-2-ol linker intermediate **181a** could be possibly due to steric factors (**Figure 2-15D**). Thus, a complete revision of the linker design was necessary.

In order to eliminate the aryl-*trans*-cycloocten-2-ol linkage, we envisaged a linker with bifunctional-*trans*-cycloocten-2-ol analog to accommodate the chloroacetamide and the NHS ester arms of the linker. In 2016, Robillard and co-workers reported the synthesis of a bifunctional-*trans*-cycloocten-2-ol (**189**) for a selective activation of drug release from an antibody−drug conjugate with tetrazines (**Figure 2-17**).[294] Compound **189** was synthesized in 6 steps from (*Z*)-cyclooct-4-ene-1-carboxylic acid (**188**). A methyl group was introduced geminal to the carboxylic acid to prevent epimerization. The hydroxy group in **189** was converted to an NHS carbonate and the carboxylic acid was converted to an NHS ester to afford **190**. The NHS carbonate in **190** was selectively reacted with doxorubicin while the NHS ester was selectively reacted with monoclonal antibody CC49 to generate the antibody–drug conjugate **190a**. It was established that equatorial isomer of **189** was 156-fold less reactive towards tetrazine **144** as compared to axial isomer of **189** towards **144**, possibly due to steric hindrance and electronic effects of the hydroxyl group. Additionally, axial-*trans*-cycloocten-2-ol **180a** reacts with tetrazine **144** with rate constant of 57.7 $M^{-1}s^{-1}$, which is ~20-fold lower in comparison to the reaction of axial-*trans*-cycloocten-4-ol with **144** (rate constant: 1,140 $M^{-1}s^{-1}$).[282]

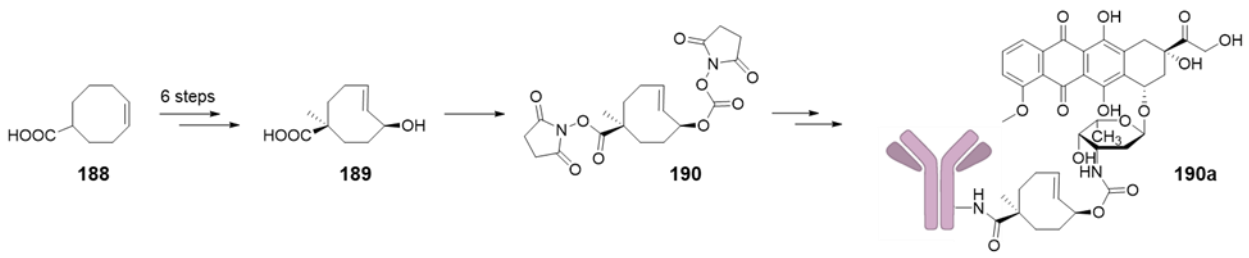

Figure 2-17 Synthesis of the functionalized *trans*-cycloocten-2-ol **189**.

Synthesis of **189** starting from (*Z*)-cyclooct-4-ene-1-carboxylic acid (**188**), and activation to compound **190**. The NHS carbonate in **190** was selectively reacted with doxorubicin while the NHS ester was selectively reacted with monoclonal antibody CC49 to generate the antibody–drug conjugate **190a**. Adapted from *Bioconjugate Chem.* **2016**, *27*, 7, 1697.[294]

In 2011, the Fox lab reported bicyclo[6.1.0]non-4-yn-9-ylmethanol (**192**), a strained *trans*-cyclooctene analog with faster reaction kinetics as compared to conventional *trans*-cyclooctene towards tetrazine ligation.[295] The authors reported that **192** reacts 160-fold faster with 3,6-diphenyl-1,2,4,5-tetrazine (**191**) (rate constant: 3,100 $M^{-1}s^{-1}$) in comparison to *trans*-cyclooctene (**194**) reaction with **191** (rate constant: 19 $M^{-1}s^{-1}$) in MeOH at 25 °C (**Figure 2-18A**).[295] The higher reactivity of **192** towards tetrazines can be attributed to the additional ring strain in this fused bicyclic system and the cyclopropane moiety locking the cyclooctene ring in the reactive "half-chair" conformer (**Figure 2-18B**). Additionally, in aqueous solution at 25 °C, it was found that a PEG-conjugated bicyclo[6.1.0]non-4-yn-9-ylmethanol (**196**) reacts with PEG-conjugated dipyridyltetrazine (**197**) with a rate constant as high as 3,300,000 $M^{-1}s^{-1}$ (**Figure 2-18C**).[296] Based on all these results, we proposed novel bifunctional *trans*-bicyclo-nonenes **207** and **208** (**Figure 2-19B**) for rapid "click-to-release" reactions with tetrazines.

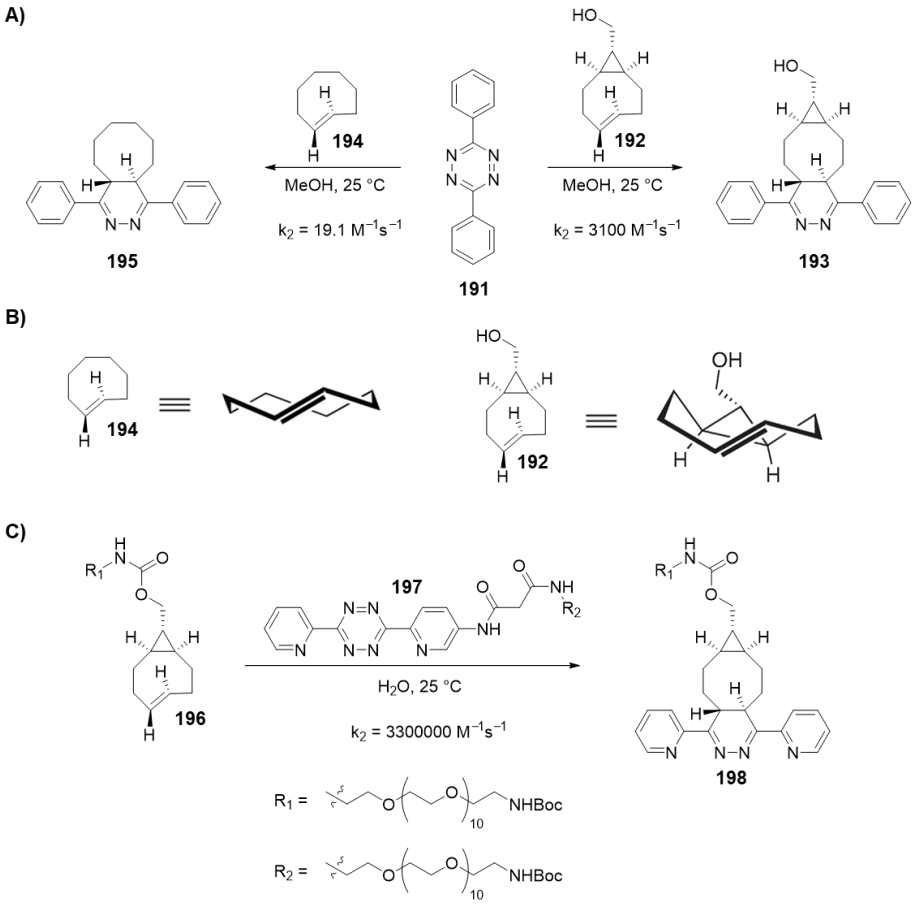

Figure 2-18 High reactivity of substituted bicyclo[6.1.0]non-4-yn-9-ylmethanol scaffolds with tetrazines. (A) Rate constants and reaction products of 3,6-diphenyl-1,2,4,5-tetrazine (**191**) with bicyclo[6.1.0]non-4-yn-9-ylmethanol (**192**) and *trans*-cyclooctene (**194**) in MeOH at 25 °C. Adapted from *J. Am. Chem. Soc.*, **2011**, 133, 25, 9646.[295] (B) Confirmations of *trans*-cyclooctenes **194** and **192**. The higher reactivity of **192** towards tetrazines can be attributed to the 'half-chair' conformation. Adapted from *J. Am. Chem. Soc.*, **2011**, 133, 25, 9646.[295] (C) Rate constant and reaction product of PEG-conjugated-3,6-di(pyridin-2-yl)-1,2,4,5-tetrazine (**197**) with PEG-conjugated-bicyclo[6.1.0]non-4-yn-9-ylmethanol (**196**) in H_2O at 25 °C. Adapted from *Chem. Sci.*, **2014**, 5, 3770.[296]

For the synthesis of **207** and **208**, we first constructed the epimeric compounds **205** and **206** (**Figure 2-19A**). The novel *trans*-bicyclo-nonenes **207** and **208** can be produced by *Z*-to-*E* photoisomerization by UV irradiation (254 nm) of compounds **205** and **206** (**Figure 2-19B**).[288] In the first batch, commercially available ethyl diazoacetate (**200**) was treated with 1,5-

cyclooctadiene (**203**) in the presence of $Rh_2(OAc)_4$ to afford diastereomers **201** and **202**, which were separated by silica gel flash chromatography (**Figure 2-19A**). Each of the diastereomers were individually converted to bifunctional *cis*-bicyclo-nonene intermediates **205** and **206** via the same route (which is illustrated here for the synthesis of compound **205** from diastereomer **201** (**Figure 2-19A**). Alkene **201** was treated with PhSeCl (**165**) in an acetonitrile/H_2O mixture to afford the mixture of compounds **203**. TBHP-mediated selenoxide elimination yielded the alcohol intermediate **204**. The hydroxy group was protected with TBDMSCl, and the ethyl ester was reduced with $LiAlH_4$ to afford the alcohol **205**. Compounds **205** and **206** were sent to the Fox lab for *Z*-to-*E* photoisomerization.[288]

TBDMS-protected *trans*-bicyclo-nonene intermediates, **207** and **208**, were prepared by photoisomerization of **205** and **206** by the Fox lab in < 20% yield (**Figure 2-19B**). Yixin Xie from the Fox lab tested these intermediates' reactivities with tetrazines with UV-Vis absorption spectroscopy.[278] Compound **207** (200 – 400 μM) reacted with tetrazine **211** (40 μM) in MeOH at 25 °C, and a rate constant of 153 $M^{-1}s^{-1}$ was observed (**Figure 2-20**). In this case, the tetrazine addition is likely hindered by the presence of bulky TBDMS group. Compound **209** was obtained by TBAF-mediated deprotection of **208**. The diol **209** indeed reacted faster with tetrazine **211** (40 μM), with a higher rate constant of 250 $M^{-1}s^{-1}$. For reference, equatorial *trans*-cycloocten-5-ol (**210**) reacted with the same tetrazine with a comparable rate constant of 358 $M^{-1}s^{-1}$. As mentioned before, a ~20-fold reduction in reactivity was observed in case of **180a** reacting with tetrazine **144** as compared to axial *trans*-cycloocten-5-ol.[282] Thus, the new *trans*-bicyclo-nonene analogs **207** and **209** are expected to react an order of magnitude faster than axial *trans*-cycloocten-2-ol (**180a**).

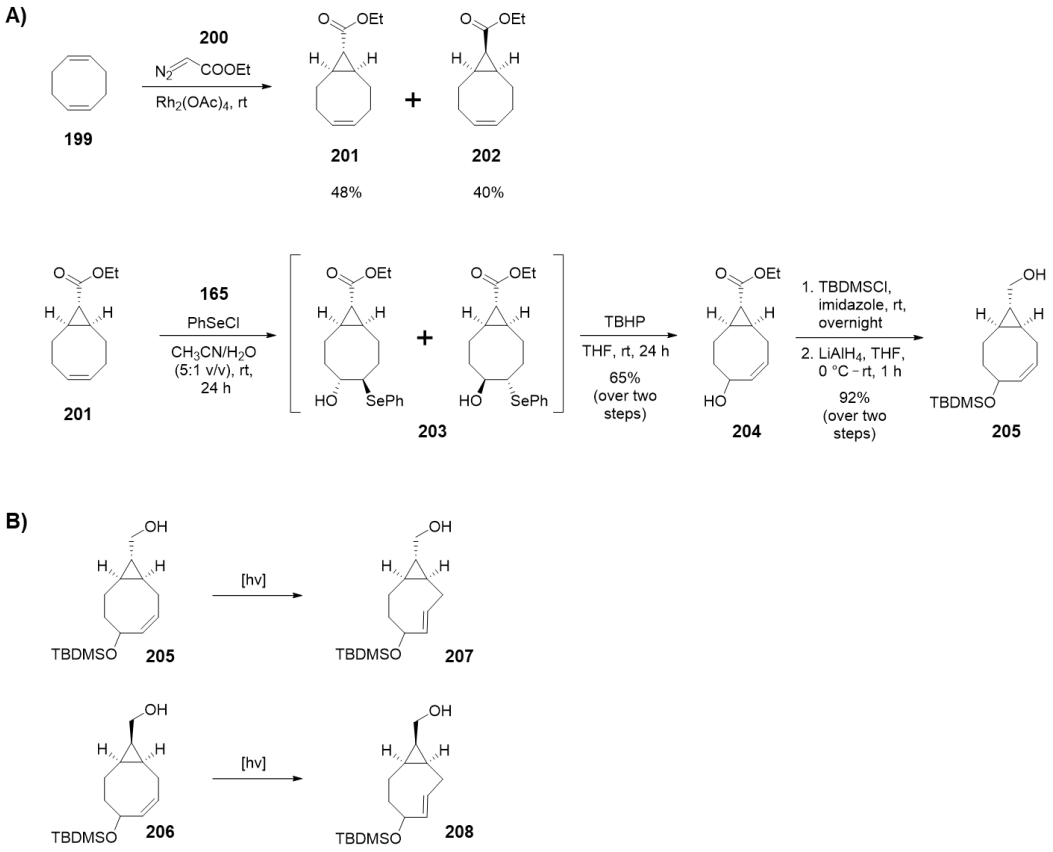

Figure 2-19 Synthetic route to bifunctional trans-bicyclo-nonenes **207** and **208**.

(A) Synthesis of *cis*-bicyclo-nonene **205**. Synthesis of epimer **206** followed a similar route. (B) TBDMS-protected *cis*-bicyclo-nonenes **205** and **206** were photoisomerized to their respective *trans*-isomers **207** and **208** by the Fox lab.

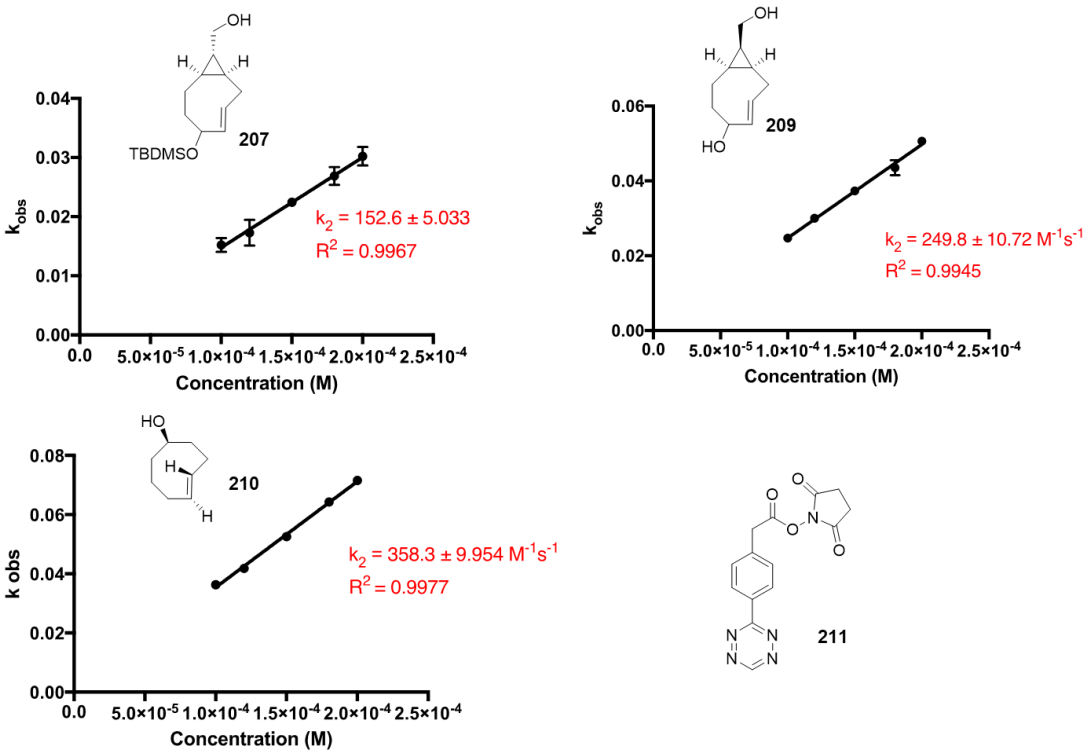

Figure 2-20 Rate constants of *trans*-bicyclo-nonene intermediates with tetrazine.

Rate constants of *trans*-bicyclo-nonene intermediates (**207** and **209**) (200–400 µM) with tetrazine **211** (40 µM) determined by UV-Vis absorption spectroscopy at 262 nm. The kinetics were measured in triplicate. The equatorial *trans*-cycloocten-5-ol (**210**) was utilized as a reference. Data generated by Yixin Xie from the Fox lab.

Both the diastereomers were found to have comparable rate constants and thus, either of the diastereomers can be utilized for the *trans*-bicyclo-nonene linker synthesis. Compound **215** was selected as an intermediate for the *trans*-bicyclo-nonene linker synthesis due to its synthetic accessibility and scalability (**Figure 2-21A**). A synthetic route was devised according to reported procedure.[297] To this end, the Rh-catalyzed cyclopropanation of commercially available reagents ethyl diazoacetate (**200**) and 1,5-cyclooctadiene (**199**) yielded compounds **201** and **202** as a mixture of diastereomers in 89% yield. Potassium *tert*-butoxide-mediated ester hydrolysis and epimerization of the diastereomeric mixture afforded (1*R*,8*S*,9*R*,*Z*)-bicyclo[6.1.0]non-4-ene-9-

carboxylic acid (**212**) as a single diastereomer in 85% yield. Next, **212** was reduced with $LiAlH_4$ to yield alcohol **213** in 67% yield, as reported earlier.[297] As explained above (**Figure 2-13**), PhSeCl (**165**) addition followed by TBHP-mediated elimination afforded the diol **215** in 64% yield (over two steps). Furthermore, the primary alcohol in **215** was selectively protected with TBDPSCl to give the TBDPS-protected *cis*-bicyclo-nonene intermediate **216** in 61% yield, which was sent to the Fox lab for *Z*-to-*E* photoisomerization.[288] All these reactions were carried out in multigram scale, indicating the scalability of this synthetic route.

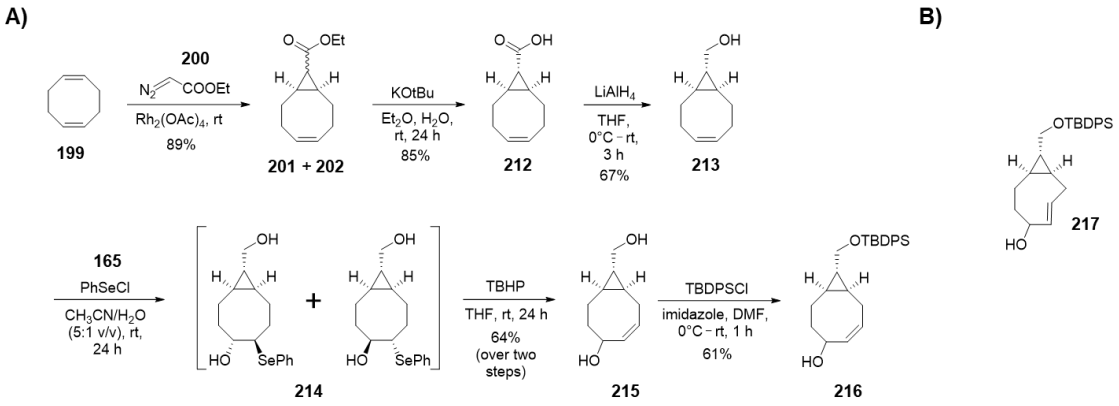

Figure 2-21 Synthesis of bifunctional *trans*-bicyclo-nonene **217**.

(A) Revised synthetic route for the synthesis of bifunctional *cis*-bicyclo-nonene **215** and TBDPS-protected compound **216**. (B) The TBDPS-protected bifunctional *trans*-bicyclo-nonene **217** (inset) is utilized for the final linker synthesis.

The Fox lab carried out *Z*-to-*E* photoisomerization reaction on **216** to afford the *trans*-isomer **217** in 18% yield (**Figure 2-21B**). Multiple attempts at this photoisomerization with varied conditions and scale of this reaction failed to improve the yield, with < 20% product (**217**) isolated (data not shown). The underlying reason for the poor yield and the fate of the majority of the reactant are still not determined and currently under investigation. In this case, the photoisomerization yielded two isomers — axial and equatorial. However, separation of these

diastereomers was not possible. Thus, **217** was utilized for the synthesis of the final linker without any purification, as a diastereomeric mixture (dr 2:1) as determined by NMR spectroscopy. However, the identity of the diastereomeric mixture is yet to be determined.

2.1.5 Synthesis of *trans*-bicyclo-nonene linker for tetrazine-activated cMOs

The *trans*-bicyclo-nonene linker synthesis was initiated from the *trans*-isomer **217** (**Figure 2-22**). The secondary alcohol in **217** was activated as an imidazole carbamate using CDI in DCM. The imidazole was displaced with DMEDA, and subsequent reaction with methyl adipoyl chloride afforded amide **218** in 51% yield (over three steps). With this arm in place (for later installation of an NHS ester), our focus was turned to installation of the chloroacetamide arm. TBAF-mediated deprotection of **218** yielded alcohol **219**. Activation with CDI, addition of DMEDA, and treatment with chloroacetyl chloride gave compound **220** in 28% yield (over three steps). The activation of methyl ester as an NHS ester was carried out by LiOH-mediated hydrolysis of the methyl ester and activation of the crude carboxylic acid as an NHS ester using TSTU in acetonitrile in presence of DIPEA as a base. The final linker **221** was purified by silica gel flash chromatography in 45% yield.

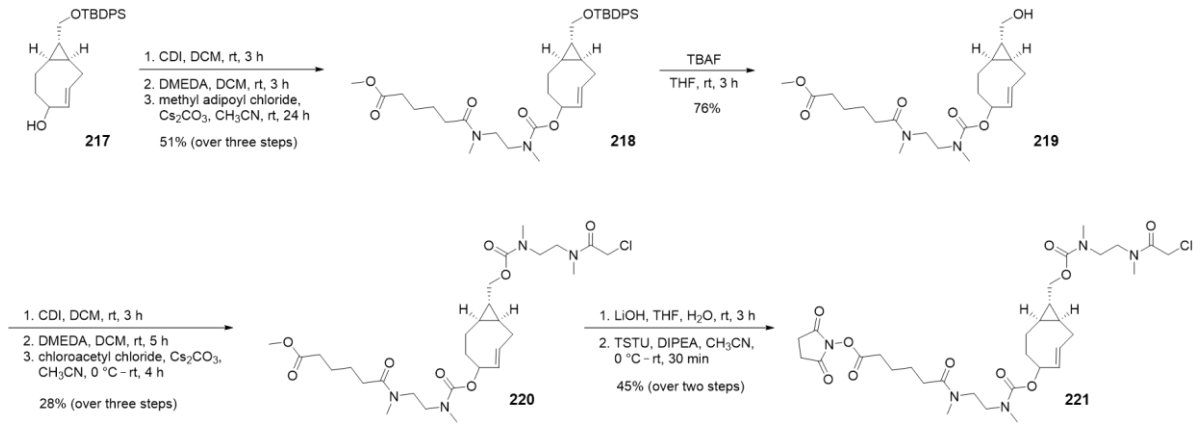

Figure 2-22 Synthesis of the final linker **221** from *trans*-bicyclo-nonene **217**.

The synthesis of this new linker took into account the pitfall of *trans*-cyclooctene instability,[290] and the design principles for higher release yields with faster kinetics.[284] The potential instability of *trans*-cyclooctene at higher temperatures and acidic pHs was avoided by carrying out all reactions at room temperature under neutral or alkaline conditions.[290] In the final reaction sequence, in which the methyl ester was hydrolysed by LiOH, the workup was performed with aqueous citric acid solution to recover the carboxylic acid at pH > 3. During the synthesis of the bifunctional *cis*-bicyclo-nonene (**215**), a methyl group was introduced geminal to the carboxylic acid to prevent epimerization.[294] As an alternative, in this new linker design, the carboxylic acid group in **212** was reduced to the alcohol by $LiAlH_4$ reduction, affording a single diastereomer **213** with no possibility of epimerization. The Weissleder lab has found that that the presence of the *N*-methylated carbamate prevents intramolecular cyclization and the formation of a tricyclic "dead-end" with no release (**Figure 2-10**).[284] This observation was incorporated in this linker design by using DMEDA to produce the desired *N*-methyl carbamate. For rapid activation of cMOs prepared using this linker, a library of tetrazines with various functionalities previously reported for "click-to-release" applications were synthesized.

The final linker **221** was used for cyclization of an *ntla* MO by Kristie Darrah (**Figure 2-23**). The commercially available *ntla* MO **222** has a 5'-amino modification and a 3'-thiol protected as a disulfide. The 5'-amine end reacts readily with the NHS ester group on the linker **221** in 0.1 M Tris buffer (pH 8) at room temperature. The formation of the conjugated amido-*ntla* MO **223** was monitored by MALDI-TOF-MS, and was purified by reversed-phase HPLC. The 3'-disulfide was reduced to a thiol using immobilized TCEP, and subsequent reaction with the chloroacetamide end of the linker in 0.1 M Tris buffer (pH 8) at room temperature afforded the cMO **224**. The formation of the *ntla* cMO **229** was monitored by MALDI-TOF-MS and purified by reverse-phase HPLC.

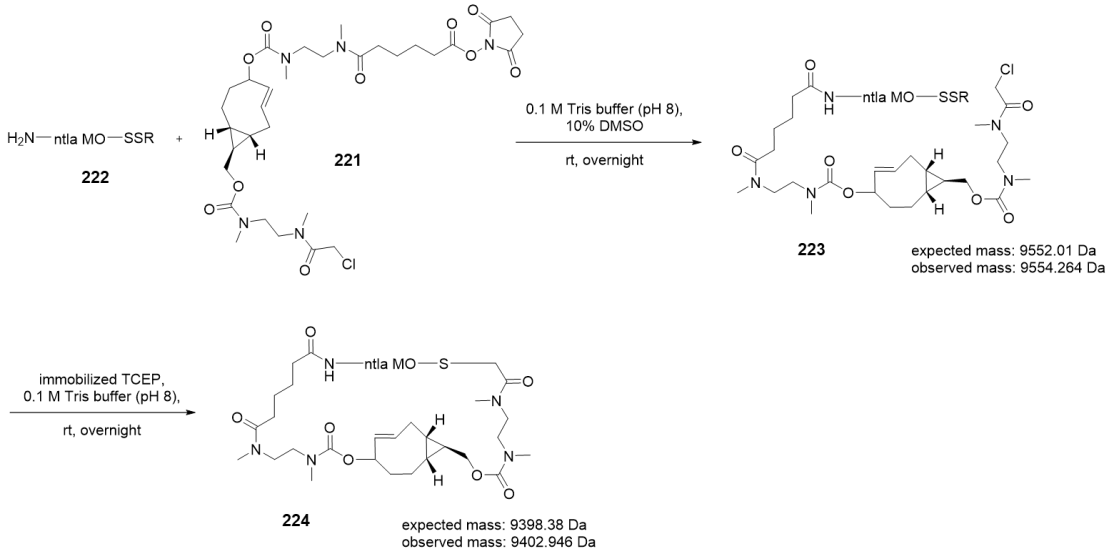

Figure 2-23 Synthesis of *ntla* cMO **224** with the novel *trans*-bicyclo-nonene linker **221**.

The reactions were monitored by MALDI-TOF-MS with the expected mass and observed mass in agreement within < 0.05% error. Data generated by Kristie Darrah.

2.1.6 Summary and future work

In summary, small molecule activation for cMO linearization was envisioned with the iEDDA reaction of tetrazine and *trans*-cycloocten-2-ol, with subsequent elimination to linearize the *ntla* cMO in zebrafish embryos. Based on the reported nitroreductase linker,[270] the linker design consisted of *trans*-cycloocten-2-ol conjugated to an aniline precursor through a carbamate linkage. The *trans*-cycloocten-2-ol-containing linker **157** has two reactive handles — an NHS ester and a chloroacetamide — to covalently link the 5'-amine and the 3'-thiol end of the *ntla* MO for cyclization. The *cis*-cycloocten-2-ol trigger was synthesized in two steps, and a *Z*-to-*E* photoisomerization was carried out by the Fox lab to afford two isomers — axial and equatorial (**180a** and **180e**, respectively). During the linker synthesis, the reduction of nitro group in **174** to an amine and subsequent carbamate synthesis to covalently link *trans*-cycloocten-2-ol to the amine group was initially challenging, but dibutyltin dilaurate-catalyzed carbamate formation delivered the desired aryl-phenyl carbamate in a rapid microwave-assisted reaction. Upon using these conditions with both *trans*-cycloocten-2-ol isomers (**180a** and **180e**) as substrates, only the equatorial isomer was successfully used to generate a carbamate. Although the equatorial isomer is the slower for 'click-to-release' applications among the two isomers, the linker intermediate **181e** was taken forward for synthesis of the final linker. Unfortunately, the synthesis of the originally designed linker as well as several variants of the final linker were unsuccessful (**Figure 2.13**). This necessitated for a change in the aryl-*trans*-cycloocten-2-ol linker design. A novel bifunctional *trans*-bicyclo-nonene was conceptualized with two alcohol functionalities for containing two reactive ends of the linker. The synthesis of the bifunctional *trans*-bicyclo-nonene was carried out on 2 isomers (**205** and **206**), and the isomers were sent to the Fox lab for *Z*-to-*E* photoisomerization. The resulting *trans*-bicyclo-nonenes (**207** and **209**) were tested for reaction

kinetics with tetrazine **211**; it is expected that these analogs exhibit faster reaction kinetics compared to the known *trans*-cycloocten-2-ol analogs. As both the *trans*-bicyclo-nonene analogs showed comparable reaction kinetics, **217** was selected based upon the ease of synthesis and scalability. One arm of the linker with **217** was constructed in 3 steps on the unprotected alcohol, while the chloroacetamide end of the linker was synthesized in 3 steps on the primary alcohol after TBDPS deprotection. Finally, the methyl ester on the first arm was hydrolyzed and activated as the NHS ester. The 5'-amine end of the *ntla* MO was conjugated to the NHS ester, and the TCEP-mediated thiol deprotection and subsequent reaction with the chloroacetamide afforded the *ntla* cMO. Along with this synthesis, a library of previously identified tetrazines were synthesized.

Hereafter, the *ntla* cMO will be injected into zebrafish embryos. The *ntla* MO produces a distinct phenotype in zebrafish embryos, we expect tetrazine-dependent induction of this phenotype in embryos injected with the *ntla* cMO. The tetrazine will be chosen with several considerations for optimization. The permeability of tetrazines in zebrafish embryos needs to be established. Low-permeability tetrazines can be injected into the embryos along with the *ntla* cMO. The toxicity of tetrazines will also be tested at various concentrations. After the initial proof-of-principle with the *ntla* cMO, the linker can theoretically be utilized to cyclize any antisense MO to dissect gene function with rapid temporal control. Finally, a novel bifunctional *trans*-bicyclo-nonene (**217**) for "click-to-release" purposes was developed as a part of this study. Compound **217** can be viewed as a novel example of decaging group with fast reaction kinetics that is activatable by small molecules, and can be utilized for various applications like controlled drug release.

2.1.7 Experimentals

All reactions were performed in flame-dried glassware under a nitrogen atmosphere with magnetic stirring. Reactions were followed by thin layer chromatography (TLC) using glass-backed silica gel plates (EMD Millipore TLC Silica Gel 60 F254: 25 Glass Plates 20x20 cm, 250 μm thickness). Anhydrous THF and acetonitrile were purchased from Acros and anhydrous DMF was purchased from Alfa Aesar. Yields refer to pure compounds unless otherwise stated. Flash chromatography was performed with silica gel (60 Å, 40-63 μm, 230 × 400 mesh, Sorbtech) as the stationary phase. High resolution mass spectrometry (HRMS) analysis was performed on a Q-Exactive (Thermo Scientific) mass spectrometer. ^{1}H NMR and ^{13}C NMR spectra were recorded on a 300 MHz or a 400 MHz Bruker NMR spectroscope. Chemical shifts are given in δ units (ppm) for ^{1}H NMR spectra and ^{13}C NMR spectra relative to the respective solvent residual peaks ($CDCl_3$: 7.26 ppm for ^{1}H NMR and 77.16 ppm for ^{13}C NMR; CD_3OD: 3.31 ppm for ^{1}H NMR and 49.00 ppm for ^{13}C NMR; $(CD_3)_2SO$: 2.50 ppm for ^{1}H NMR and 39.52 ppm for ^{13}C NMR).[197]

((1*R*,8*S*,9*R*,*Z*)-Bicyclo[6.1.0]non-4-en-9-yl)methanol (**213**) (from **199**),[297] **3,6-di(pyridin-2-yl)-1,2,4,5-tetrazine** (**144**),[298] **3,6-diphenyl-1,2,4,5-tetrazine** (**191**),[298] **2-(6-(pyridin-2-yl)-1,2,4,5-tetrazin-3-yl)ethan-1-aminium chloride** (**155**),[285] and **2-(6-(pyrimidin-2-yl)-1,2,4,5-tetrazin-3-yl)ethan-1-aminium chloride (156**)[285] were synthesized according to a reported procedures.

Phenylselenyl chloride (165). Diphenyl diselenide (5.54 g, 17.75 mmol, 1.0 eq) was dissolved in anhydrous DCM (30 mL), and the solution was cooled in an ice-water mixture. Sulfuryl chloride (1.40 mL, 17.75 mmol, 1.0 eq) was slowly added to this solution at 0 °C, and the resulting dark red solution was stirred for 1 h at 0 °C. The reaction was warmed to room temperature and the

volatiles were evaporated under reduced pressure. Compound **165** was obtained as an orange solid (6.75 g, 99%). ^{1}H NMR (400 MHz, $CDCl_3$) δ 7.89 – 7.78 (m, 2H), 7.40 – 7.38 (m, 3H). The NMR data obtained was in accordance with the reported data.[299]

2-(Phenylselanyl)cyclooctan-1-ol (167). Compound **166** (100 mg, 0.91 mmol, 1.0 eq) was dissolved in acetonitrile (5 mL) and water (1 mL) was added to this solution. Compound **165** (174 mg, 0.91 mmol, 1.0 eq) was added to the solution, and the reaction mixture was stirred at room temperature for 24 h. Acetonitrile was evaporated under reduced pressure, and the residue was resuspended in ethyl acetate (5 mL) and H_2O (5 mL) mixture. The ethyl acetate layer was separated, and the aqueous layer was extracted with ethyl acetate (2 × 5 mL). The combined organic extracts were dried over sodium sulfate (1 g), filtered, and concentrated under reduced pressure. The product was purified from the residue by silica gel flash column chromatography (elution with 1:9 ethyl acetate/hexanes) to afford **167** as a white solid (190 mg, 74%). The NMR data obtained was in accordance with the reported data.[300]

(*Z*)-Cyclooct-2-en-1-ol (168). Compound **167** (100 mg, 0.35 mmol, 1.0 eq) was dissolved in THF (4 mL), and *tert*-butyl hydroperoxide (TBHP, 1 mL, 70 wt% in H_2O) was added to this solution at room temperature. The reaction mixture was stirred at room temperature for 20 h. The reaction was quenched with aqueous saturated sodium bicarbonate solution (5 mL), and THF was evaporated under reduced pressure. The aqueous layer was washed with ethyl acetate (3 × 5 mL), and the combined organic extracts were dried over sodium sulfate (1 g), filtered, and concentrated under reduced pressure. The product was purified from the crude residue by silica gel flash column

chromatography (elution with 1:4 ethyl acetate/hexanes) to yield **168** as a colorless oil (32 mg, 72%). The NMR data obtained was in accordance with the reported data.[287]

***Tert*-butyldimethyl((1-(4-nitrophenyl)but-3-en-1-yl)oxy)silane (171).** *Tert*-butyldimethyl chlorosilane (TBDMSCl, 624 mg, 4.14 mmol, 2.0 eq) was added to a stirred solution of **170** (400 mg, 2.07 mmol, 1.0 eq) in anhydrous DMF (10 mL). To this solution, imidazole (423 mg, 6.21 mmol, 3.0 eq) was added and the reaction mixture was stirred overnight at room temperature. On consumption of **170** as confirmed by TLC, the reaction was diluted with water (100 mL) and extracted with ethyl acetate (3 × 20 mL). The combined organic extracts were washed with brine (20 mL), dried over sodium sulfate (2 g), filtered, and concentrated under reduced pressure. The product was purified from the residual oil by silica gel flash column chromatography in 1:20 ethyl acetate/hexanes to obtain **155** as a yellow oil (610 mg, 96%). ^{1}H NMR (300 MHz, $CDCl_3$) δ 8.18 (d, *J*=8.50 Hz, 2 H), 7.47 (d, *J*=8.69 Hz, 2 H), 5.65 − 5.80 (m, 1 H), 4.94 − 5.07 (m, 2 H), 4.80 (t, *J*=5.95 Hz, 1 H), 2.34 − 2.51 (m, 2 H), 0.86 − 0.93 (m, 10 H), 0.00 − 0.12 (m, 3 H), −0.10 (s, 3 H); HRMS (ESI) calcd. for $C_{16}H_{26}O_3NSi$ $(M+H)^+$ 308.1677, found: 308.1686.

3-((*Tert*-butyldimethylsilyl)oxy)-3-(4-nitrophenyl)propan-1-ol (172). Compound **171** (2.0 g, 6.50 mmol, 1.0 eq) was dissolved in MeOH (100 mL) and this solution was cooled to −78 °C in a dry ice-acetone bath. Ozone gas was passed till the solution was saturated as seen by dark blue color of the solution and the gas flow was maintained for another 15 min. The gas flow was stopped and $NaBH_4$ (1.2 g, 32.52 mmol, 5.0 eq) was very slowly added to this solution at −78 °C over 30 min to keep the effervescence to a minimum. After complete addition of $NaBH_4$, the solution was stirred at room temperature for 1 h while allowing the solution to warm to room temperature. The

reaction was quenched by ice-water mixture (20 mL) and MeOH was evaporated under reduced pressure. The aqueous layer was washed with ethyl acetate (3 × 20 mL). The combined organic extracts were washed with brine (20 mL), dried over sodium sulfate (2 g), filtered, and concentrated under reduced pressure. The residual oil was loaded onto a silica gel column and the product was eluted out in 1:4 ethyl acetate/hexanes to yield **157** as a pale-yellow oil (1.7 g, 86%). ^{1}H NMR (400 MHz, $CDCl_3$) δ 8.33 (d, *J*=8.80 Hz, 2 H), 7.63 (d, *J*=8.56 Hz, 2 H), 5.17 (dd, *J*=7.34, 4.40 Hz, 1 H), 3.78 − 3.92 (m, 2 H), 1.97 − 2.12 (m, 3 H), 1.01 − 1.05 (m, 9 H), 0.19 − 0.22 (m, 3 H), −0.02 − 0.01 (m, 3 H); HRMS (ESI) calcd. for $C_{15}H_{26}O_4NSi$ $(M+H)^+$ 312.1626, found: 312.1635.

3-((*Tert*-butyldimethylsilyl)oxy)-*N*-methyl-3-(4-nitrophenyl)propan-1-amine (173). To a solution of **172** (500 mg, 1.61 mmol, 1.0 eq) in anhydrous DCM (20 mL), mesyl chloride (190 µL, 2.46 mmol, 1.5 eq) was added at room temperature. This solution was cooled to 0 °C and triethylamine (340 µL, 2.46 mmol, 1.5 eq) was dropwise added. The resulting solution was warmed to room temperature and stirred at room temperature for 3 h. On consumption of **172** as confirmed by TLC, the reaction was concentrated under reduced pressure. The residual oil was loaded on a silica gel column and the product was eluted out in 1:6 ethyl acetate/hexanes to yield 3-((*tert*-butyldimethylsilyl)oxy)-3-(4-nitrophenyl)propyl methanesulfonate as a pale-yellow oil (570 mg, 91%). This oil (570 mg, 1.46 mmol, 1.0 eq) was further dissolved in THF (20 mL) and 40% aqueous solution of methylamine (20 mL, 234 mmol, 160 eq, 40% aq. solution) was added to the solution at room temperature. The reaction mixture was heated to 50 °C and stirred overnight to 50 °C. The reaction was cooled to room temperature and diluted with water (20 mL). The reaction mixture was extracted with ethyl acetate (3 × 10 mL) and the combined extracts were washed with

brine (20 mL), dried over sodium sulfate (1 g), filtered, and concentrated under reduced pressure. The product was purified from the residual mass by silica gel flash column chromatography in 1:1 ethyl acetate/hexanes to yield **173** as a pale-yellow oil (445 mg, 75% from **172**). ^{1}H NMR (400 MHz, $CDCl_3$) δ 8.32 (d, *J*=8.80 Hz, 2 H), 7.62 (d, *J*=8.56 Hz, 2 H), 5.80 (br s, 1 H), 5.04 (dd, *J*=7.34, 4.65 Hz, 1 H), 2.94 − 2.95 (m, 1 H), 2.93 (d, *J*=4.89 Hz, 7 H), 2.69 − 2.87 (m, 2 H), 2.56 (s, 3 H), 2.11 (s, 9 H), 1.94 − 2.07 (m, 2 H), 1.03 (s, 9 H), 0.20 (s, 3 H), 0.00 (s, 3 H); HRMS (ESI) calcd. for $C_{16}H_{29}O_3N_2Si$ $(M+H)^+$ 325.1942, found: 325.1954.

Methyl 6-((3-((*tert*-butyldimethylsilyl)oxy)-3-(4-nitrophenyl)propyl)(methyl)amino)-6-oxohexanoate (174). Methyl adipoyl chloride (0.96 mL, 6.16 mmol, 1.0 eq) was added to a solution of **173** (2.0 g, 6.16 mmol, 1.0 eq) in anhydrous acetonitrile (30 mL) at room temperature. Cesium carbonate (2.4 g, 7.40 mmol, 1.2 eq) was added to this solution and the resultant suspension was stirred at room temperature for 24 h. After stirring for 24 h at room temperature, the reaction mixture was diluted by water (30 mL) and acetonitrile was evaporated under reduced pressure. The aqueous layer was extracted with multiple portions of ethyl acetate (3 × 20 mL). The combined organic extracts were washed with brine (10 mL), dried over sodium sulfate (2 g), filtered, and concentrated under reduced pressure. The residual oil was loaded onto a silica gel column and the product was eluted out in 1:3 ethyl acetate/hexanes to obtain **174** as a yellow oil (1.91 g, 70%). ^{1}H NMR (400 MHz, $CDCl_3$) δ 8.13 − 8.22 (m, 2 H), 7.49 (d, *J*=8.56 Hz, 2 H), 4.77 − 4.85 (m, 1 H), 3.60 − 3.66 (m, 3 H), 3.42 − 3.55 (m, 1 H), 3.21 − 3.34 (m, 2 H), 2.79 − 2.94 (m, 3 H), 2.26 − 2.35 (m, 2 H), 2.23 (br s, 2 H), 1.77 − 1.98 (m, 3 H), 1.62 − 1.73 (m, 2 H), 0.84 − 0.93 (m, 9 H), 0.01 − 0.08 (m, 3 H), −0.19 − −0.13 (m, 3 H). HRMS (ESI) calcd. for $C_{16}H_{26}O_3NSi$ $(M+H)^+$ 467.2572, found: 467.2569.

Methyl 6-((3-(4-aminophenyl)-3-((*tert*-butyldimethylsilyl)oxy)propyl)(methyl)amino)-6-oxohexanoate (175). Ammonium formate (68 mg, 1.07 mmol, 10.0 eq) was added to a solution of **174** (50 mg, 0.11 mmol, 1.0 eq) in a mixture of anhydrous THF (1 mL) and anhydrous MeOH (1 mL) at room temperature. Pd/C (1 mg, 0.01 mmol, 0.1 eq) was added to this suspension and the reaction flask was sealed. The reaction mixture was allowed to stir at room temperature for 30 min. The reaction flask was opened carefully and the reaction mixture was diluted by ethyl acetate (5 mL). The suspension was filtered over a column of celite (packed in a glass pipette). The ethyl acetate layer was washed with water (5 mL), brine (5 mL), dried over sodium sulfate (200 mg), filtered, and concentrated under reduced pressure. The product was purified from the residual oil by silica gel flash column chromatography to obtain **175** as a colorless oil (40 mg, 85%). ^{1}H NMR (400 MHz, $CDCl_3$) δ 7.01 − 7.11 (m, 2 H), 6.60 − 6.68 (m, 2 H), 4.54 − 4.64 (m, 1 H), 3.65 (d, *J*=4.40 Hz, 3 H), 3.11 − 3.51 (m, 4 H), 2.86 (d, *J*=15.77 Hz, 3 H), 2.27 − 2.35 (m, 2 H), 2.13 − 2.27 (m, 2 H), 1.73 − 1.92 (m, 2 H), 1.54 − 1.68 (m, 4 H), 0.86 (d, *J*=9.54 Hz, 9 H), 0.00 (d, *J*=7.83 Hz, 3 H), −0.18 (d, *J*=6.97 Hz, 3 H); HRMS (ESI) calcd. for $C_{23}H_{41}O_4N_2Si$ $(M+H)^+$ 437.2830, found: 437.2830.

Methyl (*Z*)-6-((3-((*tert*-butyldimethylsilyl)oxy)-3-(4-(((cyclooct-2-en-1-yloxy)carbonyl) amino)phenyl)propyl)(methyl)amino)-6-oxohexanoate (177). Triphosgene (15 mg, 0.05 mmol, 0.5 eq) was added to a solution of **175** (45 mg, 0.10 mmol, 1.0 eq) in anhydrous toluene (5 mL) at room temperature. This solution was heated to 100 °C and stirred for 10 min. The reaction mixture was concentrated to yield a **176** as a pale-yellow oil (42 mg, 90%). This oil was quickly dissolved in anhydrous THF (1 mL). A solution of **168** in anhydrous THF (1 mL) was prepared in another

vial and cooled to 0 °C. Sodium hydride (1.2 eq) was added to the solution of **168** with stirring at 0 °C and the suspension was stirred at 0 °C for 15 min. The solution of **176** (in THF) was slowly added to the reaction mixture containing **168** at 0 °C and the resulting reaction mixture was stirred for 2 h while allowing to warm to room temperature. The reaction was quenched with ice-water mixture (5 mL) and the aqueous layer was washed with ethyl acetate (3 × 5 mL). The combined organic extracts were washed with brine (10 mL), dried over sodium sulfate (1 g), filtered, and concentrated under reduced pressure. Compound **177** was purified from the residual oil by silica gel flash column chromatography in 1:3 ethyl acetate/hexanes as a yellow oil (6.0 mg, 10% yield from amine **175**). ^{1}H NMR (400 MHz, $CDCl_3$) δ 7.29 − 7.38 (m, 1 H), 7.30 (br s, 1 H), 7.20 − 7.25 (m, 2 H), 6.59 − 6.73 (m, 1 H), 5.61 − 5.73 (m, 2 H), 5.44 − 5.56 (m, 1 H), 4.63 − 4.74 (m, 1 H), 3.66 (d, *J*=4.89 Hz, 3 H), 3.14 − 3.57 (m, 2 H), 2.86 (d, *J*=14.31 Hz, 3 H), 2.26 − 2.35 (m, 3 H), 2.08 − 2.21 (m, 3 H), 2.00 (br d, *J*=3.79 Hz, 2 H), 1.82 − 1.93 (m, 3 H), 1.63 − 1.75 (m, 4 H), 1.52 (br s, 3 H), 1.40 (br dd, *J*=4.83, 2.87 Hz, 2 H), 0.88 (br d, *J*=10.39 Hz, 9 H), 0.02 (d, *J*=8.44 Hz, 3 H), −0.17 (d, *J*=8.80 Hz, 3 H); HRMS (ESI) calcd. for $C_{32}H_{53}O_6N_2Si$ $(M+H)^+$ 589.3667, found: 589.3660.

Methyl 6-((3-((*tert*-butyldimethylsilyl)oxy)-3-(4-((phenoxycarbonyl)amino)phenyl)propyl) (methyl)amino)-6-oxohexanoate (179). Compound **175** (45 mg, 0.10 mmol, 1.0 eq) was dissolved in anhydrous DCM (5 mL) and this solution was cooled in ice-water bath. Compound **178** (20 µL, 0.16 mmol, 1.5 eq) and, subsequently, pyridine (20 µL, 0.26 mmol, 2.5 eq) was added to the solution at 0 °C while stirring. The reaction mixture was stirred for 30 min while allowing to warm to room temperature. A white precipitate was observed in the reaction mixture after pyridine addition. The precipitate was filtered by a glass pipette with a cotton plug. The white

precipitate was washed with DCM (3 mL) and the filtrate was concentrated under reduced pressure. The product was purified from the residual oil by silica gel flash column chromatography (elution with 1:1 ethyl acetate/hexanes) to afford **167** as a colorless oil (53 mg, 92%). ^{1}H NMR (400 MHz, $CDCl_3$) δ 6.79 – 7.41 (m, 10 H), 4.67 – 4.74 (m, 1 H), 3.64 – 3.68 (m, 3 H), 3.40 – 3.55 (m, 1 H), 3.17 – 3.28 (m, 2 H), 2.76 – 2.90 (m, 3 H), 2.16 – 2.24 (m, 2 H), 2.25 (br s, 2 H), 1.76 – 2.02 (m, 3 H), 1.59 – 1.69 (m, 2 H), 0.80 – 0.92 (m, 9 H), 0.00 – 0.07 (m, 3 H), −0.18 – −0.13 (m, 3 H); LRMS (ESI) calcd. for $C_{30}H_{45}O_6N_2Si$ $(M+H)^+$ 557.30, found: 557.00.

Methyl (*E*)-6-((3-((*tert*-butyldimethylsilyl)oxy)-3-(4-(((cyclooct-2-en-1-yloxy)carbonyl) amino)phenyl)propyl)(methyl)amino)-6-oxohexanoate (181e). To a 10 mL microwave reactor vial equipped with a stir bar, **179** (110 mg, 0.20 mmol, 1.0 eq) was added and dissolved in anhydrous toluene (5 mL). Compound **180e** (30 mg, 0.24 mmol, 1.2 eq) and dibutyltin dilaurate (150 mg, 0.24 mmol, 1.2 eq) was added to this vial at room temperature and the vial was sealed. The vial was heated to 100 °C in a microwave reactor and the reaction was stirred at 100 °C for 20 min. The vial was allowed to cool to room temperature and the vial was carefully opened. The reaction mixture was concentrated under reduced pressure. The residual oil was loaded on a silica gel column and the product was eluted out in 1:1 ethyl acetate/hexanes to afford **181e** as a pale-yellow oil (91 mg, 78%). ^{1}H NMR (400 MHz, $CDCl_3$) δ 7.32 – 7.38 (m, 2 H), 7.22 – 7.26 (m, 2 H), 6.82 – 6.84 (m, 1 H), 6.20 – 6.26 (m, 1 H), 5.80 – 5.88 (m, 1 H), 5.48 – 5.58 (m, 1 H), 4.66 – 4.75 (m, 1 H), 3.69 (d, *J*=4.57 Hz, 3 H), 3.23 – 3.66 (m, 2 H), 2.99 (d, *J*=12.78 Hz, 3 H), 2.36 – 2.46 (m, 3 H), 2.23 – 2.32 (m, 3 H), 2.18 (br d, *J*=4.12 Hz, 2 H), 1.89 – 1.99 (m, 3 H), 1.66 – 1.83 (m, 4 H), 1.55 (br s, 3 H), 1.46 (m, 2 H), 0.95 (br d, *J*=10.21 Hz, 9 H), 0.04 (d, *J*=8.65 Hz, 3 H),

−0.17 (d, *J*=8.99 Hz, 3 H); HRMS (ESI) calcd. for $C_{32}H_{53}O_6N_2Si$ $(M+H)^+$ 589.3667, found: 589.3679.

Ethyl (1*S*,8*R*,9*S*,*Z*)-5-hydroxybicyclo[6.1.0]non-3-ene-9-carboxylate (204). Compound **201** (3.50 g, 18.02 mmol, 1.0 eq) was dissolved in acetonitrile (50 mL), and water (10 mL) was added to this solution. Compound **165** (4.14 g, 21.62 mmol, 1.2 eq) was added to this solution, and the reaction mixture was stirred at room temperature for 24 h. Acetonitrile was evaporated under reduced pressure, and the residue was resuspended in ethyl acetate (50 mL) and H_2O (50 mL) mixture. The ethyl acetate layer was separated, and the aqueous layer was extracted with ethyl acetate (2 × 30 mL). The combined organic extracts were dried over sodium sulfate (10 g), filtered, and concentrated under reduced pressure to yield a yellow gum (6.20 g). The yellow gum was dissolved in THF (40 mL), and *tert*-butyl hydroperoxide (TBHP, 10 mL, 70 wt% in H_2O) was added to this solution at room temperature, and the reaction mixture was stirred for 24 h. The reaction was quenched with aqueous saturated $NaHCO_3$ (40 mL), and THF was evaporated under reduced pressure. The aqueous layer was washed with ethyl acetate (3 × 30 mL), and the combined organic extracts were dried over sodium sulfate (10 g), filtered, and concentrated under reduced pressure. The product was purified from the crude residue by silica gel flash column chromatography, eluting with ethyl acetate/hexanes (1:4) to yield **204** as a colorless viscous oil (2.48 g, 70%). ^{1}H NMR (400 MHz, $CDCl_3$) δ 5.72 – 5.81 (m, 1 H), 5.63 – 5.71 (m, 1 H), 4.31 – 4.39 (m, 1 H), 4.05 – 4.14 (m, 2 H), 2.32 – 2.43 (m, 2 H), 1.83 – 1.92 (m, 1 H), 1.61 – 1.80 (m, 4 H), 1.33 – 1.44 (m, 2 H), 1.21 – 1.28 (m, 4 H); LRMS (ESI) calcd. for $C_{12}H_{18}O_3$ $(M+H)^+$ 211.13, found: 211.00.

((1*S*,8*R*,9*S*,*Z*)-5-((*tert*-butyldimethylsilyl)oxy)bicyclo[6.1.0]non-3-en-9-yl)methanol (205). **Procedure A:** Compound **204** (5.0 g, 23.78 mmol, 1.0 eq) was dissolved in anhydrous DMF (30 mL) and imidazole (4.9 g, 71.34 mmol, 3.0 eq) was added to this solution. *Tert*-butyldiphenylchlorosilane (TBDMSCl, 5.4 g, 35.67 mmol, 1.5 eq) was added to this solution at room temperature. The reaction mixture was stirred overnight at room temperature. The reaction mixture was poured into water (200 mL) and the aqueous layer was washed with ethyl acetate (3 × 50 mL). The combined organic extracts were dried over sodium sulfate (20 g), filtered, and concentrated under reduced pressure. The product was purified from the crude residue by silica gel flash column chromatography (elution with 1:20 ethyl acetate/hexanes) to afford a clear oil. The oil was dissolved in anhydrous diethyl ether (30 mL) and this solution was cooled to 0 °C. Lithium aluminum hydride ($LiAlH_4$, 2.6 g, 37.95 mmol, 3.0 eq) was added to this solution at 0 °C with stirring. The resulting suspension was stirred at 0 °C for 1 h. Saturated aqueous ammonium chloride solution (50 mL) was slowly added to the reaction mixture at 0 °C with the formation of a white precipitate. The white precipitate was filtered and the diethyl ether layer was separated. The aqueous layer was washed with diethyl ether (3 × 30 mL). The combined diethyl ether layers were washed with brine (20 mL), dried over sodium sulfate (10 g), filtered, and concentrated under reduced pressure. The product was purified from the residual oil by silica gel flash column chromatography, eluting with ethyl acetate/hexanes (1:4) to yield **205** as a colorless oil (6.0 g, 92%). ^{1}H NMR (300 MHz, $CDCl_3$) δ 5.58 – 5.75 (m, 2 H), 4.26 (br d, *J*=9.63 Hz, 1 H), 3.44 (dd, *J*=6.70, 1.61 Hz, 2 H), 2.23 – 2.38 (m, 2 H), 1.48 – 1.87 (m, 3 H), 1.06 – 1.26 (m, 1 H), 0.78 – 0.93 (m, 12 H), 0.58 – 0.71 (m, 1 H), 0.01 – 0.08 (m, 6 H); LRMS (ESI) calcd. for $C_{16}H_{31}O_2Si$ $(M+H)^+$ 283.21, found: 283.00.

((1*S*,8*R*,9*R*,*Z*)-5-((*tert*-butyldimethylsilyl)oxy)bicyclo[6.1.0]non-3-en-9-yl)methanol (206). Procedure A, 5.4 g, 89%. ^{1}H NMR (300 MHz, $CDCl_3$) δ 5.56 – 5.77 (m, 2 H), 4.29 (br d, *J*=9.82 Hz, 1 H), 3.73 – 3.90 (m, 2 H), 2.02 – 2.18 (m, 2 H), 1.65 – 1.93 (m, 3 H), 1.04 – 1.45 (m, 5 H), 0.88 (s, 9 H), 0.04 (s, 6 H); LRMS (ESI) calcd. for $C_{16}H_{31}O_2Si$ $(M+H)^+$ 283.21, found: 283.00.

(1*R*,8*S*,9*S*,*Z*)-9-(Hydroxymethyl)bicyclo[6.1.0]non-5-en-4-ol (215). Compound **213** (5.20 g, 34.16 mmol, 1.0 eq) was dissolved in acetonitrile (100 mL), and water (20 mL) was added to this solution. Compound **165** (6.74 g, 35.18 mmol, 1.0 eq) was added to this solution, and the reaction mixture was stirred at room temperature for 24 h. Acetonitrile was evaporated under reduced pressure, and the residue was resuspended in ethyl acetate (50 mL) and H_2O (50 mL) mixture. The ethyl acetate layer was separated, and the aqueous layer was extracted with ethyl acetate (2 × 50 mL). The combined organic extracts were dried over sodium sulfate (20 g), filtered, and concentrated under reduced pressure to yield crude mixture **214** as a yellow gum (HRMS (ESI) calcd. for $C_{16}H_{23}O_2Se$ $(M+H)^+$ 327.08578, found: 327.08472). The yellow gum **214** was dissolved in THF (100 mL), and *tert*-butyl hydroperoxide (TBHP, 25 mL, 70 wt% in H_2O) was added to this solution at room temperature, and the reaction mixture was stirred for 24 h. The reaction was quenched with aqueous saturated $NaHCO_3$ (50 mL), and THF was evaporated under reduced pressure. The aqueous layer was washed with ethyl acetate (5 × 50 mL), and the combined organic extracts were dried over sodium sulfate (20 g), filtered, and concentrated under reduced pressure. The product was purified from the crude residue by silica gel flash column chromatography, eluting with MeOH/DCM (1:9) to yield **215** as a white solid (3.69 g, 64%). ^{1}H NMR (400 MHz, $CDCl_3$) δ 5.66 – 5.83 (m, 1 H), 5.60 – 5.66 (m, 1 H), 4.29 – 4.38 (m, 1 H), 3.39 – 3.47 (m, 2 H), 2.26 – 2.38 (m, 2 H), 1.68 – 1.89 (m, 4 H), 1.57 (td, *J*=12.17, 10.03 Hz, 1 H), 1.14 – 1.30 (m, 1

H), 0.79 – 0.91 (m, 2 H), 0.58 – 0.79 (m, 1 H); ^{13}C NMR (101 MHz, $CDCl_3$) δ 137.50, 129.56, 73.46, 66.51, 41.09, 29.58, 28.16, 27.23, 26.94, 20.35; HRMS (ESI) calcd. for $C_{10}H_{17}O_2$ $(M+H)^+$ 169.12231, found: 169.12241.

(1*R*,8*S*,9*S*,*Z*)-9-(((*Tert*-butyldiphenylsilyl)oxy)methyl)bicyclo[6.1.0]non-5-en-4-ol (216). Compound **215** (3.69 g, 21.93 mmol, 1.0 eq) was dissolved in anhydrous DMF (30 mL), and imidazole (2.99 g, 43.87 mmol, 2.0 eq) was added to this solution. The resulting solution was cooled in an ice-water mixture, and *tert*-butyldiphenylchlorosilane (TBDMSCl, 5.70 mL, 21.93 mmol, 1.0 eq) was slowly added dropwise to this solution at this temperature. The reaction mixture was stirred for 3 h while allowing the reaction mixture to warm to room temperature. The reaction was quenched with water (300 mL), and the aqueous layer was washed with ethyl acetate (3 × 50 mL). The combined organic extracts were dried over sodium sulfate (20 g), filtered, and concentrated under reduced pressure. The crude residue was purified by silica gel flash column chromatography, eluting with ethyl acetate/hexanes (1:4) to yield **216** as a clear oil (5.40 g, 61%). ^{1}H NMR (400 MHz, $CDCl_3$) δ 7.66 – 7.71 (m, 4 H), 7.36 – 7.45 (m, 6 H), 5.69 – 5.74 (m, 1 H), 5.59 – 5.63 (m, 1 H), 4.32 – 4.35 (m, 1 H), 3.48 – 3.60 (m, 2 H), 2.18 – 2.35 (m, 2 H), 1.81 – 1.87 (m, 1 H), 1.66 – 1.74 (m, 2 H), 1.52 – 1.57 (m, 1 H), 1.13 – 1.22 (m, 1 H), 1.05 – 1.07 (m, 9 H), 0.68 – 0.81 (m, 2 H), 0.52 – 0.56 (m, 1 H); ^{13}C NMR (101 MHz, $CDCl_3$) δ 137.21, 135.74, 134.25, 129.91, 129.66, 127.69, 73.55, 67.07, 41.28, 29.41, 28.21, 27.29, 27.00, 26.84, 20.09, 19.34; HRMS (ESI) calcd. for $C_{26}H_{35}O_2Si$ $(M+H)^+$ 407.24008, found: 407.23874.

Methyl 6-((2-(((((1*R*,8*S*,9*S*,*E*)-9-(((*tert*-butyldiphenylsilyl)oxy)methyl)bicyclo[6.1.0]non-5-en-4-yl)oxy)carbonyl)(methyl)amino)ethyl)(methyl)amino)-6-oxohexanoate (218).

Compound **217** (50 mg, 0.18 mmol, 1.0 eq) was dissolved in anhydrous DCM (3 mL), and 1,1'-carbonyldiimidazole (CDI, 57 mg, 0.35 mmol, 2.0 eq) was added to this solution and stirred for 3 h at room temperature. *N*,*N'*-Dimethylethylenediamine (DMEDA, 95 µL, 0.88 mmol, 5.0 eq) was added to the reaction mixture at room temperature, and the reaction was stirred at room temperature for another 3 h. The volatiles were evaporated under reduced pressure to yield crude amine intermediate as a yellow oil (HRMS (ESI) calcd. for $C_{31}H_{45}O_3N_2Si$ $(M+H)^+$ 521.31940, found: 521.31902). The crude residue was dissolved in anhydrous acetonitrile (5 mL), and cesium carbonate (290 mg, 0.88 mmol, 5.0 eq) was added to this reaction at room temperature. Methyl adipoyl chloride (83 µL, 0.53 mmol, 3.0 eq) was added to this suspension at room temperature, and stirred for 24 h. The reaction was quenched with water (20 mL), and the acetonitrile was evaporated under reduced pressure. The aqueous layer was washed with ethyl acetate (3 × 10 mL) and the combined organic extracts were dried over sodium sulfate (2 g), filtered, and concentrated under reduced pressure. The residue was purified by silica gel flash column chromatography, eluted with ethyl acetate/DCM (1:1) to yield **222** as a yellow oil (48 mg, 51%). ^{1}H NMR (400 MHz, $CDCl_3$) δ 7.63 – 7.65 (m, 4 H), 7.34 – 7.41 (m, 6 H), 5.14 – 5.75 (m, 2 H), 3.64 – 3.66 (m, 3 H), 3.34 – 3.56 (m, 5 H), 2.99 (s, 2 H), 2.91 – 2.96 (m, 4 H), 2.19 – 2.38 (m, 6 H), 1.82 – 2.04 (m, 2 H), 1.53 – 1.73 (m, 6 H), 1.14 – 1.33 (m, 2 H), 0.99 – 1.06 (m, 9 H), 0.69 – 0.91 (m, 2 H), 0.45 – 0.57 (m, 1 H); HRMS (ESI) calcd. for $C_{38}H_{55}O_6N_2Si$ $(M+H)^+$ 663.38239, found: 663.38213.

Methyl 6-((2-(((((1*R*,8*S*,9*S*,*E*)-9-(hydroxymethyl)bicyclo[6.1.0]non-5-en-4-yl)oxy)carbonyl)-(methyl)amino)ethyl)-(methyl)amino)-6-oxohexanoate (219). Compound **218** (80 mg, 0.12 mmol, 1.0 eq) was dissolved in anhydrous THF (5 mL), and TBAF (0.8 mL, 0.80 mmol, 6.7 eq, 1 M in THF) was added to this solution at room temperature. The reaction mixture was stirred at

room temperature for 3 h. The solvent was evaporated under reduced pressure and the residue was suspended in ethyl acetate (5 mL) and H_2O (5 mL). The ethyl acetate layer was separated and the aqueous layer was washed with ethyl acetate (2 × 5 mL). The combined organic fractions were dried over sodium sulfate (1 g), filtered, and concentrated under reduced pressure. The residue was purified by silica gel flash column chromatography, eluted with MeOH/ethyl acetate (1:20) to yield **219** (39 mg, 76%) as a colorless oil. ^{1}H NMR (400 MHz, $CDCl_3$) δ 5.05 – 6.06 (m, 2 H), 3.62 – 3.63 (m, 3 H), 3.29 – 3.48 (m, 5 H), 2.96 – 2.99 (m, 2 H), 2.89 – 2.92 (m, 4 H), 2.56 – 2.82 (m, 1 H), 2.22 – 2.39 (m, 6 H), 1.85 – 1.99 (m, 1 H), 1.54 – 1.67 (m, 6 H), 1.14 – 1.36 (m, 2 H), 0.83 – 0.95 (m, 2 H), 0.60 – 0.66 (m, 1 H); HRMS (ESI) calcd. for $C_{22}H_{37}O_6N_2$ $(M+H)^+$ 425.26461, found: 425.26478.

Methyl 6-((2-(((((1*R*,8*S*,9*S*,*E*)-9-((((2-(2-chloro-*N*-methylacetamido)ethyl)(methyl) carbamoyl)oxy)methyl) bicyclo[6.1.0]non-5-en-4-yl)oxy)carbonyl)(methyl)amino)ethyl) (methyl)amino)-6-oxohexanoate (220). Compound **219** (39 mg, 0.09 mmol, 1.0 eq) was dissolved in anhydrous DCM (3 mL) and 1,1'-carbonyldiimidazole (CDI, 23 mg, 0.14 mmol, 1.5 eq) was added to this solution and stirred at room temperature for 3 h. *N*,*N*'-Dimethylethylenediamine (DMEDA, 50 µL, 0.47 mmol, 5.0 eq) was added to the reaction mixture, and stirred at room temperature for another 5 h. The volatiles were evaporated under reduced pressure to yield crude amine intermediate as a yellow oil (HRMS (ESI) calcd. for $C_{27}H_{47}O_7N_4$ $(M+H)^+$ 539.34393, found: 539.34440). The crude residue was dissolved in anhydrous acetonitrile (3 mL), and cesium carbonate (307 mg, 0.94 mmol, 10.0 eq) was added to this solution at room temperature. The suspension was cooled in an ice-water mixture, and chloroacetyl chloride (38 µL, 0.47 mmol, 5.0 eq) was slowly added at 0 °C. The reaction was stirred for 4 h while allowing

the reaction mixture to warm to room temperature. The reaction was quenched with water (10 mL), and acetonitrile was evaporated under reduced pressure. The aqueous layer was washed with ethyl acetate (5 × 5 mL), and the combined organic extracts were dried over sodium sulfate (1 g), filtered, and concentrated under reduced pressure. The residue was purified by silica gel flash column chromatography, eluting with ethyl acetate/DCM (1:1) to yield **220** (16 mg, 28%) as a colorless oil. ^{1}H NMR (400 MHz, $CDCl_3$) δ 4.94 – 6.14 (m, 2 H), 3.78 – 4.33 (m, 3 H), 3.65 (s, 3 H), 3.24 – 3.60 (m, 8 H), 3.07 – 3.22 (m, 2 H), 2.96 – 3.04 (m, 4 H), 2.89 – 2.96 (m, 5 H), 2.22 – 2.40 (m, 6 H), 1.80 – 2.21 (m, 2 H), 1.64 (br d, *J*=2.93 Hz, 6 H), 1.14 – 1.37 (m, 3 H), 0.79 – 1.04 (m, 2 H), 0.71 (br dd, *J*=4.34, 2.75 Hz, 1 H). HRMS (ESI) calcd. for $C_{29}H_{48}O_8N_4Cl$ $(M+H)^+$ 615.31552, found: 615.31503.

2,5-Dioxopyrrolidin-1-yl 6-((2-(((((1*R*,8*S*,9*S*,*E*)-9-((((2-(2-chloro-*N*-methylacetamido)ethyl)-(methyl)carbamoyl)oxy)methyl)bicyclo[6.1.0]non-5-en-4-yl)oxy)carbonyl)-(methyl)amino)-ethyl)-(methyl)amino)-6-oxohexanoate (221). Compound **220** (8.0 mg, 0.013 mmol, 1.0 eq) was dissolved in THF (0.5 mL), and 2 M aqueous LiOH solution (0.5 mL) was slowly added to this solution at room temperature, and the resulting mixture was vigorously stirred at room temperature for 3 h. The reaction mixture was diluted with water (2 mL), and the aqueous phase was washed with Et_2O (3 × 1 mL). The aqueous layer was acidified with 1 M aqueous citric acid to a pH of 3-4. The aqueous phase was washed with ethyl acetate (3 × 2 mL). The combined organic extracts were dried over sodium sulfate (200 mg), filtered, and concentrated under reduced pressure to afford the crude acid as a colorless oil (5.6 mg, 72%). The acid was dissolved in anhydrous acetonitrile (1 mL), and the solution was cooled in an ice-water mixture. TSTU (4.2 mg, 0.014 mmol, 1.5 eq) and then *N*,*N*-diisopropylethylamine (3.3 µL, 0.019 mmol, 2.0 eq) was added to this

solution at 0 °C. The reaction mixture was stirred for 30 min while allowing the reaction mixture to warm to room temperature. The reaction mixture was concentrated under reduced pressure. The crude residue was purified by silica gel flash column chromatography, eluting with MeOH/ethyl acetate (1:20) to yield **221** as a colorless oil (2.9 mg, 45%). ^{1}H NMR (400 MHz, $CDCl_3$) δ 5.11 – 5.80 (m, 2 H), 4.06 (s, 1 H), 3.84 – 3.94 (m, 1 H), 3.64 – 3.75 (m, 2 H), 3.33 – 3.60 (m, 5 H), 3.09 – 3.16 (m, 3 H), 2.98 – 3.04 (m, 2 H), 2.91 – 2.97 (m, 4 H), 2.79 – 2.89 (m, 4 H), 2.69 – 2.78 (m, 1 H), 2.59 – 2.69 (m, 2 H), 2.27 – 2.38 (m, 4 H), 2.09 – 2.17 (m, 1 H), 1.84 – 1.95 (m, 1 H), 1.67 – 1.83 (m, 4 H), 1.47 – 1.54 (m, 6 H), 1.24 – 1.27 (m, 2 H), 0.81 – 0.99 (m, 2 H), 0.64 – 0.79 (m, 1 H); LRMS (ESI) calcd. for $C_{32}H_{49}ClN_5O_{10}$ $(M+H)^+$ 698.32, found: 698.00.

Representative procedure for the synthesis of tetrazines.

Synthetic procedure for the synthesis of 3-methyl-6-(pyridin-2-yl)-1,2,4,5-tetrazine and 3,6-dimethyl-1,2,4,5-tetrazine. The procedure was adapted from a reported procedure.[301] 2-Cyanopyridine (300 mg, 2.88 mmol, 1.0 eq) and acetonitrile (1.5 mL, 28.82 mmol, 10.0 eq) were dissolved in absolute ethanol (3 mL) and 3-mercaptopropanoic acid (250 µL, 2.88 mmol, 1.0 eq) was added to this solution at room temperature. Hydrazine monohydrate (2.8 mL, 57.63 mmol, 20.0 eq) was slowly added to this solution at room temperature and the reaction was stirred at room temperature for 72 h. The resulting orange-colored solution was transferred to a 100 mL round bottom flask and this solution was cooled in ice-water mixture. Aqueous 1 M citric acid solution (10 mL) was added to this solution at 0 °C until the pH of the solution is 3–4. Solid sodium nitrite (10 eq) was slowly added in portions at 0 °C and effervescence was observed during this time. After complete sodium nitrite addition, the solution was stirred at 0 °C for 4 h to yield a bright red

solution. The solution was transferred to a separatory funnel and saturated with solid sodium chloride. The organic fractions were extracted with ethyl acetate (3 × 20 mL) or until the red color in aqueous solution almost vanished. The combined organic extracts were dried over sodium sulfate (5 g), filtered, and concentrated under reduced pressure. The residual mass was loaded on a silica gel column and the products were eluted out in the following solvent mixtures. The symmetrical tetrazine (3,6-dimethyl-1,2,4,5-tetrazine) was eluted out in 1:10 ethyl acetate/hexanes and obtained as a red solid (110 mg, 22%). The unsymmetrical tetrazine (3-methyl-6-(pyridin-2-yl)-1,2,4,5-tetrazine) was eluted out in 1:1 ethyl acetate/hexanes and then the crude product was filtered with DCM. 3-Methyl-6-(pyridin-2-yl)-1,2,4,5-tetrazine was obtained as a red solid (140 mg, 11%).

3,6-Dimethyl-1,2,4,5-tetrazine (146). Procedure B, 110 mg, 22% yield. ^{1}H NMR (400 MHz, $CDCl_3$) δ 3.05 (s, 3 H). The NMR data obtained was in accordance with the reported data.[282]

2,2'-(1,2,4,5-Tetrazine-3,6-diyl)bis(ethan-1-ol). Procedure B, 202 mg, 9% yield. ^{1}H NMR (400 MHz, $CDCl_3$) δ 4.27 (t, *J*=5.75 Hz, 2 H), 3.59 (t, *J*=5.81 Hz, 2 H), 2.17 (br s, 2 H). The NMR data obtained was in accordance with the reported data.[302]

3-Methyl-6-(pyridin-2-yl)-1,2,4,5-tetrazine. Procedure B, 140 mg, 11% yield. ^{1}H NMR (400 MHz, $CDCl_3$) δ 8.93 – 8.96 (m, 1H), 8.59 (d, *J*=7.95 Hz, 1H), 7.89 (td, *J*=7.87, 1.73 Hz, 1H), 7.51 (ddd, *J*=7.59, 4.83, 1.19 Hz, 1H), 3.17 (s, 3H). The NMR data obtained was in accordance with the reported data.[282]

3-Methyl-6-(pyrimidin-2-yl)-1,2,4,5-tetrazine (151). Procedure B, 54 mg, 4% yield. ^{1}H NMR (400 MHz, $CDCl_3$) δ 9.11 (d, *J*=4.89 Hz, 2 H), 7.58 (t, *J*=4.89 Hz, 1 H), 3.20 (s, 3 H). The NMR data obtained was in accordance with the reported data.[303]

2-(6-(Pyridin-2-yl)-1,2,4,5-tetrazin-3-yl)ethan-1-ol. Procedure B, 257 mg, 44% yield. ^{1}H NMR (400 MHz, $CDCl_3$) δ 8.85 − 8.90 (m, 1 H), 8.57 (d, *J*=7.95 Hz, 1 H), 7.94 (td, *J*=7.76, 1.71 Hz, 1 H), 7.52 (ddd, *J*=7.58, 4.77, 0.98 Hz, 1 H), 4.29 (t, *J*=5.87 Hz, 2 H), 3.54 − 3.72 (m, 3 H). The NMR data obtained was in accordance with the reported data.[285]

2-(6-(Pyrimidin-2-yl)-1,2,4,5-tetrazin-3-yl)ethan-1-ol (150). Procedure B, 60 mg, 10% yield. ^{1}H NMR (400 MHz, $CDCl_3$) δ 9.13 (d, *J*=4.89 Hz, 1 H), 7.60 (t, *J*=4.89 Hz, 1 H), 4.35 (t, *J*=5.81 Hz, 2 H), 3.75 (t, *J*=5.80 Hz, 2 H), 2.09 (br s, 2 H). The NMR data obtained was in accordance with the reported data.[285]

***Tert*-butyl (2-(6-(pyridin-2-yl)-1,2,4,5-tetrazin-3-yl)ethyl)carbamate.** Procedure B, 435 mg, 50% yield. ^{1}H NMR (300 MHz, $CDCl_3$) δ 8.87 − 8.93 (m, 1 H), 8.58 (d, *J*=7.98 Hz, 1 H), 7.94 (td, *J*=7.79, 1.74 Hz, 1 H), 7.52 (ddd, *J*=7.59, 4.79, 1.01 Hz, 1 H), 3.76 (q, *J*=5.75 Hz, 2 H), 3.54 − 3.64 (m, 2 H), 1.32 (s, 9 H). The NMR data obtained was in accordance with the reported data.[285]

***Tert*-butyl (2-(6-(pyrimidin-2-yl)-1,2,4,5-tetrazin-3-yl)ethyl)carbamate.** Procedure B, 187 mg, 22% yield. ^{1}H NMR (300 MHz, $CDCl_3$) δ 9.09 (d, *J*=4.95 Hz, 2 H), 7.57 (t, *J*=4.91 Hz, 1 H), 3.74 − 3.84 (m, 2 H), 3.58 − 3.74 (m, 2 H), 1.32 − 1.37 (m, 9 H). The NMR data obtained was in accordance with the reported data.[285]

2.2 Enzyme-based activation of cMOs

2.2.1 Introduction

β-lactam antibiotics are the most frequently used antibiotics in hospitals due to their broad spectrum of activity, efficacy, and safety.[304] The antibacterial nature of penicillin was discovered by Dr. Alexander Fleming in 1928. Due to the difficulty of purification, the first animal experiment with penicillin did not begin until 1940; in this study, penicillin proved effective in treating a streptococcal infection in a mice model in 1940. Hodgkin et al. later described the penicillin's chemical structure by X-ray crystallography.[305] The currently available β-lactam antibiotics all have a 4-membered strained cyclic amide. In three of the four classes of β-lactam antibiotics — penicillins, cephalosporins, and carbapenems — the lactam further elaborated as part of a bicyclic ring system, whereas in monobactams, only the single four-membered ring is present (**Figure 2-24**).[304] A number of antibiotics have been approved by FDA in each of these categories.

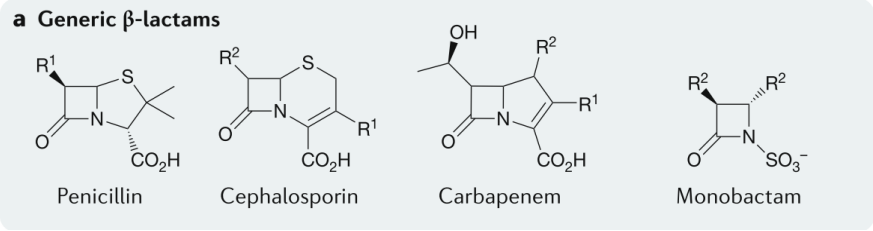

Figure 2-24 Classes of β-lactams antibiotics with different ring systems.

Adapted from *Nat. Rev. Microbiol.*, **2019**, 17, 295.[304]

β-lactam antibiotics have bactericidal activity and inhibit the synthesis of the peptidoglycan layer in the bacterial cell wall.[306] Bacteria require the peptidoglycan layer is

necessary to maintain the structural integrity of the cell wall. The integrity of the cell wall is important to maintain cell shape and osmotic stability. The cell wall consists of alternating *N*-acetylmuramic acid (NAM) and *N*-acetylglucosamine (NAG) units. A pentapeptide is attached to each NAM unit. The rigidity of the cell wall is conferred by crosslinking of these pentapeptides, and the final step of transpeptidation is facilitated by transpeptidases, which act as the targets of β-lactams (penicillin-binding proteins (PBPs)). β-lactams act by acylation of a conserved serine residue in the active site of these PBPs. The acylation is irreversible during the lifetime of a bacterial cell, leading to inactivation of the PBPs.

There are four mechanisms of resistance that bacteria have developed to counter the action of β-lactam antibiotics.[307-308] First, resistance has been achieved by changes to the active site of PBPs to reduce the binding affinity of these antibiotics. This type of resistance is seen in methicillin-resistant *Staphylococcus aureus* (MRSA).[309] Second, porin channels that β-lactam antibiotics must pass through to enter the periplasm have been observed to mutate to exclude these antibiotics, as seen in *Pseudomonas aeruginosa*.[310] This mechanism of resistance has rendered some strains of gram-negative bacteria resistant toward powerful carbapenem antibiotics.[308] Third, some strains, particularly of gram-negative species, have evolved drug efflux pumps capable of exporting a wide range of substrates, decreasing susceptibility to penicillins, cephalosporins, and carbapenems.[308] Fourth, the most common mechanism of β-lactam antibiotics resistance is by the production of β-lactamases.[307-308]

β-lactamases are enzymes produced and secreted by gram-negative bacteria, especially when β-lactam antibiotics are present in the surroundings. The first β-lactamase was identified in *Escherichia coli* before the clinical use of penicillin.[311] The significance of β-lactamases was later realized observed when a strain *S. aureus* found to have developed resistance to penicillin. Later,

as more β-lactam antibiotics were developed, resistance to multiple antibiotics was observed.[312] A multitude of β-lactamases have evolved in general, such as *Klebsiellae*, *Enterobacter*, and *P. aeruginosa*. To date, > 2,000 β-lactamases have been identified.[313]

β-lactamases are bacterial hydrolases that bind and acylate β-lactam antibiotics, resulting in the hydrolysis of the 4-membered β-lactam ring before the antibiotics reach their target.[307] Similar to PBPs, the activity is initiated by nucleophilic attack of serine on the carbonyl carbon in the β-lactam (**Figure 2-25**).[313] Next, a water molecule deacylates the intermediate to a carboxylic acid and an active serine residue. This process deactivates the antibiotic molecule and regnerates the enzyme, which can go on to inactivate additional antibiotic molecules. The transition state for the initial serine acylation step requires activation of the serine nucleophile. β-lactamases have been classified based on which nearby residue activates serine; glutamic acid,[314] a lysine and tyrosine pair,[315] and carbamylated lysine[316] may all serve this function. An interesting alternative mechanism is found in metallo-β-lactamase (MBL), in which a hydroxide group coordinated to two Zn^{2+} ions is responsible for β-lactam cleavage.[317] One Zn^{2+} is held in place by three histidine residues and the other Zn^{2+} by cysteine, histidine and aspartic acid. These classes of β-lactamases specifically target penicillins, cephalosporins, and carbapenems.

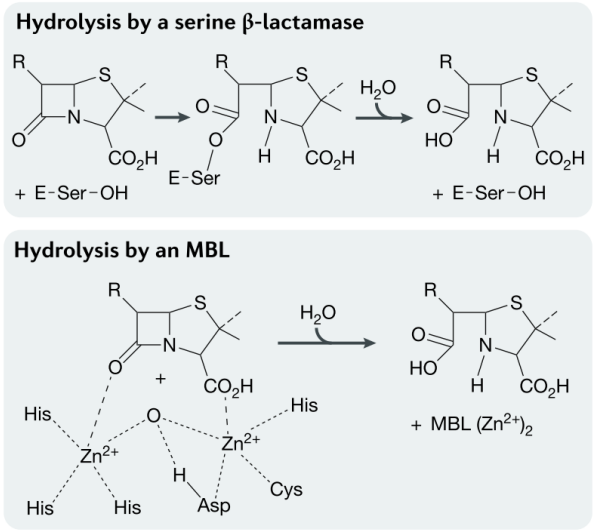

Figure 2-25 Mechanism of cyclic amide hydrolysis by a serine β-lactamase and metallo-β-lactamase (MBL). Adapted from *Nat. Rev. Microbiol.*, **2019**, 17, 295.[304]

In 1998, the Tsien lab developed a fluorescent probe for β-lactamase activity.[318] The probe, **CCF2**, contains a cephalosporin core elaborated with two fluorophores — hydroxycoumarin and fluorescein — forming a fluorescence resonance energy transfer (FRET) pair (**Figure 2-26**). The FRET pair is separated in the presence of β-lactamase, which hydrolyzes the lactam ring to generate the free amine, that eliminates and separates the acceptor fluorophore. This separation of the FRET pair is detected by a substantial change in fluorescence emission profile. Upon analyzing different ring systems activated by β-lactamase, only cephalosporins were found to respond through this elimination pathway. Moreover, β-lactamase expression was also monitored in live zebrafish embryos utilizing **CCF2**,[319] indicating that the probe functions in live zebrafish embryos. Thus, β-lactamase can act as an enzyme-based trigger for cMO linearization in zebrafish embryos.

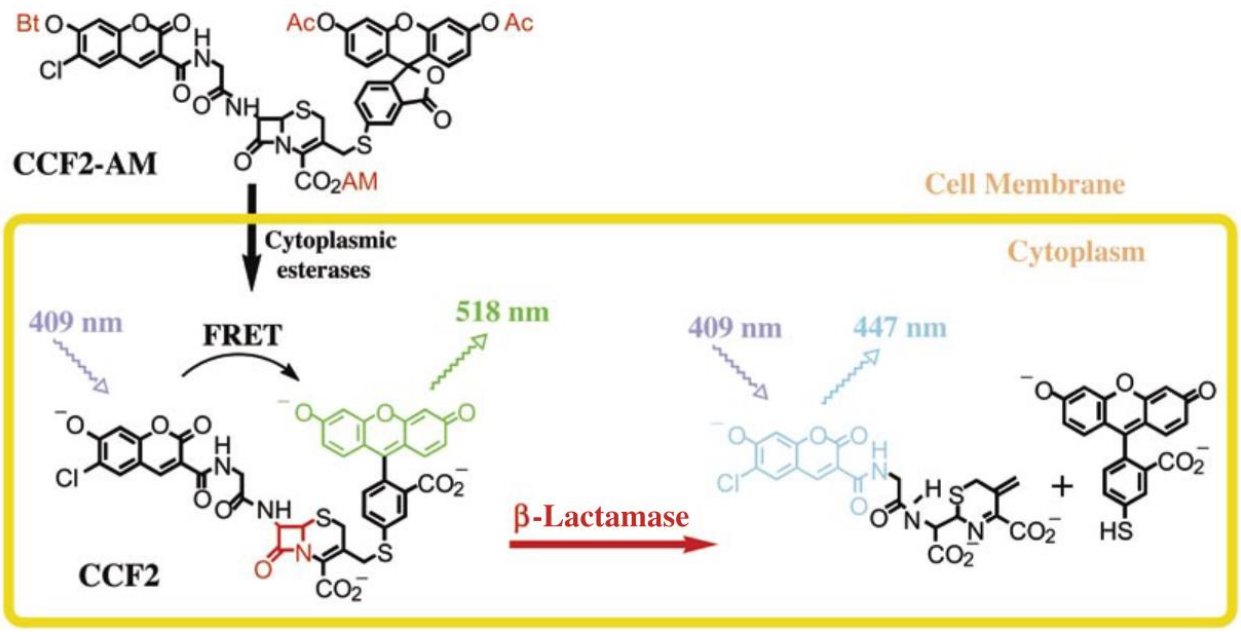

Figure 2-26 The esterified fluoroscent probe **CCF2-AM**.

CCF2-AM is hydrolyzed by cytoplasmic esterases to **CCF2** upon entering a cell. The hydroxycoumarin is excited at 409 nm, and a green fluorescence of 518 nm is emitted by fluorescein due to FRET. After β-lactamase cleavage, the FRET pair is separated, and a blue fluorescence of 447 nm from hydroxycoumarin is emitted upon excitation at 409 nm. Ac: acetyl; Bt: butyryl; AM: acetoxymethyl. Adapted from *BioTechniques*, **2007**, *42* (1), 91-96.[320]

2.2.2 Linker synthesis for β-lactamase activated cMOs

As described in previous sections, the cephalosporin-containing linker **225** was envisioned to undergo selective activation by β-lactamase (**Figure 2-27**). The original cMO linker design contained two orthogonal reactive ends — an NHS carbonate for 5'-amine conjugation (via a carbamate, which serves as a leaving group for linearization), and a chloroacetamide for conjugation to a 3'-thiol-modified MO. The proposed mechanism of cMO linearization is β-lactamase-mediated amide hydrolysis of the lactam ring, leading to the formation of amine **227**.

The amine in **227** is expected to undergo an elimination with the carbamate (**228**) to release the 5'-amine end of the morpholino leading to linearization of the cMO (**229**).

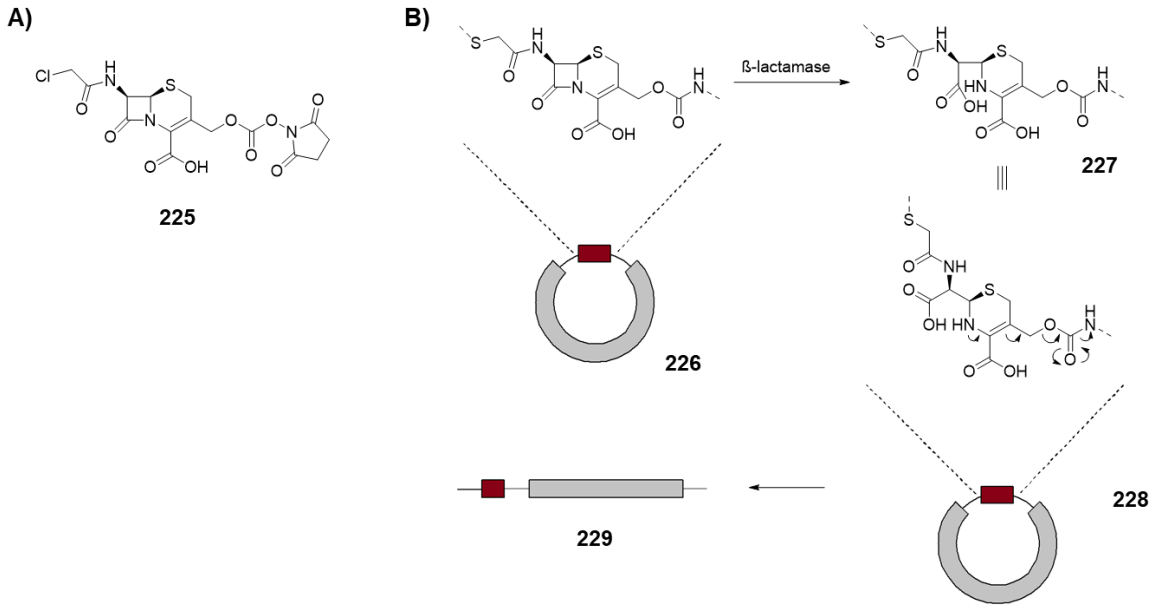

Figure 2-27 β-lactamase activated linker design and proposed mechanism of cMO linearization.

(A) The proposed cephem-containing linker **225** with chloroacetamide and NHS carbonate reactive ends. (B) Proposed mechanism of β-lactamase activation and cMO linearization.

Synthesis of the linker was initiated from commercially available 7-aminocephalosporanic acid (**230**) (**Figure 2-28**). Compound **230** was treated with *t*-butyl acetate in presence of *p*-toluene sulfonic acid (TsOH) and concentrated sulfuric acid (H_2SO_4) to obtain the *t*-butyl ester **231**.[321] The addition of chloroacetyl chloride to the amine in **231** afforded the chloroacetamide **232**. After optimization of reaction conditions, a biphasic mixture of **231** in DCM with aqueous sodium hydrogen carbonate with slow addition of chloroacetyl chloride was found to yield the best results. Next, the selective hydrolysis of the acetate group in the presence of the *t*-butyl ester was attempted to obtain the alcohol for subsequent activation as the NHS carbonate. However, both the esters (*t*-

butyl ester as well as acetate) were susceptible to base-mediated hydrolysis with NaOH or KOH (data not shown). Even with using substoichiometric amounts of the base, both the esters were affected.

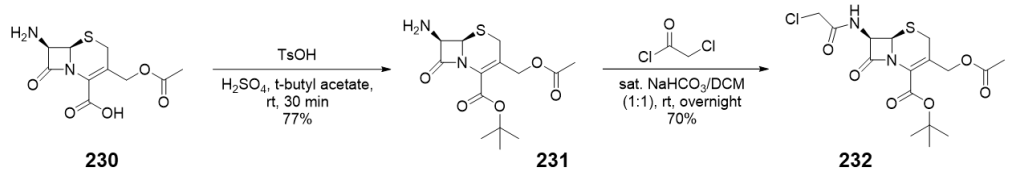

Figure 2-28 Synthesis of the cephalosporin-containing linker intermediate **232**.

Synthesis of **232** was initiated from 7-aminocephalosporanic acid (**230**), and the chloroacetamide end of the linker was installed in two steps.

This result necessitated the use of a different acid protecting group. Compound **236** was synthesized with a diphenylmethanol protecting group, according to a reported procedure.[321] Diazodiphenylmethane (**234**) was generated by treating diphenylhydrazone with HgO in basic conditions, and it was added to a solution of acid **235** to yield the ester **236** (**Figure 2-29A**). However, the base-mediated hydrolysis once again failed to selectively cleave the acetate in **236** (data not shown). Next, hydrolysis of the acetate group in **235** was attempted by potassium hydroxide, followed by protection of the acid group with **234**. Unfortunately, isolation of the hydrolyzed product **236** was unsuccessful. As an alternative, the photocleavable protecting group, 4-methoxy-7-nitroindoline (MNI, **238**), was explored as a potential option. Because this strategy would protect the acid as an amide, it was expected to be stable to treatment with base. The MNI group was synthesized according to the reported protocol.[322] A number of reaction conditions were screened with the use of different peptide coupling agents (**Figure 2-29B**). However, none of the conditions were successful in the synthesis of the MNI-protected acid (**239**).

Selective acetate cleavage can be achieved by lipase-mediated hydrolysis. Acetate hydrolysis was reported on a similar scaffold by *Candida Antarctica* Lipase B (CAL B).[321] CAL B is a serine hydrolase extracted from a yeast species, *Candida antarctica*. Upon modifying the reported reaction conditions, the acetate was incubated with CAL B at 50 °C in THF/hexanes mixture under anhydrous conditions, maintained by molecular sieves (**Figure 2-29C**). The alcohol, 2-butanol, was added as a cofactor for transesterification. Using this chemoenzymatic strategy, the desired alcohol **240** was obtained in 80% yield.

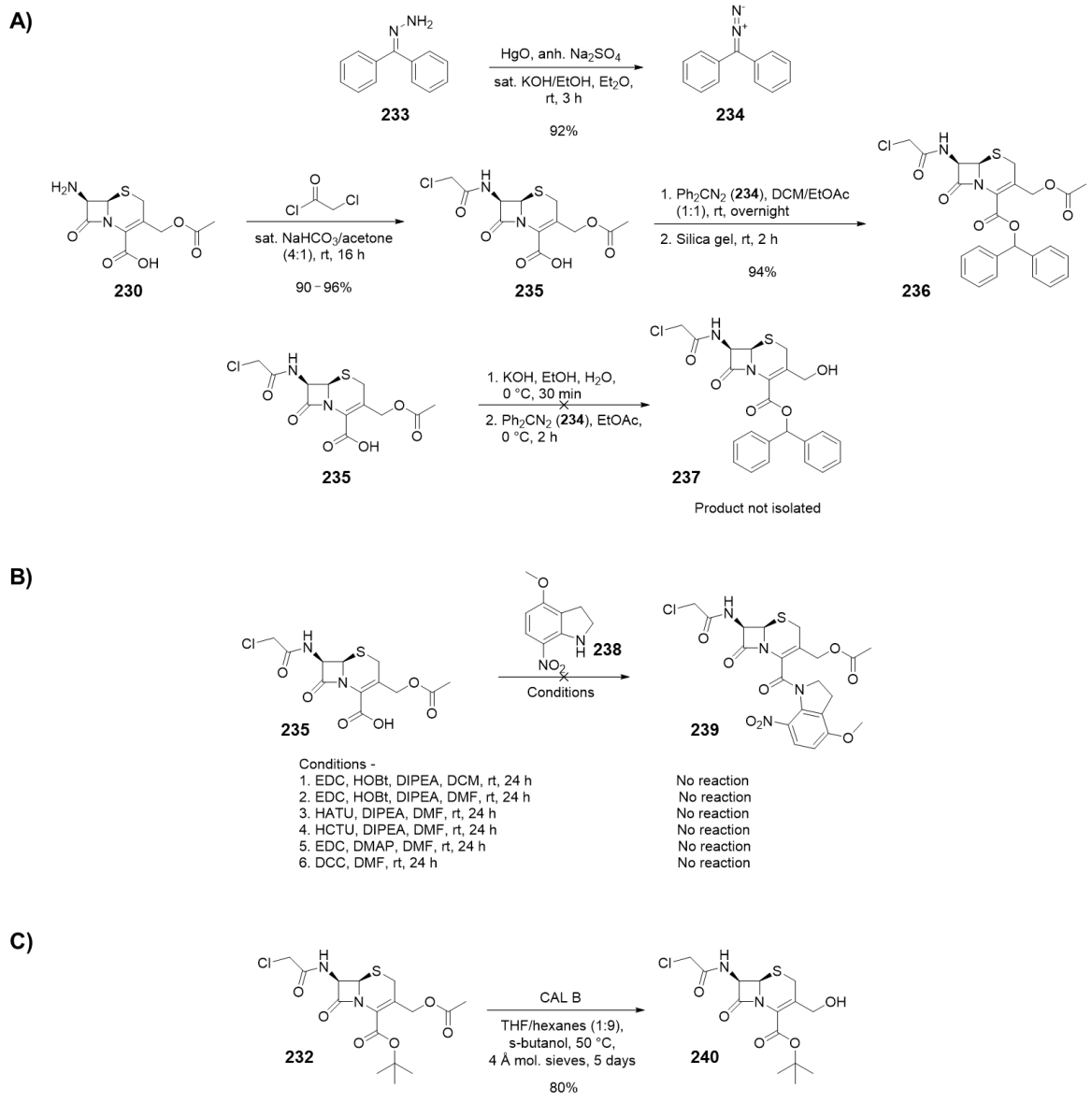

Figure 2-29 Synthetic attempts for selective acetate hydrolysis of intermediate **232**.

(A) Diazodiphenylmethane (**234**) was synthesized from hydrazone **233** and utilized in the synthesis of compound **236**. However, selective acetate hydrolysis of **236** was unsuccessful. Hydrolysis of the acetate in **235** followed by protection of the acid group with **234** was unsuccessful in the synthesis of compound **237**. (B) Failed attempts to synthesize amide **239** from acid **235**. (C) Successful synthesis of compound **240** with CAL B-mediated acetate hydrolysis of **232**.

The alcohol **242** was treated with *N*,*N*′-disuccinimidyl carbonate (DSC) in presence of DMAP in an attempt to generate the corresponding NHS carbonate. However, the synthesis and

purification of the NHS carbonate was unsuccessful due to its instability to air exposure, probably due to hydrolysis of the carbonate (data not shown). Consequently, the linker design was altered to use an NHS ester as an alternative handle. A variety of spacers with an ester linkage were attempted to install the acid end to be converted into the necessary NHS ester. Various attempts at addition of a terephthalic acid spacer proved futile (data not shown).

Next, a carbamate linkage was considered for the addition of a spacer with the acid end. The alcohol **240** was treated with succinic anhydride and glutamic anhydride to install spacers containing succinic and glutaric acid motifs (**Figure 2-30A**). However, these efforts were unsuccessful in the synthesis of these compounds (**242** and **243**, respectively). We were unable to determine the characterize the by-products formed in this reaction by NMR spectroscopy. Inspired from the *trans*-cycloocten-2-ol-linker synthesis, a three-step synthesis comprising CDI activation, DMEDA addition, and methyl adipoyl chloride was tried (**Figure 2-30B**). Unfortunately, the route did not yield the desired methyl ester **244** and we were unable to characterize the obtained by-products by NMR spectroscopy. To optimize the reaction conditions for installation of carbamate linkages, a number of reaction conditions were screened with methyl 4-isocyanatobenzoate (**245**, synthesized from methyl 4-aminobenzoate[323]). Finally, the use of dibutyltin dilaurate allowed for installation of the carbamate under mild conditions (**Figure 2-30C**). Compound **246** was synthesized from the alcohol **240** and the isocyanate **245** in 76% yield.

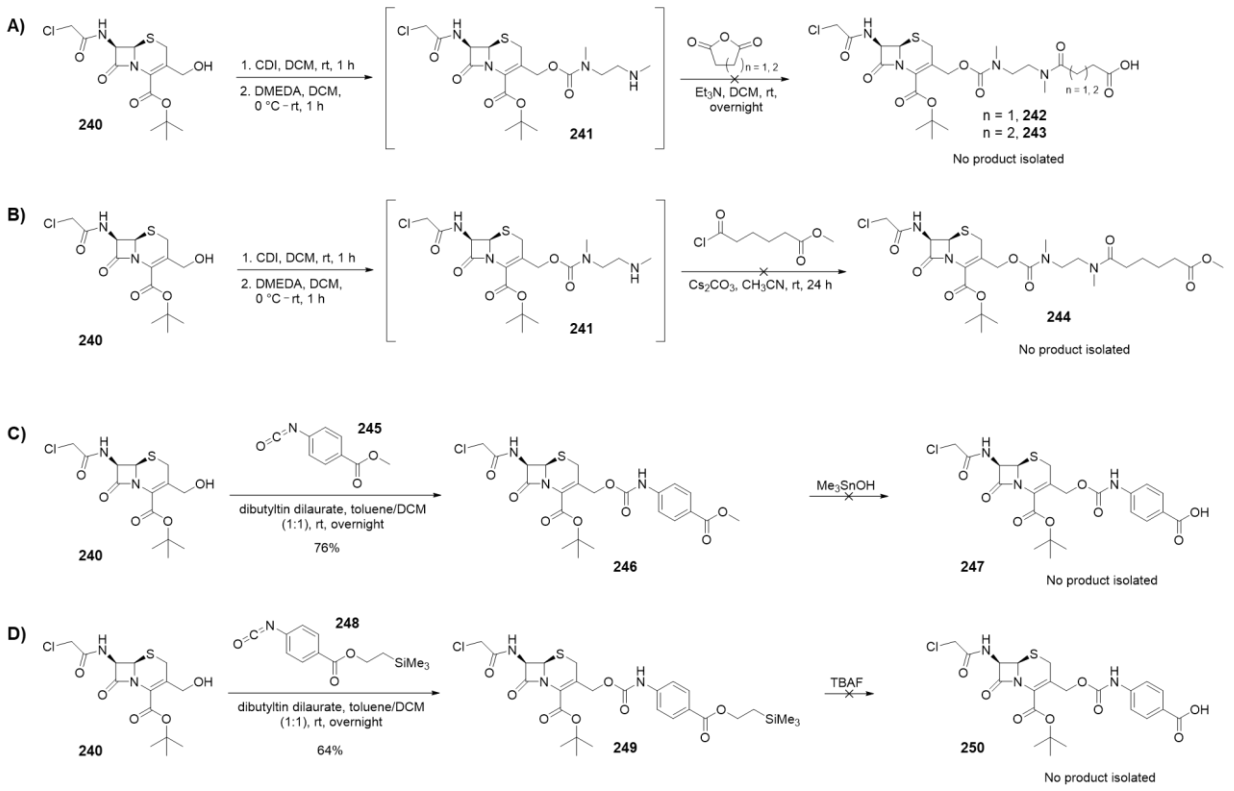

Figure 2-30 Synthetic attempts to install the spacer with an NHS ester on compound **240**.

(A) Unsuccessful attempts to synthesize compounds **242** and **243** from the alcohol **240** with succinic and glutaric acid as spacers. (B) Unsuccessful attempts to synthesize compound **244** with an adipic acid spacer from the alcohol **240**. (C) The carbamate **246** was synthesized from **240**, but the synthesis of acid product **247** was not successful. (D) The carbamate **249** was synthesized from **240**, but the synthesis of acid product **249** was not successful.

The Nicolaou lab reported trimethyltin hydroxide-mediated selective hydrolysis of a methyl ester on various scaffolds.[324] Unfortunately, the desired acid **247** was not obtained using this methodology (**Figure 2-30C**) and we were unable to determine the identity of the products formed by NMR spectroscopy. A one-pot synthesis with the generation of the acid **250** and subsequent conversion to an NHS ester was attempted using DSC (data not shown). However, this strategy did not yield the activated NHS ester of the acid **247**. In another strategy, trimethylsilylethyl ester **249** was synthesized from **240** (**Figure 2-30D**). An orthogonal

deprotection using TBAF for ester hydrolysis of the spacer was attempted on **249**, but this procedure did not afford the desired acid **250**. Unfortunately, we were unsuccessful in determination of the identity of the by-products formed in this reaction.

Since no carboxylate-containing intermediate could be isolated for the installation of an NHS ester handle, the linker design (**255**) was revised to contain an azide handle instead (**Figure 2-31)**. Concurrently, the MO was modified with an alkyne on the 5' end for linker conjugation via Cu-catalyzed azide-alkyne cycloaddition (CuAAC). For the synthesis of azide end, 3-azidopropan-1-amine (**252**) was synthesized from the corresponding alkyl chloride **254** by a reported protocol.[325] Compound **252** was converted to the isocyanate **253** by treatment with diphosgene in 78% yield. The isocyanate **253** was added to a solution of the alcohol **240** in the presence of dibutyltin dilaurate. This procedure yielded carbamate **254** with an azide handle. The final step of *t*-butyl ester deprotection was accomplished by treating **254** with trifluoroacetic acid (TFA) in DCM in the presence of triethylsilane (Et_3SiH) to afford the final linker **255**.

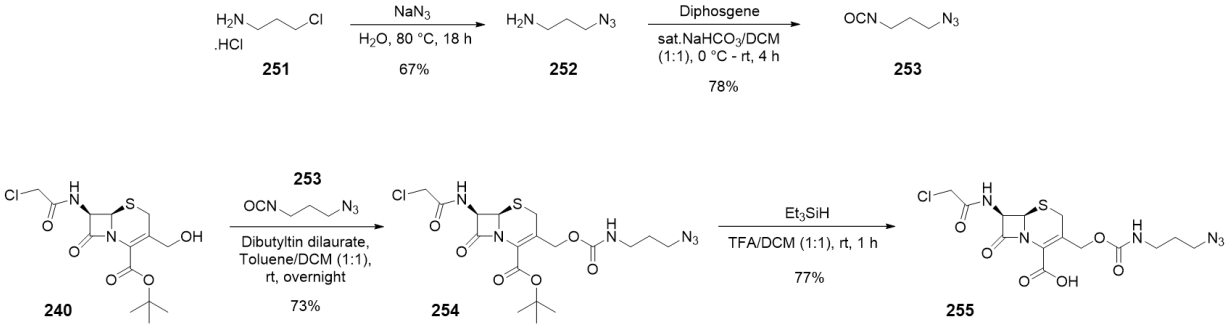

Figure 2-31 Synthesis of the final linker **258** containing chloroacetamide and azide handles.

Cyclization of an alkyne/disulfide-modified *ntla* MO with the *t*-butyl protected linker **254** and preliminary studies for monitoring the cleavage of the linker were performed by Kristie Darrah (**Figure 2-32**). The commercially available *ntla* MO (**222**) has a 5'-amine and a 3'-disulfide. To

construct the necessary alkyne handle on the amine end of *ntla* MO, pent-4-ynoic acid (**256**) was activated to NHS ester **257** using TSTU in acetonitrile with Et_3N as a base. The *ntla* MO (**222**) was treated with **257** in 0.1 M Tris buffer (pH 8.5) to yield alkyne-functionalized MO **258**. The *t*-butyl protected linker **254** was conjugated by CuAAC with Cu(II)-TBTA complex as the catalyst to yield the triazole product **259**. Deprotection of the protected thiol using immobilized TCEP yielded the 3'-thiol, and subsequent macrocyclization with the chloroacetamide handle occurred spontaneously. The deprotection and cyclization afforded the cMO **260**. All the intermediates and the products were purified by reversed-phase HPLC and characterized by MALDI-TOF-MS.

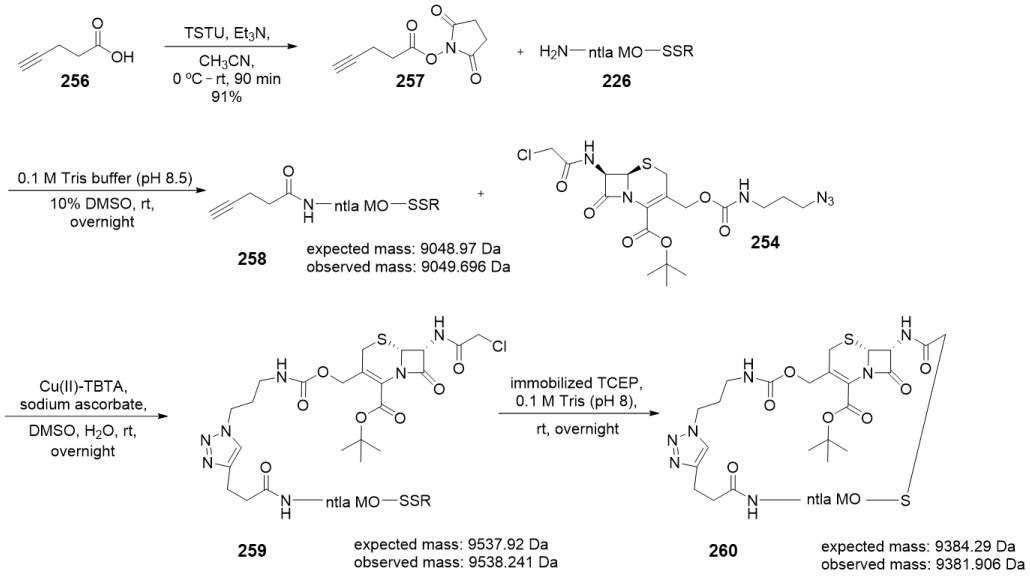

Figure 2-32 Synthesis of *ntla* cMO **260** with *t*-butyl protected linker **254**. Synthesis performed by Kristie Darrah.

2.2.3 Analysis of cleavage of β-lactamase activated linker

In an initial experiment, we monitored the cleavage of the *t*-butyl protected linker **254** by β-lactamase (**Figure 2-33**). For this purpose, recombinant β-lactamase was generated by Kristie

Darrah. Upon incubation of the linker **254** with recombinant β-lactamase, the enzyme completely cleaved **254** in 24 h, as monitored by LCMS. In comparison, the linker **254** was not hydrolyzed in absence of the enzyme.

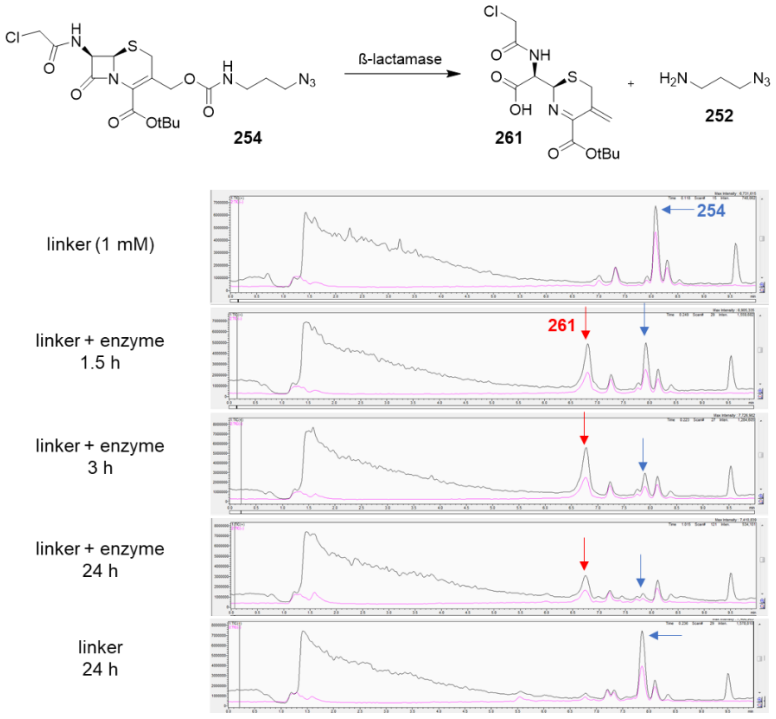

Figure 2-33 Initial *in vitro* studies with the *t-butyl* protected linker **254** and recombinant β-lactamase monitored by LCMS at different time points.

Gradual consumption of **254** (blue arrow) was observed after incubation with the enzyme, resulting in the formation of the hydrolyzed and cleaved product **261** (red arrow). Hydrolysis of β-lactam in **254** was not observed in absence of the enzyme. Data generated by Kristie Darrah.

Kristie Darrah validated β-lactamase activity in a test tube, in lysed mammalian cells, and in lysed zebrafish embryos using a nitrocefin assay (**Figure 2-34**).[326] Nitrocefin (**262**) is a chromogenic β-lactamase substrate with cephalosporin core. Compound **262** exhibits a yellow color (λ_{max} = 390 nm at pH 7.0), but upon hydrolysis of the β-lactam ring (**263**), a color change to

red (λ_{max} = 486 nm at pH 7.0) is observed (**Figure 2-34A**). Recombinant β-lactamase (0.01 μg/μL) completely cleaved the **262** in ~12 min (**Figure 2-34B**). Next, HA-tagged β-lactamase was cloned into a PCS2 vector and transfected into HEK293T cells (**Figure 2-34C**). The cells were lysed, and the cell lysate was incubated for 2 min with **262** before readout of β-lactamase activity by the nitrocefin assay. The readout revealed a ~3-fold increase in A_{486}, indicating the β-lactamase can be detected in a cell lysate. Finally, HA-β-lactamase mRNA (400 pg) was injected into the yolk sac of 1- to 2-cell stage zebrafish embryos, which were incubated for 24 hpf before manual dechorionation and lysis. The embryo lysate was incubated with **262** for 60 min before readout. The readout revealed a ~2-fold increase in A_{486} (**Figure 2-34D**). Thus, the recombinant β-lactamase is active in the lysate from zebrafish embryos, although further studies are necessary to optimize the increase in the readout.

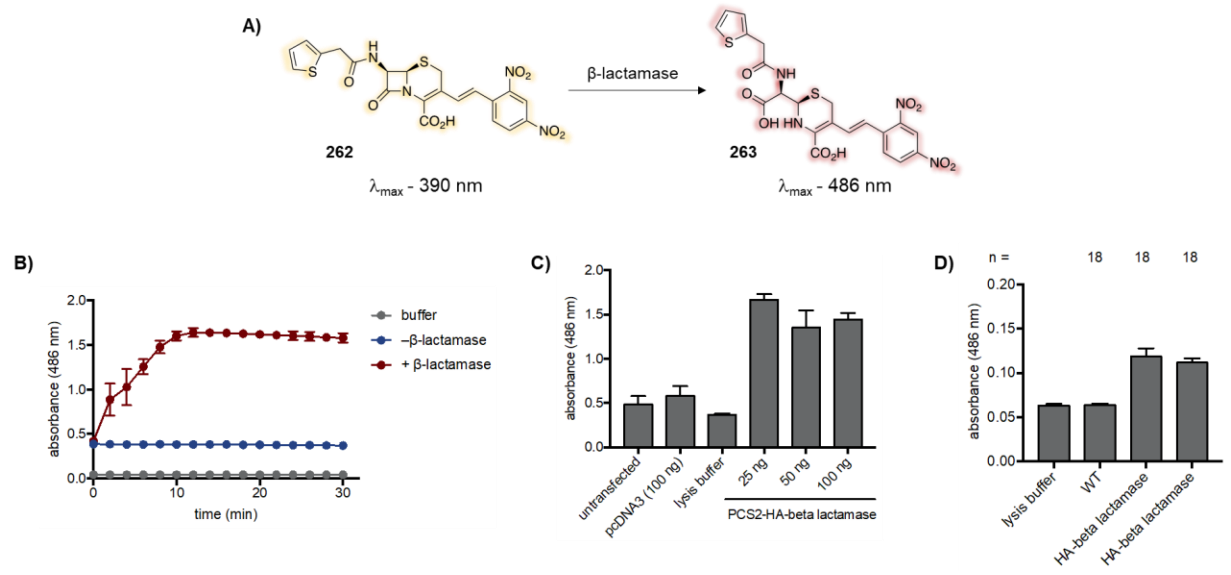

Figure 2-34 Nitrocefin assay for β-lactamase activity.

(A) A yellow-to-red color change is observed in the nitrocefin assay in proportion to β-lactamase activity . (B) *In vitro* nitrocefin assay to detect recombinant β-lactamase activity (enzyme concentration = 0.01 μg/μL). (C) Lysate from HEK293T cells transfected with PCS2-HA-β-lactamase was incubated with **262** for 2 min before readout for β-lactamase activity, which was elevated ~3-fold above that of an empty vector control. (D) HA-β-lactamase mRNA (400 pg) was injected into 18 zebrafish embryos, which were incubated for 24 hpf then manually dechorionated and lysed. The embryo lysate was incubated with **262** for 60 min before readout for β-lactamase activity. Data generated by Kristie Darrah.

2.2.4 Summary and future work

In summary, a β-lactamase activatable linker **225** for caging MOs was developed for linearization of *ntla* MO in zebrafish embryos. Taking inspiration from the FRET-based fluorescent probe **CCF2**,[318] the original linker design (**225**) comprised of a cephalosporin core with a chloroacetamide reactive handle for covalently linking to the 3'-thiol end and an NHS carbonate for linking to the 5'-amine end of the *ntla* MO. The linker synthesis began with

commercially available 7-aminocephalosporanic acid (**230**), and the chloroacetamide-containing intermediate **232** was synthesized in two steps. A roadblock was encountered during selective hydrolysis of the acetate group in **232** in presence of the *t*-butyl ester. After many attempts, a lipase, CAL B, was identified to selectively cleave the acetate group in **232** yielding the necessary alcohol **240**. The alcohol **240** was converted to an NHS carbonate, but the purification of this linker intermediate proved unsuccessful due to the potential instability of the NHS carbonate group. Attempts were made to install a spacer with an NHS ester as the reactive group, but synthesis of an ester linkage was unsuccessful. Subsequently, a carbamate linkage was proposed to install the spacer, and after trying out different conditions, a dibutyltin dilaurate-catalyzed carbamate linkage formation was successful. Later, the hydrolysis of the terminal ester in compounds **246** and **249** posed some problems, and the idea to activate this ester to the NHS ester was scrapped. Finally, in the new linker design, a spacer containing an azide group was envisioned, as it could be conjugated to *ntla* MO modified with a terminal alkyne by CuAAC. The new azide-containing linker **254** was synthesized from the alcohol **240** and 3-azidopropan-1-amine (**252**) in two steps. The *t*-butyl group in **254** was deprotected with TFA to yield the final linker **255**. On the 5'-amine end of *ntla* MO, an alkyne handle was installed, and the cyclization of the *ntla* MO was carried out with the *t*-butyl protected linker **254** in three steps. A test cleavage reaction with the isolated linker **254** revealed a successful hydrolysis using recombinant β-lactamase after 24 h. β-lactamase activity of the recombinant enzyme as well as lysates from mammalian cells and zebrafish embryos expressing the enzyme was confirmed by nitrocefin assay.

Along with the confirmation of cleavage of the *t*-butyl protected linker **254** with β-lactamase, the synthesis of the *ntla* cMO with the final linker **255** is currently underway, using similar conditions as used for preparation of cMO **260**. The final cMO will be injected into

zebrafish embryos (embryos injected with mRNA for HA-β-lactamase). The phenotypic effects of *ntla* knockdown in zebrafish embryos has been well-documented, and the reported phenotype is expected from the embryos with β-lactamase cleaved and linearized *ntla* cMO. Furthermore, other MOs with known phenotypic effects in zebrafish embryos can be cyclized with the final linker **255**.

2.2.5 Experimentals

All reactions were performed in flame-dried glassware under a nitrogen atmosphere and were stirred magnetically. Reactions were followed by thin layer chromatography (TLC) using glass-backed silica gel plates (EMD Millipore TLC Silica Gel 60 F254: 25 Glass Plates 20x20 cm, 250 μm thickness). Anhydrous THF and acetonitrile were purchased from Acros, and anhydrous DMF was purchased from Alfa Aesar. Yields refer to pure compounds unless otherwise stated. Flash column chromatography was performed with silica gel (60 Å, 40–63 μm, 230 × 400 mesh, Sorbtech) as a stationary phase. High resolution mass spectral analysis (HRMS) was performed on a Q-Exactive (Thermo Scientific) mass spectrometer. ^{1}H NMR and ^{13}C NMR spectra were recorded on a 300 MHz or a 400 MHz Bruker NMR spectroscope. Chemical shifts are given in δ units (ppm) for ^{1}H NMR spectra and ^{13}C NMR spectra relative to the respective solvent residual peaks ($CDCl_3$: 7.26 ppm for ^{1}H NMR and 77.16 ppm for ^{13}C NMR; CD_3OD: 3.31 ppm for ^{1}H NMR and 49.00 ppm for ^{13}C NMR; $(CD_3)_2SO$: 2.50 ppm for ^{1}H NMR and 39.52 ppm for ^{13}C NMR).[197]

Compounds **231**,[321] **234**,[327] and **252**[325] were synthesized according to reported procedures.

***Tert*-butyl (6*R*,7*R*)-3-(acetoxymethyl)-7-(2-chloroacetamido)-8-oxo-5-thia-1-azabicyclo-[4.2.0]-oct-2-ene-2-carboxylate (232).** Compound **231** (500 mg, 0.91 mmol, 1.0 eq) was suspended in a mixture of DCM (10 mL) and saturated aqueous $NaHCO_3$ (10 mL). Chloroacetyl chloride (600 μL, 7.61 mmol, 5.0 eq) was added in ten fractions of 0.5 eq each with 15 min intervals between each fraction. The resulting suspension was stirred overnight at room temperature. The organic layer was separated, and the aqueous layer was extracted with DCM (3 × 5 mL). The combined DCM layers were washed with brine (10 mL), dried over sodium sulfate (1 g), filtered, and concentrated under reduced pressure. The resulting residue was purified by silica gel flash column chromatography, eluting with ethyl acetate/hexanes (1:4) to yield compound **232** as a white solid (352 mg, 57%). ^{1}H NMR (400 MHz, $CDCl_3$) δ 7.20 (br d, *J*=9.05 Hz, 1 H), 5.82 (dd, *J*=9.17, 5.01 Hz, 1 H), 4.99 – 5.09 (m, 2 H), 4.82 (d, *J*=13.20 Hz, 1 H), 4.12 (s, 2 H), 3.54 – 3.61 (m, 1 H), 3.37 – 3.43 (m, 1 H), 2.09 (s, 3 H), 1.54 (s, 9 H); ^{13}C NMR (101 MHz, $CDCl_3$) δ 170.78, 166.46, 160.34, 127.54, 123.58, 84.18, 63.18, 59.27, 56.93, 42.38, 27.91, 26.51, 20.92; HRMS (ESI) calcd. for $C_{16}H_{20}O_6N_2ClS$ $(M-H)^-$ 403.07251, found: 403.07346.

(6*R*,7*R*)-3-(Acetoxymethyl)-7-(2-chloroacetamido)-8-oxo-5-thia-1-azabicyclo[4.2.0]oct-2-ene-2-carboxylic acid (235). To a solution of **230** (500 mg, 1.84 mmol, 1.0 eq) in a mixture of acetone (4 mL) and saturated aqueous sodium bicarbonate solution (16 mL), chloroacetyl chloride (300 μL, 3.76 mmol, 2.0 eq) was slowly added over a period of 15 min at room temperature. The reaction was stirred at room temperature for 16 h. The reaction mixture was acidified with 1 N aqueous HCl solution (20 mL) to a pH of 2. The DCM layer was separated and the aqueous layer was washed with DCM (3 × 10 mL). The combined DCM layers were dried over sodium sulfate (2 g), filtered, and concentrated under reduced pressure. The product was purified from the residual

solid by silica gel flash column chromatography (elution with 1:4 ethyl acetate/DCM) to yield **235** as a pale-yellow solid (615 mg, 96%). ^{1}H NMR (400 MHz, $(CD_3)_2SO$) δ 9.25 (br s, 1H), 5.73 (dd, J=9.11, 5.05 Hz, 1H), 4.91 – 5.07 (m, 2 H), 4.73 (d, *J*=13.03 Hz, 1 H), 4.06 (s, 2 H), 3.59 – 3.61 (m, 1 H), 3.35 – 3.40 (m, 1 H), 2.05 (s, 3 H).

Benzhydryl (6*R*,7*R*)-3-(acetoxymethyl)-7-(2-chloroacetamido)-8-oxo-5-thia-1-azabicyclo [4.2.0] oct-2-ene-2-carboxylate (236). A solution of **234** (1.7 g, 8.60 mmol, 2.0 eq) in DCM (10 mL) was prepared and slowly added, at room temperature, to a solution of **235** (1.5 g, 4.30 mmol, 1.0 eq) in ethyl acetate (10 mL) over a period of 15 min with stirring. Effervescence was observed during addition with the solution turning pink in color. After overnight stirring at room temperature, silica gel (1.0 g) was added to the reaction mixture and stirred for another 2 h at room temperature. The pink color was seen to be vanished after stirring for 2 h at room temperature. The reaction mixture was concentrated under reduced pressure and the product was purified from the silica gel residue by silica gel flash column chromatography (elution with 1:4 ethyl acetate/hexanes) to afford **236** as a pale-yellow solid (2.0 g, 94%). ^{1}H NMR (400 MHz, $CDCl_3$) δ 7.20 – 7.36 (m, 11 H), 6.92 (s, 1H), 5.78 (dd, J=9.15, 4.93 Hz, 1 H), 4.95 – 5.12 (m, 2 H), 4.78 (d, J=13.15 Hz, 1 H), 4.10 (s, 2 H), 3.54 – 3.59 (m, 1H), 3.33 – 3.43 (m, 1 H), 2.07 (s, 3 H).

***Tert*-butyl (6*R*,7*R*)-7-(2-chloroacetamido)-3-(hydroxymethyl)-8-oxo-5-thia-1-azabicyclo [4.2.0]-oct-2-ene-2-carboxylate (240).** Compound **232** (300 mg, 0.74 mmol, 1.0 eq) was dissolved in anhydrous THF (2.4 mL) and hexanes (22.6 mL) was added to the THF solution, forming a colorless gel. Lipase acrylic resin (CAL B, Sigma Aldrich Cat. No. L4777) (200 mg, 67 wt%), 2-butanol (1.2 mL, 13 mmol, 18 eq) and 4 Å mol. sieves (300 mg, 1.0 eq) were added to

this suspension at room temperature. The resulting suspension was heated to 50 °C and stirred for 5 days. The reaction mixture was filtered, the residue was washed with ethyl acetate (30 mL), and the filtrate was concentrated under reduced pressure. The resulting residue was purified by silica gel flash column chromatography, eluting with ethyl acetate/hexanes (1:1) to yield **240** as a pale-yellow solid (215 mg, 80%). ^{1}H NMR (400 MHz, $CDCl_3$) δ 7.41 (br d, *J*=8.56 Hz, 1 H), 5.83 (br dd, *J*=8.74, 4.71 Hz, 1 H), 4.97 (br d, *J*=4.52 Hz, 1 H), 4.49 (br d, *J*=12.59 Hz, 1 H), 4.11 (s, 2 H), 3.80 – 4.02 (m, 1 H), 3.51 – 3.68 (m, 2 H), 2.78 (s, 1 H), 1.54 (s, 9 H); ^{13}C NMR (101 MHz, $CDCl_3$) δ 166.63, 163.90, 161.56, 130.18, 126.83, 84.38, 62.15, 59.25, 56.71, 42.37, 27.92, 27.62; HRMS (ESI) calcd. for $C_{14}H_{18}O_5N_2ClS$ $(M-H)^-$ 361.06195, found: 361.05946.

***Tert*-butyl (6*R*,7*R*)-7-(2-chloroacetamido)-3-((((4-(methoxycarbonyl)phenyl)carbamoyl) oxy)methyl)-8-oxo-5-thia-1-azabicyclo[4.2.0]oct-2-ene-2-carboxylate (246).** To a solution of **240** (30 mg, 0.08 mmol, 1.0 eq) in a mixture of anhydrous toluene (1 mL) and anhydrous DCM (1 mL), **245** (18 mg, 0.10 mmol, 1.2 eq) was added at room temperature with stirring. Dibutyltin dilaurate (63 mg, 0.10 mmol, 1.2 eq) was added to the reaction mixture at room temperature and the reaction mixture was stirred overnight at room temperature. The reaction mixture was concentrated under reduced pressure and the residue was loaded on a silica gel column. The product was eluted out in 1:1 ethyl acetate/hexanes to afford **246** as a pale-yellow solid (34 mg, 76%). ^{1}H NMR (400 MHz, $CDCl_3$) δ 7.99 (d, *J*=8.80 Hz, 2 H), 7.46 (d, *J*=8.80 Hz, 2 H), 7.22 – 7.26 (m, 1 H), 7.11 (s, 1 H), 5.83 (dd, *J*=9.05, 4.89 Hz, 1 H), 5.17 (d, *J*=13.08 Hz, 1 H), 5.01 (d, *J*=5.01 Hz, 1 H), 4.87 – 4.99 (m, 1 H), 4.12 – 4.13 (m, 2 H), 3.89 – 3.90 (m, 3 H), 3.60 (d, *J*=18.46 Hz, 1 H), 3.41 – 3.54 (m, 1 H), 1.55 (s, 9 H); LRMS (ESI) calcd. for $C_{23}H_{25}O_8N_3ClS$ $(M-H)^-$ 538.10, found: 538.00.

***Tert*-butyl (6*R*,7*R*)-7-(2-chloroacetamido)-8-oxo-3-((((4-((2-(trimethylsilyl)ethoxy)carbonyl)-phenyl)carbamoyl)oxy)methyl)-5-thia-1-azabicyclo[4.2.0]oct-2-ene-2-carboxylate (249).** To a solution of **240** (30 mg, 0.08 mmol, 1.0 eq) in a mixture of anhydrous toluene (1 mL) and anhydrous DCM (1 mL), **248** (26 mg, 0.10 mmol, 1.2 eq) was added at room temperature with stirring. Dibutyltin dilaurate (63 mg, 0.10 mmol, 1.2 eq) was added to the reaction mixture at room temperature and the reaction mixture was stirred overnight at room temperature. The reaction mixture was concentrated under reduced pressure and the residue was loaded on a silica gel column. The product was eluted out in 1:1 ethyl acetate/hexanes to afford **246** as a pale-yellow oil (33 mg, 64%). ^{1}H NMR (400 MHz, $CDCl_3$) δ 7.99 (d, *J*=8.68 Hz, 2 H), 7.46 (br d, *J*=8.68 Hz, 2 H), 7.32 (d, *J*=9.17 Hz, 1 H), 7.22 (s, 1 H), 5.82 (dd, *J*=9.11, 4.95 Hz, 1 H), 5.16 (d, *J*=13.08 Hz, 1 H), 4.97 – 5.04 (m, 1 H), 4.93 (d, *J*=12.96 Hz, 1 H), 4.32 – 4.47 (m, 2 H), 4.11 (s, 2 H), 3.59 (d, *J*=18.34 Hz, 1 H), 3.40 – 3.53 (m, 1 H), 1.54 (s, 9 H), 1.08 – 1.15 (m, 2 H), 0.07 (s, 9 H); LRMS (ESI) calcd. for $C_{27}H_{35}O_8N_3ClS$ $(M-H)^-$ 624.16, found: 624.00.

1-Azido-3-isocyanatopropane (253). Compound **255** (50 mg, 0.5 mmol, 0.5 eq) was suspended in a mixture of DCM (1 mL) and saturated aqueous $NaHCO_3$ solution (1 mL), and cooled in an ice-water mixture. Diphosgene (240 μL, 2.0 mmol, 2.0 eq) was added to this solution at room temperature, and the suspension was stirred at room temperature for 3 h. The DCM layer was separated and washed with saturated aqueous $NaHCO_3$ solution (2 × 1 mL). The DCM layer was dried over sodium sulfate (1 g), filtered, and concentrated under reduced pressure. Compound **255** was obtained as a clear oil and was used further without purification (49 mg, 78%). ^{1}H NMR (400 MHz, $CDCl_3$) δ 3.41 – 3.48 (m, 4 H), 1.84 (quin, *J*=6.42 Hz, 2 H).

***Tert*-butyl (6*R*,7*R*)-3-((((3-azidopropyl)carbamoyl)oxy)methyl)-7-(2-chloroacetamido)-8-oxo-5-thia-1-azabicyclo[4.2.0]oct-2-ene-2-carboxylate (254).** Compound **240** (50 mg, 0.14 mmol, 1.0 eq) was dissolved in DCM (3 mL) and toluene (3 mL). The isocyanate **253** (86 mg, 5.0 eq) was added to this solution at room temperature. Dibutyltin dilaurate (40 μL, 0.069 mmol, 0.5 eq) was added to the reaction mixture, which was stirred overnight at room temperature. The reaction mixture was concentrated and purified by silica gel flash column chromatography, eluting with Et_2O/DCM (1:10) to yield **254** as a yellow oil (49 mg, 73%). ^{1}H NMR (400 MHz, $CDCl_3$) δ 7.22 – 7.29 (m, 1 H), 5.81 (dd, *J*=9.11, 4.95 Hz, 1 H), 4.96 – 5.07 (m, 3 H), 4.82 (br d, *J*=13.20 Hz, 1 H), 4.11 (s, 2 H), 3.49 – 3.60 (m, 1 H), 3.35 – 3.47 (m, 3 H), 3.22 – 3.35 (m, 2 H), 1.79 (quin, *J*=6.54 Hz, 3 H), 1.54 (s, 9 H); ^{13}C NMR (101 MHz, $CDCl_3$) δ 166.51, 84.10, 59.25, 56.96, 42.37, 27.94, 26.35; HRMS (ESI) calcd. for $C_{18}H_{24}O_6N_6ClS$ $(M-H)^-$ 487.11611, found: 487.11476.

(6*R*,7*R*)-3-((((3-Azidopropyl)carbamoyl)oxy)methyl)-7-(2-chloroacetamido)-8-oxo-5-thia-1-azabicyclo[4.2.0]oct-2-ene-2-carboxylic acid (255). Compound **254** (19 mg, 0.039 mmol, 1.0 eq) was dissolved in anhydrous DCM (0.5 mL), and triethylsilane (12 μL, 0.078 mmol, 2.0 eq) was added to this solution at room temperature. TFA (0.5 mL) was added to the reaction and the reaction mixture was stirred at room temperature for 1 h. The volatiles were evaporated under reduced pressure, and the remaining TFA was co-evaporated with MeOH. The residue was dissolved in MeOH (0.5 mL) and precipitated with Et_2O (5 mL). The precipitated solid was centrifuged at 5000 rpm to a pellet. The supernatant was discarded. This process was repeated twice, and the solid pellet was dried under reduced pressure to yield **255** as a yellow solid (13 mg, 77%). ^{1}H NMR (400 MHz, CD_3OD) δ 5.74 (d, *J*=4.65 Hz, 1 H), 5.02 – 5.20 (m, 2 H), 4.83 (br d, *J*=13.33 Hz, 1 H), 4.12 (s, 2 H), 3.58 – 3.72 (m, 2 H), 3.44 – 3.57 (m, 2 H), 3.36 (t, *J*=6.72 Hz, 2

H), 3.18 (t, *J*=6.72 Hz, 2 H), 2.97 – 3.05 (m, 1 H), 1.86 – 1.94 (m, 1 H), 1.75 (quin, *J*=6.69 Hz, 2 H); ^{13}C NMR (101 MHz, CD_3OD) δ 169.87, 165.61, 64.53, 60.72, 58.66, 42.63, 39.16, 38.47, 30.08, 27.92, 26.89; HRMS (ESI) calcd. for $C_{14}H_{16}O_6N_6ClS$ $(M-H)^-$ 431.05351, found: 431.05149.

3.0 Caged mRNA 5’-cap for spatiotemporal activation of mRNA translation

3.1 Introduction

Messenger RNA (mRNA) processing initiates on the nascent RNA molecules during the transcription process when RNA molecules reach a length of 25-30 nucleotides. A modified guanosine cap is installed on the 5’-end of the pre-mRNA transcript. In eukaryotic and viral systems, the mRNA contains a cap structure which is a *N*7-methylated guanosine (m^7G, **Figure 3-4**) attached to the first nucleotide of the RNA molecule by an inverted 5’ to 5’ triphosphate bridge. Cap formation is the first co-transcriptional 5′-end modification of nascent messenger RNA (mRNA).[328] The 5’-cap is a characteristic feature of eukaryotic and viral mRNAs, while being absent in bacterial and archaeal transcripts. Before the identification of the mRNA cap, it was believed that 5’-ends of eukaryotic mRNAs and bacteriophage mRNA had triphosphorylated pppN modifications.[329] Biochemical analyses carried out in the mid-1970s by Wei et al.[330] and Furuichi et al.[331] revealed the presence of methylated guanosine residues on the 5’-end of mRNA in HeLa cells and reoviruses, respectively.

The mRNA cap plays essential roles in regulation of mRNA stability, mRNA maturation, mRNA export from the nucleus to cytoplasm, and translation initiation.[332] The cap physically protects the mRNA from 5’ → 3’ exonucleases, thus contributing to its stability. The cap must be removed by enzymes like Dcp2 (mRNA-decapping enzyme 2) to generate a 5’-monophosphorylated RNA which can be a substrate for 5′ → 3′ exoribonucleases such as Xrn1/Rat1.[333] Additionally, the 5’-cap is necessary for effective mRNA splicing. An important and specific interaction between the nuclear cap-binding complex and m^7G-cap promotes efficient

interactions between small nuclear ribonucleoproteins (snRNPs) and 5'-splice sites.[334] The interaction between the nuclear cap-binding complex and the 5'-cap also facilitates the formation of spliceosome assembly for packaging and exporting mRNA to the cytoplasm.[335]

The most important function of the m^7G-cap is the initiation of protein synthesis.[336] The presence of the cap serves as an anchor for directing the translational machinery to the 5'-end of the protein coding mRNA and the 5′ to 3′ looping of mRNA during translation.[337] The recruitment of the 40S ribosomal subunit to the 5'-end of mRNA is the rate-limiting step. Eukaryotic initiation factor 4E (eIF4E) directly binds to the m^7G mRNA cap (**Figure 3-1**).Once the eIF4E/ mRNA complex is formed, it then binds to the scaffolding protein eIF4G and the DEAD-box RNA helicase eIF4A forming the eIF4F complex.[338] Additionally, the eIF4G protein binds to poly-A-binding protein (PABP).[339] The eIF4F complex binds the cap structure via the eIF4E subunit, and is thought to subsequently unwind the mRNA 5' untranslated region (5'-UTR) secondary structure to facilitate 40S ribosomal subunit binding.[340] The 40S subunit, eIF3, and the ternary complex (consisting of eIF2, GTP, and methionine-tRNA-initiator) forms the 43S complex.[339]

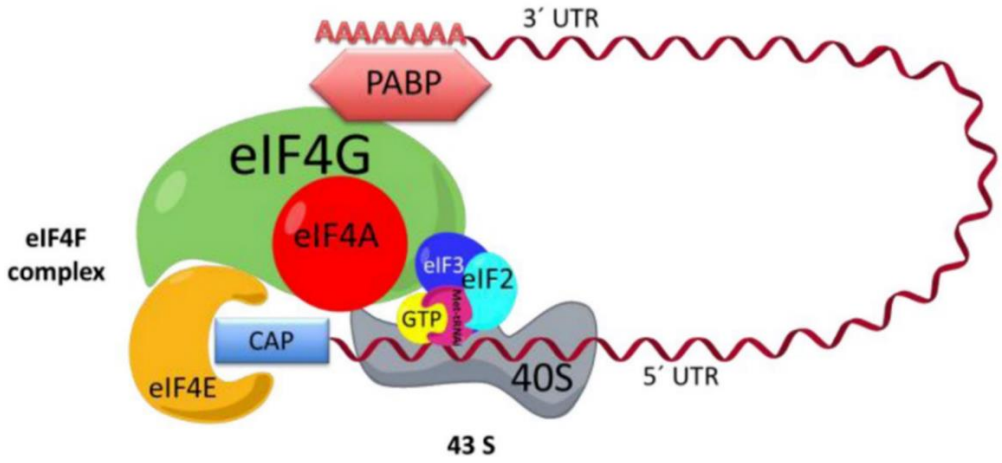

Figure 3-1 Schematic representation of translation initiation complex.

The interaction between eIF4F complex, 43S, and the mRNA is shown. The eIF4F complex is formed by eIF4G, eIF4A, and eIF4E. The 43S complex is formed by 40S subunit, eIF3, and the ternary complex (consisting of eIF2, GTP, and methionine-tRNA-initiator). Adapted from *Viruses*, **2015**, 7(2), 739.[339]

The biochemical pathway for the synthesis of the m^7G cap proceeds through three steps and each step is catalyzed sequentially by RNA triphosphatase, RNA guanylyltransferase and RNA guanine-*N*7 methyltransferase (**Figure 3-2**).[341] RNA triphosphatase is the first enzyme to act on nascent mRNAs (p_γ-p_β-p_α-RNA) by removing the γ-phosphate on the 5'-end to yield a diphosphorylated end (p_β-p_α-RNA). RNA triphosphatases differ in terms of structure and catalytic mechanism and are classified into two families: metal-dependent RNA triphosphatases (for e.g., Cet1 from budding yeast) and metal-independent triphosphatases. The Cet1 active site is composed of several basic residues that are presumed to coordinate the triphosphate moiety on the 5'-end and several acidic residues that coordinate two metal ions which further interact with the triphosphate moiety.[342-343] Metal-independent RNA triphosphatases catalyze removal of the γ-phosphate through a two-step reaction through a covalent protein-cysteinyl-*S*-phosphate intermediate and subsequent hydrolysis of this intermediate to liberate inorganic phosphate.[344] In the second

reaction, the 5’ diphosphorylated end is then capped by RNA guanylyltransferase which acts by transferring guanosine monophosphate (GMP) from a guanosine triphosphate (GTP) substrate to the 5’-end to form capped RNA (G-p_α-p_β-p_α-RNA).[345] This transfer proceeds in a two-step reaction involving formation of a covalent enzyme-(lysyl-*N*)-GMP intermediate and transfer of the GMP to the diphosphorylated end of the RNA. In the third reaction, the guanosine cap is methylated at the *N*7-position by RNA guanine-*N*7 methyltransferase through transferring the methyl group from a methyl donor, *S*-adenosylmethionine (AdoMet) to complete the synthesis of the 5’-cap (m^7G-p_α-p_β-p_α-RNA).[341]

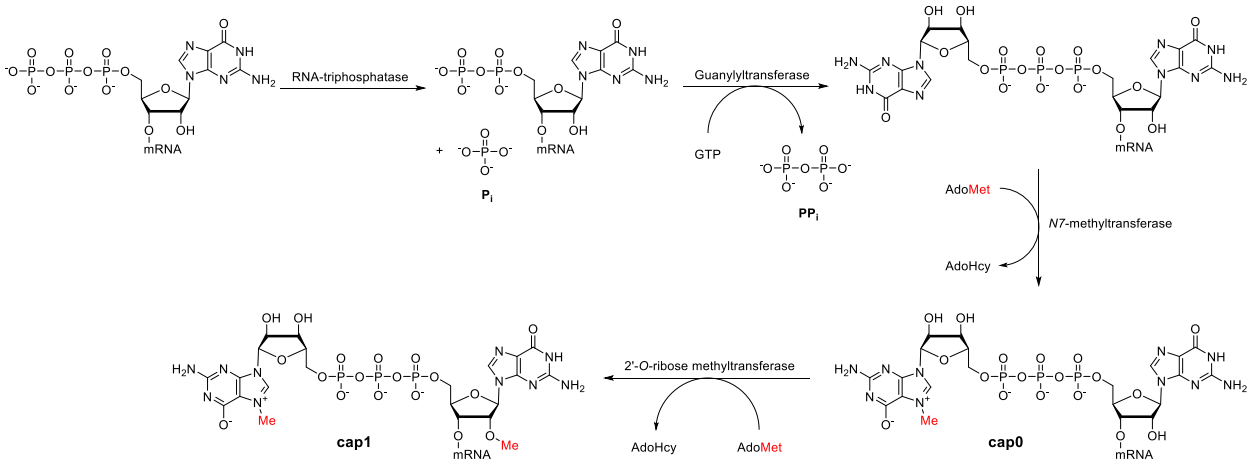

Figure 3-2 The biochemical synthetic pathway of capping nascent mRNA.

RNA-triphosphatase removes the γ-phosphate (P_i) from the 5’-triphosphate end. Next, RNA guanylyltransferase transfers a GMP from the GTP substrate to the 5’-end with the expulsion of inorganic pyrophosphate (PP_i). Finally, RNA guanine-*N*7 methyltransferase transfers a methyl group on the *N*7-position of the guanosine cap to generate the cap0 structure. The cap1 structure was produced by 2’-OH methylation on the first nucleotide of the mRNA by 2’-*O*-ribose methyltransferase. Both methylation reactions utilize AdoMet as a methyl donor. Adapted from *Beilstein J. Org. Chem*,. **2017**, *13*, 2819.[346]

Along with m^7G-capped RNA (m^7G-p_α-p_β-p_α-RNA or m^7GpppNpNp-), other cap structures also exist. The native cap (m^7GpppNpNp-, also denoted as cap0) is further methylated by 2'-*O*-ribose methyltransferase on the 2'-OH of the first mRNA nucleotide to generate a cap1 structure (m^7Gppp-$m^{2'\text{-}O}$NpNp-). This process is m^7G-cap dependent and occurs in the nucleus. In addition to the cap1 structure, cap2 structures have also been reported, where the first two mRNA nucleotides are methylated at the 2'-OH group (m^7Gppp-$m^{2'\text{-}O}$Np-$m^{2'\text{-}O}$Np-). Subsequent methylations of the m^7G-capped RNA are catalyzed by RNA methyltransferases and utilize the AdoMet methyl donor. These modifications provide significant resistance against 5'-exonucleases. Hypermethylation of the cap structures is observed in trypanosomatids (*Leishmania* and *Trypanosoma*) with the first four nucleotides of the nascent mRNA methylated to generate the cap4 structure.[347] Unique 5'-cap structures are found in non-coding small nuclear RNAs (snRNAs). Sm-class snRNAs (snRNAs that bind to Sm proteins) are characterized by hypermethylated 5′-trimethylguanosine caps while LSm-class snRNAs (snRNAs that bind to LSm proteins) contain monomethylphosphate caps.[348] In bacteria, some RNAs are capped with NAD^+, NADH, or 3′-dephospho-coenzyme A.[349-350]

In addition to the biochemical pathway for the synthesis of 5'-capped mRNAs, *in vitro* synthesis of 5'-capped mRNAs are classified into three categories – enzymatic, chemical, and chemoenzymatic methods.[346] *In vitro* enzymatic preparation of large RNA molecules can be achieved by *in vitro* transcription (IVT) using a DNA template, while shorter RNA sequences can be synthesized by solid-phase synthesis. IVT produces RNA molecules with uncapped 5'-triphosphate ends and a 5'-cap can be installed on these RNA transcripts either by post-transcriptional capping or co-transcriptional capping. In the case of solid-phase synthesis, the cap can be installed during the synthesis of the RNA sequence.

In post-transcriptional capping, the RNA from IVT is subjected to a dedicated enzymatic capping reaction. These enzymes originate from different eukaryotic organisms or DNA viruses and are expressed recombinantly in *E. coli*.[351-352] A pioneering work by the Rosenberg group described the use of capping enzymes isolated from Vaccinia virus for capping RNA transcripts *in vitro*.[353] These capping enzymes are still in use for post-transcriptional mRNA capping and consists of two viral proteins D1 and D12. The large protein D1 is primarily responsible for the capping reaction with the triphosphatase and guanylyltransferase activity present in the N-terminal half of the protein while the methyltransferase activity is present in the C-terminal half.[354-355] The small protein D12 is responsible for the activation of D1. These enzymes are reported to be inefficient in capping mRNAs[355-358] and the capping reactions are limited to a small scale.[359] To address these scalability issues, Fuchs et al. have developed an expression and purification protocol for the Vaccinia enzymes. The substrate specificity for these enzymes is relaxed with cap modifications and non-natural cap analogs identified as substrates for guanylyltransferase activity. For example, ribavirin was utilized as a substrate by the Vaccinia capping enzyme to generate a ribavirin-capped mRNA;[360] however, other synthetic caps were not tested with this enzyme[361] (**Figure 3-3**).

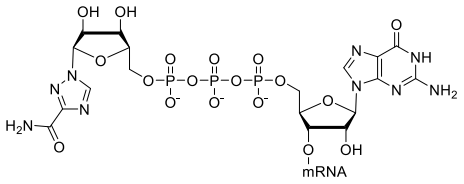

Figure 3-3 Ribavirin capped mRNA prepared by Vaccinia capping enzyme.

Ribavirin was identified as a substrate for guanylyltransferase activity. Adapted from *J. Biol. Chem.*, **2004**, 279 (21), 22124.[360]

In co-transcriptional capping, the cap analogs are directly added to the IVT process.[346] Due to the relaxed substrate specificity of RNA polymerases from bacteriophages (such as T3, T7, and SP6), the cap analog acts as a substrate for RNA polymerization and the cap is incorporated at the 5'-end of the mRNA transcript. The most commonly used cap analog is m^7GpppG (**263**) as RNA polymerases can utilize this cap analog as a substrate (**Figure 3-4**). In this case, RNA polymerases initiate the RNA elongation on the guanosine end with m^7G acting as a 5'-cap. Interestingly, the cap analog competes with GTP present in the IVT mix for initiation of transcription. GTP as an initiator nucleotide produces uncapped mRNAs and these mRNAs will not be translated.[362] This issue can be resolved by reducing the GTP concentration or by digesting the uncapped mRNA with triphosphate on the 5'-end by 5'-phosphatase-mediated exonuclease activity. Another concern with the cap analog **263** is the possibility of initiation of RNA elongation from the other end of the cap analog. The polymerization on the 3'-OH of the m^7G group produces a miscapped RNA. This problem can be resolved by synthesis of anti-reverse cap analog (ARCA).[363-364] ARCAs contain a methylated or deoxygenated 3'-OH on the m^7G group ($m_2^{7,3'\text{-O}}$GpppG, **264** or $m^{7,3'\text{-}d}$GpppG) which prevents the RNA polymerization in the 'wrong direction'. Interestingly, methylation at the 2′-OH end of m^7G also prevented reverse incorporation of the cap analog.[365] The orientation problem can also be circumvented by the another cap analog m^7GpppA with T7 class II promotor phi2.5 for higher 5'-capping homogeneity as ATP is used as an initiator.[366]

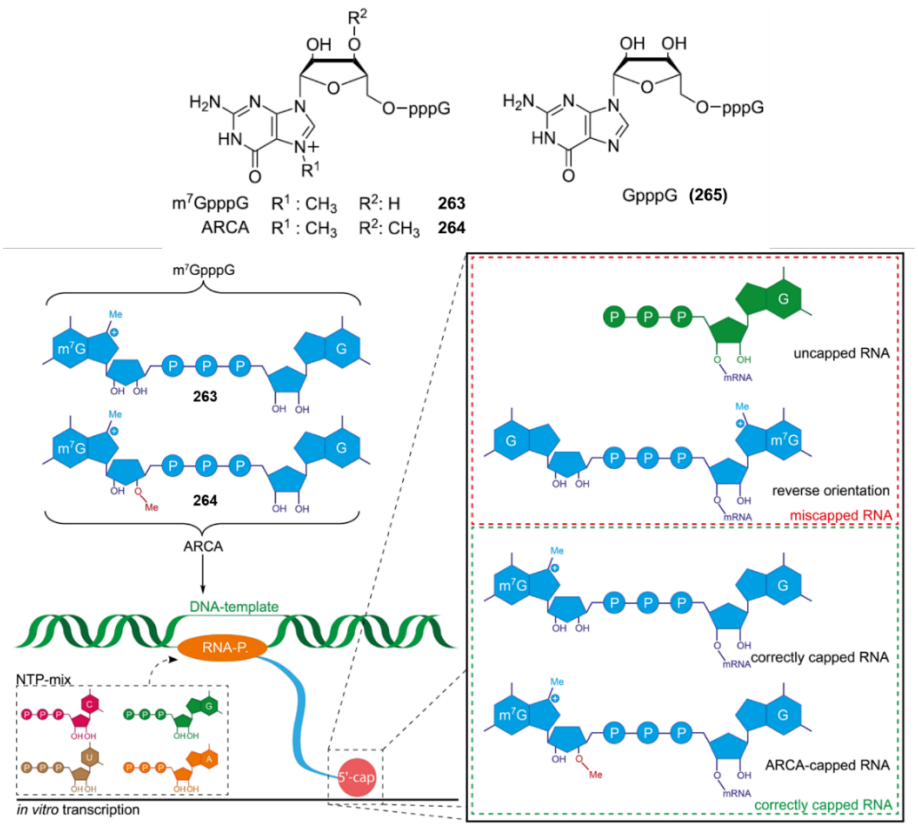

Figure 3-4 Schematic representation of a co-transcriptional capping reaction.

There are two possibilities of capping with **263** in IVT – correctly capped RNA and miscapped RNA. The reverse orientation capping of mRNA can be eliminated by utilizing ARCA **264**, which produces only correctly capped RNA. Adapted from *Beilstein J. Org. Chem.*, **2017**, *13*, 2819.[346]

The cap analog m^7GpppG (**263**) is chemically synthesized from GMP (**267**) and guanosine diphosphate (GDP, **266**) as the triphosphate can be achieved by coupling these parts (**Figure 3-5**).[367] Compounds **266** and **267** can be synthesized by phosphorylation of guanosine. Compound **267** is activated as a GMP-imidazolide (**269**). Methylation of **266** yields *N*7-methylated-GDP (m^7Gpp, **268**) with high regioselectivity. Here, **268** acts as a nucleophile and the activated **269** as an electrophile with imidazole as a leaving group. The final coupling step to synthesize the cap analog **263** is achieved with Lewis acids like $ZnCl_2$ as a catalyst.

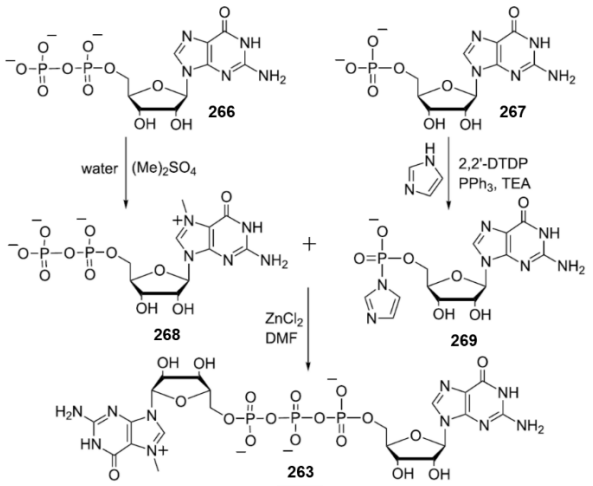

Figure 3-5 Synthetic scheme for the synthesis of standard cap **263**.

Adapted from *Beilstein J. Org. Chem.*, **2017**, *13*, 2819.[346]

Over the years, various modifications to the m^7G cap with improved stability and translational efficiency has been pursued. These properties are important in the efforts to develop potential mRNA therapeutics.[368] A cap with a locked nucleic acid ($m^{7(LNA)}GpppG$) exhibited 1.61-fold, 1.28-fold and 4.23-fold higher stability as compared to standard cap (m^7GpppG, **263**), ARCA ($m_2^{7,3'\text{-}O}GpppG$, **264**), and uncapped (pppG) RNA, respectively, as demonstrated using luciferase mRNA (*in vitro* transcription carried out by T7 RNA polymerase).[369] Additionally, luciferase mRNA capped with $m^{7(LNA)}GpppG$ (**270**) translated with higher efficiency (3.2-fold) as compared to **263** (**Figure 3-6**). Another cap analog containing 3'-*O*-propargyl modification (**271**) exhibited a 3-fold higher translational efficiency in comparison to the standard cap (**263**) (**Figure 3-6**, *in vitro* transcription carried out by T7 RNA polymerase).[370] Both these cap analogs produced correctly capped RNA similar to ARCA. A *N*7-modified ARCA cap analog, *N*7-(4-chlorophenoxyethyl)-$m^{3'\text{-}O}GpppG$ (**272**), was studied by Kore et al. (**Figure 3-6**).[371] A higher translational efficiency (> 1.5-fold) was observed in the case of luciferase mRNA capped with this

as compared to the standard cap (*in vitro* transcription carried out by T7 RNA polymerase). Additionally, a number of other cap analogs with modifications including tetraphosphate (*in vitro* transcription carried out by T7 RNA polymerase)[372] and tetraphosphates with methylene(bisphosphonate) moieties (*in vitro* transcription carried out by SP6 RNA polymerase)[373] were reported with improved binding to eIF4E and higher translational efficiency. Furthermore, cap analogs containing phosphorothioate linkages displayed higher affinity to eIF4E, improved stability, and translationally activity (*in vitro* transcription carried out by T7 RNA polymerase).[374-375]

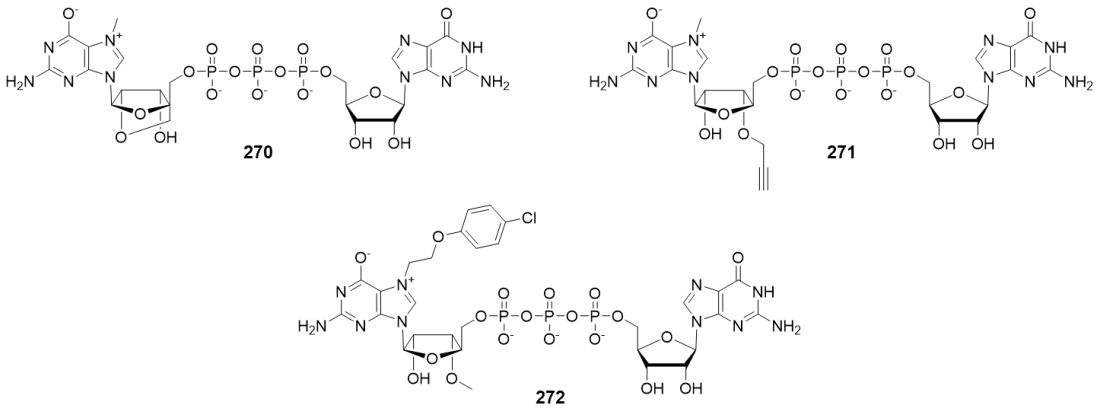

Figure 3-6 Modifications to the m^7G cap with improved stability and translational efficiency.

Over the years, strategies to disrupt the eIF4E/mRNA cap interactions for translational inhibition were pursued. A study by Wendel et al. identified eIF4E as a potent oncogene.[376] The oncogenic activity of eIF4E is activated by phosphorylation of Ser 209 in mouse models. Phospho-eIF4E promotes tumorigenesis by suppressing apoptosis via regulation of its downstream target, the anti-apoptotic protein Mcl-1. In 2012, a detailed SAR study and identification of a guanine-based potent small molecule eIF4E inhibitor was reported by Chen et al.[377] Other studies to

modulate eIF4E activity include a cap analog with *N*7-benzyl and 5'-phosphate modifications.[378] Interestingly, light-mediated reversible activation of protein translation was reported with 2-meta-methyl-phenylazo cap on the 5'-end of the Venus (an improved version of yellow fluorescent protein) mRNA (**Figure 3-7**).[379] The author demonstrated that the phenylazo cap could control mRNA translation in a reversible manner by *cis*-*trans* photoisomerization with 370 nm and 430 nm light. In zebrafish embryos, the *cis*-form of the 5'-cap was translationally active with 7-fold higher translational efficiency while the *trans*-form was inactive. The C2-position of the phenylazo moiety was selected to modulate the eIF4E/mRNA cap interactions.

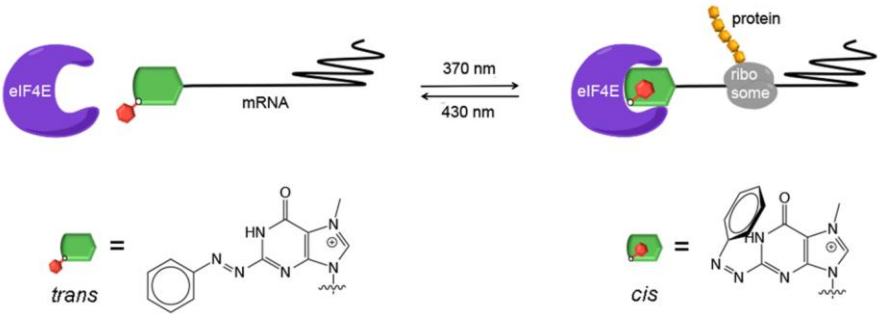

Figure 3-7 Schematic representation of 2-*meta*-methyl-phenylazo 5'-cap.

The *trans*-isomer is translationally inactive with unfavorable eIF4E/mRNA cap interactions, while the eIF4E binds to the *cis*-isomer and 'turns-on' mRNA translation. The *cis* and *trans*-isomers can be reversibly switched by illumination with 370 nm and 430 nm light. Adapted from *ACS Chem. Biol.*, **2017**, *12*, *2*, 351.[379]

Utilizing this information, we propose a method for light-mediated spatiotemporal activation of mRNA translation. We envision an *N*1-caged 5'-cap analog **273** with a photocleavable caging group present at the *N*1-position (**Figure 3-8A**). This cap analog is expected to interfere with the eIF4E/mRNA cap interactions. A closer inspection at the crystal structure of eIF4E and m^7GTP (PDB code: 1IPC, **Figure 3-8B**) revealed polar interactions between

neighboring residues and the m^7G moiety.[377] The eIF4E/m^7GTP interactions consist of hydrogen-bonds between *N*1 and N^2-groups and a glutamic acid residue at the 103 position (E103) while the negatively charged phosphate groups are in close proximity with positively charged arginine and lysine residues forming a salt bridge. Furthermore, the m^7G moiety has stabilizing pi stacking interactions with tryptophan residues at positions 56 and 102 (W56 and W102). Thus, we propose that the caging group present at the *N*1 and N^2-positions can effectively disrupt the eIF4E/mRNA cap interactions and lead to translational inhibition. A light-mediated removal of the caging group will lead to the generation of a standard 5'-cap structure with a translational activation of the caged cap mRNA.

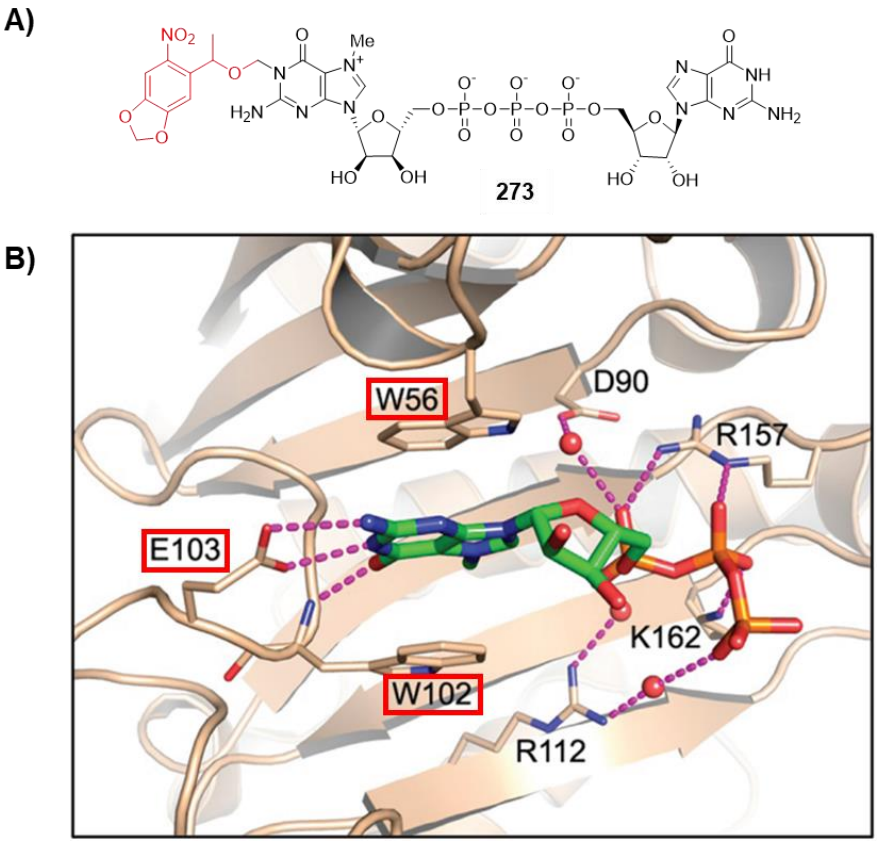

Figure 3-8 Light-mediated activation of mRNA translation.

(A) A mRNA cap analog **273** proposed for light-mediated activation of mRNA translation. (B) A closer look at the crystal structure of eIF4E bound to m^{7}GTP (PDB code: 1IPC). The *N*1 and *N*^{2}-positions on m^{7}G group has stabilizing hydrogen-bonded interactions with E103 residue in eIF4E, while the m^{7}G moiety has stabilizing pi stacking interactions with W56 and W102 (highlighted by red boxes). The *N*1 and *N*^{2}-positions are selected for caging with a photocleavable group. Adapted from *J. Med. Chem.*, **2012**, *55*, 3837.[377]

3.2 Synthesis of an *N*1-caged mRNA 5'-cap analog

A 2-nitrobenzyl caging group was modified and installed with a methylene spacer, as reported (**Figure 3-9**).[380] The synthesis of this caging group was initiated from commercially

available 6-nitropiperonal (**274**) following published reports. The aldehyde **274** was then converted to the secondary alcohol **275** in excellent yield. The methylene spacer was added to the alcohol **275** as a thioether to afford **276**. The thioether **276** was further converted into compound **277**. The chloride **276** was utilized in the addition reaction to the *N*1-position of guanosine. For selective *N*1-caging of the guanosine by **277**, all the groups other than *N*1 were protected (**Figure 3-9**). All the hydroxy groups on the ribose moiety in guanosine (**278**) were protected by TBDMS groups to yield compound **279**.[381] Next, the N^2-position in **279** was protected through reaction with *N*,*N*-dimethylformamide dimethyl acetal to afford the formimidamide **280**. Compound **277** was added to the *N*1-position on protected guanosine **280** by utilizing DBU as a base. The caged nucleoside **281** was obtained in 67% yield. TBAF deprotection of all TBDMS groups in **281** delivered **282** in good yield.

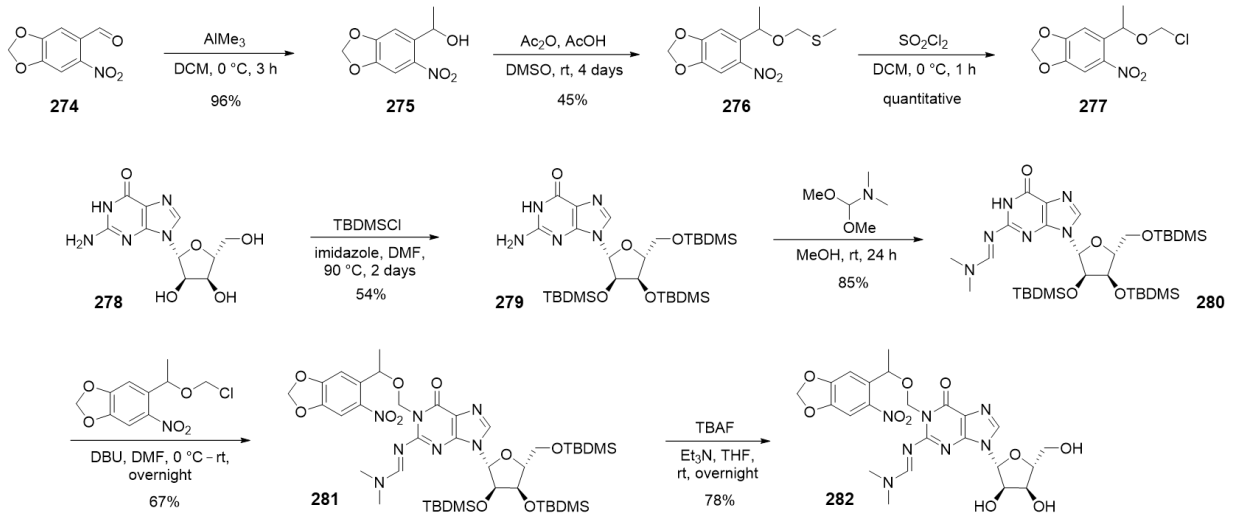

Figure 3-9 Synthetic scheme for the synthesis of *N*1-caged protected guanosine **282**.

The formimidamide protection was removed by methylamine and ammonium hydroxide treatment to afford the *N*1-caged guanosine (**283**, **Figure 3-10A**). Attempts were made to

phosphorylate the 5'-OH group in **283** (**Figure 3-10B**). The conventional method of utilizing $POCl_3$ (**285**) in $PO(OMe)_3$ at 0 °C to phosphorylate guanosine was utilized here.[382] However, this procedure resulted in uncaging of the NPOM group with the formation of GMP (**270**) observed upon monitoring the reaction with LCMS. This uncaging was likely attributed to the acidic nature of the reaction mixture. Hence, the subsequent efforts were targeted to achieve this transformation in a basic reaction mixture. A number of organic bases were added to the reaction, however, these reaction conditions either facilitated uncaging of the reactant **283** followed by mono-phosphorylation to yield the uncaged GMP (**270**) or consumption of the reactant with unknown products formed. Thus, our initial assumption of NPOM group uncaging due to acidic nature of the reaction mixture proved false and the exact mechanisms of the uncaging of NPOM group in **285** could not be determined. Even attempts to add the organic phosphates (such as dibenzyl phosphorochloridate and diphenyl phosphorochloridate) to the 5'-OH failed to produce the desired product (data not shown).[383] Finally, replacing **285** with an alternate reagent for phosphorylation was tried to achieve this conversion.

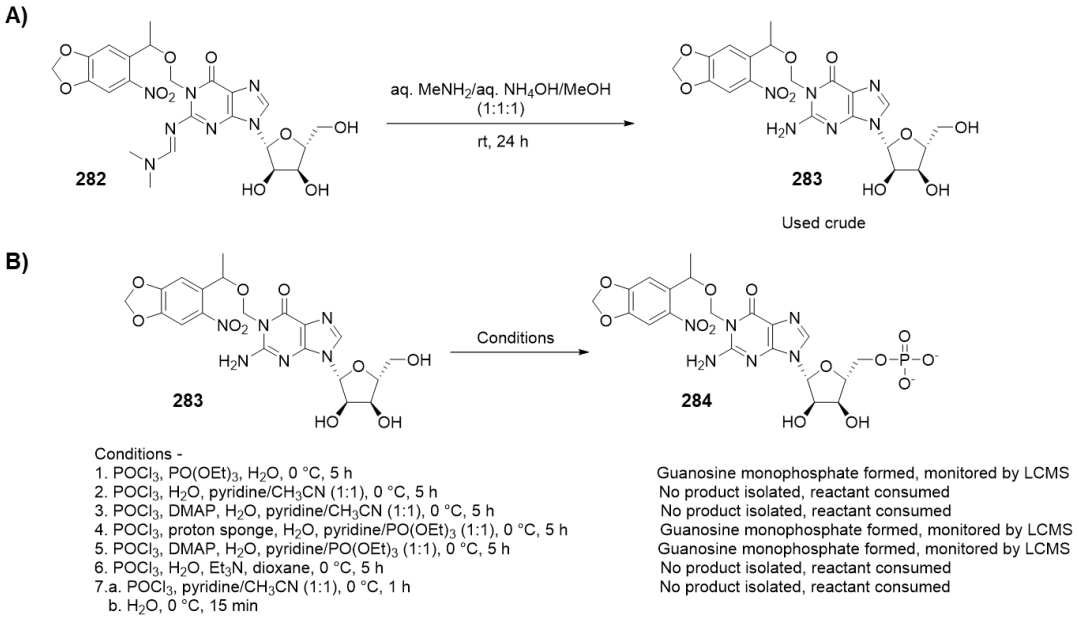

Figure 3-10 Attempts for the synthesis of *N*1-caged GMP **284**.

(A) The *N*1-caged guanosine **283** was synthesized from the protected guanosine **282**. (B) A number of reaction conditions were tried for the synthesis of **284**, but were unsuccessful in yielding the desired product. The products in some of these conditions were not determined while the rest resulted in separation of the caging group to yield uncaged GMP (**270**).

Kulikowski and co-workers reported a triazole-based reagent **287** for phosphorylation of thiol-modified nucleosides.[384] The reagent **287** was prepared and utilized for the synthesis of **284** (**Figure 3-11**). The reagent **287** was prepared by treating **285** and 1,2,4-triazole (**286**) with Et_3N as a base in dioxane solvent, as adapted from the reported procedure.[384] The above reaction mixture was filtered and the filtrate was added directly to the solution of **283** in acetonitrile and dioxane at 0 °C. The identity of **287** could not be confirmed by NMR spectroscopy and LCMS as the reagent was readily hydrolysable even with air moisture (as evidenced by formation of a white precipitate; utilization of the hydrolyzed reagent for the synthesis of **284** was found to affect the yield of **284**, data not shown). Thus, the reaction mixture containing **287** was directly added to the solution

containing **283** even without concentration of the filtrate. This procedure afforded the desired product **284** in 77% yield and purified by DEAE Sephadex ion exchange column chromatography.

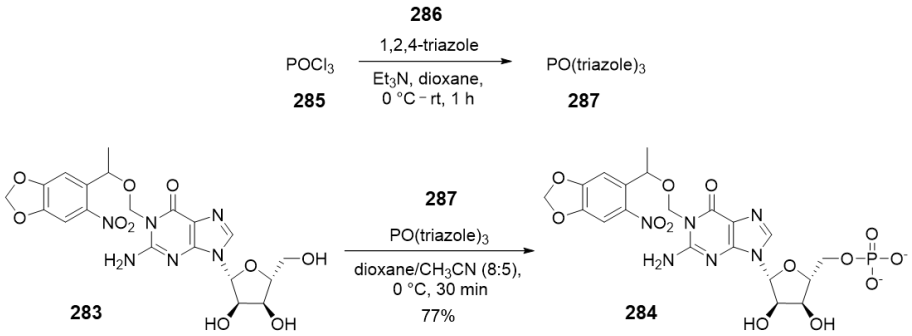

Figure 3-11 Optimized synthetic route for the synthesis of *N*1-caged GMP **284**.

Then, the *N*7-methylation of **284** was carried out with methyl iodide in DMSO (**Figure 3-12A**).[385] However, due to lower polarity of **288**, DEAE Sephadex ion exchange column was ineffective in the purification of **288**. The nature of impurities formed in this reaction include multiple instances of GMP methylation and other impurities of similar polarity. Furthermore, attempts at reverse phase HPLC purification of **288** were unsuccessful probably due to minimal change in the structure and polarity of **288** from the impurities. Thus, **288** was used without purification in the subsequent reactions. The identity of **288** could not be confirmed by NMR spectroscopy as multiple signals were present at the expected *N7*-Me signal (δ ~ 4.0 ppm) in the ^{1}H NMR spectrum of the impure sample of **288**, while the product mass was observed in LRMS of this sample (LRMS (ESI) calcd. for $C_{21}H_{24}O_{13}N_6P$ $(M–H)^-$ 599.11, found: 599.00). For the construction of the other end of the mRNA cap analog **273**, GDP (**269**) was utilized to form the triphosphate bridge. Compound **269** was activated to the GDP-imidazolide **289** by treating with triphenylphosphine, 2,2'-dipyridyldisulfide, and imidazole with Et_3N as a base in DMF in 90%

yield.[365] Compound **289** was purified by precipitation as a sodium salt in acetone solution and obtained in > 90% purity as determined by NMR spectroscopy, following reported procedure.[365]

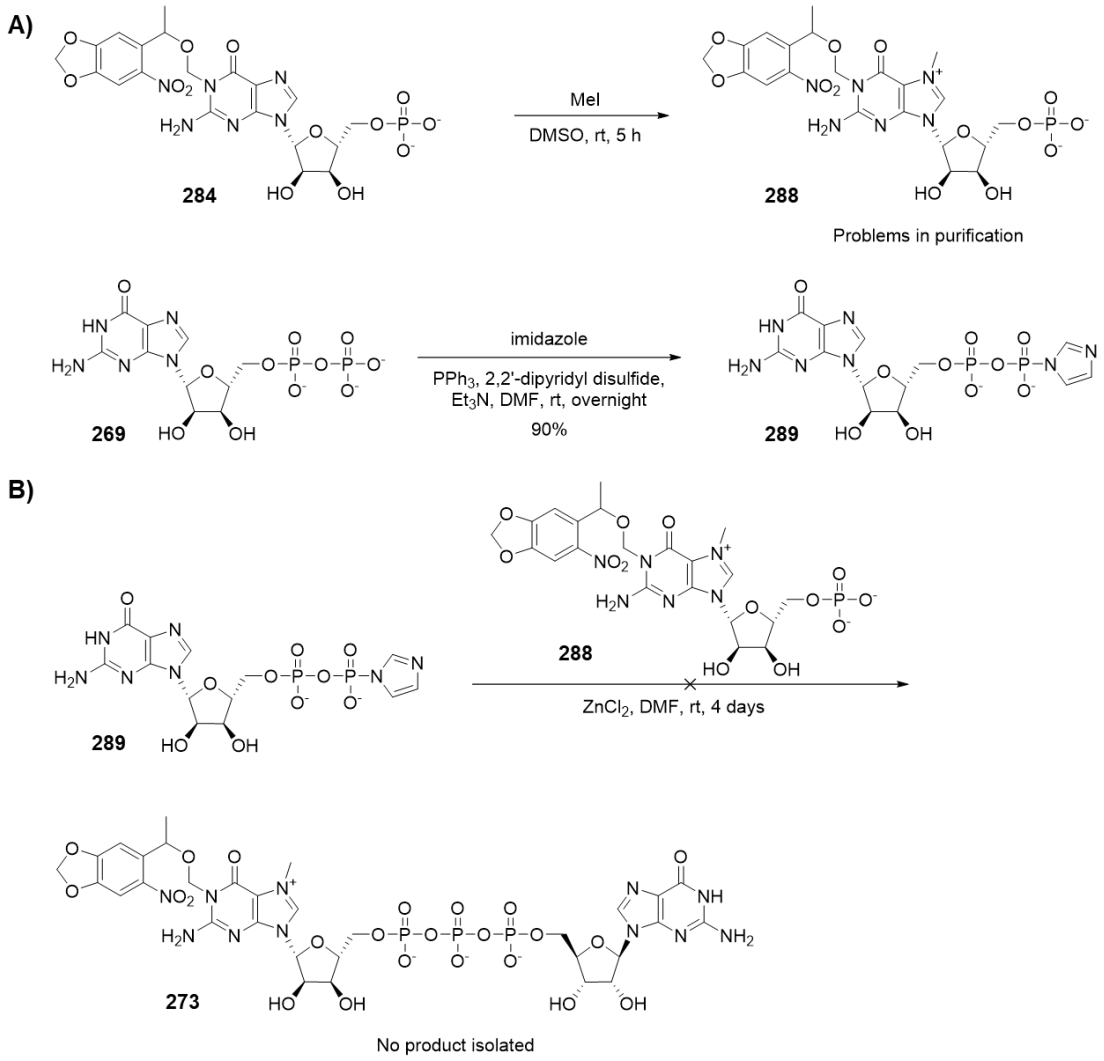

Figure 3-12 Synthetic attempt for the synthesis of *N*1-caged cap analog **273**.

(A) Synthesis of **288** and **289**. (B) The final coupling step of **288** and **289** with $ZnCl_2$ as a catalyst was unsuccessful.

Subsequently, **289** was reacted with impure **288** in the presence of $ZnCl_2$ for the final coupling reaction (**Figure 3-12B**). However, multiple attempts at this reaction did not yield the *N*1-caged cap analog **273**. To optimize the reaction conditions for the final coupling reaction, the

reaction conditions were screened for the synthesis of the native mRNA cap analog **266** (data not shown). In these efforts, the addition of $ZnCl_2$ as a catalyst proved to be the best conditions for the final coupling. Again, translating these exact reaction conditions for the final coupling of **288** and **289** were unsuccessful. Moreover, a number of catalysts such as $MgCl_2$, $MnCl_2$ and $Zn(OTf)_2$ were screened without a positive outcome. With the synthesis of *N*1-caged cap **273** proving difficult, the process of capping mRNAs was revisited.

3.3 Synthesis and analysis of *N*1-caged GTP as capping reagent

A dedicated capping reaction on nascent mRNA has been achieved by Vaccinia virus capping enzymes. This viral capping reaction involves a three-step process of removal of γ-phosphate (RNA triphosphatase) leaving a diphosphate, GMP transfer to the 5'-end of mRNA from GTP (RNA guanylyltransferase), and *N*7-methylation of the guanosine cap using AdoMet as a methyl donor (RNA guanine-*N*7 methyltransferase).[341] As GTP is utilized as a substrate for capping mRNA, the Vaccinia capping enzyme system was employed for installing *N*1-caged 5'-cap with *N*1-caged GTP (**292**) as a substrate.

Synthesis of **292** was initiated from the *N*1-caged GMP (**284**) (**Figure 3-13**). Compound **284** was activated to the imidazolide **290**, analogous to the reaction conditions described for the synthesis of **289**. The pyrophosphate **291** was added to the imidazolide **290** to yield **292** in 29% yield.

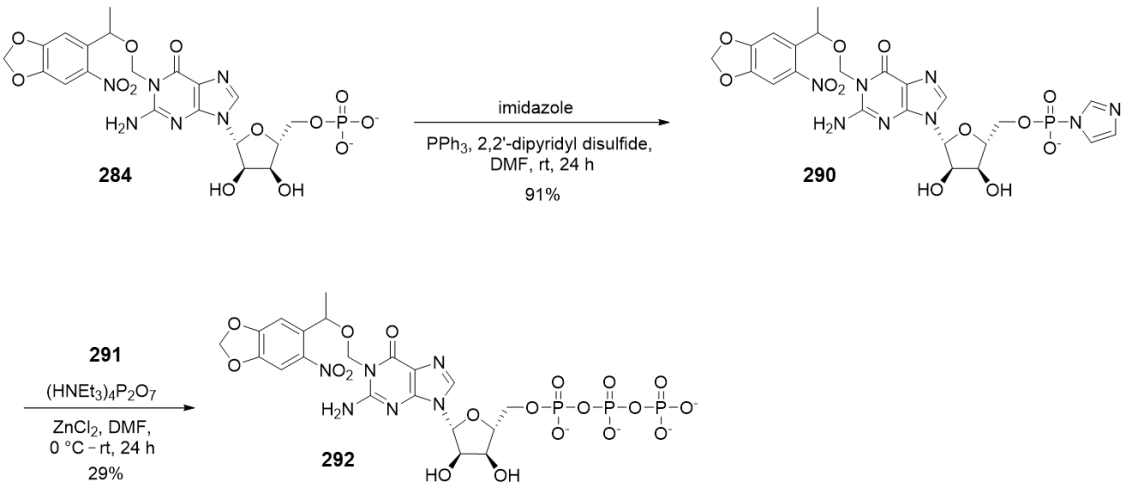

Figure 3-13 Synthetic route for the synthesis of *N*1-caged GTP **292**.

Compound **284** was activated as an imidazolide **290** and further reacted with pyrophosphate **291** to afford the *N*1-caged GTP **292**.

Compound **292** was utilized for *in vitro* capping of *Renilla* luciferase (Rluc) mRNA (**Figure 3-14**). These experiments were performed by Wes Brown. The *in vitro* capping reaction was carried out with **292** and the native cap (**263**) and each mRNA was loaded onto 0.8% agarose gel containing ethidium bromide. (**Figure 3-14A**; Ladder is Tridye 1 kbp ladder (NEB). Lane 1 – mMessage mMachine was used to synthesize native capped Rluc mRNA following standard manufacturer protocol; Lane 2 – SP6 megascript was used to transcribe non-capped Rluc mRNA following standard manufacturer protocol; Lane 3 – GTP (1.5 mM) : **263** (6 mM) ratio used in SP6 megascript reaction following manufacturer protocol; Lane 4 – GTP (0.68 mM) : **263** (6.82 mM) used in SP6 megascript reaction following manufacturer protocol; Lane 5 – **292** (0.5 mM) used in vaccinia capping reaction (Manufacturer: New England Biolabs, Inc. (NEB), catalog # M2080S) of Rluc mRNA generated from SP6 megascript transcription). Compound **292** (0.5 mM in DMSO solution) was added in place of GTP (0.5 mM in DMSO solution) to the Vaccinia capping kit (NEB) for installing the *N*1-caged cap to the Rluc mRNA. Along with 0.5 mM concentration of

292, a higher concentration (2.0 mM) was also utilized for the *in vitro* capping reaction. The capped mRNA was isolated and injected into zebrafish embryos at one-cell stage. An uncapped luciferase mRNA was injected as a control. Some of the injected embryos was exposed to UV light (365 nm) for 5 min directly after injection. The embryos were collected at 24 hpf, lysed, and analyzed in the luciferase assay. Upon analyzing the luciferase readout, no significant difference was observed in Rluc expression with or without exposure to UV light (**Figure 3-14B**). The negative control of uncapped mRNA produced minimal Rluc expression. The possible explanation for such a result could be the inability of Vaccinia capping enzymes to utilize the *N*1-caged GTP **292** as a substrate for guanylyltransferase activity. Also, GTP may be present as a contaminant in the enzyme mix in this kit and the Rluc mRNA produced were capped with the standard m^7G cap. Further studies are necessary to ascertain the reasons for this result.

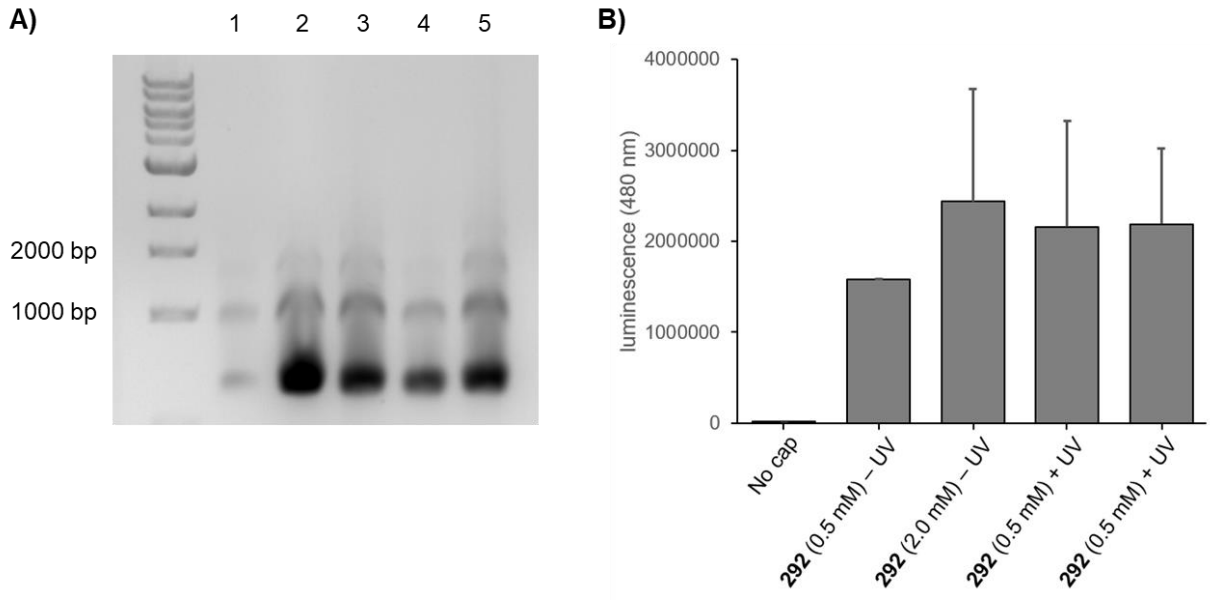

Figure 3-14 Compound **292** as a substate for capping *Renilla* luciferase mRNA with the Vaccinia capping kit. (A) The *in vitro* capping reaction was carried out by **292** and the native cap (**263**) and each mRNA was loaded onto 0.8% agarose gel containing ethidium bromide. The Rluc mRNA appears as two distinct bands (due to folding differences) demonstrating the integrity of the mRNA across the multiple conditions mentioned. (B) The negative control of uncapped mRNA (No cap) produced low Rluc expression. The isolated Rluc mRNA was injected in zebrafish embryos. Some of the embryos were exposed to 365 nm UV light at 1 hpf and all the embryos were lysed at 24 hpf. The lysate was analyzed in a luciferase assay. No significant difference is observed in Rluc expression with or without UV light exposure. Errors bars represent standard deviations from three independent experiments. Data generated by Wes Brown.

3.4 Synthesis of N^2-caged mRNA 5'-cap analog

In addition to the efforts for installing *N*1-caged 5'-cap with the Vaccinia capping system and **292** as a substrate, synthesis of the N^2-caged cap analog **300** was attempted. The crystal structure of eIF4E and m^7GTP revealed the presence of hydrogen-bonded interactions between *N*1

and N^2-groups on the m^7G moiety with the glutamic acid residue at 103 position (E103) stabilizing the binding interactions between eIF4E and m^7GTP (**Figure 3-8**).[377] Thus, light-mediated translational activation was also envisioned to be achieved by caging the N^2-position with a photocleavable group.

Synthesis of the N^2-caged 5'-cap analog **300** was initiated with the protection of the *N*1-position to install the caging group selectively on the N^2-position (**Figure 3-15**). As the *N*1-position is an amide, the protecting group was placed on the oxygen end. In order to minimize the synthetic steps for N^2-caged guanosine **297**, 2-(trimethylsilyl)ethan-1-ol (**294**) was used as a protecting group.[386] The protecting group **294** can be deprotected in the same step as TBDMS deprotection by TBAF. Compound **295** was synthesized by Mitsunobu reaction conditions from **279** and **294** using triphenylphosphine and DIAD in THF solvent.[387] Furthermore, the caging group **275** was activated as an imidazole carbamate by the reaction with CDI to yield **293**. Compound **293** was reacted with protected guanosine **295** in the presence of NaH to afford the N^2-caged protected guanosine **296** in 75% yield. Finally, N^2-caged guanosine **297** was obtained by a global TBAF deprotection to remove all silyl-protecting groups.

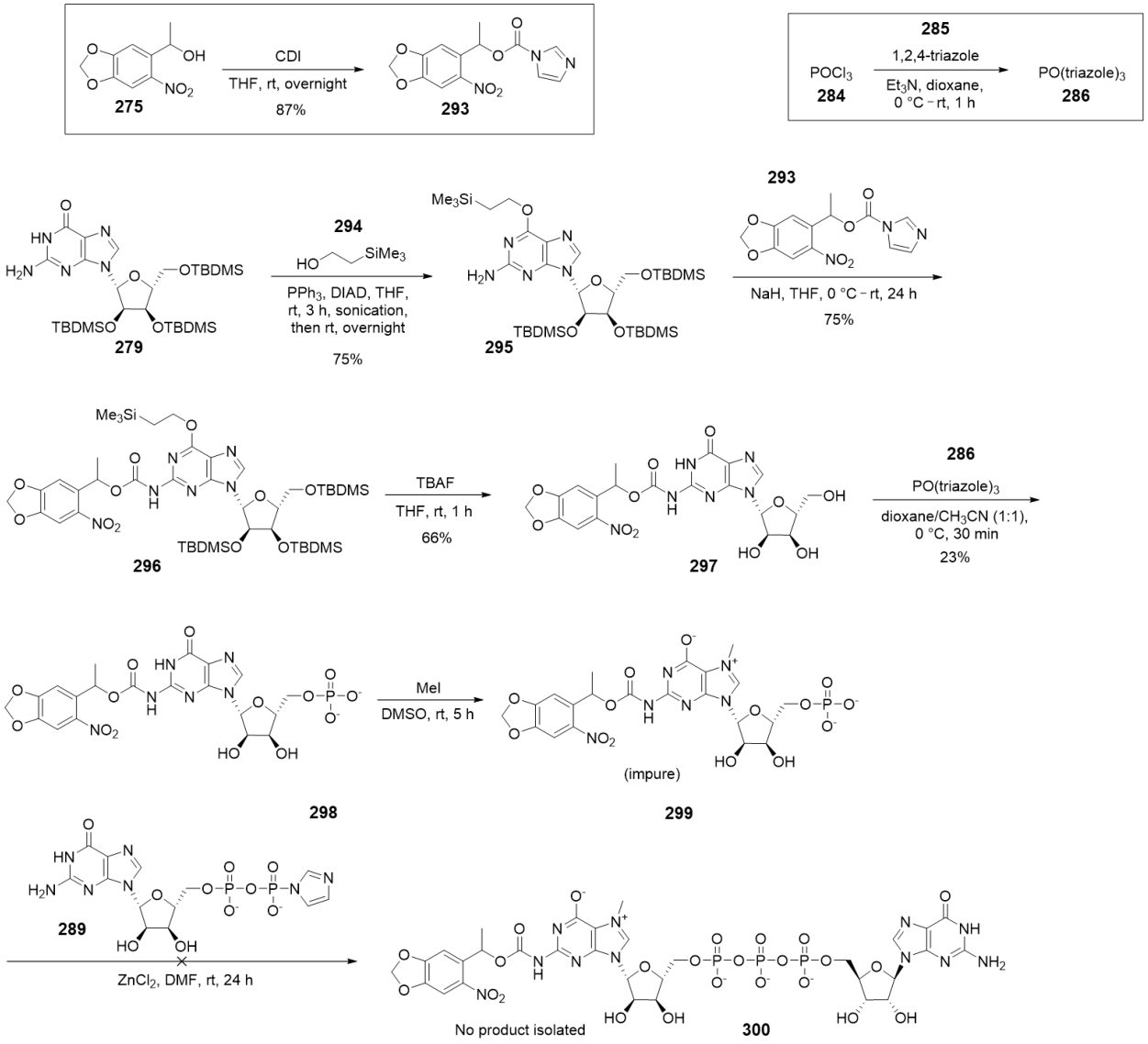

Figure 3-15 Synthetic scheme for the failed synthesis of N^2-caged cap analog **300**.

The final step of coupling **289** and **299** with $ZnCl_2$ as a catalyst was unsuccessful.

The N^2-caged guanosine **297** was monophosphorylated at the 5'-OH group by the similar procedure optimized for the synthesis of **284** (**Figure 3-15**). Compound **297** was treated with the triazole reagent **286** in dioxane and acetonitrile mixture to yield the N^2-caged GMP **298**. Compound **298** was obtained in 23% yield with ~60% purity as determined by ^{1}H NMR spectroscopy (^{13}C NMR not recorded due to low purity of **298**, while LCMS analysis showed the

desired product mass – LRMS (ESI) calcd. for $C_{20}H_{20}O_{14}N_6P$ $(M–H)^-$ 599.08, found: 599.00). In this reaction, 60% of the reactant **297** was recovered back. Subsequently, compound **298** was *N*7-methylated by methyl iodide in DMSO solution to afford the **299**. In this case as well, the purification of **299** by DEAE Sephadex ion exchange column was not successful. Again, for the construction of the other end of the mRNA cap analog, GDP-imidazolide **289** was utilized. The final step of coupling **289** and **299** was attempted in the presence of $ZnCl_2$ as a catalyst. However, the initial efforts at this coupling reaction were unsuccessful.

3.5 Summary and future work

A caged cap analog with a photocleavable caging group was proposed upon analyzing the eIF4E/m^7GTP interactions (**Figure 3-8**). The *N*1-position was selected to be caged by a photocleavable group as it was expected to disrupt hydrogen-bond interactions between the m^7G cap and Glu103 residue of eIF4E.[377] To selectively cage the *N*1-position on guanosine, all the hydroxy groups on the ribose were protected with TBDMS groups and the *N*2-position as a formimidamide **280**. The *N*1-position was caged by a previously reported photocleavable caging group **277**.[380] Final steps of deprotection of all the protecting groups yielded the *N*1-caged guanosine. Further attempts were carried out for the synthesis of *N*1-caged GMP **284**, as many of the conventional methods of phosphorylation failed. Finally, a milder triazole-based reagent **287** was successful in yielding **284** in good yields. Compound **288** was further methylated at the *N*7-position. For the construction of the other end of the cap analog, GDP (**269**) was activated as a GDP-imidazolide **289**. Unfortunately, the final coupling of **288** and **289** was unsuccessful with $ZnCl_2$ as a catalyst. Efforts to synthesize the *N*1-caged cap analog **273** with different Lewis acids

as catalysts also failed. Another approach consisted of utilizing *N*1-caged GTP **292** as a substrate for Vaccinia virus capping enzyme system. Compound **292** was synthesized from *N*1-caged GMP-imidazolide **290** and a pyrophosphate **291**. However, after numerous efforts, the installation of the *N*1-caged cap on luciferase mRNA was unsuccessful. Further efforts are necessary to ascertain the reasons for this result and to circumvent this problem. Another approach was pursued with the synthesis of N^2-caged cap analog **300**. The synthesis of the N^2-caged guanosine end of the cap analog was initiated with **279**. To selectively cage the N^2-position, the *N*1-amide was protected with 2-(trimethylsilyl)ethan-1-ol (**294**) to afford the protected guanosine **295**. The N^2-position was caged with an activated imidazole carbamate of the caging group **293** to yield **296**. A global TBAF deprotection on **296** yielded the N^2-caged guanosine **297**. The mono-phosphorylation and *N*7-methylation was carried out with similar procedures as utilized for the synthesis of **284**. Again, in this case, the final step of coupling **289** and **299** to synthesize the N^2-caged cap analog **300** was unsuccessful with $ZnCl_2$ as a catalyst.

In the future, to resolve the problem of final coupling in the synthesis of **300**, different activating groups on the GDP end can be tried.[388] GDP can be activated with cyanuric chloride or triisopropylbenzenesulfonyl chloride and the final coupling can be achieved by $MgBr_2$ as a catalyst. GDP can also be activated with sulfonylimidazolium salts for phosphate coupling.[389] Although the catalyst used for such couplings are $ZnCl_2$ or $MgCl_2$, these coupling reactions can be completed within minutes. The use of $ZnCl_2$ or $MgCl_2$ can also be eliminated by the activation of phosphates as phosphoromorpholidates.[388] The activated phosphoromorpholidates can undergo diphosphate bond formation with phosphates in the presence of tetrazoles. The reaction conditions selected for the diphosphate bond formation can be translated to the triphosphate bond formation

in the synthesis of **300**. Additionally, utilizing **292** as a substrate for the *N*1-caged mRNA capping with the Vaccinia capping system will be pursued further.

3.6 Experimentals

All reactions were performed in flame-dried glassware under a nitrogen atmosphere and stirred magnetically unless otherwise stated. Reactions were followed by thin layer chromatography (TLC) using glass-backed silica gel plates (EMD Millipore TLC Silica Gel 60 F254: 25 Glass Plates 20x20 cm, 250 μm thickness) and LCMS (Shimadzu Ultra Fast Liquid Chromatography with electrospray ionization (ESI) on positive and negative modes). Anhydrous THF, DMSO, and dioxane were purchased from Acros. Yields refer to pure compounds unless otherwise stated. Organic compounds were purified by silica gel flash column chromatography, performed on silica gel (EMD Millipore TLC Silica Gel 60 F254: 25 Glass Plates 20x20 cm, 250 μm thickness) as a stationary phase. Nucleotides were separated by ion-exchange chromatography on a DEAE Sephadex A-25 (HCO_3^- form) using a step-wise gradient of TEAB buffer, pH 7.5. Eluates containing product fractions were evaporated to dryness by co-evaporation with absolute ethanol and acetonitrile. High resolution mass spectral analysis (HRMS) was performed on a Q-Exactive (Thermo Scientific) mass spectrometer. Sonication was performed by VWR Ultrasonic Bath (model number: 150D). The ^{1}H NMR and ^{13}C NMR spectra were recorded on a 400 MHz Varian NMR instrument. Chemical shifts are given in δ units (ppm) for ^{1}H NMR spectra and ^{13}C NMR spectra relative to the respective solvent residual peaks ($CDCl_3$: 7.26 ppm for ^{1}H NMR and 77.16 ppm for ^{13}C NMR; CD_3OD: 3.31 ppm for ^{1}H NMR and 49.00 ppm for ^{13}C NMR; $(CD_3)_2SO$: 2.50 ppm for ^{1}H NMR and 39.52 ppm for ^{13}C NMR).[197]

Ion-exchange column purification: Triethylammonium bicarbonate (TEAB) buffer (1 M, pH = 7.5) was prepared by bubbling CO_2 (obtained by sublimation of dry ice) through an aqueous solution of triethylamine. The dry DEAE Sephadex A-25 resin (3 g) was suspended in start buffer (10 mM TEAB, 50 mL) resulting in swelling of the resin. The resin was packed in an ISCO flash chromatography load cartridge (careful to keep the resin wet). The resin was washed with 3 column volumes of elution buffer (10 mM TEAB + 1 M NaCl). Finally, the resin was again washed with 3 column volumes of start buffer to prepare the column for purification. For purification of a sample, the sample was dissolved in water and filtered before addition to the column. Upon addition of the sample, the column was washed with 3 column volumes of start buffer to remove the non-polar impurities. The column was then eluted by increasing step-wise gradient of TEAB buffer starting from 0.1 M to 1.0 M with 3 column volumes of each concentration. The column was washed with 3 column volumes of elution buffer. The column was regenerated again with 3 column volumes of start buffer (For storage, the column was washed with 3 column volumes of 20% aqueous ethanol and regenerated again with 3 column volumes of start buffer). The fractions collected were analyzed by LCMS and the fractions containing the desired product were collected together. The solvent was co-evaporated with ethanol and acetonitrile under reduced pressure.

Compounds **279**[381] and **289**[365] were synthesized according to a known procedures.

2-Amino-9-((2*R*,3*R*,4*S*,5*R*)-3,4-dihydroxy-5-(hydroxymethyl)tetrahydrofuran-2-yl)-1-((1-(6-nitrobenzo[*d*][1,3]dioxol-5-yl)ethoxy)methyl)-1,9-dihydro-6*H*-purin-6-one (283). To a solution of **282** (120 mg, 0.21 mmol, 1.0 eq) in MeOH (1 mL), ammonium hydroxide (1 mL, 26 mmol, 120 eq) and methylamine (1 mL, 12 mmol, 55 eq, 40 wt% in H_2O) were added at room

temperature. The reaction mixture was stirred at room temperature for 24 h. The volatiles were evaporated under reduced pressure to yield **283** as a yellow oil (108 mg, quantitative). ^{1}H NMR (400 MHz, CD_3OD) δ 7.79 (d, *J*=16.26 Hz, 1 H), 7.21 (d, *J*=9.05 Hz, 1 H), 7.02 (d, *J*=3.79 Hz, 1 H), 5.87 - 6.02 (m, 2 H), 5.68 (dd, *J*=12.96, 5.75 Hz, 1 H), 5.58 (dd, *J*=19.99, 11.80 Hz, 1 H), 5.18 - 5.30 (m, 2 H), 4.41 - 4.54 (m, 1 H), 4.17 - 4.23 (m, 1 H), 3.99 (dq, *J*=6.25, 3.13 Hz, 1 H), 3.70 - 3.80 (m, 1 H), 3.60 - 3.69 (m, 1 H), 1.41 (dd, *J*=6.30, 1.16 Hz, 3 H); ^{13}C NMR (101 MHz, CD_3OD) δ 158.30, 155.68, 153.61, 148.62, 143.45, 138.30, 107.17, 105.56, 104.79, 90.05, 87.40, 75.92, 75.22, 72.38, 71.82, 63.70, 63.32, 59.65, 53.74, 24.01; HRMS (ESI) calcd. for $C_{20}H_{23}O_{10}N_6$ $(M+H)^+$ 507.14702, found: 507.14656.

((2*R*,3*S*,4*R*,5*R*)-5-(2-Amino-1-((1-(6-nitrobenzo[*d*][1,3]dioxol-5-yl)ethoxy)methyl)-6-oxo-1,6-dihydro-9*H*-purin-9-yl)-3,4-dihydroxytetrahydrofuran-2-yl)methyl phosphate (284). Compound **286** (90 mg, 1.30 mmol, 12 eq) was dissolved in anhydrous dioxane (2.5 mL) and triethylamine (140 µL, 0.96 mmol, 10 eq) was added to this solution with cooling in an ice-water bath. In another vial, **285** (30 µL, 0.32 mmol, 3.0 eq) was dissolved in anhydrous dioxane (0.5 mL) and was added to the first solution at 0 °C. The reaction was stirred vigorously for 1 h while allowing the reaction mixture to warm to room temperature, while a white suspension forms. The suspension was filtered (with a cotton filter in a glass pipette and the filtrate was collected in a vial) and the filtrate containing **287** was taken up in a 3 mL syringe. In another vial, **283** (50 mg, 0.10 mmol, 1.0 eq) was dissolved in acetonitrile (3 mL) in an open vial and this solution was cooled in an ice-water bath with stirring. The filtrate in the syringe was slowly added dropwise to this solution at 0 °C, over a period of 15 min. The reaction was stirred in an open vial for another 15 mins. The reaction was added to water (3 mL) and the solvents dioxane and acetonitrile were

evaporated under reduced pressure. The product was purified from the residual aqueous solution by DEAE Sephadex ion-exchange column chromatography and elution with 0.3 M TEAB buffer to yield **284** as a pale-yellow oil (44 mg, 77%). ^{1}H NMR (400 MHz, CD_3OD) δ 7.95 (s, 1 H), 7.23 (d, *J*=1.96 Hz, 1 H), 7.05 (d, *J*=7.21 Hz, 1 H), 5.90 - 6.02 (m, 2 H), 5.67 - 5.78 (m, 1 H), 5.48 - 5.62 (m, 1 H), 5.20 - 5.32 (m, 2 H), 4.52 - 4.66 (m, 1 H), 4.22 - 4.31 (m, 1 H), 3.83 (dt, *J*=7.27, 5.10 Hz, 1 H), 3.62 - 3.67 (m, 1 H), 3.37 - 3.42 (m, 1 H), 1.42 (d, *J*=6.24 Hz, 3 H); HRMS (ESI) calcd. for $C_{20}H_{24}O_{13}N_6P$ $(M+H)^+$ 587.11335, found: 587.11346.

((2*R*,3*S*,4*R*,5*R*)-5-(2-Amino-1-((1-(6-nitrobenzo[*d*][1,3]dioxol-5-yl)ethoxy)methyl)-6-oxo-1,6-dihydro-9*H*-purin-9-yl)-3,4-dihydroxytetrahydrofuran-2-yl)methyl phosphate (288). Compound **285** (30 mg, 0.05 mmol, 1.0 eq) was dissolved in anhydrous DMSO (0.5 mL) and methyl iodide (30 µL, 0.51 mmol, 10 eq) was added to this solution at room temperature. The reaction was stirred for 5 h at room temperature and added to water (3 mL). The aqueous solution was washed with diethyl ether (3 × 1 mL). The aqueous solution was concentrated under reduced pressure by co-evaporation with absolute ethanol and acetonitrile. The crude product **288** was obtained as a yellow residue (27 mg, 87%). LRMS (ESI) calcd. for $C_{21}H_{24}O_{13}N_6P$ $(M–H)^–$ 599.11, found: 599.00.

2-Amino-9-((2*R*,3*R*,4*S*,5*R*)-5-((((((((((2*R*,3*S*,4*R*,5*R*)-5-(2-amino-6-oxo-1,6-dihydro-9*H*-purin-9-yl)-3,4-dihydroxytetrahydrofuran-2-yl)methoxy)(hydroxy)phosphoryl)oxy)oxidophosphoryl)oxy)oxidophosphoryl)oxy)methyl)-3,4-dihydroxytetrahydrofuran-2-yl)-7-methyl-1-((1-(6-nitrobenzo[*d*][1,3]dioxol-5-yl)ethoxy)methyl)-6-oxo-6,9-dihydro-1*H*-purin-7-ium (273). Compounds **289** (10 mg, 0.02 mmol, 1.0 eq) and **288** (18 mg, 0.03 mmol, 1.5 eq) were suspended

in anhydrous DMF (0.3 mL), and $ZnCl_2$ (11 mg, 0.08 mmol, 4.0 eq) was added to the suspension at room temperature with vigorous stirring. After 15 min of vigorous stirring to dissolve the reactants, the reaction was stirred at room temperature with normal stirring for 4 days. LCMS analysis did not reveal the formation of **273**.

((2*R*,3*S*,4*R*,5*R*)-5-(2-Amino-1-((1-(6-nitrobenzo[*d*][1,3]dioxol-5-yl)ethoxy)methyl)-6-oxo-1,6-dihydro-9*H*-purin-9-yl)-3,4-dihydroxytetrahydrofuran-2-yl)methyl hydrogen (1*H*-imidazol-1-yl)phosphonate (290). To a solution of **284** (50 mg, 0.08 mmol, 1.0 eq) in anhydrous DMF (3 mL), triphenylphosphine (67 mg, 0.26 mmol, 3.0 eq), imidazole (58 mg, 0.85 mmol, 10 eq), and 2,2'-dipyridyl disulfide (56 mg, 0.26 mmol, 3.0 eq) were added at room temperature. The reaction mixture was stirred for 24 h at room temperature. The reaction mixture was then added to a solution of sodium perchlorate (42 mg, 0.34 mmol, 4.0 eq) dissolved in 30 mL acetone. The resulting suspension was added to a 50 mL ultracentrifuge tube and spun down at 5000 rpm for 10 mins. The supernatant liquid was decanted and the solid pellet was suspended in 30 mL acetone. This process was repeated twice. The solid pellet was dried under vacuum over phosphorus pentoxide to yield **290** as a yellow solid (53 mg, 94%). ^{1}H NMR (400 MHz, $(CD_3)_2SO$) δ 7.82 (d, *J*=16.36 Hz, 1 H), 7.67 (s, 1 H), 7.25 (d, *J*=8.96 Hz, 1 H), 7.16 (d, *J*=7.12 Hz, 1 H), 7.08 (d, *J*=7.19 Hz, 1 H), 6.87 (d, *J*=7.21 Hz, 1 H), 5.94 - 6.06 (m, 2 H), 5.73 - 5.82 (m, 1 H), 5.53 - 5.67 (m, 1 H), 5.21 - 5.30 (m, 2 H), 4.50 - 4.61 (m, 1 H), 4.22 - 4.30 (m, 1 H), 3.86 (m, 1 H), 3.63 - 3.69 (m, 1 H), 3.37 - 3.43 (m, 1 H), 1.41 (d, *J*=6.32 Hz, 3 H); HRMS (ESI) calcd. for $C_{23}H_{26}O_{12}N_8P$ $(M+H)^+$ 637.14023, found: 637.14031.

((2*R*,3*S*,4*R*,5*R*)-5-(2-Amino-1-((1-(6-nitrobenzo[*d*][1,3]dioxol-5-yl)ethoxy)methyl)-6-oxo-1,6-dihydro-9*H*-purin-9-yl)-3,4-dihydroxytetrahydrofuran-2-yl)methyl triphosphate (292). Compound **290** (120 mg, 0.18 mmol, 1.0 eq) and tetrakis(triethylamine) diphosphate (151 mg, 0.55 mmol, 3.0 eq) were suspended in anhydrous DMF (4 mL), and the suspension was cooled in ice-water mixture. $ZnCl_2$ (250 mg, 1.82 mmol, 10 eq) was added to the suspension at 0 °C with vigorous stirring. After 30 min of vigorous stirring to dissolve the reactants while allowing the reaction to warm to room temperature, the reaction was stirred at room temperature with normal stirring for 24 h. The reaction mixture was then added to a solution of sodium perchlorate (200 mg, 1.64 mmol, 9 eq) dissolved in 40 mL acetone. The resulting suspension was added to a 50 mL ultracentrifuge tube and spun down at 5000 rpm for 10 mins. The supernatant liquid was decanted and the solid pellet was suspended in 20 mL acetone. This process was repeated twice. The solid pellet was dried under vacuum. Compound **292** (2.3 mg, 29%) was purified by reverse phased-HPLC from a portion of the pellet (8.0 mg) and obtained as a white solid. ^{1}H NMR (400 MHz, $(CD_3)_2SO$) δ 7.81 (m, 1 H), 7.27 (d, *J*=9.06 Hz, 1 H), 7.05 (m, 1 H), 5.93 - 6.07 (m, 2 H), 5.73 - 5.82 (m, 1 H), 5.54 - 5.69 (m, 1 H), 5.29 - 5.36 (m, 2 H), 4.53 - 4.62 (m, 1 H), 4.22 - 4.29 (m, 1 H), 3.88 (m, 1 H), 3.61 - 3.71 (m, 1 H), 3.34 - 3.44 (m, 1 H), 1.42 (d, *J*=7.24 Hz, 3 H); HRMS (ESI) calcd. for $C_{23}H_{26}O_{12}N_8P$ $(M+H)^+$ 747.04601, found: 747.04586.

1-(6-Nitrobenzo[*d*][1,3]dioxol-5-yl)ethyl-1*H*-imidazole-1-carboxylate (293). Compound **275** (50 mg, 0.24 mmol, 1.0 eq) was dissolved in anhydrous THF (3 mL). 1,1'-Carbonyldiimidazole (58 mg, 0.36 mmol, 1.5 eq) was added to this solution at room temperature. The reaction mixture was stirred overnight at room temperature. The solvent was evaporated under reduced pressure with an oily residue remaining and the product was purified from this residue by silica gel flash

column chromatography, elution with ethyl acetate/DCM (1:1) to yield **275** as a pale-yellow solid (63 mg, 87%). ^{1}H NMR (400 MHz, $CDCl_3$) δ 8.11 (s, 1 H), 7.46 (s, 1 H), 7.39 (s, 1 H), 7.03 (s, 1 H), 6.98 – 7.01 (m, 1 H), 6.56 (q, *J*=6.44 Hz, 1 H), 6.10 (dd, *J*=7.76, 1.04 Hz, 2 H), 1.75 (d, *J*=6.36 Hz, 3 H); ^{13}C NMR (101 MHz, $CDCl_3$) δ 152.65, 147.81, 147.59, 141.80, 137.02, 133.16, 130.84, 117.09, 105.46, 105.41, 103.40, 72.86, 21.83. HRMS (ESI) calcd. for $C_{13}H_{12}O_6N_3$ $(M+H)^+$ 306.07206, found: 306.07164.

9-((2*R*,3*R*,4*R*,5*R*)-3,4-Bis((*tert*-butyldimethylsilyl)oxy)-5-(((*tert*-butyldimethylsilyl)oxy)-methyl)-tetrahydrofuran-2-yl)-6-(2-(trimethylsilyl)ethoxy)-9*H*-purin-2-amine (295). Compounds **279** (628 mg, 2.40 mmol, 5.0 eq) and **294** (340 μL, 2.40 mmol, 5.0 eq) were dissolved in anhydrous THF (5 mL) and diisopropyl azodicarboxylate (470 μL, 2.40 mmol, 5.0 eq) was slowly added to this solution at room temperature. The reaction mixture was sonicated at room temperature for 3 h and then stirred overnight at room temperature. The volatiles were evaporated under reduced pressure to an oily residue. The product was purified from this residue by silica gel flash column chromatography, elution with ethyl acetate/hexanes (1:10) to yield **295** as a white solid (262 mg, 75%). ^{1}H NMR (400 MHz, $CDCl_3$) δ 7.90 (s, 1 H), 5.91 (d, *J*=5.87 Hz, 1 H), 5.36 (br s, 2 H), 4.48 – 4.59 (m, 2 H), 4.46 (dd, *J*=5.62, 4.65 Hz, 1 H), 4.25 (dd, *J*=4.16, 3.06 Hz, 1 H), 4.07 (q, *J*=2.73 Hz, 1 H), 3.93 (dd, *J*=11.37, 3.55 Hz, 1 H), 3.75 (dd, *J*=11.25, 2.45 Hz, 1 H), 1.19 – 1.25 (m, 2 H), 0.92 (d, *J*=3.06 Hz, 18 H), 0.76 (s, 9 H), 0.11 (dd, *J*=7.15, 3.61 Hz, 12 H), 0.06 (s, 9 H), –0.07 (s, 3 H), –0.22 (s, 3 H); ^{13}C NMR (101 MHz, $CDCl_3$) δ 161.39, 159.60, 153.76, 137.35, 115.71, 87.23, 85.61, 76.61, 72.50, 64.83, 62.93, 26.19, 26.00, 25.79, 18.62, 18.20, 18.05, 17.63, –1.29, –4.12, –4.61, –4.63, –4.98, –5.27, –5.33; HRMS (ESI) calcd. for $C_{33}H_{68}O_5N_5Si_4$ $(M+H)^+$ 726.42920, found: 726.42716.

1-(6-Nitrobenzo[*d*][1,3]dioxol-5-yl)ethyl (9-((2*R*,3*R*,4*R*,5*R*)-3,4-bis((*tert*-butyldimethylsilyl)-oxy)-5-(((*tert*-butyldimethylsilyl)oxy)methyl)tetrahydrofuran-2-yl)-6-(2-(trimethylsilyl)-ethoxy)-9*H*-purin-2-yl)carbamate (296). Compound **295** (250 mg, 0.34 mmol, 1.0 eq) was dissolved in anhydrous THF (10 mL) and this solution was cooled in ice-water mixture. Sodium hydride (17 mg, 0.41 mmol, 1.2 eq, 60% in mineral oil) was added to the solution containing **295** at 0 °C while stirring. The resulting suspension was stirred at 0 °C for 15 min. Compound **293** (210 mg, 0.69 mmol, 2.0 eq) was added to the reaction mixture with stirring at 0 °C. The reaction mixture was allowed to warm to room temperature and stirred for 24 h at room temperature. The reaction was slowly quenched by adding water (5 mL) and the organic fractions were extracted with ethyl acetate (3 × 15 mL). The combined organic extracts were dried over sodium sulfate (1 g), filtered, and concentrated under reduced pressure. The product was purified by silica gel flash column chromatography, elution with ethyl acetate/hexanes (1:5) to yield **296** as a pale yellow solid (247 mg, 75%). ^{1}H NMR (400 MHz, $CDCl_3$) δ 8.08 (d, *J*=12.10 Hz, 1 H), 7.51 (d, *J*=2.69 Hz, 1 H), 7.34 (d, *J*=4.52 Hz, 1 H), 7.08 – 7.21 (m, 1 H), 6.39 – 6.49 (m, 1 H), 6.05 – 6.10 (m, 2 H), 5.86 – 5.98 (m, 1 H), 4.66 – 4.82 (m, 1 H), 4.60 – 4.66 (m, 2 H), 4.24 – 4.28 (m, 1 H), 4.04 – 4.10 (m, 1 H), 3.94 – 4.03 (m, 1 H), 3.75 (dd, *J*=11.19, 2.14 Hz, 1 H), 1.66 (dd, *J*=6.36, 0.98 Hz, 3 H), 1.21 – 1.28 (m, 3 H), 0.91 (dd, *J*=6.24, 4.40 Hz, 18 H), 0.75 (d, *J*=7.09 Hz, 9 H), 0.06 – 0.11 (m, 21 H), –0.10 (d, *J*=8.68 Hz, 3 H), –0.32 (d, *J*=10.51 Hz, 3 H); ^{13}C NMR (101 MHz, $CDCl_3$) δ 161.21, 152.68, 152.55, 151.65, 150.02, 147.23, 141.55, 140.70, 136.16, 118.80, 105.95, 105.42, 103.12, 88.33, 85.85, 75.18, 72.37, 69.72, 65.89, 62.85, 26.18, 25.96, 25.77, 22.37, 18.37, 17.79, –1.29, –4.37, –4.67, –4.50, –5.06, –5.35; HRMS (ESI) calcd. for $C_{43}H_{75}O_{11}N_6Si_4$ $(M+H)^+$ 963.45654, found: 963.45423.

1-(6-Nitrobenzo[*d*][1,3]dioxol-5-yl)ethyl (9-((2*R*,3*R*,4*S*,5*R*)-3,4-dihydroxy-5-(hydroxy-methyl)-tetrahydrofuran-2-yl)-6-oxo-6,9-dihydro-1*H*-purin-2-yl)carbamate (297). Compound **296** (200 mg, 0.20 mmol, 1.0 eq) was dissolved in anhydrous THF (6 mL) and TBAF (2.08 mL, 2.1 mmol, 10 eq, 1 M in THF) was added to this solution at room temperature. The reaction mixture was stirred for 2 h at room temperature. The volatiles were evaporated under reduced pressure to an oily residue. The product was purified from this residue by silica gel flash column chromatography, elution with MeOH/DCM (1:9) to yield **297** as a yellow oil (71 mg, 66%). ^{1}H NMR (400 MHz, CD_3OD) δ 8.24 (s, 1 H), 7.52 (s, 1 H), 7.18 (d, *J*=1.34 Hz, 1 H), 6.40 (q, *J*=6.40 Hz, 1 H), 6.13 – 6.18 (m, 2 H), 5.95 (d, *J*=5.14 Hz, 1 H), 4.49 – 4.56 (m, 1 H), 4.32 (td, *J*=4.71, 1.96 Hz, 1 H), 4.07 (q, *J*=3.55 Hz, 1 H), 3.85 (dd, *J*=12.29, 3.12 Hz, 1 H), 3.71 – 3.81 (m, 1 H), 3.21 – 3.27 (m, 1 H), 1.70 (d, *J*=6.36 Hz, 3 H); ^{13}C NMR (101 MHz, CD_3OD) δ 155.36, 154.14, 150.77, 149.18, 143.19, 139.67, 135.29, 120.97, 89.66, 86.87, 76.31, 71.77, 62.61, 59.51, 54.08, 22.06; LRMS (ESI) calcd. for $C_{20}H_{21}O_{11}N_6$ $(M+H)^+$ 521.13, found: 521.00.

((2*R*,3*S*,4*R*,5*R*)-3,4-Dihydroxy-5-(2-(((1-(6-nitrobenzo[*d*][1,3]dioxol-5-yl)ethoxy)carbonyl)-amino)-6-oxo-1,6-dihydro-9*H*-purin-9-yl)tetrahydrofuran-2-yl)methyl phosphate (298). Compound **286** (90 mg, 1.30 mmol, 12 eq) was dissolved in anhydrous dioxane (2.5 mL) and triethylamine (140 µL, 0.96 mmol, 10 eq) was added to this solution with cooling in an ice-water bath. In another vial, **285** (30 µL, 0.32 mmol, 3.0 eq) was dissolved in anhydrous dioxane (0.5 mL) and was added to the first solution at 0 °C. The reaction was stirred vigorously for 1 h while allowing the reaction mixture to warm to room temperature, while a white suspension forms. The suspension was filtered (with a cotton filter in a glass pipette and the filtrate was collected in a

vial) and the filtrate containing **287** was taken up in a 3 mL syringe. In another vial, **297** (50 mg, 0.096 mmol, 1.0 eq) was dissolved in acetonitrile (3 mL) in an open vial and this solution was cooled in an ice-water bath with stirring. The filtrate in the syringe was slowly added dropwise to this solution at 0 °C, over a period of 5 min. The reaction was stirred in an open vial for another 25 mins. The reaction was added to water (3 mL) and the solvents dioxane and acetonitrile were evaporated under reduced pressure. The product was purified from the residual aqueous solution by DEAE Sephadex ion-exchange column chromatography and elution with 0.5 M TEAB buffer to yield **298** as a pale-yellow oil (17 mg, 23%). ^{1}H NMR (400 MHz, CD_3OD) δ 8.12 (s, 1 H), 7.32 (s, 1 H), 7.02 (s, 1 H), 6.23 (q, *J*=6.36 Hz, 1 H), 6.19 – 6.27 (m, 2 H), 5.82 (d, *J*=5.01 Hz, 1 H), 4.71 – 4.76 (m, 1 H), 4.52 – 4.48 (m, 1 H), 4.33 – 4.37 (m, 1 H), 4.20 – 4.26 (m, 2 H), 1.81 (d, *J*=6.28 Hz, 3 H); LRMS (ESI) calcd. for $C_{20}H_{20}O_{14}N_6P$ $(M–H)^-$ 599.08, found: 599.00. (^{13}C NMR not recorded due to low purity of **298**, ~60% purity).

((2*R*,3*S*,4*R*,5*R*)-3,4-Dihydroxy-5-(7-methyl-2-(((1-(6-nitrobenzo[*d*][1,3]dioxol-5-yl)ethoxy)-carbonyl)amino)-6-oxo-1,6-dihydro-9*H*-purin-7-ium-9-yl)tetrahydrofuran-2-yl)methyl phosphate (299). Compound **298** (10 mg, 0.016 mmol, 1.0 eq) was dissolved in anhydrous DMSO (0.3 mL) and methyl iodide (10 µL, 0.16 mmol, 10 eq) was added to this solution at room temperature. The reaction was stirred for 5 h at room temperature and added to water (3 mL). The aqueous solution was washed with diethyl ether (3 × 1 mL). The aqueous solution was concentrated under reduced pressure by co-evaporation with absolute ethanol and acetonitrile. The crude product **299** was obtained as a yellow residue (8.9 mg, 90%). LRMS (ESI) calcd. for $C_{21}H_{22}O_{14}N_6P$ $(M–H)^-$ 613.09, found: 613.00.

9-((2*R*,3*R*,4*S*,5*R*)-5-((((((((((2*R*,3*S*,4*R*,5*R*)-5-(2-Amino-6-oxo-1,6-dihydro-9*H*-purin-9-yl)-3,4-dihydroxytetrahydrofuran-2-yl)methoxy)(hydroxy)phosphoryl)oxy)oxidophosphoryl)-oxy) oxidophosphoryl)oxy)methyl)-3,4-dihydroxytetrahydrofuran-2-yl)-7-methyl-2-(((1-(6-nitro benzo[*d*][1,3]dioxol-5-yl)ethoxy)carbonyl)amino)-9*H*-purin-7-ium-6-olate (300). Compounds **289** (8 mg, 0.016 mmol, 1.0 eq) and **299** (15 mg, 0.024 mmol, 1.5 eq) were suspended in anhydrous DMF (0.3 mL), and $ZnCl_2$ (22 mg, 0.163 mmol, 10 eq) was added to the suspension at room temperature with vigorous stirring. After 15 min of vigorous stirring to dissolve the reactants, the reaction was stirred at room temperature with normal stirring for 24 h. LCMS analysis did not reveal the formation of **300**.

Bibliography

1. Almeida, M. I.; Reis, R. M.; Calin, G. A., MicroRNA history: discovery, recent applications, and next frontiers. *Mutation Research/Fundamental and Molecular Mechanisms of Mutagenesis* **2011,** *717* (1), 1-8.

2. Kozomara, A.; Griffiths-Jones, S., miRBase: annotating high confidence microRNAs using deep sequencing data. *Nucleic Acids Research* **2014,** *42* (D1), D68-D73.

3. Hafner, M.; Landthaler, M.; Burger, L.; Khorshid, M.; Hausser, J.; Berninger, P.; Rothballer, A.; Ascano Jr, M.; Jungkamp, A.-C.; Munschauer, M., Transcriptome-wide identification of RNA-binding protein and microRNA target sites by PAR-CLIP. *Cell* **2010,** *141* (1), 129-141.

4. Lee, R. C.; Feinbaum, R. L.; Ambros, V., The C. elegans heterochronic gene lin-4 encodes small RNAs with antisense complementarity to lin-14. *Cell* **1993,** *75* (5), 843-854.

5. Reinhart, B. J.; Slack, F. J.; Basson, M.; Pasquinelli, A. E.; Bettinger, J. C.; Rougvie, A. E.; Horvitz, H. R.; Ruvkun, G., The 21-nucleotide let-7 RNA regulates developmental timing in Caenorhabditis elegans. *Nature* **2000,** *403* (6772), 901-906.

6. Lagos-Quintana, M.; Rauhut, R.; Lendeckel, W.; Tuschl, T., Identification of novel genes coding for small expressed RNAs. *Science* **2001,** *294* (5543), 853-858.

7. Lau, N. C.; Lim, L. P.; Weinstein, E. G.; Bartel, D. P., An abundant class of tiny RNAs with probable regulatory roles in Caenorhabditis elegans. *Science* **2001,** *294* (5543), 858-862.

8. Lee, R. C.; Ambros, V., An extensive class of small RNAs in Caenorhabditis elegans. *Science* **2001,** *294* (5543), 862-864.

9. Rodriguez, A.; Griffiths-Jones, S.; Ashurst, J. L.; Bradley, A., Identification of mammalian microRNA host genes and transcription units. *Genome Research* **2004,** *14* (10a), 1902-1910.

10. Cai, X.; Hagedorn, C. H.; Cullen, B. R., Human microRNAs are processed from capped, polyadenylated transcripts that can also function as mRNAs. *RNA* **2004,** *10* (12), 1957-1966.

11. Lee, Y.; Ahn, C.; Han, J.; Choi, H.; Kim, J.; Yim, J.; Lee, J.; Provost, P.; Rådmark, O.; Kim, S., The nuclear RNase III Drosha initiates microRNA processing. *Nature* **2003,** *425* (6956), 415-419.

12. Park, J.-E.; Heo, I.; Tian, Y.; Simanshu, D. K.; Chang, H.; Jee, D.; Patel, D. J.; Kim, V. N., Dicer recognizes the 5′ end of RNA for efficient and accurate processing. *Nature* **2011,** *475* (7355), 201-205.

13. Alarcón, C. R.; Lee, H.; Goodarzi, H.; Halberg, N.; Tavazoie, S. F., N 6-methyladenosine marks primary microRNAs for processing. *Nature* **2015,** *519* (7544), 482-485.

14. Okada, C.; Yamashita, E.; Lee, S. J.; Shibata, S.; Katahira, J.; Nakagawa, A.; Yoneda, Y.; Tsukihara, T., A high-resolution structure of the pre-microRNA nuclear export machinery. *Science* **2009,** *326* (5957), 1275-1279.

15. Hutvágner, G.; McLachlan, J.; Pasquinelli, A. E.; Bálint, É.; Tuschl, T.; Zamore, P. D., A cellular function for the RNA-interference enzyme Dicer in the maturation of the let-7 small temporal RNA. *Science* **2001,** *293* (5531), 834-838.

16. Yoda, M.; Kawamata, T.; Paroo, Z.; Ye, X.; Iwasaki, S.; Liu, Q.; Tomari, Y., ATP-dependent human RISC assembly pathways. *Nature Structural & Molecular Biology* **2010,** *17* (1), 17.

17. Rana, T. M., Illuminating the silence: understanding the structure and function of small RNAs. *Nature Reviews Molecular Cell Biology* **2007,** *8* (1), 23-36.

18. Okamura, K.; Chung, W.-J.; Lai, E. C., The long and short of inverted repeat genes in animals: microRNAs, mirtrons and hairpin RNAs. *Cell Cycle* **2008,** *7* (18), 2840-2845.

19. Ha, M.; Kim, V. N., Regulation of microRNA biogenesis. *Nature Reviews Molecular Cell Biology* **2014,** *15* (8), 509-524.

20. Kawamata, T.; Tomari, Y., Making risc. *Trends in Biochemical Sciences* **2010,** *35* (7), 368-376.

21. Jo, M. H.; Shin, S.; Jung, S.-R.; Kim, E.; Song, J.-J.; Hohng, S., Human Argonaute 2 has diverse reaction pathways on target RNAs. *Molecular Cell* **2015,** *59* (1), 117-124.

22. Jonas, S.; Izaurralde, E., Towards a molecular understanding of microRNA-mediated gene silencing. *Nature Reviews Genetics* **2015,** *16* (7), 421-433.

23. Christie, M.; Boland, A.; Huntzinger, E.; Weichenrieder, O.; Izaurralde, E., Structure of the PAN3 pseudokinase reveals the basis for interactions with the PAN2 deadenylase and the GW182 proteins. *Molecular Cell* **2013,** *51* (3), 360-373.

24. Behm-Ansmant, I.; Rehwinkel, J.; Doerks, T.; Stark, A.; Bork, P.; Izaurralde, E., mRNA degradation by miRNAs and GW182 requires both CCR4: NOT deadenylase and DCP1: DCP2 decapping complexes. *Genes & Development* **2006,** *20* (14), 1885-1898.

25. Braun, J. E.; Truffault, V.; Boland, A.; Huntzinger, E.; Chang, C.-T.; Haas, G.; Weichenrieder, O.; Coles, M.; Izaurralde, E., A direct interaction between DCP1 and

XRN1 couples mRNA decapping to 5′ exonucleolytic degradation. *Nature Structural & Molecular Biology* **2012,** *19* (12), 1324.

26. Xu, W.; San Lucas, A.; Wang, Z.; Liu, Y., Identifying microRNA targets in different gene regions. *BMC Bioinformatics* **2014,** *15* (S7), S4.

27. Ellwanger, D. C.; Büttner, F. A.; Mewes, H.-W.; Stümpflen, V., The sufficient minimal set of miRNA seed types. *Bioinformatics* **2011,** *27* (10), 1346-1350.

28. Broughton, J. P.; Lovci, M. T.; Huang, J. L.; Yeo, G. W.; Pasquinelli, A. E., Pairing beyond the seed supports microRNA targeting specificity. *Molecular Cell* **2016,** *64* (2), 320-333.

29. Ghildiyal, M.; Zamore, P. D., Small silencing RNAs: an expanding universe. *Nature Reviews Genetics* **2009,** *10* (2), 94-108.

30. Forman, J. J.; Legesse-Miller, A.; Coller, H. A., A search for conserved sequences in coding regions reveals that the let-7 microRNA targets Dicer within its coding sequence. *Proceedings of the National Academy of Sciences* **2008,** *105* (39), 14879-14884.

31. Zhang, J.; Zhou, W.; Liu, Y.; Liu, T.; Li, C.; Wang, L., Oncogenic role of microRNA-532-5p in human colorectal cancer via targeting of the 5'UTR of RUNX3. *Oncology Letters* **2018,** *15* (5), 7215-7220.

32. Dharap, A.; Pokrzywa, C.; Murali, S.; Pandi, G.; Vemuganti, R., MicroRNA miR-324-3p induces promoter-mediated expression of RelA gene. *PLoS One* **2013,** *8* (11).

33. Vasudevan, S.; Steitz, J. A., AU-rich-element-mediated upregulation of translation by FXR1 and Argonaute 2. *Cell* **2007,** *128* (6), 1105-1118.

34. Garzon, R.; Marcucci, G.; Croce, C. M., Targeting microRNAs in cancer: rationale, strategies and challenges. *Nature Reviews Drug Discovery* **2010,** *9* (10), 775-789.

35. Lu, M.; Zhang, Q.; Deng, M.; Miao, J.; Guo, Y.; Gao, W.; Cui, Q., An analysis of human microRNA and disease associations. *PloS One* **2008,** *3* (10), e3420.

36. Esquela-Kerscher, A.; Slack, F. J., Oncomirs—microRNAs with a role in cancer. *Nature Reviews Cancer* **2006,** *6* (4), 259-269.

37. Hwang, H.; Mendell, J., MicroRNAs in cell proliferation, cell death, and tumorigenesis. *British Journal of Cancer* **2006,** *94* (6), 776-780.

38. Volinia, S.; Calin, G. A.; Liu, C.-G.; Ambs, S.; Cimmino, A.; Petrocca, F.; Visone, R.; Iorio, M.; Roldo, C.; Ferracin, M., A microRNA expression signature of human solid tumors defines cancer gene targets. *Proceedings of the National academy of Sciences of the United States of America* **2006,** *103* (7), 2257-2261.

39. Baffa, R.; Fassan, M.; Volinia, S.; O'Hara, B.; Liu, C. G.; Palazzo, J. P.; Gardiman, M.; Rugge, M.; Gomella, L. G.; Croce, C. M., MicroRNA expression profiling of human

metastatic cancers identifies cancer gene targets. *The Journal of Pathology* **2009,** *219* (2), 214-221.

40. Calin, G. A.; Croce, C. M., MicroRNA signatures in human cancers. *Nature Reviews Cancer* **2006,** *6* (11), 857-866.

41. Bonci, D.; Coppola, V.; Musumeci, M.; Addario, A.; Giuffrida, R.; Memeo, L.; D'Urso, L.; Pagliuca, A.; Biffoni, M.; Labbaye, C., The miR-15a–miR-16-1 cluster controls prostate cancer by targeting multiple oncogenic activities. *Nature Medicine* **2008,** *14* (11), 1271-1277.

42. Cimmino, A.; Calin, G. A.; Fabbri, M.; Iorio, M. V.; Ferracin, M.; Shimizu, M.; Wojcik, S. E.; Aqeilan, R. I.; Zupo, S.; Dono, M., miR-15 and miR-16 induce apoptosis by targeting BCL2. *Proceedings of the National Academy of Sciences of the United States of America* **2005,** *102* (39), 13944-13949.

43. Gruszka, R.; Zakrzewska, M., The oncogenic relevance of miR-17-92 cluster and its paralogous miR-106b-25 and miR-106a-363 clusters in brain tumors. *International Journal of Molecular Sciences* **2018,** *19* (3), 879.

44. Li, Y.; Wang, Y.; Shen, X.; Han, X., miR-128 Functions as an OncomiR for the Downregulation of HIC1 in Breast Cancer. *Frontiers in Pharmacology* **2019,** *10*, 1202.

45. Pfeffer, S.; Zavolan, M.; Grässer, F. A.; Chien, M.; Russo, J. J.; Ju, J.; John, B.; Enright, A. J.; Marks, D.; Sander, C., Identification of virus-encoded microRNAs. *Science* **2004,** *304* (5671), 734-736.

46. Andersson, M. G.; Haasnoot, P. J.; Xu, N.; Berenjian, S.; Berkhout, B.; Akusjärvi, G., Suppression of RNA interference by adenovirus virus-associated RNA. *Journal of Virology* **2005,** *79* (15), 9556-9565.

47. Sullivan, C. S.; Grundhoff, A. T.; Tevethia, S.; Pipas, J. M.; Ganem, D., SV40-encoded microRNAs regulate viral gene expression and reduce susceptibility to cytotoxic T cells. *Nature* **2005,** *435* (7042), 682-686.

48. Gatto, G.; Rossi, A.; Rossi, D.; Kroening, S.; Bonatti, S.; Mallardo, M., Epstein–Barr virus latent membrane protein 1 trans-activates miR-155 transcription through the NF-κB pathway. *Nucleic Acids Research* **2008,** *36* (20), 6608-6619.

49. Linnstaedt, S. D.; Gottwein, E.; Skalsky, R. L.; Luftig, M. A.; Cullen, B. R., Virally induced cellular microRNA miR-155 plays a key role in B-cell immortalization by Epstein-Barr virus. *Journal of Virology* **2010,** *84* (22), 11670-11678.

50. Huang, J.; Wang, F.; Argyris, E.; Chen, K.; Liang, Z.; Tian, H.; Huang, W.; Squires, K.; Verlinghieri, G.; Zhang, H., Cellular microRNAs contribute to HIV-1 latency in resting primary CD4+ T lymphocytes. *Nature Medicine* **2007,** *13* (10), 1241-1247.

51. Keller, A.; Leidinger, P.; Lange, J.; Borries, A.; Schroers, H.; Scheffler, M.; Lenhof, H.-P.; Ruprecht, K.; Meese, E., Multiple sclerosis: microRNA expression profiles accurately differentiate patients with relapsing-remitting disease from healthy controls. *PloS One* **2009,** *4* (10).

52. Pogribny, I. P.; Starlard-Davenport, A.; Tryndyak, V. P.; Han, T.; Ross, S. A.; Rusyn, I.; Beland, F. A., Difference in expression of hepatic microRNAs miR-29c, miR-34a, miR-155, and miR-200b is associated with strain-specific susceptibility to dietary nonalcoholic steatohepatitis in mice. *Laboratory Investigation* **2010,** *90* (10), 1437-1446.

53. Cheung, O.; Puri, P.; Eicken, C.; Contos, M. J.; Mirshahi, F.; Maher, J. W.; Kellum, J. M.; Min, H.; Luketic, V. A.; Sanyal, A. J., Nonalcoholic steatohepatitis is associated with altered hepatic MicroRNA expression. *Hepatology* **2008,** *48* (6), 1810-1820.

54. Martins, M.; Rosa, A.; Guedes, L. C.; Fonseca, B. V.; Gotovac, K.; Violante, S.; Mestre, T.; Coelho, M.; Rosa, M. M.; Martin, E. R., Convergence of miRNA expression profiling, α-synuclein interacton and GWAS in Parkinson's disease. *PloS One* **2011,** *6* (10).

55. Hébert, S. S.; Horré, K.; Nicolaï, L.; Papadopoulou, A. S.; Mandemakers, W.; Silahtaroglu, A. N.; Kauppinen, S.; Delacourte, A.; De Strooper, B., Loss of microRNA cluster miR-29a/b-1 in sporadic Alzheimer's disease correlates with increased BACE1/β-secretase expression. *Proceedings of the National Academy of Sciences* **2008,** *105* (17), 6415-6420.

56. Zhang, S.; Chen, L.; Jung, E. J.; Calin, G. A., Targeting microRNAs with small molecules: Between Dream and Reality. *Clinical Pharmacology and Therapeutics* **2010,** *87* (6), 754.

57. Papagiannakopoulos, T.; Shapiro, A.; Kosik, K. S., MicroRNA-21 targets a network of key tumor-suppressive pathways in glioblastoma cells. *Cancer Research* **2008,** *68* (19), 8164-8172.

58. Kloosterman, W. P.; Plasterk, R. H., The diverse functions of microRNAs in animal development and disease. *Developmental Cell* **2006,** *11* (4), 441-450.

59. Ding, M.; Li, J.; Yu, Y.; Liu, H.; Yan, Z.; Wang, J.; Qian, Q., Integrated analysis of miRNA, gene, and pathway regulatory networks in hepatic cancer stem cells. *Journal of Translational Medicine* **2015,** *13* (1), 1.

60. Tong, A.; Nemunaitis, J., Modulation of miRNA activity in human cancer: a new paradigm for cancer gene therapy? *Cancer Gene Therapy* **2008,** *15* (6), 341-355.

61. Iorio, M. V.; Croce, C. M., MicroRNA dysregulation in cancer: diagnostics, monitoring and therapeutics. A comprehensive review. *EMBO Molecular Medicine* **2012,** *4* (3), 143-159.

62. Meister, G.; Landthaler, M.; Dorsett, Y.; Tuschl, T., Sequence-specific inhibition of microRNA-and siRNA-induced RNA silencing. *RNA* **2004,** *10* (3), 544-550.

63. Boutla, A.; Delidakis, C.; Tabler, M., Developmental defects by antisense-mediated inactivation of micro-RNAs 2 and 13 in Drosophila and the identification of putative target genes. *Nucleic Acids Research* **2003,** *31* (17), 4973-4980.

64. Hutvágner, G.; Simard, M. J.; Mello, C. C.; Zamore, P. D., Sequence-specific inhibition of small RNA function. *PLoS Biology* **2004,** *2* (4), e98.

65. Wang, H.; Garzon, R.; Sun, H.; Ladner, K. J.; Singh, R.; Dahlman, J.; Cheng, A.; Hall, B. M.; Qualman, S. J.; Chandler, D. S., NF-κB–YY1–miR-29 regulatory circuitry in skeletal myogenesis and rhabdomyosarcoma. *Cancer Cell* **2008,** *14* (5), 369-381.

66. Krützfeldt, J.; Rajewsky, N.; Braich, R.; Rajeev, K. G.; Tuschl, T.; Manoharan, M.; Stoffel, M., Silencing of microRNAs in vivo with 'antagomirs'. *Nature* **2005,** *438* (7068), 685-689.

67. Kawasaki, A. M.; Casper, M. D.; Freier, S. M.; Lesnik, E. A.; Zounes, M. C.; Cummins, L. L.; Gonzalez, C.; Cook, P. D., Uniformly modified 2'-deoxy-2'-fluoro-phosphorothioate oligonucleotides as nuclease-resistant antisense compounds with high affinity and specificity for RNA targets. *Journal of Medicinal Chemistry* **1993,** *36* (7), 831-841.

68. Zhang, Y.; Roccaro, A. M.; Rombaoa, C.; Flores, L.; Obad, S.; Fernandes, S. M.; Sacco, A.; Liu, Y.; Ngo, H.; Quang, P., LNA-mediated anti–miR-155 silencing in low-grade B-cell lymphomas. *Blood* **2012,** *120* (8), 1678-1686.

69. Elmen, J.; Lindow, M.; Silahtaroglu, A.; Bak, M.; Christensen, M.; Lind-Thomsen, A.; Hedtjärn, M.; Hansen, J. B.; Hansen, H. F.; Straarup, E. M., Antagonism of microRNA-122 in mice by systemically administered LNA-antimiR leads to up-regulation of a large set of predicted target mRNAs in the liver. *Nucleic Acids Research* **2008,** *36* (4), 1153-1162.

70. Gebert, L. F.; Rebhan, M. A.; Crivelli, S. E.; Denzler, R.; Stoffel, M.; Hall, J., Miravirsen (SPC3649) can inhibit the biogenesis of miR-122. *Nucleic Acids Research* **2014,** *42* (1), 609-621.

71. Choi, W.-Y.; Giraldez, A. J.; Schier, A. F., Target protectors reveal dampening and balancing of Nodal agonist and antagonist by miR-430. *Science* **2007,** *318* (5848), 271-274.

72. Aagaard, L.; Rossi, J. J., RNAi therapeutics: principles, prospects and challenges. *Advanced Drug Delivery Reviews* **2007,** *59* (2), 75-86.

73. Zhao, X.; Pan, F.; Holt, C. M.; Lewis, A. L.; Lu, J. R., Controlled delivery of antisense oligonucleotides: a brief review of current strategies. *Expert Opinion on Drug Delivery* **2009,** *6* (7), 673-686.

74. Karikó, K.; Bhuyan, P.; Capodici, J.; Weissman, D., Small interfering RNAs mediate sequence-independent gene suppression and induce immune activation by signaling through toll-like receptor 3. *The Journal of Immunology* **2004,** *172* (11), 6545-6549.

75. Gilleron, J.; Querbes, W.; Zeigerer, A.; Borodovsky, A.; Marsico, G.; Schubert, U.; Manygoats, K.; Seifert, S.; Andree, C.; Stöter, M., Image-based analysis of lipid nanoparticle-mediated siRNA delivery, intracellular trafficking and endosomal escape. *Nature Biotechnology* **2013,** *31* (7), 638-646.

76. Ankenbruck, N.; Naro, Y.; Kumbhare, R.; Deiters, A., Discovery and Therapeutic Relevance of Small Molecule Modifiers of MicroRNA Function. In *MicroRNAs in Diseases and Disorders*, 2019; pp 323-363.

77. Uttamchandani, M.; Yao, S. Q., *Small Molecule Microarrays*. Springer: 2017.

78. Pai, J.; Hyun, S.; Hyun, J. Y.; Park, S.-H.; Kim, W.-J.; Bae, S.-H.; Kim, N.-K.; Yu, J.; Shin, I., Screening of pre-miRNA-155 binding peptides for apoptosis inducing activity using peptide microarrays. *Journal of the American Chemical Society* **2016,** *138* (3), 857-867.

79. Chirayil, S.; Chirayil, R.; Luebke, K. J., Discovering ligands for a microRNA precursor with peptoid microarrays. *Nucleic Acids Research* **2009,** *37* (16), 5486-5497.

80. Connelly, C. M.; Boer, R. E.; Moon, M. H.; Gareiss, P.; Schneekloth Jr, J. S., Discovery of inhibitors of microRNA-21 processing using small molecule microarrays. *ACS Chemical Biology* **2017,** *12* (2), 435-443.

81. Disney, M. D.; Labuda, L. P.; Paul, D. J.; Poplawski, S. G.; Pushechnikov, A.; Tran, T.; Velagapudi, S. P.; Wu, M.; Childs-Disney, J. L., Two-dimensional combinatorial screening identifies specific aminoglycoside− RNA internal loop partners. *Journal of the American Chemical Society* **2008,** *130* (33), 11185-11194.

82. Disney, M. D.; Angelbello, A. J., Rational design of small molecules targeting oncogenic noncoding RNAs from sequence. *Accounts of Chemical Research* **2016,** *49* (12), 2698-2704.

83. Velagapudi, S. P.; Costales, M. G.; Vummidi, B. R.; Nakai, Y.; Angelbello, A. J.; Tran, T.; Haniff, H. S.; Matsumoto, Y.; Wang, Z. F.; Chatterjee, A. K., Approved anti-cancer drugs target oncogenic non-coding RNAs. *Cell Chemical Biology* **2018,** *25* (9), 1086-1094. e7.

84. Davies, B. P.; Arenz, C., A fluorescence probe for assaying micro RNA maturation. *Bioorganic & Medicinal Chemistry* **2008,** *16* (1), 49-55.

85. Davies, B. P.; Arenz, C., A homogenous assay for micro RNA maturation. *Angewandte Chemie International Edition* **2006,** *45* (33), 5550-5552.

86. Vo, D. D.; Staedel, C.; Zehnacker, L.; Benhida, R.; Darfeuille, F.; Duca, M., Targeting the production of oncogenic microRNAs with multimodal synthetic small molecules. *ACS Chemical Biology* **2014,** *9* (3), 711-721.

87. Bose, D.; Jayaraj, G. G.; Kumar, S.; Maiti, S., A molecular-beacon-based screen for small molecule inhibitors of miRNA maturation. *ACS Chemical Biology* **2013,** *8* (5), 930-938.

88. Klemm, C. M.; Berthelmann, A.; Neubacher, S.; Arenz, C., Short and Efficient Synthesis of Alkyne-Modified Amino Glycoside Building Blocks. *European Journal of Organic Chemistry* **2009,** *2009* (17), 2788-2794.

89. Vo, D. D.; Tran, T. P. A.; Staedel, C.; Benhida, R.; Darfeuille, F.; Di Giorgio, A.; Duca, M., Oncogenic MicroRNAs Biogenesis as a Drug Target: Structure–Activity Relationship Studies on New Aminoglycoside Conjugates. *Chemistry–A European Journal* **2016,** *22* (15), 5350-5362.

90. Roos, M.; Pradère, U.; Ngondo, R. P.; Behera, A.; Allegrini, S.; Civenni, G.; Zagalak, J. A.; Marchand, J.-R. m.; Menzi, M.; Towbin, H., A small-molecule inhibitor of Lin28. *ACS Chemical Biology* **2016,** *11* (10), 2773-2781.

91. Lim, D.; Byun, W. G.; Koo, J. Y.; Park, H.; Park, S. B., Discovery of a small-molecule inhibitor of protein–microRNA interaction using binding assay with a site-specifically labeled Lin28. *Journal of the American Chemical Society* **2016,** *138* (41), 13630-13638.

92. Lightfoot, H. L.; Miska, E. A.; Balasubramanian, S., Identification of small molecule inhibitors of the Lin28-mediated blockage of pre-let-7g processing. *Organic & Biomolecular Chemistry* **2016,** *14* (43), 10208-10216.

93. Wang, L.; Rowe, R. G.; Jaimes, A.; Yu, C.; Nam, Y.; Pearson, D. S.; Zhang, J.; Xie, X.; Marion, W.; Heffron, G. J., Small-molecule inhibitors disrupt let-7 oligouridylation and release the selective blockade of let-7 processing by LIN28. *Cell Reports* **2018,** *23* (10), 3091-3101.

94. Tan, G. S.; Chiu, C.-H.; Garchow, B. G.; Metzler, D.; Diamond, S. L.; Kiriakidou, M., Small molecule inhibition of RISC loading. *ACS Chemical Biology* **2012,** *7* (2), 403-410.

95. Lorenz, D. A.; Song, J. M.; Garner, A. L., High-throughput platform assay technology for the discovery of pre-microRNA-selective small molecule probes. *Bioconjugate Chemistry* **2015,** *26* (1), 19-23.

96. Lorenz, D. A.; Vander Roest, S.; Larsen, M. J.; Garner, A. L., Development and implementation of an HTS-compatible assay for the discovery of selective small-molecule ligands for pre-microRNAs. *SLAS DISCOVERY: Advancing Life Sciences R&D* **2018,** *23* (1), 47-54.

97. Baell, J. B.; Holloway, G. A., New substructure filters for removal of pan assay interference compounds (PAINS) from screening libraries and for their exclusion in bioassays. *Journal of Medicinal Chemistry* **2010,** *53* (7), 2719-2740.

98. Thorne, N.; Inglese, J.; Auld, D. S., Illuminating insights into firefly luciferase and other bioluminescent reporters used in chemical biology. *Chemistry & Biology* **2010,** *17* (6), 646-657.

99. Thorne, N.; Auld, D. S.; Inglese, J., Apparent activity in high-throughput screening: origins of compound-dependent assay interference. *Current Opinion in Chemical Biology* **2010,** *14* (3), 315-324.

100. Auld, D. S.; Thorne, N.; Nguyen, D.-T.; Inglese, J., A specific mechanism for nonspecific activation in reporter-gene assays. ACS Publications: 2008.

101. Shan, G.; Li, Y.; Zhang, J.; Li, W.; Szulwach, K. E.; Duan, R.; Faghihi, M. A.; Khalil, A. M.; Lu, L.; Paroo, Z., A small molecule enhances RNA interference and promotes microRNA processing. *Nature Biotechnology* **2008,** *26* (8), 933.

102. Daniels, S. M.; Melendez-Peña, C. E.; Scarborough, R. J.; Daher, A.; Christensen, H. S.; El Far, M.; Purcell, D. F.; Lainé, S.; Gatignol, A., Characterization of the TRBP domain required for dicer interaction and function in RNA interference. *BMC Molecular Biology* **2009,** *10* (1), 38.

103. Gumireddy, K.; Young, D. D.; Xiong, X.; Hogenesch, J. B.; Huang, Q.; Deiters, A., Small-molecule inhibitors of microrna miR-21 function. *Angewandte Chemie International Edition* **2008,** *47* (39), 7482-7484.

104. Jiang, C.-s.; Wang, X.-m.; Zhang, S.-q.; Meng, L.-s.; Zhu, W.-h.; Xu, J.; Lu, S.-m., Discovery of 4-benzoylamino-N-(prop-2-yn-1-yl) benzamides as novel microRNA-21 inhibitors. *Bioorganic & Medicinal Chemistry* **2015,** *23* (19), 6510-6519.

105. Naro, Y.; Ankenbruck, N.; Thomas, M.; Tivon, Y.; Connelly, C. M.; Gardner, L.; Deiters, A., Small molecule inhibition of MicroRNA miR-21 rescues chemosensitivity of renal-cell carcinoma to topotecan. *Journal of Medicinal Chemistry* **2018,** *61* (14), 5900-5909.

106. Naro, Y.; Thomas, M.; Stephens, M. D.; Connelly, C. M.; Deiters, A., Aryl amide small-molecule inhibitors of microRNA miR-21 function. *Bioorganic & Medicinal Chemistry Letters* **2015,** *25* (21), 4793-4796.

107. Frankel, L. B.; Christoffersen, N. R.; Jacobsen, A.; Lindow, M.; Krogh, A.; Lund, A. H., Programmed cell death 4 (PDCD4) is an important functional target of the microRNA miR-21 in breast cancer cells. *Journal of Biological Chemistry* **2008,** *283* (2), 1026-1033.

108. Young, D. D.; Connelly, C. M.; Grohmann, C.; Deiters, A., Small molecule modifiers of microRNA miR-122 function for the treatment of hepatitis C virus infection and hepatocellular carcinoma. *Journal of the American Chemical Society* **2010,** *132* (23), 7976-7981.

109. Xiao, Z.; Li, C. H.; Chan, S. L.; Xu, F.; Feng, L.; Wang, Y.; Jiang, J.-D.; Sung, J. J.; Cheng, C. H.; Chen, Y., A small-molecule modulator of the tumor-suppressor miR34a inhibits the growth of hepatocellular carcinoma. *Cancer Research* **2014,** *74* (21), 6236-6247.

110. Zhu, T.; Cao, S.; Su, P.-C.; Patel, R.; Shah, D.; Chokshi, H. B.; Szukala, R.; Johnson, M. E.; Hevener, K. E., Hit identification and optimization in virtual screening: practical

recommendations based on a critical literature analysis: miniperspective. *Journal of Medicinal Chemistry* **2013,** *56* (17), 6560-6572.

111. Tan, S.-B.; Huang, C.; Chen, X.; Wu, Y.; Zhou, M.; Zhang, C.; Zhang, Y., Small molecular inhibitors of miR-1 identified from photocycloadducts of acetylenes with 2-methoxy-1, 4-naphthalenequinone. *Bioorganic & Medicinal Chemistry* **2013,** *21* (20), 6124-6131.

112. Guo, R.; Abdelmohsen, K.; Morin, P. J.; Gorospe, M., Novel microRNA reporter uncovers repression of let-7 by GSK-3β. *Plos One* **2013,** *8* (6).

113. Todd, A.; Anderson, R.; Groundwater, P. W., Rational drug design-identifying and characterising a target. *The Pharmaceutical Journal* **2009,** *283* (7559), 19-20.

114. Mathews, D. H.; Disney, M. D.; Childs, J. L.; Schroeder, S. J.; Zuker, M.; Turner, D. H., Incorporating chemical modification constraints into a dynamic programming algorithm for prediction of RNA secondary structure. *Proceedings of the National Academy of Sciences* **2004,** *101* (19), 7287-7292.

115. Velagapudi, S. P.; Gallo, S. M.; Disney, M. D., Sequence-based design of bioactive small molecules that target precursor microRNAs. *Nature Chemical Biology* **2014,** *10* (4), 291.

116. Velagapudi, S. P.; Cameron, M. D.; Haga, C. L.; Rosenberg, L. H.; Lafitte, M.; Duckett, D. R.; Phinney, D. G.; Disney, M. D., Design of a small molecule against an oncogenic noncoding RNA. *Proceedings of the National Academy of Sciences* **2016,** *113* (21), 5898-5903.

117. Haga, C. L.; Velagapudi, S. P.; Strivelli, J. R.; Yang, W.-Y.; Disney, M. D.; Phinney, D. G., Small molecule inhibition of miR-544 biogenesis disrupts adaptive responses to hypoxia by modulating ATM-mTOR signaling. *ACS Chemical Biology* **2015,** *10* (10), 2267-2276.

118. Childs-Disney, J. L.; Disney, M. D., Small molecule targeting of a MicroRNA associated with hepatocellular carcinoma. *ACS Chemical Biology* **2016,** *11* (2), 375-380.

119. Murata, A.; Otabe, T.; Zhang, J.; Nakatani, K., BzDANP, a small-molecule modulator of pre-miR-29a maturation by Dicer. *ACS Chemical Biology* **2016,** *11* (10), 2790-2796.

120. Schmidt, M. F.; Korb, O.; Abell, C., MicroRNA-specific argonaute 2 protein inhibitors. *ACS Chemical Biology* **2013,** *8* (10), 2122-2126.

121. Shi, Z.; Zhang, J.; Qian, X.; Han, L.; Zhang, K.; Chen, L.; Liu, J.; Ren, Y.; Yang, M.; Zhang, A., AC1MMYR2, an inhibitor of dicer-mediated biogenesis of oncomir miR-21, reverses epithelial–mesenchymal transition and suppresses tumor growth and progression. *Cancer Research* **2013,** *73* (17), 5519-5531.

122. Girard, M.; Jacquemin, E.; Munnich, A.; Lyonnet, S.; Henrion-Caude, A., miR-122, a paradigm for the role of microRNAs in the liver. *Journal of Hepatology* **2008,** *48* (4), 648-656.

123. Landgraf, P.; Rusu, M.; Sheridan, R.; Sewer, A.; Iovino, N.; Aravin, A.; Pfeffer, S.; Rice, A.; Kamphorst, A. O.; Landthaler, M., A mammalian microRNA expression atlas based on small RNA library sequencing. *Cell* **2007,** *129* (7), 1401-1414.

124. Lagos-Quintana, M.; Rauhut, R.; Yalcin, A.; Meyer, J.; Lendeckel, W.; Tuschl, T., Identification of tissue-specific microRNAs from mouse. *Current Biology* **2002,** *12* (9), 735-739.

125. Chang, J.; Nicolas, E.; Marks, D.; Sander, C.; Lerro, A.; Buendia, M. A.; Xu, C.; Mason, W. S.; Moloshok, T.; Bort, R., miR-122, a mammalian liver-specific microRNA, is processed from hcr mRNA and maydownregulate the high affinity cationic amino acid transporter CAT-1. *RNA Biology* **2004,** *1* (2), 106-113.

126. Wienholds, E.; Kloosterman, W. P.; Miska, E.; Alvarez-Saavedra, E.; Berezikov, E.; de Bruijn, E.; Horvitz, H. R.; Kauppinen, S.; Plasterk, R. H., MicroRNA expression in zebrafish embryonic development. *Science* **2005,** *309* (5732), 310-311.

127. Li, J.; Ghazwani, M.; Zhang, Y.; Lu, J.; Li, J.; Fan, J.; Gandhi, C. R.; Li, S., miR-122 regulates collagen production via targeting hepatic stellate cells and suppressing P4HA1 expression. *Journal of Hepatology* **2013,** *58* (3), 522-528.

128. Jopling, C., Liver-specific microRNA-122: Biogenesis and function. *RNA Biology* **2012,** *9* (2), 137-142.

129. Filipowicz, W.; Großhans, H., The liver-specific microRNA miR-122: biology and therapeutic potential. In *Epigenetics and Disease*, Springer: 2011; pp 221-238.

130. Hsu, S.-h.; Wang, B.; Kota, J.; Yu, J.; Costinean, S.; Kutay, H.; Yu, L.; Bai, S.; La Perle, K.; Chivukula, R. R., Essential metabolic, anti-inflammatory, and anti-tumorigenic functions of miR-122 in liver. *The Journal of Clinical Investigation* **2012,** *122* (8), 2871-2883.

131. Laudadio, I.; Manfroid, I.; Achouri, Y.; Schmidt, D.; Wilson, M. D.; Cordi, S.; Thorrez, L.; Knoops, L.; Jacquemin, P.; Schuit, F., A feedback loop between the liver-enriched transcription factor network and miR-122 controls hepatocyte differentiation. *Gastroenterology* **2012,** *142* (1), 119-129.

132. Esau, C.; Davis, S.; Murray, S. F.; Yu, X. X.; Pandey, S. K.; Pear, M.; Watts, L.; Booten, S. L.; Graham, M.; McKay, R., miR-122 regulation of lipid metabolism revealed by in vivo antisense targeting. *Cell Metabolism* **2006,** *3* (2), 87-98.

133. Davoodian, N.; Lotfi, A. S.; Soleimani, M.; Mowla, S. J., MicroRNA-122 overexpression promotes hepatic differentiation of human adipose tissue-derived stem cells. *Journal of Cellular Biochemistry* **2014,** *115* (9), 1582-1593.

134. Deng, X. G.; Qiu, R. L.; Wu, Y. H.; Li, Z. X.; Xie, P.; Zhang, J.; Zhou, J. J.; Zeng, L. X.; Tang, J.; Maharjan, A., Overexpression of miR-122 promotes the hepatic differentiation

and maturation of mouse ESCs through a miR-122/FoxA1/HNF4a-positive feedback loop. *Liver International* **2014,** *34* (2), 281-295.

135. Doddapaneni, R.; Chawla, Y. K.; Das, A.; Kalra, J. K.; Ghosh, S.; Chakraborti, A., Overexpression of microRNA-122 enhances in vitro hepatic differentiation of fetal liver-derived stem/progenitor cells. *Journal of Cellular Biochemistry* **2013,** *114* (7), 1575-1583.

136. Nakao, K.; Miyaaki, H.; Ichikawa, T., Antitumor function of microRNA-122 against hepatocellular carcinoma. *Journal of Gastroenterology* **2014,** *49* (4), 589-593.

137. Kishikawa, T.; Otsuka, M.; Tan, P. S.; Ohno, M.; Sun, X.; Yoshikawa, T.; Shibata, C.; Takata, A.; Kojima, K.; Takehana, K., Decreased miR122 in hepatocellular carcinoma leads to chemoresistance with increased arginine. *Oncotarget* **2015,** *6* (10), 8339.

138. Fukuhara, T.; Kambara, H.; Shiokawa, M.; Ono, C.; Katoh, H.; Morita, E.; Okuzaki, D.; Maehara, Y.; Koike, K.; Matsuura, Y., Expression of microRNA miR-122 facilitates an efficient replication in nonhepatic cells upon infection with hepatitis C virus. *Journal of Virology* **2012,** *86* (15), 7918-7933.

139. Gatfield, D.; Le Martelot, G.; Vejnar, C. E.; Gerlach, D.; Schaad, O.; Fleury-Olela, F.; Ruskeepää, A.-L.; Oresic, M.; Esau, C. C.; Zdobnov, E. M., Integration of microRNA miR-122 in hepatic circadian gene expression. *Genes & Development* **2009,** *23* (11), 1313-1326.

140. Coulouarn, C.; Factor, V. M.; Andersen, J. B.; Durkin, M. E.; Thorgeirsson, S. S., Loss of miR-122 expression in liver cancer correlates with suppression of the hepatic phenotype and gain of metastatic properties. *Oncogene* **2009,** *28* (40), 3526-3536.

141. Xu, H.; He, J.-H.; Xiao, Z.-D.; Zhang, Q.-Q.; Chen, Y.-Q.; Zhou, H.; Qu, L.-H., Liver-enriched transcription factors regulate MicroRNA-122 that targets CUTL1 during liver development. *Hepatology* **2010,** *52* (4), 1431-1442.

142. Bhattacharyya, S. N.; Habermacher, R.; Martine, U.; Closs, E. I.; Filipowicz, W., Relief of microRNA-mediated translational repression in human cells subjected to stress. *Cell* **2006,** *125* (6), 1111-1124.

143. Wang, X.; Yu, B.; Ren, W.; Mo, X.; Zhou, C.; He, H.; Jia, H.; Wang, L.; Jacob, S. T.; Lee, R. J., Enhanced hepatic delivery of siRNA and microRNA using oleic acid based lipid nanoparticle formulations. *Journal of Controlled Release* **2013,** *172* (3), 690-698.

144. Thakral, S.; Ghoshal, K., miR-122 is a unique molecule with great potential in diagnosis, prognosis of liver disease, and therapy both as miRNA mimic and antimir. *Current Gene Therapy* **2015,** *15* (2), 142-150.

145. Liu, K.-c.; Lin, B.-s.; Zhao, M.; Wang, K.-y.; Lan, X.-p., Cutl1: a potential target for cancer therapy. *Cellular Signalling* **2013,** *25* (1), 349-354.

146. Fornari, F.; Gramantieri, L.; Giovannini, C.; Veronese, A.; Ferracin, M.; Sabbioni, S.; Calin, G. A.; Grazi, G. L.; Croce, C. M.; Tavolari, S., MiR-122/cyclin G1 interaction

modulates p53 activity and affects doxorubicin sensitivity of human hepatocarcinoma cells. *Cancer Research* **2009,** *69* (14), 5761-5767.

147. Lin, C. J.-F.; Gong, H.-Y.; Tseng, H.-C.; Wang, W.-L.; Wu, J.-L., miR-122 targets an anti-apoptotic gene, Bcl-w, in human hepatocellular carcinoma cell lines. *Biochemical and Biophysical Research Communications* **2008,** *375* (3), 315-320.

148. Jopling, C. L.; Yi, M.; Lancaster, A. M.; Lemon, S. M.; Sarnow, P., Modulation of hepatitis C virus RNA abundance by a liver-specific MicroRNA. *Science* **2005,** *309* (5740), 1577-1581.

149. Lanford, R. E.; Hildebrandt-Eriksen, E. S.; Petri, A.; Persson, R.; Lindow, M.; Munk, M. E.; Kauppinen, S.; Ørum, H., Therapeutic silencing of microRNA-122 in primates with chronic hepatitis C virus infection. *Science* **2010,** *327* (5962), 198-201.

150. Jangra, R. K.; Yi, M.; Lemon, S. M., Regulation of hepatitis C virus translation and infectious virus production by the microRNA miR-122. *Journal of Virology* **2010,** *84* (13), 6615-6625.

151. Henke, J. I.; Goergen, D.; Zheng, J.; Song, Y.; Schüttler, C. G.; Fehr, C.; Jünemann, C.; Niepmann, M., microRNA-122 stimulates translation of hepatitis C virus RNA. *The EMBO Journal* **2008,** *27* (24), 3300-3310.

152. Shimakami, T.; Yamane, D.; Welsch, C.; Hensley, L.; Jangra, R. K.; Lemon, S. M., Base pairing between hepatitis C virus RNA and microRNA 122 3′ of its seed sequence is essential for genome stabilization and production of infectious virus. *Journal of Virology* **2012,** *86* (13), 7372-7383.

153. Luna, J. M.; Scheel, T. K.; Danino, T.; Shaw, K. S.; Mele, A.; Fak, J. J.; Nishiuchi, E.; Takacs, C. N.; Catanese, M. T.; de Jong, Y. P., Hepatitis C virus RNA functionally sequesters miR-122. *Cell* **2015,** *160* (6), 1099-1110.

154. Tricoli, L.; Niture, S.; Chimeh, U.; Kumar, D., Role of microRNAs in the development of hepatocellular carcinoma and acquired drug resistance. *Frontiers in Bioscience* **2019,** *24*, 545-554.

155. van der Ree, M. H.; van der Meer, A. J.; van Nuenen, A. C.; de Bruijne, J.; Ottosen, S.; Janssen, H. L.; Kootstra, N. A.; Reesink, H. W., Miravirsen dosing in chronic hepatitis C patients results in decreased microRNA-122 levels without affecting other microRNAs in plasma. *Alimentary Pharmacology & Therapeutics* **2016,** *43* (1), 102-113.

156. Cheng, A. M.; Byrom, M. W.; Shelton, J.; Ford, L. P., Antisense inhibition of human miRNAs and indications for an involvement of miRNA in cell growth and apoptosis. *Nucleic Acids Research* **2005,** *33* (4), 1290-1297.

157. Yu, C.; Qian, L.; Uttamchandani, M.; Li, L.; Yao, S. Q., Single-Vehicular Delivery of Antagomir and Small Molecules to Inhibit miR-122 Function in Hepatocellular Carcinoma

Cells by using “Smart” Mesoporous Silica Nanoparticles. *Angewandte Chemie* **2015,** *54* (36), 10574-10578.

158. Slowing, I.; Trewyn, B. G.; Lin, V. S.-Y., Effect of surface functionalization of MCM-41-type mesoporous silica nanoparticles on the endocytosis by human cancer cells. *Journal of the American Chemical Society* **2006,** *128* (46), 14792-14793.

159. Nilsson, A.; NILSHEDEN, C., STRUCTURAL EFFECTS ON SELECTIVE ALIPHATIC HYDROGEN-EXCHANGE IN ALKYL-SUBSTITUTED AROMATIC-COMPOUNDS IN DEUTERIATED TRIFLUOROACETIC-ACID. *Acta Chemica Scandinavica. Series B. Organic Chemistry and Biochemistry* **1985,** *39* (1), 25-30.

160. Van Den Berge, E.; Robiette, R., Development of a regioselective N-methylation of (benz) imidazoles providing the more sterically hindered isomer. *The Journal of Organic Chemistry* **2013,** *78* (23), 12220-12223.

161. Tokunaga, T.; Hume, W. E.; Kitoh, M.; Nagata, R., Pyrrole derivatives. Google Patents: 2004.

162. Pu, J.; Kreft, A. F.; Aschmies, S. H.; Atchison, K. P.; Berkowitz, J.; Caggiano, T. J.; Chlenov, M.; Diamantidis, G.; Harrison, B. L.; Hu, Y., Synthesis and structure–activity relationship of a novel series of heterocyclic sulfonamide γ-secretase inhibitors. *Bioorganic & Medicinal Chemistry* **2009,** *17* (13), 4708-4717.

163. Suwiński, J.; Salwińska, E., Reactions of 1-arenesulfonyl-4-nitroimidazoles with aniline in aqueous methanol solution. *Tetrahedron* **1994,** *50* (19), 5741-5752.

164. Che, Z.; Zhang, S.; Shao, Y.; Fan, L.; Xu, H.; Yu, X.; Zhi, X.; Yao, X.; Zhang, R., Synthesis and quantitative structure–activity relationship (QSAR) study of novel N-arylsulfonyl-3-acylindole arylcarbonyl hydrazone derivatives as nematicidal agents. *Journal of Agricultural and Food Chemistry* **2013,** *61* (24), 5696-5705.

165. Auld, D. S.; Thorne, N.; Maguire, W. F.; Inglese, J.; Collins, F. A., Mechanism of PTC124 Activity in Cell-Based Luciferase Assays of Nonsense Codon Suppression. *Proceedings of the National Academy of Sciences of the United States of America* **2009,** *106* (9), 3585-3590.

166. McKeown, S. C.; Hall, A.; Blunt, R.; Brown, S. H.; Chessell, I. P.; Chowdhury, A.; Giblin, G. M.; Healy, M. P.; Johnson, M. R.; Lorthioir, O., Identification of novel glycine sulfonamide antagonists for the EP 1 receptor. *Bioorganic & Medicinal Chemistry Letters* **2007,** *17* (6), 1750-1754.

167. Sultane, P. R.; Mete, T. B.; Bhat, R. G., Chemoselective N-deacetylation under mild conditions. *Organic & Biomolecular Chemistry* **2014,** *12* (2), 261-264.

168. Auld, D. S.; Inglese, J., *Interferences with Luciferase Reporter Enzymes*. Eli Lilly & Company and the National Center for Advancing Translational Sciences: 2016.

169. Pagé, D.; Walpole, C.; Yang, H., Benzimidazole derivatives, compositions containing them, preparation thereof and uses thereof. Google Patents: 2007.

170. Herr, R. J., 5-Substituted-1H-tetrazoles as carboxylic acid isosteres: medicinal chemistry and synthetic methods. *Bioorganic & Medicinal Chemistry* **2002,** *10* (11), 3379-3393.

171. Lassalas, P.; Gay, B.; Lasfargeas, C.; James, M. J.; Tran, V.; Vijayendran, K. G.; Brunden, K. R.; Kozlowski, M. C.; Thomas, C. J.; Smith, A. B.; Huryn, D. M.; Ballatore, C., Structure Property Relationships of Carboxylic Acid Isosteres. *Journal of Medicinal Chemistry* **2016,** *59* (7), 3183-3203.

172. Roh, J.; Vávrová, K.; Hrabálek, A., Synthesis and functionalization of 5-substituted tetrazoles. *European Journal of Organic Chemistry* **2012,** *2012* (31), 6101-6118.

173. Livak, K. J.; Schmittgen, T. D., Analysis of Relative Gene Expression Data Using Real-Time Quantitative PCR and the 2−ΔΔCT Method. *Methods* **2001,** *25* (4), 402-408.

174. Gumireddy, K.; Young, D. D.; Xiong, X.; Hogenesch, J. B.; Huang, Q.; Deiters, A., Small Molecule Inhibitors of MicroRNA miR-21 Function. *Angewandte Chemie International Edition* **2008,** *47* (39), 7482-7484.

175. Wang, N.; Wang, Q.; Shen, D.; Sun, X.; Cao, X.; Wu, D., Downregulation of microRNA-122 promotes proliferation, migration, and invasion of human hepatocellular carcinoma cells by activating epithelial–mesenchymal transition. *OncoTargets and Therapy* **2016,** *9*, 2035-2047.

176. Li, Z.-Y.; Xi, Y.; Zhu, W.-N.; Zeng, C.; Zhang, Z.-Q.; Guo, Z.-C.; Hao, D.-L.; Liu, G.; Feng, L.; Chen, H.-Z.; Chen, F.; Lv, X.; Liu, D.-P.; Liang, C.-C., Positive regulation of hepatic miR-122 expression by HNF4α. *Journal of Hepatology* **2011,** *55* (3), 602-611.

177. Laudadio, I.; Manfroid, I.; Achouri, Y.; Schmidt, D.; Wilson, M. D.; Cordi, S.; Thorrez, L.; Knoops, L.; Jacquemin, P.; Schuit, F.; Pierreux, C. E.; Odom, D. T.; Peers, B.; Lemaigre, F. P., A Feedback Loop Between the Liver-Enriched Transcription Factor Network and Mir-122 Controls Hepatocyte Differentiation. *Gastroenterology* **2012,** *142* (1), 119-129.

178. Farré, D.; Roset, R.; Huerta, M.; Adsuara, J. E.; Roselló, L.; Albà, M. M.; Messeguer, X., Identification of patterns in biological sequences at the ALGGEN server: PROMO and MALGEN. *Nucleic Acids Research* **2003,** *31* (13), 3651-3653.

179. Messeguer, X.; Escudero, R.; Farré, D.; Núñez, O.; Martínez, J.; Albà, M. M., PROMO: Detection of known transcription regulatory elements using species-tailored searches. *Bioinformatics* **2002,** *18* (2), 333-334.

180. Kiselyuk, A.; Lee, S.-H.; Farber-Katz, S.; Zhang, M.; Athavankar, S.; Cohen, T.; Pinkerton, Anthony B.; Ye, M.; Bushway, P.; Richardson, Adam D.; Hostetler, Heather A.; Rodriguez-Lee, M.; Huang, L.; Spangler, B.; Smith, L.; Higginbotham, J.; Cashman, J.; Freeze, H.; Itkin-Ansari, P.; Dawson, Marcia I.; Schroeder, F.; Cang, Y.; Mercola, M.;

Levine, F., HNF4α Antagonists Discovered by a High-Throughput Screen for Modulators of the Human Insulin Promoter. *Chemistry & Biology* **2012,** *19* (7), 806-818.

181. Levy, G.; Habib, N.; Guzzardi, M. A.; Kitsberg, D.; Bomze, D.; Ezra, E.; Uygun, B. E.; Uygun, K.; Trippler, M.; Schlaak, J. F.; Shibolet, O.; Sklan, E. H.; Cohen, M.; Timm, J.; Friedman, N.; Nahmias, Y., Nuclear receptors control pro-viral and antiviral metabolic responses to hepatitis C virus infection. *Nature Chemical Biology* **2016,** *12*, 1037.

182. Janssen, H. L. A.; Reesink, H. W.; Lawitz, E. J.; Zeuzem, S.; Rodriguez-Torres, M.; Patel, K.; van der Meer, A. J.; Patick, A. K.; Chen, A.; Zhou, Y.; Persson, R.; King, B. D.; Kauppinen, S.; Levin, A. A.; Hodges, M. R., Treatment of HCV Infection by Targeting MicroRNA. *The New England Journal of Medicine* **2013,** *368* (18), 1685-1694.

183. Ottosen, S.; Parsley, T. B.; Yang, L.; Zeh, K.; van Doorn, L. J.; van der Veer, E.; Raney, A. K.; Hodges, M. R.; Patick, A. K., In vitro antiviral activity and preclinical and clinical resistance profile of miravirsen, a novel anti-hepatitis C virus therapeutic targeting the human factor miR-122. *Antimicrobial Agents and Chemotherapy* **2015,** *59* (1), 599-608.

184. Li, Y.; Masaki, T.; Yamane, D.; McGivern, D. R.; Lemon, S. M., Competing and noncompeting activities of miR-122 and the 5′exonuclease Xrn1 in regulation of hepatitis C virus replication. *Proceedings of the National Academy of Sciences of the United States of America* **2013,** *110* (5), 1881-1886.

185. Mortimer, S. A.; Doudna, J. A., Unconventional miR-122 binding stabilizes the HCV genome by forming a trimolecular RNA structure. *Nucleic Acids Research* **2013,** *41* (7), 4230-4240.

186. Henke, J. I.; Goergen, D.; Zheng, J.; Song, Y.; Schüttler, C. G.; Fehr, C.; Jünemann, C.; Niepmann, M., microRNA-122 stimulates translation of hepatitis C virus RNA. *The EMBO Journal* **2008,** *27* (24), 3300-3310.

187. Roberts, A. P.; Lewis, A. P.; Jopling, C. L., miR-122 activates hepatitis C virus translation by a specialized mechanism requiring particular RNA components. *Nucleic Acids Research* **2011,** *39* (17), 7716-7729.

188. Masaki, T.; Arend, Kyle C.; Li, Y.; Yamane, D.; McGivern, David R.; Kato, T.; Wakita, T.; Moorman, Nathaniel J.; Lemon, Stanley M., miR-122 Stimulates Hepatitis C Virus RNA Synthesis by Altering the Balance of Viral RNAs Engaged in Replication versus Translation. *Cell Host & Microbe* **2015,** *17* (2), 217-228.

189. Wang, L.; Jeng, K.-S.; Lai, M. M. C., Poly(C)-binding protein 2 interacts with sequences required for viral replication in the hepatitis C virus (HCV) 5' untranslated region and directs HCV RNA replication through circularizing the viral genome. *Journal of Virology* **2011,** *85* (16), 7954-7964.

190. Li, Y.; Yamane, D.; Masaki, T.; Lemon, S. M., The yin and yang of hepatitis C: synthesis and decay of hepatitis C virus RNA. *Nature Reviews Microbiology* **2015,** *13* (9), 544-558.

191. Berezhna, S. Y.; Supekova, L.; Sever, M. J.; Schultz, P. G.; Deniz, A. A., Dual regulation of hepatitis C viral RNA by cellular RNAi requires partitioning of Ago2 to lipid droplets and P-bodies. *RNA* **2011,** *17* (10), 1831-1845.

192. Liu, F.; Shimakami, T.; Murai, K.; Shirasaki, T.; Funaki, M.; Honda, M.; Murakami, S.; Yi, M.; Tang, H.; Kaneko, S., Efficient Suppression of Hepatitis C Virus Replication by Combination Treatment with miR-122 Antagonism and Direct-acting Antivirals in Cell Culture Systems. *Scientific Reports* **2016,** *6*, 30939.

193. Sorbo, M. C.; Cento, V.; Di Maio, V. C.; Howe, A. Y. M.; Garcia, F.; Perno, C. F.; Ceccherini-Silberstein, F., Hepatitis C virus drug resistance associated substitutions and their clinical relevance: Update 2018. *Drug Resistance Updates* **2018,** *37*, 17-39.

194. Crouchet, E.; Wrensch, F.; Schuster, C.; Zeisel, M. B.; Baumert, T. F., Host-targeting therapies for hepatitis C virus infection: current developments and future applications. *Therapeutic Advances in Gastroenterology* **2018,** *11*, 1756284818759483.

195. Fernández-Hernando, C.; Ramírez, C. M.; Goedeke, L.; Suárez, Y., MicroRNAs in Metabolic Disease. *Arteriosclerosis, Thrombosis, and Vascular Biology* **2013,** *33* (2), 178-185.

196. Rautio, J.; Meanwell, N. A.; Di, L.; Hageman, M. J., The expanding role of prodrugs in contemporary drug design and development. *Nature Reviews Drug Discovery* **2018,** *17* (8), 559.

197. Fulmer, G. R.; Miller, A. J.; Sherden, N. H.; Gottlieb, H. E.; Nudelman, A.; Stoltz, B. M.; Bercaw, J. E.; Goldberg, K. I., NMR chemical shifts of trace impurities: common laboratory solvents, organics, and gases in deuterated solvents relevant to the organometallic chemist. *Organometallics* **2010,** *29* (9), 2176-2179.

198. Vorona, S.; Artamonova, T.; Zevatskii, Y.; Myznikov, L., An improved protocol for the preparation of 5-substituted tetrazoles from organic thiocyanates and nitriles. *Synthesis* **2014,** *46* (06), 781-786.

199. Brockunier, L. L.; He, J.; Colwell, L. F.; Habulihaz, B.; He, H.; Leiting, B.; Lyons, K. A.; Marsilio, F.; Patel, R. A.; Teffera, Y., Substituted piperazines as novel dipeptidyl peptidase IV inhibitors. *Bioorganic & Medicinal Chemistry Letters* **2004,** *14* (18), 4763-4766.

200. Blaazer, A. R.; Lange, J. H.; van der Neut, M. A.; Mulder, A.; den Boon, F. S.; Werkman, T. R.; Kruse, C. G.; Wadman, W. J., Novel indole and azaindole (pyrrolopyridine) cannabinoid (CB) receptor agonists: Design, synthesis, structure–activity relationships, physicochemical properties and biological activity. *European Journal of Medicinal Chemistry* **2011,** *46* (10), 5086-5098.

201. Itsenko, O.; Kihlberg, T.; Långström, B., Photoinitiated carbonylation with [11C] carbon monoxide using amines and alkyl iodides. *The Journal of Organic Chemistry* **2004,** *69* (13), 4356-4360.

202. Cheng, Y.; Zhang, C., MicroRNA-21 in cardiovascular disease. *Journal of Cardiovascular Translational Research* **2010,** *3* (3), 251-255.

203. Chan, J. A.; Krichevsky, A. M.; Kosik, K. S., MicroRNA-21 is an antiapoptotic factor in human glioblastoma cells. *Cancer Research* **2005,** *65* (14), 6029-6033.

204. Wang, H.; Tan, Z.; Hu, H.; Liu, H.; Wu, T.; Zheng, C.; Wang, X.; Luo, Z.; Wang, J.; Liu, S., microRNA-21 promotes breast cancer proliferation and metastasis by targeting LZTFL1. *BMC Cancer* **2019,** *19* (1), 738.

205. Zhao, J.; Zhang, Y.; Zhao, G., Emerging role of microRNA-21 in colorectal cancer. *Cancer Biomarkers* **2015,** *15* (3), 219-226.

206. Markou, A.; Zavridou, M.; Lianidou, E. S., miRNA-21 as a novel therapeutic target in lung cancer. *Lung Cancer: Targets and Therapy* **2016,** *7*, 19.

207. Sicard, F.; Gayral, M.; Lulka, H.; Buscail, L.; Cordelier, P., Targeting miR-21 for the therapy of pancreatic cancer. *Molecular Therapy* **2013,** *21* (5), 986-994.

208. Luu, H. N.; Lin, H.-Y.; Sørensen, K. D.; Ogunwobi, O. O.; Kumar, N.; Chornokur, G.; Phelan, C.; Jones, D.; Kidd, L.; Batra, J., miRNAs associated with prostate cancer risk and progression. *BMC Urology* **2017,** *17* (1), 18.

209. Sekar, D.; Krishnan, R.; Thirugnanasambantham, K.; Rajasekaran, B.; Islam, V. I. H.; Sekar, P., Significance of microRNA 21 in gastric cancer. *Clinics and Research in Hepatology and Gastroenterology* **2016,** *40* (5), 538-545.

210. Volinia, S.; Calin, G. A.; Liu, C.-G.; Ambs, S.; Cimmino, A.; Petrocca, F.; Visone, R.; Iorio, M.; Roldo, C.; Ferracin, M., A microRNA expression signature of human solid tumors defines cancer gene targets. *Proceedings of the National Academy of Sciences* **2006,** *103* (7), 2257-2261.

211. del Mar Díaz-González, S.; Rodríguez-Aguilar, E. D.; Meneses-Acosta, A.; Valadez-Graham, V.; Deas, J.; Gómez-Cerón, C.; Tavira-Montalván, C. A.; Arizmendi-Heras, A.; Ramírez-Bello, J.; Zurita-Ortega, M. E., Transregulation of microRNA miR-21 promoter by AP-1 transcription factor in cervical cancer cells. *Cancer Cell International* **2019,** *19* (1), 1-15.

212. Zhu, S.; Wu, H.; Wu, F.; Nie, D.; Sheng, S.; Mo, Y.-Y., MicroRNA-21 targets tumor suppressor genes in invasion and metastasis. *Cell Research* **2008,** *18* (3), 350-359.

213. Gabriely, G.; Wurdinger, T.; Kesari, S.; Esau, C. C.; Burchard, J.; Linsley, P. S.; Krichevsky, A. M., MicroRNA 21 Promotes Glioma Invasion by Targeting Matrix Metalloproteinase Regulators. *Molecular and Cellular Biology* **2008,** *28* (17), 5369-5380.

214. Asangani, I. A.; Rasheed, S. A.; Nikolova, D.; Leupold, J.; Colburn, N.; Post, S.; Allgayer, H., MicroRNA-21 (miR-21) post-transcriptionally downregulates tumor suppressor Pdcd4

and stimulates invasion, intravasation and metastasis in colorectal cancer. *Oncogene* **2008,** *27* (15), 2128-2136.

215. Asangani, I.; Rasheed, S.; Nikolova, D.; Leupold, J.; Colburn, N.; Post, S.; Allgayer, H., MicroRNA-21 (miR-21) post-transcriptionally downregulates tumor suppressor Pdcd4 and stimulates invasion, intravasation and metastasis in colorectal cancer. *Oncogene* **2008,** *27* (15), 2128-2136.

216. Yang, H.-S.; Knies, J. L.; Stark, C.; Colburn, N. H., Pdcd4 suppresses tumor phenotype in JB6 cells by inhibiting AP-1 transactivation. *Oncogene* **2003,** *22* (24), 3712-3720.

217. Sun, Q.; Miao, J.; Luo, J.; Yuan, Q.; Cao, H.; Su, W.; Zhou, Y.; Jiang, L.; Fang, L.; Dai, C., The feedback loop between miR-21, PDCD4 and AP-1 functions as a driving force for renal fibrogenesis. *Journal of Cell Science* **2018,** *131* (6), jcs202317.

218. Clark, J. C.; Thomas, D. M.; Choong, P. F.; Dass, C. R., RECK—a newly discovered inhibitor of metastasis with prognostic significance in multiple forms of cancer. *Cancer and Metastasis Reviews* **2007,** *26* (3-4), 675.

219. Zhang, Z.; Li, Z.; Gao, C.; Chen, P.; Chen, J.; Liu, W.; Xiao, S.; Lu, H., miR-21 plays a pivotal role in gastric cancer pathogenesis and progression. *Laboratory Investigation* **2008,** *88* (12), 1358-1366.

220. Sayed, D.; Rane, S.; Lypowy, J.; He, M.; Chen, I.-Y.; Vashistha, H.; Yan, L.; Malhotra, A.; Vatner, D.; Abdellatif, M., MicroRNA-21 targets Sprouty2 and promotes cellular outgrowths. *Molecular Biology of the Cell* **2008,** *19* (8), 3272-3282.

221. Wu, Y.; Song, Y.; Xiong, Y.; Wang, X.; Xu, K.; Han, B.; Bai, Y.; Li, L.; Zhang, Y.; Zhou, L., MicroRNA-21 (Mir-21) promotes cell growth and invasion by repressing tumor suppressor PTEN in colorectal cancer. *Cellular Physiology and Biochemistry* **2017,** *43* (3), 945-958.

222. Shi, G.-h.; Ye, D.-w.; Yao, X.-d.; Zhang, S.-l.; Dai, B.; Zhang, H.-l.; Shen, Y.-j.; Zhu, Y.; Zhu, Y.-p.; Xiao, W.-j., Involvement of microRNA-21 in mediating chemo-resistance to docetaxel in androgen-independent prostate cancer PC3 cells. *Acta Pharmacologica Sinica* **2010,** *31* (7), 867-873.

223. Si, M.; Zhu, S.; Wu, H.; Lu, Z.; Wu, F.; Mo, Y., miR-21-mediated tumor growth. *Oncogene* **2007,** *26* (19), 2799-2803.

224. Medina, P. P.; Nolde, M.; Slack, F. J., OncomiR addiction in an in vivo model of microRNA-21-induced pre-B-cell lymphoma. *Nature* **2010,** *467* (7311), 86-90.

225. Schmittgen, T. D.; Jiang, J.; Liu, Q.; Yang, L., A high-throughput method to monitor the expression of microRNA precursors. *Nucleic Acids Research* **2004,** *32* (4), e43-e43.

226. Cheng, Y.; Liu, X.; Zhang, S.; Lin, Y.; Yang, J.; Zhang, C., MicroRNA-21 protects against the H 2 O 2-induced injury on cardiac myocytes via its target gene PDCD4. *Journal of Molecular and Cellular Cardiology* **2009,** *47* (1), 5-14.

227. Lopez-Lázaro, M., Dual role of hydrogen peroxide in cancer: possible relevance to cancer chemoprevention and therapy. *Cancer Letters* **2007,** *252* (1), 1-8.

228. Ankenbruck, N.; Kumbhare, R.; Naro, Y.; Thomas, M.; Gardner, L.; Emanuelson, C.; Deiters, A., Small molecule inhibition of microRNA-21 expression reduces cell viability and microtumor formation. *Bioorganic & Medicinal Chemistry* **2019,** *27* (16), 3735-3743.

229. Thorne, N.; Shen, M.; Lea, W. A.; Simeonov, A.; Lovell, S.; Auld, D. S.; Inglese, J., Firefly luciferase in chemical biology: a compendium of inhibitors, mechanistic evaluation of chemotypes, and suggested use as a reporter. *Chemistry & Biology* **2012,** *19* (8), 1060-1072.

230. Scudiero, D. A.; Shoemaker, R. H.; Paull, K. D.; Monks, A.; Tierney, S.; Nofziger, T. H.; Currens, M. J.; Seniff, D.; Boyd, M. R., Evaluation of a soluble tetrazolium/formazan assay for cell growth and drug sensitivity in culture using human and other tumor cell lines. *Cancer Research* **1988,** *48* (17), 4827-4833.

231. Du, G.; Cao, D.; Meng, L., miR-21 inhibitor suppresses cell proliferation and colony formation through regulating the PTEN/AKT pathway and improves paclitaxel sensitivity in cervical cancer cells. *Molecular Medicine Reports* **2017,** *15* (5), 2713-2719.

232. Gu, J.-B.; Bao, X.-B.; Ma, Z., Effects of miR-21 on proliferation and apoptosis in human gastric adenocarcinoma cells. *Oncology Letters* **2018,** *15* (1), 618-622.

233. Zhou, B.; Wang, D.; Sun, G.; Mei, F.; Cui, Y.; Xu, H., Effect of miR-21 on apoptosis in lung cancer cell through inhibiting the PI3K/Akt/NF-κB signaling pathway in vitro and in vivo. *Cellular Physiology and Biochemistry* **2018,** *46* (3), 999-1008.

234. Najafi, Z.; Sharifi, M.; Javadi, G., Degradation of miR-21 induces apoptosis and inhibits cell proliferation in human hepatocellular carcinoma. *Cancer Gene Therapy* **2015,** *22* (11), 530-535.

235. Wagenaar, T. R.; Zabludoff, S.; Ahn, S.-M.; Allerson, C.; Arlt, H.; Baffa, R.; Cao, H.; Davis, S.; Garcia-Echeverria, C.; Gaur, R., Anti–miR-21 suppresses hepatocellular carcinoma growth via broad transcriptional network deregulation. *Molecular Cancer Research* **2015,** *13* (6), 1009-1021.

236. Lam, H. C.; Liu, H.-J.; Baglini, C. V.; Filippakis, H.; Alesi, N.; Nijmeh, J.; Du, H.; Lope, A. L.; Cottrill, K. A.; Handen, A., Rapamycin-induced miR-21 promotes mitochondrial homeostasis and adaptation in mTORC1 activated cells. *Oncotarget* **2017,** *8* (39), 64714.

237. Wang, P.; Guan, Q.; Zhou, D.; Yu, Z.; Song, Y.; Qiu, W., miR-21 inhibitors modulate biological functions of gastric cancer cells via PTEN/PI3K/mTOR pathway. *DNA and Cell Biology* **2018,** *37* (1), 38-45.

238. Yao, Q.; Xu, H.; Zhang, Q.-Q.; Zhou, H.; Qu, L.-H., MicroRNA-21 promotes cell proliferation and down-regulates the expression of programmed cell death 4 (PDCD4) in HeLa cervical carcinoma cells. *Biochemical and Biophysical Research Communications* **2009,** *388* (3), 539-542.

239. Zhang, H. L.; Si, L. B.; Zeng, A.; Long, F.; Qi, Z.; Zhao, R.; Bai, M., MicroRNA-21 antisense oligonucleotide improves the sensitivity of A375 human melanoma cell to Cisplatin: An in vitro study. *Journal of Cellular Biochemistry* **2018,** *119* (4), 3129-3141.

240. Misawa, A.; Katayama, R.; Koike, S.; Tomida, A.; Watanabe, T.; Fujita, N., AP-1-Dependent miR-21 expression contributes to chemoresistance in cancer stem cell-like SP cells. *Oncology Research Featuring Preclinical and Clinical Cancer Therapeutics* **2010,** *19* (1), 23-33.

241. Chen, B.; Chen, X.; Wu, X.; Wang, X.; Wang, Y.; Lin, T.-Y.; Kurata, J.; Wu, J.; Vonderfecht, S.; Sun, G., Disruption of microRNA-21 by TALEN leads to diminished cell transformation and increased expression of cell–environment interaction genes. *Cancer Letters* **2015,** *356* (2), 506-516.

242. Xiong, G.; Huang, Z.; Jiang, H.; Pan, Z.; Xie, J.; Wang, S., Inhibition of microRNA-21 decreases the invasiveness of fibroblast-like synoviocytes in rheumatoid arthritis via TGFβ/Smads signaling pathway. *Iranian Journal of Basic Medical Sciences* **2016,** *19* (7), 787.

243. Yang, C. H.; Yue, J.; Pfeffer, S. R.; Handorf, C. R.; Pfeffer, L. M., MicroRNA miR-21 regulates the metastatic behavior of B16 melanoma cells. *Journal of Biological Chemistry* **2011,** *286* (45), 39172-39178.

244. Nedaeinia, R.; Sharifi, M.; Avan, A.; Kazemi, M.; Nabinejad, A.; Ferns, G. A.; Ghayour-Mobarhan, M.; Salehi, R., Inhibition of microRNA-21 via locked nucleic acid-anti-miR suppressed metastatic features of colorectal cancer cells through modulation of programmed cell death 4. *Tumor Biology* **2017,** *39* (3), 1010428317692261.

245. Liu, Z.-L.; Wang, H.; Liu, J.; Wang, Z.-X., MicroRNA-21 (miR-21) expression promotes growth, metastasis, and chemo-or radioresistance in non-small cell lung cancer cells by targeting PTEN. *Molecular and Cellular Biochemistry* **2013,** *372* (1-2), 35-45.

246. Bose, D.; Jayaraj, G.; Suryawanshi, H.; Agarwala, P.; Pore, S. K.; Banerjee, R.; Maiti, S., The tuberculosis drug streptomycin as a potential cancer therapeutic: inhibition of miR-21 function by directly targeting its precursor. *Angewandte Chemie International Edition* **2012,** *51* (4), 1019-1023.

247. Summerton, J. E., Morpholino, siRNA, and S-DNA compared: impact of structure and mechanism of action on off-target effects and sequence specificity. *Current Topics in Medicinal Chemistry* **2007,** *7* (7), 651-660.

248. Zamecnik, P. C.; Stephenson, M. L., Inhibition of Rous sarcoma virus replication and cell transformation by a specific oligodeoxynucleotide. *Proceedings of the National Academy of Sciences* **1978,** *75* (1), 280-284.

249. Eckstein, F., Phosphorothioate oligodeoxynucleotides: what is their origin and what is unique about them? *Antisense and Nucleic Acid Drug Development* **2000,** *10* (2), 117-121.

250. Guga, P.; Koziołkiewicz, M., Phosphorothioate nucleotides and oligonucleotides–recent progress in synthesis and application. *Chemistry & Biodiversity* **2011,** *8* (9), 1642-1681.

251. Krieg, A. M.; Stein, C., Phosphorothioate oligodeoxynucleotides: antisense or anti-protein? *Antisense Research and Development* **1995,** *5* (4), 241-241.

252. Summerton, J.; WELLER, D., Morpholino antisense oligomers: design, preparation, and properties. *Antisense and Nucleic Acid Drug Development* **1997,** *7* (3), 187-195.

253. Corey, D. R.; Abrams, J. M., Morpholino antisense oligonucleotides: tools for investigating vertebrate development. *Genome Biology* **2001,** *2* (5), 1-3.

254. Robu, M. E.; Larson, J. D.; Nasevicius, A.; Beiraghi, S.; Brenner, C.; Farber, S. A.; Ekker, S. C., p53 activation by knockdown technologies. *PLOS Genetics* **2007,** *3* (5), e78.

255. Stein, D.; FOSTER, E.; HUANG, S.-B.; WELLER, D.; SUMMERTON, J., A specificity comparison of four antisense types: morpholino, 2′-O-methyl RNA, DNA, and phosphorothioate DNA. *Antisense and Nucleic Acid Drug Development* **1997,** *7* (3), 151-157.

256. Kloosterman, W. P.; Wienholds, E.; Ketting, R. F.; Plasterk, R. H., Substrate requirements for let-7 function in the developing zebrafish embryo. *Nucleic Acids Research* **2004,** *32* (21), 6284-6291.

257. Flynt, A. S.; Li, N.; Thatcher, E. J.; Solnica-Krezel, L.; Patton, J. G., Zebrafish miR-214 modulates Hedgehog signaling to specify muscle cell fate. *Nature Genetics* **2007,** *39* (2), 259-263.

258. Kloosterman, W. P.; Lagendijk, A. K.; Ketting, R. F.; Moulton, J. D.; Plasterk, R. H., Targeted inhibition of miRNA maturation with morpholinos reveals a role for miR-375 in pancreatic islet development. *PLoS Biology* **2007,** *5* (8), e203.

259. Nasevicius, A.; Ekker, S. C., Effective targeted gene ‘knockdown’in zebrafish. *Nature Genetics* **2000,** *26* (2), 216-220.

260. Kos, R.; Reedy, M. V.; Johnson, R. L.; Erickson, C. A., The winged-helix transcription factor FoxD3 is important for establishing the neural crest lineage and repressing melanogenesis in avian embryos. *Development* **2001,** *128* (8), 1467-1479.

261. Howard, E. W.; Newman, L. A.; Oleksyn, D. W.; Angerer, R. C.; Angerer, L. M., SpKrl: a direct target of beta-catenin regulation required for endoderm differentiation in sea urchin embryos. *Development* **2001,** *128* (3), 365-375.

262. Shestopalov, I. A.; Sinha, S.; Chen, J. K., Light-controlled gene silencing in zebrafish embryos. *Nature Chemical Biology* **2007,** *3* (10), 650-651.

263. Schulte-Merker, S.; Ho, R.; Herrmann, B.; Nusslein-Volhard, C., The protein product of the zebrafish homologue of the mouse T gene is expressed in nuclei of the germ ring and the notochord of the early embryo. *Development* **1992,** *116* (4), 1021-1032.

264. Halpern, M. E.; Ho, R. K.; Walker, C.; Kimmel, C. B., Induction of muscle pioneers and floor plate is distinguished by the zebrafish no tail mutation. *Cell* **1993,** *75* (1), 99-111.

265. Tomasini, A. J.; Schuler, A. D.; Zebala, J. A.; Mayer, A. N., PhotoMorphs™: A novel light-activated reagent for controlling gene expression in zebrafish. *Genesis* **2009,** *47* (11), 736-743.

266. Tallafuss, A.; Gibson, D.; Morcos, P.; Li, Y.; Seredick, S.; Eisen, J.; Washbourne, P., Turning gene function ON and OFF using sense and antisense photo-morpholinos in zebrafish. *Development* **2012,** *139* (9), 1691-1699.

267. Deiters, A.; Garner, R. A.; Lusic, H.; Govan, J. M.; Dush, M.; Nascone-Yoder, N. M.; Yoder, J. A., Photocaged morpholino oligomers for the light-regulation of gene function in zebrafish and Xenopus embryos. *Journal of the American Chemical Society* **2010,** *132* (44), 15644-15650.

268. Yamazoe, S.; Shestopalov, I. A.; Provost, E.; Leach, S. D.; Chen, J. K., Cyclic caged morpholinos: conformationally gated probes of embryonic gene function. *Angewandte Chemie International Edition* **2012,** *51* (28), 6908-6911.

269. Yamazoe, S.; Liu, Q.; McQuade, L. E.; Deiters, A.; Chen, J. K., Sequential Gene Silencing Using Wavelength-Selective Caged Morpholino Oligonucleotides. *Angewandte Chemie International Edition* **2014,** *53* (38), 10114-10118.

270. Yamazoe, S.; McQuade, L. E.; Chen, J. K., Nitroreductase-activatable morpholino oligonucleotides for in vivo gene silencing. *ACS Chemical Biology* **2014,** *9* (9), 1985-1990.

271. Ash, C.; Dubec, M.; Donne, K.; Bashford, T., Effect of wavelength and beam width on penetration in light-tissue interaction using computational methods. *Lasers in Medical Science* **2017,** *32* (8), 1909-1918.

272. Sletten, E. M.; Bertozzi, C. R., Bioorthogonal chemistry: fishing for selectivity in a sea of functionality. *Angewandte Chemie International Edition* **2009,** *48* (38), 6974-6998.

273. Prescher, J. A.; Dube, D. H.; Bertozzi, C. R., Chemical remodelling of cell surfaces in living animals. *Nature* **2004,** *430* (7002), 873-877.

274. Stöckmann, H.; Neves, A. A.; Stairs, S.; Brindle, K. M.; Leeper, F. J., Exploring isonitrile-based click chemistry for ligation with biomolecules. *Organic & Biomolecular Chemistry* **2011,** *9* (21), 7303-7305.

275. McKay, C. S.; Finn, M., Click chemistry in complex mixtures: bioorthogonal bioconjugation. *Chemistry & Biology* **2014,** *21* (9), 1075-1101.

276. Chen, Y.; Kamlet, A. S.; Steinman, J. B.; Liu, D. R., A biomolecule-compatible visible-light-induced azide reduction from a DNA-encoded reaction-discovery system. *Nature Chemistry* **2011,** *3* (2), 146.

277. Rieder, U.; Luedtke, N., Alkene-tetrazine ligation for imaging cellular DNA. *Angewandte Chemie International Edition* **2014,** *53* (35), 9168.

278. Blackman, M. L.; Royzen, M.; Fox, J. M., Tetrazine ligation: fast bioconjugation based on inverse-electron-demand Diels− Alder reactivity. *Journal of the American Chemical Society* **2008,** *130* (41), 13518-13519.

279. Knall, A.-C.; Slugovc, C., Inverse electron demand Diels–Alder (iEDDA)-initiated conjugation: a (high) potential click chemistry scheme. *Chemical Society Reviews* **2013,** *42* (12), 5131-5142.

280. Presolski, S. I.; Hong, V. P.; Finn, M., Copper-Catalyzed Azide–Alkyne Click Chemistry for Bioconjugation. *Current Protocols in Chemical Biology* **2011**, 153-162.

281. Shelbourne, M.; Chen, X.; Brown, T.; El-Sagheer, A. H., Fast copper-free click DNA ligation by the ring-strain promoted alkyne-azide cycloaddition reaction. *Chemical Communications* **2011,** *47* (22), 6257-6259.

282. Versteegen, R. M.; Rossin, R.; ten Hoeve, W.; Janssen, H. M.; Robillard, M. S., Click to release: instantaneous doxorubicin elimination upon tetrazine ligation. *Angewandte Chemie International Edition* **2013,** *52* (52), 14112-14116.

283. Fan, X.; Ge, Y.; Lin, F.; Yang, Y.; Zhang, G.; Ngai, W. S. C.; Lin, Z.; Zheng, S.; Wang, J.; Zhao, J., Optimized tetrazine derivatives for rapid bioorthogonal decaging in living cells. *Angewandte Chemie International Edition* **2016,** *55* (45), 14046-14050.

284. Carlson, J. C.; Mikula, H.; Weissleder, R., Unraveling tetrazine-triggered bioorthogonal elimination enables chemical tools for ultrafast release and universal cleavage. *Journal of the American Chemical Society* **2018,** *140* (10), 3603-3612.

285. Sarris, A. J.; Hansen, T.; de Geus, M. A.; Maurits, E.; Doelman, W.; Overkleeft, H. S.; Codée, J. D.; Filippov, D. V.; van Kasteren, S. I., Fast and pH-Independent Elimination of trans-Cyclooctene by Using Aminoethyl-Functionalized Tetrazines. *Chemistry–A European Journal* **2018,** *24* (68), 18075-18081.

286. Toshimitsu, A.; Aoai, T.; Owada, H.; Uemura, S.; Okano, M., Phenylselenenyl chloride in acetonitrile-water: A highly convenient reagent for hydroxyselenation of olefins and preparation of cyclic ethers from dienes. *Tetrahedron* **1985,** *41* (22), 5301-5306.

287. Becker, N.; Carreira, E. M., Hydroxyl-directed nitrile oxide cycloaddition reactions with cyclic allylic alcohols. *Organic Letters* **2007,** *9* (19), 3857-3858.

288. Royzen, M.; Yap, G. P.; Fox, J. M., A photochemical synthesis of functionalized trans-cyclooctenes driven by metal complexation. *Journal of the American Chemical Society* **2008,** *130* (12), 3760-3761.

289. Chen, X.; Zhou, X.-Y.; Wu, H.; Lei, Y.-Z.; Li, J.-H., Highly efficient reduction of nitro compounds: Recyclable Pd/C-catalyzed transfer hydrogenation with ammonium formate or hydrazine hydrate as hydrogen source. *Synthetic Communications* **2018,** *48* (19), 2475-2484.

290. Fang, Y.; Judkins, J. C.; Boyd, S. J.; am Ende, C. W.; Rohlfing, K.; Huang, Z.; Xie, Y.; Johnson, D. S.; Fox, J. M., Studies on the stability and stabilization of trans-cyclooctenes through radical inhibition and silver (I) metal complexation. *Tetrahedron* **2019,** *75* (32), 4307-4317.

291. Reddy, V. V.; Naga Brahmeswara Rao, M. V.; Reddy, G. M.; Mukkanti, K.; Reddy, G. M., Synthesis and spectral characterization of related substances of Vardenafil, an erectile dysfunction drug. *Synthetic Communications* **2012,** *42* (23), 3513-3523.

292. Rulev, A. Y., Aza-Michael reaction: achievements and prospects. *Russian Chemical Reviews* **2011,** *80* (3), 197.

293. Versteegen, R. M.; ten Hoeve, W.; Rossin, R.; de Geus, M. A.; Janssen, H. M.; Robillard, M. S., Click-to-Release from trans-Cyclooctenes: Mechanistic Insights and Expansion of Scope from Established Carbamate to Remarkable Ether Cleavage. *Angewandte Chemie International Edition* **2018,** *57* (33), 10494-10499.

294. Rossin, R.; van Duijnhoven, S. M.; Ten Hoeve, W.; Janssen, H. M.; Kleijn, L. H.; Hoeben, F. J.; Versteegen, R. M.; Robillard, M. S., Triggered drug release from an antibody–drug conjugate using fast "click-to-release" chemistry in mice. *Bioconjugate Chemistry* **2016,** *27* (7), 1697-1706.

295. Taylor, M. T.; Blackman, M. L.; Dmitrenko, O.; Fox, J. M., Design and synthesis of highly reactive dienophiles for the tetrazine–trans-cyclooctene ligation. *Journal of the American Chemical Society* **2011,** *133* (25), 9646-9649.

296. Darko, A.; Wallace, S.; Dmitrenko, O.; Machovina, M. M.; Mehl, R. A.; Chin, J. W.; Fox, J. M., Conformationally strained trans-cyclooctene with improved stability and excellent reactivity in tetrazine ligation. *Chemical Science* **2014,** *5* (10), 3770-3776.

297. O'Brien, J. G.; Chintala, S. R.; Fox, J. M., Stereoselective Synthesis of Bicyclo [6.1. 0] nonene Precursors of the Bioorthogonal Reagents s-TCO and BCN. *The Journal of Organic Chemistry* **2017,** *83* (14), 7500-7503.

298. Bakkali, H.; Marie, C.; Ly, A.; Thobie-Gautier, C.; Graton, J.; Pipelier, M.; Sengmany, S.; Léonel, E.; Nédélec, J. Y.; Evain, M., Functionalized 2, 5-Dipyridinylpyrroles by Electrochemical Reduction of 3, 6-Dipyridinylpyridazine Precursors. *European Journal of Organic Chemistry* **2008,** *2008* (12), 2156-2166.

299. Xing, L.; Zhang, Y.; Li, B.; Du, Y., In situ formation of RSCl/ArSeCl and their application to the synthesis of 4-chalcogenylisocumarins/pyrones from o-(1-alkynyl) benzoates and (z)-2-alken-4-ynoates. *Organic Letters* **2019,** *21* (10), 3620-3624.

300. Chen, X.; Wu, H.; Su, W.; Xu, R.; Liu, M.; Ding, J., Active metallic indium-mediated ring-opening of epoxides with diphenyl diselenides: a novel one-pot synthesis of β-hydroxy selenides in aqueous media. *Journal of Chemical Research* **2007,** *2007* (6), 325-327.

301. Mao, W.; Shi, W.; Li, J.; Su, D.; Wang, X.; Zhang, L.; Pan, L.; Wu, X.; Wu, H., Organocatalytic and Scalable Syntheses of Unsymmetrical 1, 2, 4, 5-Tetrazines by Thiol-Containing Promotors. *Angewandte Chemie International Edition* **2019,** *58* (4), 1106.

302. Feng, H.; Zhang, H.; Wang, M.; Vannam, R.; Wang, H.; Yan, X.; Ouyang, W.; Jia, X.; Fox, J.; Li, Z., Improving Tumor-to-Background Contrast Through Hydrophilic Tetrazines: The Construction of 18F Labeled PET Agents Targeting Non-Small Cell Lung Carcinoma. *Chemistry–A European Journal* **2020**.

303. Davies, S.; Oliveira, B. L.; Bernardes, G. J., Development of a self-immolative linker for tetrazine-triggered release of alcohols in cells. *Organic & Biomolecular Chemistry* **2019,** *17* (23), 5725-5730.

304. Bush, K.; Bradford, P. A., Interplay between β-lactamases and new β-lactamase inhibitors. *Nature Reviews Microbiology* **2019,** *17* (5), 295.

305. Crowfoot, D.; Bunn, C. W.; Rogers-Low, B. W.; Turner-Jones, A., X-ray crystallographic investigation of the structure of penicillin. *The Chemistry of Penicillin* **1949**, 310-367.

306. Zeng, X.; Lin, J., Beta-lactamase induction and cell wall metabolism in Gram-negative bacteria. *Frontiers in Microbiology* **2013,** *4*, 128.

307. Drawz, S. M.; Bonomo, R. A., Three decades of β-lactamase inhibitors. *Clinical Microbiology Reviews* **2010,** *23* (1), 160-201.

308. Papp-Wallace, K. M.; Endimiani, A.; Taracila, M. A.; Bonomo, R. A., Carbapenems: past, present, and future. *Antimicrobial Agents and Chemotherapy* **2011,** *55* (11), 4943-4960.

309. Gurusamy, K. S.; Koti, R.; Toon, C. D.; Wilson, P.; Davidson, B. R., Antibiotic therapy for the treatment of methicillin-resistant Staphylococcus aureus (MRSA) infections in surgical wounds. *Cochrane Database of Systematic Reviews* **2013,** (8).

310. Hancock, R. E.; Woodruff, W. A., Roles of porin and β-lactamase in β-lactam resistance of Pseudomonas aeruginosa. *Clinical Infectious Diseases* **1988,** *10* (4), 770-775.

311. Abraham, E.; Chain, E., An enzyme from bacteria able to destroy penicillin. 1940. *Reviews of Infectious Diseases* **1988,** *10* (4), 677.

312. Massova, I.; Mobashery, S., Kinship and diversification of bacterial penicillin-binding proteins and β-lactamases. *Antimicrobial Agents and Chemotherapy* **1998,** *42* (1), 1-17.

313. Bonomo, R. A., β-Lactamases: a focus on current challenges. *Cold Spring Harbor Perspectives in Medicine* **2017,** *7* (1), a025239.

314. Minasov, G.; Wang, X.; Shoichet, B. K., An ultrahigh resolution structure of TEM-1 β-lactamase suggests a role for Glu166 as the general base in acylation. *Journal of the American Chemical Society* **2002,** *124* (19), 5333-5340.

315. Chen, Y.; McReynolds, A.; Shoichet, B. K., Re-examining the role of Lys67 in class C β-lactamase catalysis. *Protein Science* **2009,** *18* (3), 662-669.

316. Verma, V.; Testero, S. A.; Amini, K.; Wei, W.; Liu, J.; Balachandran, N.; Monoharan, T.; Stynes, S.; Kotra, L. P.; Golemi-Kotra, D., Hydrolytic mechanism of OXA-58 enzyme, a carbapenem-hydrolyzing class D β-lactamase from Acinetobacter baumannii. *Journal of Biological Chemistry* **2011,** *286* (43), 37292-37303.

317. Garau, G.; Di Guilmi, A. M.; Hall, B. G., Structure-based phylogeny of the metallo-β-lactamases. *Antimicrobial Agents and Chemotherapy* **2005,** *49* (7), 2778-2784.

318. Zlokarnik, G.; Negulescu, P. A.; Knapp, T. E.; Mere, L.; Burres, N.; Feng, L.; Whitney, M.; Roemer, K.; Tsien, R. Y., Quantitation of transcription and clonal selection of single living cells with β-lactamase as reporter. *Science* **1998,** *279* (5347), 84-88.

319. Raz, E.; Zlokarnik, G.; Tsien, R. Y.; Driever, W., β-lactamase as a marker for gene expression in live zebrafish embryos. *Developmental Biology* **1998,** *203* (2), 290-294.

320. Qureshi, S. A., β-Lactamase: an ideal reporter system for monitoring gene expression in live eukaryotic cells. *BioTechniques* **2007,** *42* (1), 91-96.

321. Patterson, L. D.; Miller, M. J., Enzymatic deprotection of the cephalosporin 3′-acetoxy group using Candida antarctica lipase B. *The Journal of Organic Chemistry* **2010,** *75* (4), 1289-1292.

322. Hayashi, K.-i.; Kusaka, N.; Yamasaki, S.; Zhao, Y.; Nozaki, H., Development of 4-methoxy-7-nitroindolinyl (MNI)-caged auxins which are extremely stable in planta. *Bioorganic & Medicinal Chemistry Letters* **2015,** *25* (20), 4464-4471.

323. Aravapalli, S.; Lai, H.; Teramoto, T.; Alliston, K. R.; Lushington, G. H.; Ferguson, E. L.; Padmanabhan, R.; Groutas, W. C., Inhibitors of Dengue virus and West Nile virus

proteases based on the aminobenzamide scaffold. *Bioorganic & Medicinal Chemistry* **2012,** *20* (13), 4140-4148.

324. Nicolaou, K.; Estrada, A. A.; Zak, M.; Lee, S. H.; Safina, B. S., A mild and selective method for the hydrolysis of esters with trimethyltin hydroxide. *Angewandte Chemie International Edition* **2005,** *44* (9), 1378-1382.

325. Sarkar, K.; Madras, G.; Chatterjee, K., Dendron conjugation to graphene oxide using click chemistry for efficient gene delivery. *RSC Advances* **2015,** *5* (62), 50196-50211.

326. O'Callaghan, C. H.; Morris, A.; Kirby, S. M.; Shingler, A., Novel method for detection of β-lactamases by using a chromogenic cephalosporin substrate. *Antimicrobial Agents and Chemotherapy* **1972,** *1* (4), 283-288.

327. de Sá, A.; Prata, M. I. M.; Geraldes, C. F.; André, J. P., Triaza-based amphiphilic chelators: Synthetic route, in vitro characterization and in vivo studies of their Ga (III) and Al (III) chelates. *Journal of Inorganic Biochemistry* **2010,** *104* (10), 1051-1062.

328. Martin, S.; Paoletti, E.; Moss, B., Purification of mRNA guanylyltransferase and mRNA (guanine-7-) methyltransferase from vaccinia virions. *Journal of Biological Chemistry* **1975,** *250* (24), 9322-9329.

329. Furuichi, Y., Discovery of m7G-cap in eukaryotic mRNAs. *Proceedings of the Japan Academy, Series B* **2015,** *91* (8), 394-409.

330. Wei, C.-M.; Gershowitz, A.; Moss, B., Methylated nucleotides block 5′ terminus of HeLa cell messenger RNA. *Cell* **1975,** *4* (4), 379-386.

331. Furuichi, Y.; Muthukrishnan, S.; Shatkin, A., 5'-Terminal m-7G (5') ppp (5') Gmp in vivo: identification in reovirus genome RNA. *Proceedings of the National Academy of Sciences* **1975,** *72* (2), 742-745.

332. Varani, G., A cap for all occasions. *Structure* **1997,** *5* (7), 855-858.

333. Liu, H.; Kiledjian, M., Decapping the message: a beginning or an end. Portland Press Ltd.: 2006.

334. Lewis, J. D.; Görlich, D.; Mattaj, I. W., A yeast cap binding protein complex (yCBC) acts at an early step in pre-mRNA splicing. *Nucleic Acids Research* **1996,** *24* (17), 3332-03336.

335. Lewis, J. D.; Izaurralde, E.; Jarmolowski, A.; McGuigan, C.; Mattaj, I. W., A nuclear cap-binding complex facilitates association of U1 snRNP with the cap-proximal 5'splice site. *Genes & Development* **1996,** *10* (13), 1683-1698.

336. Muthukrishnan, S.; Both, G.; Furuichi, Y.; Shatkin, A., 5′-Terminal 7-methylguanosine in eukaryotic mRNA is required for translation. *Nature* **1975,** *255* (5503), 33-37.

337. Gingras, A.-C.; Raught, B.; Sonenberg, N., eIF4 initiation factors: effectors of mRNA recruitment to ribosomes and regulators of translation. *Annual Review of Biochemistry* **1999,** *68* (1), 913-963.

338. Merrick, W., The pathway and mechanism of eukaryotic protein synthesis. *Translational Control* **1996**, 31-69.

339. Montero, H.; García-Román, R.; Mora, S. I., eIF4E as a control target for viruses. *Viruses* **2015,** *7* (2), 739-750.

340. Sonenberg, N., eIF4E, the mRNA cap-binding protein: from basic discovery to translational research. *Biochemistry and Cell Biology* **2008,** *86* (2), 178-183.

341. Ghosh, A.; Lima, C. D., Enzymology of RNA cap synthesis. *Wiley Interdisciplinary Reviews: RNA* **2010,** *1* (1), 152-172.

342. Bisaillon, M.; Shuman, S., Structure-function analysis of the active site tunnel of yeast RNA triphosphatase. *Journal of Biological Chemistry* **2001,** *276* (20), 17261-17266.

343. Gong, C.; Martins, A.; Shuman, S., Structure-function analysis of Trypanosoma brucei RNA triphosphatase and evidence for a two-metal mechanism. *Journal of Biological Chemistry* **2003,** *278* (51), 50843-50852.

344. Takagi, T.; Moore, C. R.; Diehn, F.; Buratowski, S., An RNA 5′-triphosphatase related to the protein tyrosine phosphatases. *Cell* **1997,** *89* (6), 867-873.

345. Shuman, S.; Lima, C. D., The polynucleotide ligase and RNA capping enzyme superfamily of covalent nucleotidyltransferases. *Current Opinion in Structural Biology* **2004,** *14* (6), 757-764.

346. Muttach, F.; Muthmann, N.; Rentmeister, A., Synthetic mRNA capping. *Beilstein Journal of Organic Chemistry* **2017,** *13* (1), 2819-2832.

347. Bangs, J. D.; Crain, P.; Hashizume, T.; McCloskey, J.; Boothroyd, J., Mass spectrometry of mRNA cap 4 from trypanosomatids reveals two novel nucleosides. *Journal of Biological Chemistry* **1992,** *267* (14), 9805-9815.

348. Matera, A. G.; Terns, R. M.; Terns, M. P., Non-coding RNAs: lessons from the small nuclear and small nucleolar RNAs. *Nature Reviews Molecular Cell Biology* **2007,** *8* (3), 209-220.

349. Bird, J. G.; Zhang, Y.; Tian, Y.; Panova, N.; Barvík, I.; Greene, L.; Liu, M.; Buckley, B.; Krásný, L.; Lee, J. K., The mechanism of RNA 5′ capping with NAD+, NADH and desphospho-CoA. *Nature* **2016,** *535* (7612), 444-447.

350. Cahová, H.; Winz, M.-L.; Höfer, K.; Nübel, G.; Jäschke, A., NAD captureSeq indicates NAD as a bacterial cap for a subset of regulatory RNAs. *Nature* **2015,** *519* (7543), 374-377.

351. Martin, S.; Moss, B., Modification of RNA by mRNA guanylyltransferase and mRNA (guanine-7-) methyltransferase from vaccinia virions. *Journal of Biological Chemistry* **1975,** *250* (24), 9330-9335.

352. Furuichi, Y.; Muthukrishnan, S.; Tomasz, J.; Shatkin, A., Mechanism of formation of reovirus mRNA 5'-terminal blocked and methylated sequence, m7GpppGmpC. *Journal of Biological Chemistry* **1976,** *251* (16), 5043-5053.

353. Rosenberg, M.; Paterson, B. M., Efficient cap-dependent translation of polycistronic prokaryotic mRNAs is restricted to the first gene in the operon. *Nature* **1979,** *279* (5715), 696-701.

354. Myette, J. R.; Niles, E. G., Domain Structure of the Vaccinia Virus mRNA Capping Enzyme Expression in Escherichia coli of a Subdomain Possessing the RNA 5′-Triphosphatase and Guanylyltransferase Activities and a Kinetic Comparison to the Full-Size Enzyme. *Journal of Biological Chemistry* **1996,** *271* (20), 11936-11944.

355. Shuman, S.; Surks, M.; Furneaux, H.; Hurwitz, J., Purification and characterization of a GTP-pyrophosphate exchange activity from vaccinia virions. Association of the GTP-pyrophosphate exchange activity with vaccinia mRNA guanylyltransferase. RNA (guanine-7-) methyltransferase complex (capping enzyme). *Journal of Biological Chemistry* **1980,** *255* (23), 11588-11598.

356. Paterson, B. M.; Rosenberg, M., Efficient translation of prokaryotic mRNAs in a eukaryotic cell-free system requires addition of a cap structure. *Nature* **1979,** *279* (5715), 692-696.

357. Contreras, R.; Cheroutre, H.; Degrave, W.; Fiers, W., Simple, efficient in vitro synthesis of capped RNA useful for direct expression of cloned eukaryoti genes. *Nucleic Acids Research* **1982,** *10* (20), 6353-6362.

358. Pelletier, J.; Sonenberg, N., Insertion mutagenesis to increase secondary structure within the 5′ noncoding region of a eukaryotic mRNA reduces translational efficiency. *Cell* **1985,** *40* (3), 515-526.

359. Fuchs, A.-L.; Neu, A.; Sprangers, R., A general method for rapid and cost-efficient large-scale production of 5′ capped RNA. *RNA* **2016,** *22* (9), 1454-1466.

360. Bougie, I.; Bisaillon, M., The broad spectrum antiviral nucleoside ribavirin as a substrate for a viral RNA capping enzyme. *Journal of Biological Chemistry* **2004,** *279* (21), 22124-22130.

361. Issur, M.; Bougie, I.; Despins, S.; Bisaillon, M., Enzymatic synthesis of RNAs capped with nucleotide analogues reveals the molecular basis for substrate selectivity of RNA capping enzyme: impacts on RNA metabolism. *PLoS One* **2013,** *8* (9), e75310.

362. Pasquinelli, A.; Dahlberg, J. E.; Lund, E., Reverse 5'caps in RNAs made in vitro by phage RNA polymerases. *RNA* **1995,** *1* (9), 957-967.

363. Peng, Z.-H.; Sharma, V.; Singleton, S. F.; Gershon, P. D., Synthesis and application of a chain-terminating dinucleotide mRNA cap analog. *Organic Letters* **2002,** *4* (2), 161-164.

364. STEPINSKI, J.; WADDELL, C.; STOLARSKI, R.; DARZYNKIEWICZ, E.; RHOADS, R. E., Synthesis and properties of mRNAs containing the novel "anti-reverse" cap analogs 7-methyl (3′-O-methyl) GpppG and 7-methyl (3′-deoxy) GpppG. *RNA* **2001,** *7* (10), 1486-1495.

365. Jemielity, J.; Fowler, T.; Zuberek, J.; Stepinski, J.; Lewdorowicz, M.; Niedzwiecka, A.; Stolarski, R.; Darzynkiewicz, E.; Rhoads, R. E., Novel "anti-reverse" cap analogs with superior translational properties. *RNA* **2003,** *9* (9), 1108-1122.

366. Coleman, T. M.; Wang, G.; Huang, F., Superior 5′ homogeneity of RNA from ATP-initiated transcription under the T7 ϕ2. 5 promoter. *Nucleic Acids Research* **2004,** *32* (1), e14-e14.

367. Kore, A. R.; Parmar, G., An industrial process for selective synthesis of 7-methyl guanosine 5′-diphosphate: versatile synthon for synthesis of mRNA cap analogues. *Nucleosides, Nucleotides and Nucleic Acids* **2006,** *25* (3), 337-340.

368. Ziemniak, M.; Strenkowska, M.; Kowalska, J.; Jemielity, J., Potential therapeutic applications of RNA cap analogs. *Future Medicinal Chemistry* **2013,** *5* (10), 1141-1172.

369. Kore, A. R.; Shanmugasundaram, M.; Charles, I.; Vlassov, A. V.; Barta, T. J., Locked nucleic acid (LNA)-modified dinucleotide mRNA cap analogue: synthesis, enzymatic incorporation, and utilization. *Journal of the American Chemical Society* **2009,** *131* (18), 6364-6365.

370. Shanmugasundaram, M.; Charles, I.; Kore, A. R., Design, synthesis and biological evaluation of dinucleotide mRNA cap analog containing propargyl moiety. *Bioorganic & Medicinal Chemistry* **2016,** *24* (6), 1204-1208.

371. Kore, A. R.; Xiao, Z.; Li, M., Synthesis and biological validation of N7-(4-chlorophenoxyethyl) substituted dinucleotide cap analogs for mRNA translation. *Bioorganic & Medicinal Chemistry* **2013,** *21* (15), 4570-4574.

372. Grudzien, E.; Stepinski, J.; Jankowska-Anyszka, M.; Stolarski, R.; Darzynkiewicz, E.; Rhoads, R. E., Novel cap analogs for in vitro synthesis of mRNAs with high translational efficiency. *RNA* **2004,** *10* (9), 1479-1487.

373. Rydzik, A. M.; Lukaszewicz, M.; Zuberek, J.; Kowalska, J.; Darzynkiewicz, Z. M.; Darzynkiewicz, E.; Jemielity, J., Synthetic dinucleotide mRNA cap analogs with tetraphosphate 5′, 5′ bridge containing methylenebis (phosphonate) modification. *Organic & Biomolecular Chemistry* **2009,** *7* (22), 4763-4776.

374. Grudzien-Nogalska, E.; Jemielity, J.; Kowalska, J.; Darzynkiewicz, E.; Rhoads, R. E., Phosphorothioate cap analogs stabilize mRNA and increase translational efficiency in mammalian cells. *RNA* **2007,** *13* (10), 1745-1755.

375. Kowalska, J.; Lewdorowicz, M.; Zuberek, J.; Grudzien-Nogalska, E.; Bojarska, E.; Stepinski, J.; Rhoads, R. E.; Darzynkiewicz, E.; Davis, R. E.; Jemielity, J., Synthesis and characterization of mRNA cap analogs containing phosphorothioate substitutions that bind tightly to eIF4E and are resistant to the decapping pyrophosphatase DcpS. *RNA* **2008,** *14* (6), 1119-1131.

376. Wendel, H.-G.; Silva, R. L.; Malina, A.; Mills, J. R.; Zhu, H.; Ueda, T.; Watanabe-Fukunaga, R.; Fukunaga, R.; Teruya-Feldstein, J.; Pelletier, J., Dissecting eIF4E action in tumorigenesis. *Genes & Development* **2007,** *21* (24), 3232-3237.

377. Chen, X.; Kopecky, D. J.; Mihalic, J.; Jeffries, S.; Min, X.; Heath, J.; Deignan, J.; Lai, S.; Fu, Z.; Guimaraes, C., Structure-guided design, synthesis, and evaluation of guanine-derived inhibitors of the eIF4E mRNA–cap interaction. *Journal of Medicinal Chemistry* **2012,** *55* (8), 3837-3851.

378. Ghosh, B.; Benyumov, A. O.; Ghosh, P.; Jia, Y.; Avdulov, S.; Dahlberg, P. S.; Peterson, M.; Smith, K.; Polunovsky, V. A.; Bitterman, P. B., Nontoxic chemical interdiction of the epithelial-to-mesenchymal transition by targeting cap-dependent translation. *ACS Chemical Biology* **2009,** *4* (5), 367-377.

379. Ogasawara, S., Duration control of protein expression in vivo by light-mediated reversible activation of translation. *ACS Chemical Biology* **2017,** *12* (2), 351-356.

380. Feng, C.; Li, Y.; Spitale, R., Photo-controlled cell-specific metabolic labeling of RNA. *Organic & Biomolecular Chemistry* **2017,** *15* (24), 5117-5120.

381. Gadakh, B.; Vondenhoff, G.; Lescrinier, E.; Rozenski, J.; Froeyen, M.; Van Aerschot, A., Base substituted 5′-O-(N-isoleucyl) sulfamoyl nucleoside analogues as potential antibacterial agents. *Bioorganic & Medicinal Chemistry* **2014,** *22* (10), 2875-2886.

382. Kore, A. R.; Bugarin, A.; Shanmugasundaram, M., Design and Facile Synthesis of New Dinucleotide Cap Analog Containing Both 2′ and 3′-OH Modification on M7Guanosine Moiety. *Nucleosides, Nucleotides and Nucleic Acids* **2015,** *34* (9), 611-619.

383. Vacca, J. P.; deSolms, S. J.; Huff, J. R.; Billington, D. C.; Baker, R.; Kulagowski, J. J.; Mawer, I. M., The total synthesis of myo-inositol polyphosphates. *Tetrahedron* **1989,** *45* (17), 5679-5702.

384. Miazga, A.; Hamy, F.; Louvel, S.; Klimkait, T.; Pietrusiewicz, Z.; Kurzyńska-Kokorniak, A.; Figlerowicz, M.; Wińska, P.; Kulikowski, T., Thiated derivatives of 2′, 3′-dideoxy-3′-fluorothymidine: Synthesis, in vitro anti-HIV-1 activity and interaction with recombinant drug resistant HIV-1 reverse transcriptase forms. *Antiviral Research* **2011,** *92* (1), 57-63.

385. Wojtczak, B. A.; Sikorski, P. J.; Fac-Dabrowska, K.; Nowicka, A.; Warminski, M.; Kubacka, D.; Nowak, E.; Nowotny, M.; Kowalska, J.; Jemielity, J., 5′-Phosphorothiolate dinucleotide cap analogues: reagents for messenger RNA modification and potent small-molecular inhibitors of decapping enzymes. *Journal of the American Chemical Society* **2018,** *140* (18), 5987-5999.

386. Hou, X.; Wang, G.; Gaffney, B. L.; Jones, R. A., Synthesis of guanosine and deoxyguanosine phosphoramidites with cross-linkable thioalkyl tethers for direct incorporation into RNA and DNA. *Nucleosides, Nucleotides and Nucleic Acids* **2009,** *28* (11-12), 1076-1094.

387. Gowda, A. P.; Lee, M.; Spratt, T. E., N2-Substituted 2′-Deoxyguanosine Triphosphate Derivatives as Selective Substrates for Human DNA Polymerase κ. *Angewandte Chemie International Edition* **2017,** *56* (10), 2628-2631.

388. Lin, T.-C.; Fang, J.-M., Diphosphate formation using cyanuric chloride or triisopropylbenzenesulfonyl chloride as the activating agents. *Tetrahedron Letters* **2011,** *52* (17), 2232-2234.

389. Mohamady, S.; Desoky, A.; Taylor, S. D., Sulfonyl imidazolium salts as reagents for the rapid and efficient synthesis of nucleoside polyphosphates and their conjugates. *Organic Letters* **2012,** *14* (1), 402-405.